STARS

University of Central Florida
STARS

Electronic Theses and Dissertations, 2004-2019

2006

Molecular Structure-nonlinear Optical Property Relationships For A Series Of Polymethine And Squaraine Molecules

Jie Fu
University of Central Florida

 Part of the Electromagnetics and Photonics Commons, and the Optics Commons
Find similar works at: https://stars.library.ucf.edu/etd
University of Central Florida Libraries http://library.ucf.edu

This Doctoral Dissertation (Open Access) is brought to you for free and open access by STARS. It has been accepted for inclusion in Electronic Theses and Dissertations, 2004-2019 by an authorized administrator of STARS. For more information, please contact STARS@ucf.edu.

STARS Citation
Fu, Jie, "Molecular Structure-nonlinear Optical Property Relationships For A Series Of Polymethine And Squaraine Molecules" (2006). *Electronic Theses and Dissertations, 2004-2019*. 1016.
https://stars.library.ucf.edu/etd/1016

University of Central Florida
STARS
Showcase of Text, Archives, Research & Scholarship

MOLECULAR STRUCTURE – NONLINEAR OPTICAL PROPERTY RELATIONSHIPS FOR A SERIES OF POLYMETHINE AND SQUARAINE MOLECULES

by

JIE FU
B.S. Tsinghua University, 1997
M.S. Tsinghua University, 2000
M.S. University of Central Florida, 2002

A dissertation submitted in partial fulfillment of the requirements
for the degree of Doctor of Philosophy
in the College of Optics and Photonics: CREOL & FPCE
at the University of Central Florida
Orlando, Florida

Fall Term
2006

Major Professors: Dr. Eric W. Van Stryland and Dr. David J. Hagan

© 2006 Jie Fu

ABSTRACT

This dissertation reports on the investigation of the relationships between molecular structure and two-photon absorption (2PA) properties for a series of polymethine and squaraine molecules. Current and emerging applications exploiting the quadratic dependence upon laser intensity, such as two-photon fluorescence imaging, three-dimensional microfabrication, optical data storage and optical limiting, have motivated researchers to find novel materials exhibiting strong 2PA. Organic materials are promising candidates because their linear and nonlinear optical properties can be optimized for applications by changing their structures through molecular engineering. Polymethine and squaraine dyes are particularly interesting because they are fluorescent and showing large 2PA.

We used three independent nonlinear spectroscopic techniques (Z-scan, two-photon fluorescence and white-light continuum pump-probe spectroscopy) to obtain the 2PA spectra revealing 2PA bands, and we confirm the experimental data by comparing the results from the different methods mentioned.

By systematically altering the structure of polyemthines and squaraines, we studied the effects of molecular symmetry, strength of donor terminal groups, conjugation length of the chromophore chain, polarity of solvents, and the effects of placing bridge molecules inside the chromophore chain on the 2PA properties. We also compared polymethine, squaraine, croconium and tetraon dyes with the same terminal groups to study the effects of the different additions inserted within the chromophore chain on their optical properties. Near IR absorbing squaraine dyes were experimentally observed to show extremely large 2PA cross sections (≈ 30000GM). A simplified three-level model was used to fit the measured 2PA spectra and

detailed quantum chemical calculations revealed the reasons for the squaraine to exhibit strong 2PA. In addition, two-photon excitation fluorescence anisotropy spectra were measured through multiple 2PA transitions. A theoretical model based on four-levels with two intermediate states was derived and used for analysis of the experimental data.

This dissertation is dedicated to my parents and my wife Xiang Wu, who have given me unending patience, support and love throughout these years.

ACKNOWLEDGMENTS

I would truly like to thank my advisors, Dr. David J. Hagan and Dr. Eric W. Van Stryland, for providing me this great opportunity and environment to complete my graduate research work in CREOL. I really appreciate their every effort to provide me the guidance whenever I needed throughout these years because both of them also take great responsibility on the CREOL and OSA at same time, so have very tight schedule.

I also deeply grateful for the opportunity to work with Dr. Olga A. Przhonska from the Institute of Physics, National Academy of Sciences of Ukraine. Without her great patience and detailed discussions, this dissertation would not have been possible. Not only I learned a lot from her about chemistry of organic molecule, but also her incredible passions and dedications on the science put herself a valuable example to anyone working with her.

The whole of the work presented in this dissertation was result of a truly broad collaborative effort. I want to sincerely thank Dr. Lazaro A. Padilha for his extensive experimental work on Z-scan measurements. He is a great friend as well. I also want to give special thanks to former student Dr. Joel M. Hales for his help and encouragement. He taught me much of what I know about femto-second lab and scientific research in my earlier years here. I also appreciate people from Institute of Organic Chemistry of National Academy of Sciences from Ukraine, Dr. Seth Marder's group at School of Chemistry and Biochemistry from Georgia Institute of Technology and Dr. Kevin Belfield's group for their great efforts on synthesizing the organic molecules studied in this dissertation.

I would like to thank the graduate students and post-docs I have worked with in the nonlinear optics group over the years. Dr. Scott Webster is a great group leader, researcher and

friend. I also appreciate all the help from Dr. Rich Lepkowicz, Ion Cohanoschi, Peter Olszak, Claudiu Cirloganu and Mihaela Balu.

Finally I want to thank all of my friends and acquaintances I've made here while in CREOL. Dr. Changching Tsai, Dr. S.T. Wu's group, Dr. Guifang Li's group, Peter Olszak, Weiyao Zhou, you all made this one of best times of my life. Thank you to everyone.

TABLE OF CONTENTS

LIST OF FIGURES

LIST OF TABLES

LIST OF NOMENCLATURE

Acronym/Unit	Description
2PA	Two-Photon Absorption
2PF	Two-Photon Fluorescence
CaF_2	Calcium Fluoride
cm	Centimeter (10^{-2} m)
D-2PA	Degenerate Two-Photon Absorption
ESA	Excited-State Absorption
eV	Electron Volt unit of energy
fs	Femtosecond (10^{-15} s)
GM	Goppert-Mayer unit for the 2PA cross-section (1 x 10^{-50} cm^4 sec photon^{-1} molecule^{-1})
GVD	Group-Velocity Dispersion
GVM	Group-Velocity Mismatch
GW	Gigawatt (10^9 W)
HOMO	Highest Occupied Molecular Orbital
ISC	Intersystem Crossing
kHz	Kilohertz (10^3 Hz)
LUMO	Lowest Unoccupied Molecular Orbital
μJ	Microjoule (10^{-6} J)
μm	Micrometer (10^{-6} m)
M	Molarity unit of concentration (Moles/Liter)

mm	Millimeter (10^{-3} m)
MW	Megawatt (10^{6} W)
ND-2PA	Nondegenerate Two-Photon Absorption
nJ	Nanojoule (10^{-9} J)
NLO	Nonlinear Optical
nm	Nanometer (10^{-9} m)
ns	Nanosecond (10^{-15} s)
OD	Optical Density
OKE	Optical Kerr Effect
OPA	Optical Parametric Amplifier
ps	Picosecond (10^{-12}s)
SOS	Sum-Over-States
THF	Tetrahydrofuran
WLC	White Light Continuum

CHAPTER 1 INTRODUCTION

1.1 Background and motivation

In 1931, Maria Goppert-Mayer first theoretically predicted that an atom or a molecule could absorb two photons simultaneously in a single quantized event [1]. The first experimental evidence for two-photon absorption (2PA) waited 30 years until the laser was invented, and then Kaiser and Garret demonstrated two-photon excitation in a $CaF_2:Eu^{3+}$ crystal [2].

The process of two-photon absorption involves simultaneous absorption of two photons from an initial state to a higher excited state within a material, and the energy difference between these two states is equal to the sum of the energies of the two photons. In the case of absorbing two photons having the same frequency or photon energy, this type of 2PA is called *Degenerate* 2PA (D-2PA). In the case of absorbing two photons having different frequency or photon energy, this type of 2PA is called *Nondegenerate* 2PA (ND-2PA).

The two-photon absorption process is different from excited state absorption (ESA). Both of them involve two photons. The difference is shown in Fig.1.1. S_0 is ground state, S_1 is the first excited state, and S_2 is the second excited state.

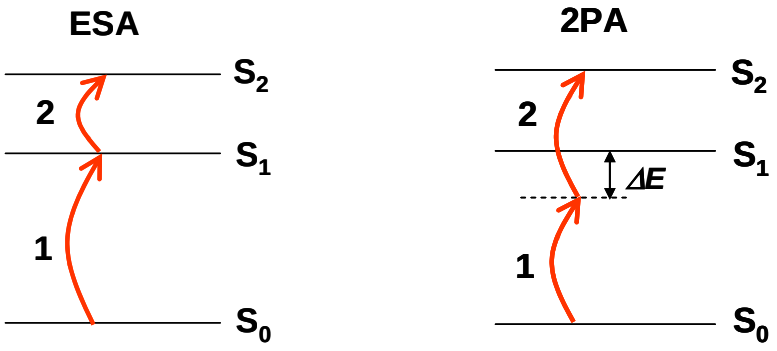

Figure 1.1 Diagram for electronic transitions for Excited State Absorption (ESA) and Two-Photon Absorption (2PA)

The following is a conceptual description of ESA and 2PA that provides some useful intuition concerning the processes. Shown in Fig. 1.1, In the ESA process, photon 1 has sufficient energy to excite a molecule from the ground state S_0 to the first excited state S_1. Because the energy mismatch, ΔE, between photon 1 and state S_1 is within the natural linewidth, excited electrons can make real transitions and stay in state S_1 for times of ~10^{-3} to 10^{-12} seconds. Thus arrival of photon 2 within this time can complete the electronic transition to the final state S_2. This describes the ESA process, which is sometimes called *resonance two-photon absorption.*

In a 2PA process, the energy mismatch ΔE between photon 1 and the first excited state S_1 is large compared to the natural linewidth and neither photon has sufficient energy to excite the ground-state molecule to excited state S_1 on its own. Thus, in order to complete the 2PA process to S_2, the second photon has to arrive within a time determined by the Uncertainty Principle [3]. The brief duration of this action (~10^{-15} seconds for 2PA in the visible) is the reason 2PA is classified as an 'instantaneous' nonlinear process. This also describes why 2PA is observed only for high intensity where the probability of finding 2 photons in the same time interval is large. 2PA is also called *non-resonance two-photon absorption.*

More accurately, the probability of 2PA depends quadratically on the irradiance of the beam (2PA $\propto I^2$). This leads to several existing and potential applications and technologies, including two-photon fluorescence microscopy [4], three-dimensional (3D) micro-fabrication [5] and optical data storage [6].

Achieving 3D spatial resolution with 2PA (or spatial localization of 2PA) is illustrated in Fig. 1.2. The solution is a fluorescent chromophore. In Fig.1.2 (a), light of wavelength λ_1 is focused into the solution. Because λ_1 is within the linear absorption spectrum, the solution shows large one-photon absorption (1PA) of the λ_1 beam at regions close to the surface, and then emits significant fluorescence from this region. In Fig.1.2 (b), the laser beam of wavelength λ_2 ($\lambda_2 = 2\lambda_1$) is focused into the solution by the same focusing geometry. Because λ_2 is not within the linear absorption range, the green solution does not experience 1PA of λ_2 at regions close to the surface, and only experiences 2PA at region near the focal point where the intensity of the laser beam is high. Fluorescence following 2PA is localized at the region of the focal point. Moreover, the λ_2 laser beam shows much less linear scattering loss (scattering loss $\propto \omega^4$) compared with a λ_1 beam, so 2PA improves the penetration depth. This is important for biological imaging.

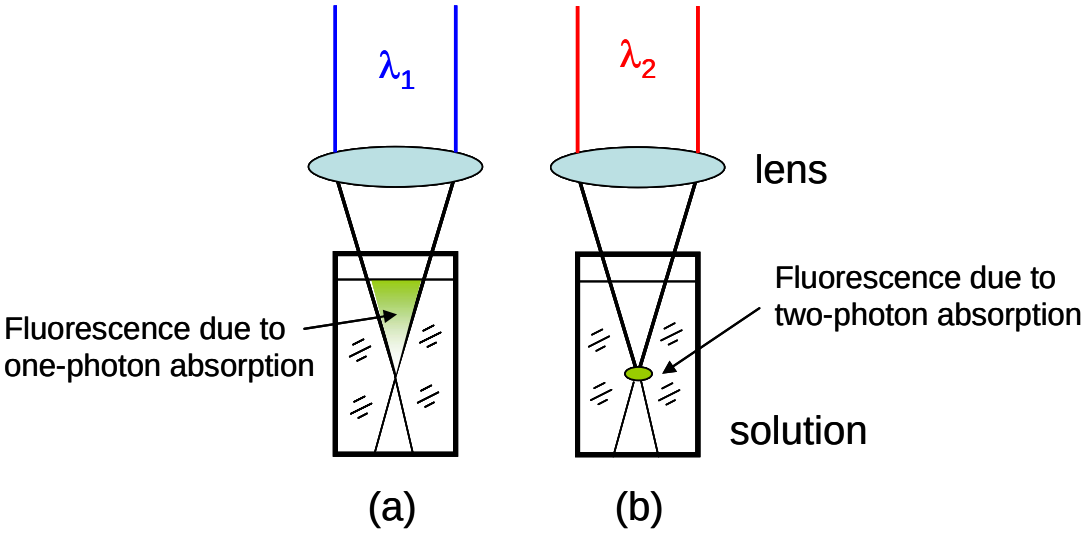

Figure 1.2 Illustration showing a comparison of fluorescence due to 1PA (a) and 2PA (b) to show the greater spatial resolution of two-photon excitation

In addition to the fluorescence that can follow the 2PA process, 2PA can also be followed by intersystem crossing (ISC) and ESA as shown in Fig.1.3. Another important application of 2PA is optical power limiting [8-10] which takes advantage of these processes.

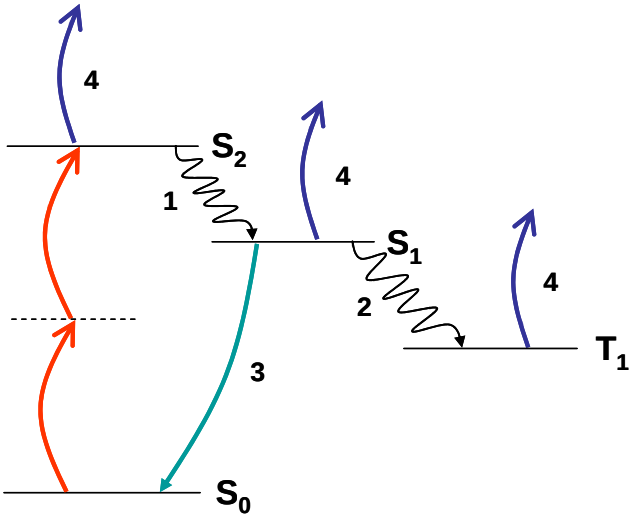

Figure 1.3 Photophysical process following 2PA (S_0, S_1 and S_2 are singlet states, T_1 is a triplet state): 1) Internal Conversion to S_1; 2) Intersystem crossing (ISC) to triplet state T_1; 3) radiative decay (fluorescence) from S_1; 4) Excited state absorption (ESA)

Organic materials are strong candidates for 2PA applications because their material properties can be tailored through molecular engineering. In particular, electron delocalization in molecules provides a strong polarizability to enhance a molecule's 2PA.

In organic structures the delocalization of electrons, similar to the free electrons in a semiconductor, is provided by π-bonding in a class of organic compounds called *π-conjugated* molecules and polymers. These conjugated molecules involve alternate single and multiple covalent bonds. A single covalent bond between two atoms (heavier than hydrogen) is formed by the axial overlap of the hybridized atomic orbitals of two atoms and is called the *σ bond* (blue bond in Fig.1.4). The additional bond involved in a double covalent bond between two atoms is formed by the lateral overlap of the un-hybridized *p* type atomic orbitals (green bond in Fig.1.4). This bond is called a *π bond*, and the electrons involved are called the π electrons. One example for π bonds in ethane is illustrated in Fig.1.4 [11].

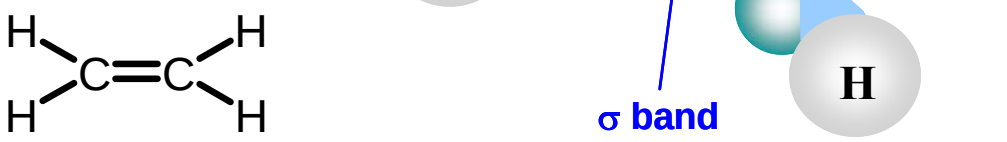

(a) (b)

Figure 1.4: (a) Molecular structure for ethane (b) illustration of covalent bands of ethane

A double covalent bond has one σ bond and one π bond, and a triple covalent bond has one σ bond and two π bonds. π electrons are loosely bound electrons and are spread (delocalized) over the entire conjugated molecular structure, hence behaving similar to free electrons in a semiconductor.

Unfortunately, most known organic molecules have relatively small 2PA cross sections δ, and criteria for the design of molecules with large δ have not been well developed. A significant breakthrough came in 1998 [12] and opened the door for design strategies for molecules with large 2PA cross sections. Researchers synthesized molecules with linear π-conjugation showing large 2PA cross sections on the basis of the concept that symmetric charge (π electrons) transfers from the ends of a conjugated system to the middle, or vice verse [12]. They also performed quantum chemical calculations to confirm this charge redistribution with experimental results.

After that, various research groups [13-26] have shown molecular design strategies for efficient 2PA by a systematic investigation of the conjugation length of the chromophores, various symmetrical and asymmetrical combinations of electron-donor and electron-acceptor terminal groups, and the addition of such groups in the middle of the chromophore to vary the charge distribution. Even though there has been considerable progress in the studies of structure-property relationships of organic molecules, much more remains to be discovered. We discuss some of this in this dissertation but also use newly developed techniques (done at CREOL) to significantly build the existing database to help elucidate structure/property relations in collaboration with materials synthesizers and quantum chemists.

1.2 Dissertation statement

The purpose of this dissertation is to investigate several sets of organic molecules whose structures have been systemically altered to determine how these structural changes will affect their two-photon absorbing capabilities. Full linear spectroscopic characterization is performed on these molecules to determine the strength, location and spectral contour of their absorption and emission spectra. Several nonlinear spectroscopic techniques are employed to characterize both the strength and location of the 2PA spectra. In addition, quantum chemical calculations are used to determine state and transition dipole moments, as well as explaining and confirming experimental results. We also measured two-photon excitation fluorescence anisotropy spectra which for the first time covered several 2PA bands, giving us more insight into the 2PA process.

Molecular structure motif changes, such as symmetry, conjugation length, donor-acceptor strength, effect of squaraine addition, croconium and tetraon are investigated. These results show definitive correlations between chemical structures and the linear and nonlinear optical properties of these molecules, and with molecules showing unprecedented 2PA cross sections. All these experimental and theoretical studies improve our understanding of the way to optimize molecular two-photon absorbing capabilities.

1.3 Dissertation outline

This work is structured according to the following: Chapter 1 introduces the concept of two-photon absorption and provides the impetus for investigating this nonlinear behavior of organic molecules. Chapter 2 describes this process in terms of light-matter interactions and presents the perturbative Sum-Over-States (SOS) formulation for the third-order susceptibility,

$\chi^{(3)}$. Chapter 3 addressed the linear and nonlinear spectroscopic techniques. Chapter 4 concentrates on the study of relationships between molecular structures and 2PA properties for polymethine molecules. The linear spectroscopic data for these molecules are also presented. Chapter 5 addresses the relationships between chemical structures and the 2PA properties of squaraines. We also compared 2PA properties for polymethines, squaraines, croconium and tetraon molecules having similar structures. Quantum chemical calculations help us understand the differences and also provide us insight into the nature of the 2PA process. In Chapter 6, two-photon excitation fluorescence anisotropy spectra of polymethines and squaraines are studied both experimentally and theoretically. We derived a new equation for two-photon anisotropy based on a two-intermediate-state, four-level model to reveal the orientation between different transition dipole moments involved in the 2PA process. Finally, Chapter 7 concludes the dissertation and suggests some future directions which might be taken.

CHAPTER 2 NONLINEAR OPTICS AND TWO-PHOTON ABSORPTION THEORY

2.1 Nonlinear optics/macroscopic polarization theory

All derivations and formulas in this chapter are based on the definition of the electric field and polarization shown below:

$$\boldsymbol{E} = \frac{1}{2}\left(\boldsymbol{E}_0 e^{-i\omega t} + \boldsymbol{E}_0^* e^{i\omega t}\right) \tag{2.1}$$

$$\boldsymbol{P} = \frac{1}{2}\left(\boldsymbol{P}_0 e^{-i\omega t} + \boldsymbol{P}_0^* e^{i\omega t}\right) \tag{2.2}$$

Nonlinear optics studies the phenomena that the response of a material system to an applied optical/electric field depends upon the strength of the optical field in a nonlinear manner, or in the other words, optical properties of a material system are changed in the presence of an intense optical field.

Responses of materials to intense optical fields depend on the frequency of the optical wave and the irradiance (i.e. for pulsed sources, the pulse energy, pulse duration, and beam spatial distribution): and on the materials; 1) displacement of electrons; 2) displacement of atoms (molecular vibrations); 3) molecular orientation in liquid and gas phase; 4) electrostriction (acousto-optics); 5) molecular orientation in solid (liquid crystal); 6) saturated absorption; 7) thermal effect. Here two-photon absorption (2PA) is one of nonlinear optical processes related to the *displacement of electrons* in the presence of an intense optical field.

Now we consider details of this interaction between materials and an externally applied optical electric field, $\boldsymbol{E}_{ex}$. The materials consist of a distribution of charged particles, namely

positively charged nuclei and negatively charged electrons. In general, the electron is "elastically" coupled to the nucleus (by "classical" picture). An externally applied oscillating optical field $\boldsymbol{E_{ex}}$ will interact with electrons in the way that electrons are "displaced" by the electric field in the vicinity, called the *local electric filed* $\boldsymbol{E_{loc}}$. This local field is due to the externally applied optical field $\boldsymbol{E_{ex}}$, but is modified by the electric field due to the presence of other electrons and nuclei. The local electric field, $\boldsymbol{E_{loc}}$, displaces the electron density from the nuclear core and creates an induced dipole moment $\boldsymbol{\mu}$ (called *microscopic polarization*).

Provided the incident optical field $\boldsymbol{E_{ex}}$ is small in magnitude, the displacement of the electron charge cloud will remain small as well, and will oscillate harmonically with the frequency of the electric field $\boldsymbol{E_{loc}}$. In this regime, the induced dipole moment or microscopic polarization $\boldsymbol{\mu}$ can be considered to be linearly proportional to the strength of the local electric field $\boldsymbol{E_{loc}}$ and an expression can be written relating the two terms:

$$\boldsymbol{\mu(\omega)} = \alpha(\omega)\boldsymbol{E}_{loc}\boldsymbol{(\omega)} \tag{2.3}$$

Here, $\boldsymbol{\mu}$ and $\boldsymbol{E_{loc}}$ are given as vector quantities and $\alpha(\omega)$ is called the *linear polarizability* of the atom or molecule. In addition, it should be noted that α is a second rank tensor for general anisotropic materials.

The *Macroscopic polarization,* $\boldsymbol{P}$, is related to the microscopic polarization $\boldsymbol{\mu}$ through the number density, N, number of molecules per unit volume, and to the external optical field $\boldsymbol{E_{ex}}$ with *macroscopic linear susceptibility* $\chi^{(1)}$ (also a second-rank tensor for anisotropic materials). In **SI** unit, the relation is:

$$\boldsymbol{P(\omega)} = N\boldsymbol{\mu(\omega)} = N\alpha(\omega)\boldsymbol{E}_{loc}\boldsymbol{(\omega)} = \varepsilon_0\chi^{(1)}(\omega)\boldsymbol{E}_{ex}\boldsymbol{(\omega)} \tag{2.4}$$

If we assume that there are only Lorentz-Lorentz interactions among the molecules, the local field can be expressed in **SI** unit as:

$$\boldsymbol{E}_{loc}(\omega) = \boldsymbol{E}_{ex}(\omega) + \frac{1}{3\varepsilon_0}\boldsymbol{P}(\omega) = \boldsymbol{E}_{ex}(\omega)\left(1 + \frac{\chi^{(1)}(\omega)}{3}\right) \tag{2.5}$$

The relationship between microscopic linear polarizability α and macroscopic linear susceptibility $\chi^{(1)}$ can be derived from Eq (2.4) and (2.5) as:

$$\alpha(\omega) = \frac{3\varepsilon_0}{N}\frac{\chi^{(1)}(\omega)}{3 + \chi^{(1)}(\omega)} \tag{2.6}$$

and

$$\chi^{(1)}(\omega) = \frac{1}{\varepsilon_0}\frac{N\alpha(\omega)}{1 - \frac{N\alpha(\omega)}{3\varepsilon_0}} \tag{2.7}$$

If we assume the linear absorption of light with frequency ω is negligible (this is a common case for nonlinear optics), the imaginary part of $\chi^{(1)}$ is set equal to zero. We then have the relation:

$$\chi^{(1)}(\omega) = \mathrm{Re}(\chi^{(1)}(\omega)) = \mathrm{Re}(\varepsilon^{(1)}(\omega)) - 1 = n(\omega) - 1 \tag{2.8}$$

Substituting Eq.(2.8) into Eq. (2.5), we get:

$$\boldsymbol{E}_{loc}(\omega) = \boldsymbol{E}_{ex}(\omega)\left(\frac{n(\omega) + 2}{3}\right) \tag{2.9}$$

and substituting Eq.(2.8) into Eq.(2.6), we get:

$$\alpha(\omega) = \frac{\varepsilon_0}{N}\left(\frac{3}{n(\omega) + 2}\right)\chi^{(1)}(\omega) \tag{2.10}$$

In nonlinear optics, the nonlinear optical response of a material can often be described by generalizing Eq. (2.4) by expressing the macroscopic polarization **P** as a power series in the externally applied optical field $\mathbf{E}_{ex}$. In **SI** units this gives:

$$\begin{aligned}\boldsymbol{P}(\boldsymbol{r},t) &= \varepsilon_0\chi^{(1)}\boldsymbol{E}_{ex}(\boldsymbol{r},t) + \varepsilon_0\chi^{(2)}\boldsymbol{E}_{ex}(\boldsymbol{r},t)\boldsymbol{E}_{ex}(\boldsymbol{r},t) + \varepsilon_0\chi^{(3)}\boldsymbol{E}_{ex}(\boldsymbol{r},t)\boldsymbol{E}_{ex}(\boldsymbol{r},t)\boldsymbol{E}_{ex}(\boldsymbol{r},t) + \cdots \\ &= \boldsymbol{P}^{(1)} + \boldsymbol{P}^{(2)} + \boldsymbol{P}^{(3)} + \cdots\cdots\end{aligned} \tag{2.11}$$

Here $\chi^{(2)}$ is called the *macroscopic second-order nonlinear susceptibilit*y and is a third-rank tensor, and $\boldsymbol{P}^{(2)} = \varepsilon_0\chi^{(2)}\boldsymbol{E}_{ex}\boldsymbol{E}_{ex}$ is referred to as the second-order nonlinear polarization; $\chi^{(3)}$ is called the *macroscopic third-order nonlinear susceptibility* and is a fouth-rank tensor, and $\boldsymbol{P}^{(3)} = \varepsilon_0\chi^{(3)}\boldsymbol{E}_{ex}\boldsymbol{E}_{ex}\boldsymbol{E}_{ex}$ is referred to as the third-order nonlinear polarization.

It is noted that some researchers in the nonlinear optics field use microscopic third-order polarizability γ (please do not confuse this γ with the γ used in the next section referring to the three-photon absorption coefficient) instead of the *macroscopic* third-order nonlinear susceptibility $\chi^{(3)}$. We can derive the relationship between these below.

With Eq (2.5) and (2.9), for the frequency degenerate 2PA case, we have in **SI** units from Eq. (2.11):

$$\begin{aligned}\boldsymbol{P}(\omega) &= N\alpha(\omega)\boldsymbol{E}_{loc}(\omega) + N\gamma(-\omega;\omega,-\omega,\omega)\boldsymbol{E}_{loc}{}^{3}(\omega) \\ &= N\alpha(\omega)\left(\boldsymbol{E}_{ex}(\omega) + \frac{1}{3\varepsilon_0}\boldsymbol{P}(\omega)\right) + N\gamma(-\omega;\omega,-\omega,\omega)\boldsymbol{E}_{loc}{}^{3}(\omega) \\ &= N\alpha(\omega)\left(\boldsymbol{E}_{ex}(\omega) + \frac{1}{3\varepsilon_0}\boldsymbol{P}(\omega)\right) + N\gamma(-\omega;\omega,-\omega,\omega)\left(\frac{n(\omega)+2}{3}\right)^{3}\boldsymbol{E}_{ex}{}^{3}(\omega)\end{aligned} \tag{2.12}$$

This equation is now solved algebraically for $\boldsymbol{P}(\omega)$ to obtain:

$$\boldsymbol{P}(\omega) = \frac{N\alpha(\omega)}{1-\frac{N\alpha(\omega)}{3\varepsilon_0}}\boldsymbol{E}_{ex}(\omega) + \frac{N\gamma(-\omega;\omega,-\omega,\omega)}{1-\frac{N\alpha(\omega)}{3\varepsilon_0}}\left(\frac{n(\omega)+2}{3}\right)^{3}\boldsymbol{E}_{ex}{}^{3}(\omega) \tag{2.13}$$

Also from Eq. (2.11), we have,

$$\boldsymbol{P}(\omega) = \varepsilon_0 \chi^{(1)}(\omega)\boldsymbol{E}_{ex}(\omega) + \varepsilon_0 \chi^{(3)}(-\omega;\omega,-\omega,\omega)\boldsymbol{E}_{ex}^{3}(\omega) \tag{2.14}$$

Comparing Eq. (2.13) and (2.14), we see the first terms must be equal to each other by Eq. (2.7), so the second terms must also be equal. Therefore we have

$$\gamma(-\omega;\omega,-\omega,\omega) = \frac{\varepsilon_0}{N}\frac{1}{\left(\frac{n(\omega)+2}{3}\right)^3}\left(1-\frac{N\alpha(\omega)}{3\varepsilon_0}\right)\chi^{(3)}(-\omega;\omega,-\omega,\omega) \tag{2.15}$$

From Eq. (2.7) and (2.10), we have,

$$\left(1-\frac{N\alpha(\omega)}{3\varepsilon_0}\right) = \frac{1}{\left(\frac{n(\omega)+2}{3}\right)} \tag{2.16}$$

and

$$\gamma(-\omega;\omega,-\omega,\omega) = \frac{\varepsilon_0}{N}\frac{1}{\left(\frac{n(\omega)+2}{3}\right)^4}\chi^{(3)}(-\omega;\omega,-\omega,\omega) = \frac{\varepsilon_0}{N}\frac{1}{L^4}\chi^{(3)}(-\omega;\omega,-\omega,\omega) \tag{2.17}$$

Usually, researchers define $L = \frac{n(\omega)+2}{3}$ as a *local field factor*.

In this dissertation, we will use the macroscopic third-order nonlinear susceptibility $\chi^{(3)}$ only.

The polarization $\boldsymbol{P}$ describes the linear and nonlinear optical phenomena through its time and space variation, $\boldsymbol{P(r,t)}$. This polarization can act as the source of new components of the electromagnetic field. This is shown by the wave equation in a media in **SI** unit:

$$\nabla\times\nabla\times\boldsymbol{E} + \frac{1}{c^2}\frac{\partial^2\boldsymbol{E}}{\partial t^2} = -\mu_0\frac{\partial^2\boldsymbol{P}}{\partial t^2} \tag{2.18}$$

We note that second-order nonlinear optical interactions ($\chi^{(2)}$, $\boldsymbol{P}^{(2)}$) can only occur in noncentrosymmetric materials, i.e. materials that do not display inversion symmetry [*inversion symmetry*: $\boldsymbol{P}^{(2)}(-\boldsymbol{r},t) = -\boldsymbol{P}^{(2)}(\boldsymbol{r},t)$]. Since liquids, gases, amorphous solids (for example, glass), even many crystals do display inversion symmetry, $\chi^{(2)}$ vanishes for such materials, and consequently they cannot show macroscopic second-order nonlinear optical interactions. On the contrary, third-order nonlinear optical interactions ($\chi^{(3)}$, $\boldsymbol{P}^{(3)}$) can occur in both centrosymmetric and noncentrosymmetric materials, i.e. all materials.

The physical phenomenon related to the second-order nonlinear susceptibility $\chi^{(2)}$ and third-order nonlinear optical susceptibility $\chi^{(3)}$ are summarized in Table 2.1 and Table 2.2 respectively.

Table 2.1 Second-order nonlinear optical processes related to second-order susceptibility $\chi^{(2)}$

Nonlinear Optical Process	**Description**	$\chi^{(2)}$
Second-Harmonic Generation (SHG)	In: single beam at ω Out: single beam at 2ω	$\chi^{(2)}(-2\omega;\ \omega,\omega)$
Sum Frequency Generation Difference Frequency Generation	In: two beams at ω_1, ω_2 Out: single beam at $\omega_3=\omega_1\pm\omega_2$	$\chi^{(2)}(-\omega_3;\ \omega_1,\pm\omega_2)$
Linear Electro-Optical Effect (Pockels Effect)	In: static field and ω-beam Out: phase shift at ω-beam	$\chi^{(2)}(-\omega;\ 0,\omega)$
Optical Rectification (OR)	In: single beam at ω Out: static electric field	$\chi^{(2)}(0;\ \omega,\omega)$

Table 2.2 Third-order nonlinear optical processes related to third-order susceptibility $\chi^{(3)}$

Nonlinear Optical Process	Description	$\chi^{(3)}$
Third-Harmonic Generation (THG)	In: single beam at ω Out: single beam at 3ω	$\chi^{(3)}(-3\omega;\ \omega,\omega,\omega)$
Nonlinear Refractive Index Degenerate Two-Photon Absorption (D-2PA)	In: single beam at ω Out: phase shift/loss at ω	$\chi^{(3)}(-\omega;\ \omega,-\omega,\omega)$
Cross-Phase Modulation (including Optical Kerr Effect) Nondegenerate Two-Photon Absorption (ND-2PA)	In: two beams at ω_1, ω_2 Out: phase shift/loss at ω_1	$\chi^{(3)}(-\omega_1;\ \omega_1,-\omega_2,\omega_2)$
Degenerate Four Wave Mixing (DFWM)	In: three beams at ω Out: new beam at ω	$\chi^{(3)}(-\omega;\ \omega,-\omega,\omega)$
General Four Wave Mixing	In: two beams at ω_1, ω_2, ω_3 Out: new beam at ω_4	$\chi^{(3)}(-\omega_4;\ \omega_1,\omega_2,\omega_3)$
Electric Field Induced Second-Harmonic Generation	In: static field and ω-beam Out: new beam at 2ω	$\chi^{(3)}(-2\omega;\ 0,-\omega,\omega)$
Quadratic Electro-Optical Effect (Kerr Electro-Optical Effect)	In: static field and ω-beam Out: phase shift at ω	$\chi^{(3)}(-\omega;\ 0,0,\omega)$

2.2 Two-photon absorption and perturbation theory

2.2.1 Two-photon absorption

One of the most prominent aspects of the third-order nonlinear susceptibility $\chi^{(3)}$ is its connection to the nonlinear refractive index n_2 and the two-photon absorption coefficient β (see Table 2.2).

Degenerate two-photon absorption (D-2PA):

If we look at the evolution of the intensity $I(z)$ of a single beam with frequency ω propagating along the z-direction in a material with $\chi^{(3)}$, it can be described by the following differential equation:

$$\frac{dI(z)}{dz} = -\alpha I - \beta I^2 - \gamma I^3 - \cdots \tag{2.19}$$

where α is called the linear absorption coefficient, β is called the two-photon absorption coefficient, and γ is called the three-photon absorption coefficient.

If we ignore 1PA and only consider pure two-photon absorption, Eq. (2.19) will become:

$$\frac{dI(z)}{dz} = -\beta I^2 \tag{2.20}$$

It can be shown that the 2PA coefficient β is related to imaginary part of the third order susceptibility $\chi^{(3)}$. For the degenerate 2PA case (two photons having the same frequency and same polarization), this relation is shown below in **SI** units:

$$\beta = \frac{3\omega}{2n^2c^2\varepsilon_0}\mathrm{Im}(\chi^{(3)}(-\omega;\omega,-\omega,\omega)) \tag{2.21}$$

where n is the linear refractive index of the beam with frequency ω, and c is speed of light in vacuum.

Besides the 2PA coefficient β, another quantity often used to describe 2PA of molecules is the *2PA cross section, δ*. The 2PA cross section, δ, is typically given in units of 1×10^{-50} cm^4 sec photon^{-1} molecule^{-1}. This unit is commonly referred as a Goppert-Mayer or GM in honor of the author who pioneered theoretical work in this field. The relationship between δ and β for the degenerate 2PA case is shown below [27]:

$$\delta = \frac{\hbar\omega\beta}{N} \tag{2.22}$$

where N is the density of molecules in units of 1/volume.

We can derive this relation based on the work of Ref. [27]. For the degenerate 2PA case, the energy exchanged between the light beam and the molecular ensemble per unit time and volume, is given by

$$\frac{dW}{dt} = \left\langle \mathbf{E} \cdot \frac{d\mathbf{P}}{dt} \right\rangle = \frac{1}{2}\omega \,\mathrm{Im}\left(E^*(\omega) \cdot P(\omega)\right) \tag{2.23}$$

With **SI** units, we have a relationship between the amplitude of the induced dipole moment to the electric field amplitude:

$$P(\omega) = \frac{3}{4}\varepsilon_0 \chi^{(3)}\left(-\omega;\omega,-\omega,\omega\right)\left|E(\omega)\right|^2 E(\omega) \tag{2.24}$$

Substituting Eq.(2.24) into Eq. (2.23), we have:

$$\frac{dW}{dt} = \frac{3}{8}\omega\varepsilon_0 \left|E(\omega)\right|^2 \left|E(\omega)\right|^2 \,\mathrm{Im}\left(\chi^{(3)}\right) \tag{2.25}$$

Using the **SI** units definition of irradiance

$$I = \frac{1}{2}\varepsilon_0 cn\left|E(\omega)\right|^2 \tag{2.26}$$

Eq. (2.25) changes to:

$$\frac{dW}{dt} = \frac{3\omega I^2}{2\varepsilon_0 c^2 n^2}\,\mathrm{Im}\left(\chi^{(3)}\right) \tag{2.27}$$

In a rate equation description, two-photon absorption is often described by a cross section δ in units of $\mathrm{cm}^4\mathrm{sec}$ as

$$\frac{dn_p}{dt} = \delta N F^2 \tag{2.28}$$

where dn_p/dt is the number of photons absorbed per unit time and unit volume, N is the density of absorbing molecules, and the photon flux is described as:

$$F = \frac{I}{\hbar\omega} \tag{2.29}$$

And $dW = dn_p \hbar\omega$, so we have

$$\delta = \frac{\hbar\omega}{NI^2}\frac{dW}{dt} \tag{2.30}$$

Substituting Eq (2.27) into Eq (2.30), we obtain:

$$\delta = \frac{3\hbar\omega^2}{2\varepsilon_0 c^2 n^2 N}\mathrm{Im}\left(\chi^{(3)}\right) \tag{2.31}$$

If we substitute Eq.(2.21) into Eq.(2.31), we can get relation shown in Eq.(2.22)

Nondegenerate two-photon absorption (ND-2PA):

If we look at two beams at different frequencies (ω_1, ω_2) incident on a material, the intensity change of the two beams in the material due to pure two-photon absorption can be described by:

$$\begin{aligned}\frac{dI_1}{dz} &= -\beta_{11}I_1^2 - 2\beta_{12}I_1I_2 \\ \frac{dI_2}{dz} &= -\beta_{22}I_2^2 - 2\beta_{21}I_1I_2\end{aligned} \tag{2.32}$$

where β_{11}, β_{22} are degenerate 2PA coefficients for beam ω_1 and beam ω_2 respectively, and their relationships to $\chi^{(3)}$ are shown in Eq.(2.21). β_{12}, β_{21} are called nondegenerate 2PA coefficients (β_{ND}), and their relationships to $\chi^{(3)}$ in *isotropic* media are shown below in **SI** units:

$$\begin{aligned}\beta_{12} &= \frac{3\omega_1}{2n_1n_2c^2\varepsilon_0}\Delta\,\mathrm{Im}(\chi_{xxxx}{}^{(3)}(-\omega_1;\omega_1,-\omega_2,\omega_2)) \\ \beta_{21} &= \frac{3\omega_2}{2n_1n_2c^2\varepsilon_0}\Delta\,\mathrm{Im}(\chi_{xxxx}{}^{(3)}(-\omega_2;\omega_2,-\omega_1,\omega_1))\end{aligned} \tag{2.33}$$

where n_1 and n_2 are linear refractive index of beam ω_1 and beam ω_2 respectively. Δ=1 for two beams having parallel polarization. Δ=1/3 for two beams having orthogonal polarization.

The relation of the nondegenerate 2PA cross section δ_{ND} to the nondegenerate 2PA coefficient β_{ND} is shown below [28]:

$$\delta_{ND} = \frac{\hbar\beta_{ND}}{N}\left(\frac{2\omega_1\omega_2}{\omega_1+\omega_2}\right) = \frac{\beta_{ND}}{N}\frac{hc}{\left(\frac{\lambda_1+\lambda_2}{2}\right)} \tag{2.34}$$

where N is number density of molecules in a unit volume (units of 1/volume).

2.2.2 Calculation for third-order nonlinear susceptibility

In order to determine the 2PA coefficient, β, or 2PA cross section, δ, we have to determine the imaginary part of the third-order nonlinear susceptibility, Im($\chi^{(3)}$). There are two ways to calculate $\chi^{(3)}$: 1) based on the "classical" model (electron "spring" model); 2) based on quantum mechanical perturbation theory of the atomic (or molecular) wave function (sum-over-states expression), where one method to derive the expression for 2PA cross section δ is following the work from Orr and Ward [31], the other method for 2PA cross section δ is following the work from McClain [33].

1) Classical model [29]:

Based on a classical electron "spring" model, the third-order nonlinear susceptibility $\chi^{(3)}$ (fourth-rank tensor) for centrosymmetric media for $\omega_4 = \omega_1 + \omega_2 + \omega_3$ can be expressed as below in **SI** units:

$$\chi^{(3)}_{ijkl}(-\omega_4;\omega_1,\omega_2,\omega_3)=\frac{Nbe^4\delta_{jk}\delta_{il}}{\varepsilon_0 m^3 D(\omega_4)D(\omega_1)D(\omega_2)D(\omega_3)} \tag{2.35}$$

where *e* is the charge of the electron, *m* is mass of the electron; *N* is the number density of atoms; *b* is a parameter that characterizes the strength of the nonlinearity; *i, j, k, l = x, y, z*; δ is the Kronecker delta function which is expressed as: $\delta_{ij}=1$ if $i=j$ and $\delta_{ij}=0$ if $i\neq j$, and

$$D(\omega)=\omega_0^2-\omega^2-i\omega\Gamma \tag{2.36}$$

where ω_0 is the resonance frequency of the electron "spring", and Γ is the damping factor of the "spring".

2) Quantum mechanical perturbation theory [30]

With quantum mechanical perturbation theory, we perform the calculation of the third-order nonlinear susceptibility $\chi^{(3)}$ based on the properties of the atomic wave functions. This method gives a clearer picture of the underlying physics of the nonlinear interaction. As the intramolecular electric forces are much stronger than the forces due to the external electric field $\boldsymbol{E_{ex}}$, the interaction of the external electric field with the molecules can be regarded as a perturbation of the molecular fields. By this theory, for a general third-order process, the third-order nonlinear susceptibility, $\chi^{(3)}$, can be expressed by a *sum over states* (SOS) method.

To derive $\mathrm{Im}\left(\chi^{(3)}\left(-\omega;\omega,-\omega,\omega\right)\right)$, we use the third-order nonlinear susceptibility $\chi^{(3)}$ expressed in **SI** units from the work of Orr and Ward [31]:

$$\chi^{(3)}_{ijkl}\left(-(\omega_1+\omega_2+\omega_3);\omega_1,\omega_2,\omega_3\right)=$$

$$\frac{N}{\varepsilon_0}\frac{\wp}{3!}\sum_{\nu,m,n}{}'\left\{\begin{array}{l}\dfrac{\mu^i_{g\nu}\overline{\mu}^j_{\nu m}\overline{\mu}^k_{mn}\mu^l_{ng}}{(\Omega_{\nu g}-\hbar\omega_1-\hbar\omega_2-\hbar\omega_3)(\Omega_{mg}-\hbar\omega_1-\hbar\omega_2)(\Omega_{ng}-\hbar\omega_1)}\\ +\dfrac{\mu^i_{g\nu}\overline{\mu}^j_{\nu m}\overline{\mu}^k_{mn}\mu^l_{ng}}{(\Omega_{\nu g}{}^*+\hbar\omega_3)(\Omega_{mg}-\hbar\omega_1-\hbar\omega_2)(\Omega_{ng}-\hbar\omega_1)}\\ +\dfrac{\mu^i_{g\nu}\overline{\mu}^j_{\nu m}\overline{\mu}^k_{mn}\mu^l_{ng}}{(\Omega_{\nu g}{}^*+\hbar\omega_1)(\Omega_{mg}{}^*+\hbar\omega_1+\hbar\omega_2)(\Omega_{ng}-\hbar\omega_3)}\\ \dfrac{\mu^i_{g\nu}\overline{\mu}^j_{\nu m}\overline{\mu}^k_{mn}\mu^l_{ng}}{(\Omega_{\nu g}{}^*+\hbar\omega_1)(\Omega_{mg}{}^*+\hbar\omega_1+\hbar\omega_2)(\Omega_{ng}+\hbar\omega_1+\hbar\omega_2+\hbar\omega_3)}\end{array}\right\}$$

$$-\frac{N}{\varepsilon_0}\frac{\wp}{3!}\sum_{\nu,n}{}'\left\{\begin{array}{l}\dfrac{\mu^i_{g\nu}\mu^j_{\nu g}\mu^k_{gn}\mu^l_{ng}}{(\Omega_{\nu g}-\hbar\omega_1-\hbar\omega_2-\hbar\omega_3)(\Omega_{\nu g}-\hbar\omega_3)(\Omega_{ng}-\hbar\omega_1)}\\ +\dfrac{\mu^i_{g\nu}\mu^j_{\nu g}\mu^k_{gn}\mu^l_{ng}}{(\Omega_{\nu g}-\hbar\omega_3)(\Omega_{ng}{}^*+\hbar\omega_2)(\Omega_{ng}-\hbar\omega_1)}\\ +\dfrac{\mu^i_{g\nu}\mu^j_{\nu g}\mu^k_{gn}\mu^l_{ng}}{(\Omega_{\nu g}{}^*+\hbar\omega_3)(\Omega_{ng}-\hbar\omega_2)(\Omega_{ng}{}^*+\hbar\omega_1)}\\ \dfrac{\mu^i_{g\nu}\mu^j_{\nu g}\mu^k_{gn}\mu^l_{ng}}{(\Omega_{\nu g}{}^*+\hbar\omega_1+\hbar\omega_2+\hbar\omega_3)(\Omega_{\nu g}{}^*+\hbar\omega_3)(\Omega_{ng}{}^*+\hbar\omega_1)}\end{array}\right\} \qquad (2.37)$$

Here *g* indicates the ground state, υ, *m*, *n* indicate excited states; $\mu_{\upsilon m}$ indicates transition dipole moments from state υ to state *m*, and $\overline{\mu}_{\nu m}=\mu_{\nu m}-\delta_{\nu m}\mu_{gg}$, μ_{gg} is ground state permanent dipole moment; $\Omega_{\upsilon m}$ is defined as $\Omega_{\nu m}=E_{\nu m}-i\Gamma_{\nu m}=\hbar\omega_{\nu m}-i\Gamma_{im}$, $E_{\upsilon m}$ is the energy between the state υ and state *m*, and $\Gamma_{\upsilon \mathrm{m}}$ is a damping factor; $\wp$ is called the intrinsic permutation parameter; $\sum'$ means summation over all states excluding the ground state *g*, and *i, j, k, l* = *x, y, z*.

Now let us consider the case for degenerate 2PA. The third-order nonlinear susceptibility responsible for degenerate 2PA is the imaginary part of $\chi^{(3)}(-\omega;\omega,\omega,-\omega)$, $\chi^{(3)}(-\omega;\omega,-\omega,\omega)$ and $\chi^{(3)}(-\omega;-\omega,\omega,\omega)$. Also let us only look at the *xxxx* component ,$\chi_{xxxx}{}^{(3)}(-\omega;\omega,\omega,-\omega)$, so Eq. (2.37) becomes:

$$\chi^{(3)}_{xxxx}(-\omega;\omega,\omega,-\omega) =$$

$$\frac{2N}{3!\varepsilon_0}\sum_{v,m,n}{}' \left\{ \begin{array}{l} \dfrac{\boldsymbol{\mu^x_{gv}\bar{\mu}^x_{vm}\bar{\mu}^x_{mn}\mu^x_{ng}}}{\boldsymbol{(\Omega_{vg}-\hbar\omega)(\Omega_{mg}-2\hbar\omega)(\Omega_{ng}-\hbar\omega)}} \\ + \dfrac{\boldsymbol{\mu^x_{gv}\bar{\mu}^x_{vm}\bar{\mu}^x_{mn}\mu^x_{ng}}}{\boldsymbol{(\Omega_{vg}{}^*-\hbar\omega)(\Omega_{mg}-2\hbar\omega)(\Omega_{ng}-\hbar\omega)}} \\ + \dfrac{\mu^x_{gv}\bar{\mu}^x_{vm}\bar{\mu}^x_{mn}\mu^x_{ng}}{(\Omega_{vg}{}^*+\hbar\omega)(\Omega_{mg}{}^*+2\hbar\omega)(\Omega_{ng}+\hbar\omega)} \\ \dfrac{\mu^x_{gv}\bar{\mu}^x_{vm}\bar{\mu}^x_{mn}\mu^x_{ng}}{(\Omega_{vg}{}^*+\hbar\omega)(\Omega_{mg}{}^*+2\hbar\omega)(\Omega_{ng}+\hbar\omega)} \end{array} \right\}$$

$$-\frac{2N}{3!\varepsilon_0}\sum_{v,n}{}' \left\{ \begin{array}{l} \dfrac{\mu^x_{gv}\mu^x_{vg}\mu^x_{gn}\mu^x_{ng}}{(\Omega_{vg}-\hbar\omega)(\Omega_{vg}+\hbar\omega)(\Omega_{ng}-\hbar\omega)} \\ + \dfrac{\mu^x_{gv}\mu^x_{vg}\mu^x_{gn}\mu^x_{ng}}{(\Omega_{vg}+\hbar\omega)(\Omega_{ng}{}^*+\hbar\omega)(\Omega_{ng}-\hbar\omega)} \\ + \dfrac{\mu^x_{gv}\mu^x_{vg}\mu^x_{gn}\mu^x_{ng}}{(\Omega_{vg}{}^*-\hbar\omega)(\Omega_{ng}-\hbar\omega)(\Omega_{ng}{}^*+\hbar\omega)} \\ \dfrac{\mu^x_{gv}\mu^x_{vg}\mu^x_{gn}\mu^x_{ng}}{(\Omega_{vg}{}^*+\hbar\omega)(\Omega_{vg}{}^*-\hbar\omega)(\Omega_{ng}{}^*+\hbar\omega)} \end{array} \right\} \qquad (2.38)$$

Here we can see only the resonance terms in **bold** in $\chi_{xxxx}^{(3)}(-\omega;\ \omega,\omega,\ -\omega)$ above where all 3 terms at denominator have minus sign, and other terms are at least two orders magnitude smaller than these **bold** terms with typical molecular parameters and can be negelected. The factor of 2 in Eq. (2.38) is a consequence of the permutation operator $\wp$ and comes from the fact that there are two possibilities of the ordering of the two positive ω's that are equivalent in $\chi_{xxxx}^{(3)}(-\omega;\ \boldsymbol{\omega},\boldsymbol{\omega},-\omega)$.

In the same way, we can calculate that $\chi_{xxxx}^{(3)}(-\omega;\ -\omega,\omega,\omega)$ does not have any such resonance term, and $\chi_{xxxx}^{(3)}(-\omega;\ \omega,\ -\omega,\omega)$ has resonance terms (**bold**) shown in Eq. (2.39):

$$\chi^{(3)}_{xxxx}(-\omega;\omega,-\omega,\omega)=$$

$$\frac{2N}{3!\varepsilon_0}\sum_{v,m,n}{}'\left\{\begin{array}{l}\dfrac{\mu^x_{gv}\overline{\mu}^x_{vm}\overline{\mu}^x_{mn}\mu^x_{ng}}{(\Omega_{vg}-\hbar\omega)\,\Omega_{mg}\,(\Omega_{ng}-\hbar\omega)}\\ +\dfrac{\mu^x_{gv}\overline{\mu}^x_{vm}\overline{\mu}^x_{mn}\mu^x_{ng}}{(\Omega_{vg}{}^*-\hbar\omega)\Omega_{mg}(\Omega_{ng}-\hbar\omega)}\\ +\dfrac{\mu^x_{gv}\overline{\mu}^x_{vm}\overline{\mu}^x_{mn}\mu^x_{ng}}{(\Omega_{vg}{}^*+\hbar\omega)\Omega_{mg}{}^*(\Omega_{ng}+\hbar\omega)}\\ \dfrac{\mu^x_{gv}\overline{\mu}^x_{vm}\overline{\mu}^x_{mn}\mu^x_{ng}}{(\Omega_{vg}{}^*+\hbar\omega)\Omega_{mg}{}^*(\Omega_{ng}+\hbar\omega)}\end{array}\right\}$$

$$-\frac{2N}{3!\varepsilon_0}\sum_{v,n}{}'\left\{\begin{array}{l}\dfrac{\boldsymbol{\mu^x_{gv}\mu^x_{vg}\mu^x_{gn}\mu^x_{ng}}}{\boldsymbol{(\Omega_{vg}-\hbar\omega)(\Omega_{vg}-\hbar\omega)(\Omega_{ng}-\hbar\omega)}}\\ +\dfrac{\boldsymbol{\mu^x_{gv}\mu^x_{vg}\mu^x_{gn}\mu^x_{ng}}}{\boldsymbol{(\Omega_{vg}-\hbar\omega)(\Omega_{ng}{}^*-\hbar\omega)(\Omega_{ng}-\hbar\omega)}}\\ +\dfrac{\mu^x_{gv}\mu^x_{vg}\mu^x_{gn}\mu^x_{ng}}{(\Omega_{vg}{}^*+\hbar\omega)(\Omega_{ng}+\hbar\omega)(\Omega_{ng}{}^*+\hbar\omega)}\\ \dfrac{\mu^x_{gv}\mu^x_{vg}\mu^x_{gn}\mu^x_{ng}}{(\Omega_{vg}{}^*+\hbar\omega)(\Omega_{vg}{}^*+\hbar\omega)(\Omega_{ng}{}^*+\hbar\omega)}\end{array}\right\} \tag{2.39}$$

Combining resonance terms from $\chi_{xxxx}^{(3)}(-\omega;\ \omega,\omega,\ -\omega)$ and $\chi_{xxxx}^{(3)}(-\omega;\ \omega,\ -\omega,\omega)$, we obtain an approximate expression for $\chi_{xxxx}^{(3)}$ for degenerate 2PA (D-2PA):

$$\chi^{(3)}_{xxxx}(D-2PA)=$$

$$\frac{2N}{3!\varepsilon_0}\sum_{v,m,n}{}'\left\{\begin{array}{l}\dfrac{\mu^x_{gv}\overline{\mu}^x_{vm}\overline{\mu}^x_{mn}\mu^x_{ng}}{(\Omega_{vg}-\hbar\omega)(\Omega_{mg}-2\hbar\omega)(\Omega_{ng}-\hbar\omega)}\\ +\dfrac{\mu^x_{gv}\overline{\mu}^x_{vm}\overline{\mu}^x_{mn}\mu^x_{ng}}{(\Omega_{vg}{}^*-\hbar\omega)(\Omega_{mg}-2\hbar\omega)(\Omega_{ng}-\hbar\omega)}\end{array}\right\}$$

$$-\frac{2N}{3!\varepsilon_0}\sum_{v,n}{}'\left\{\begin{array}{l}\dfrac{\mu^x_{gv}\mu^x_{vg}\mu^x_{gn}\mu^x_{ng}}{(\Omega_{vg}-\hbar\omega)(\Omega_{vg}-\hbar\omega)(\Omega_{ng}-\hbar\omega)}\\ +\dfrac{\mu^x_{gv}\mu^x_{vg}\mu^x_{gn}\mu^x_{ng}}{(\Omega_{vg}-\hbar\omega)(\Omega_{ng}{}^*-\hbar\omega)(\Omega_{ng}-\hbar\omega)}\end{array}\right\} \tag{2.40}$$

For a three-state model (see Fig.2.1), we only consider three electronic states (ground state g, and two excited states e and e'). We also assume that only one excited state e is strongly coupled to the ground state g in a 1-photon transition, which means that the transition dipole moment between these two states is non-zero, $\mu_{ge}\neq 0$ and $\mu_{eg}\neq 0$, and $\mu_{ge'}=0$ and $\mu_{e'g}=0$. In addition, we assume that coupling between the two excited states is strong, which means $\mu_{ee'}\neq 0$ and $\mu_{e'e}\neq 0$. Finally, we assume that the permanent dipole moment of the 'molecule' in the ground state g and in the excited state e are non-zero: $\mu_{gg}\neq 0$ and $\mu_{ee}\neq 0$, and possibly different.

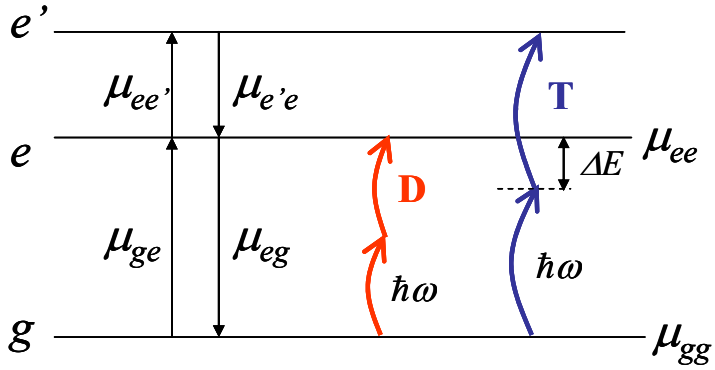

Figure 2.1 Three state model for Sum-Over-State (SOS) expression

Based on these assumptions, $\chi_{xxxx}^{(3)}(D\text{-}2PA)$ in Eq. (2.40) becomes:

$$\chi^{(3)}_{xxxx}(D-2PA)=$$

$$\frac{2N}{3!\varepsilon_0}\left\{\begin{array}{ll}\dfrac{\mu^x_{ge}\bar{\mu}^x_{ee}\bar{\mu}^x_{ee}\mu^x_{eg}}{(\Omega_{eg}-\hbar\omega)(\Omega_{eg}-2\hbar\omega)(\Omega_{eg}-\hbar\omega)} & \text{D}\\ +\dfrac{\mu^x_{ge}\bar{\mu}^x_{ee}\bar{\mu}^x_{ee}\mu^x_{eg}}{(\Omega_{eg}*-\hbar\omega)(\Omega_{eg}-2\hbar\omega)(\Omega_{eg}-\hbar\omega)} & \text{D}\\ +\dfrac{\mu^x_{ge}\bar{\mu}^x_{ee'}\bar{\mu}^x_{e'e}\mu^x_{eg}}{(\Omega_{eg}-\hbar\omega)(\Omega_{e'g}-2\hbar\omega)(\Omega_{eg}-\hbar\omega)} & \text{T}\\ +\dfrac{\mu^x_{ge}\bar{\mu}^x_{ee'}\bar{\mu}^x_{e'e}\mu^x_{eg}}{(\Omega_{eg}*-\hbar\omega)(\Omega_{e'g}-2\hbar\omega)(\Omega_{eg}-\hbar\omega)} & \text{T}\end{array}\right.$$

$$-\frac{2N}{3!\varepsilon_0}\left\{\begin{array}{ll}\dfrac{\mu^x_{ge}\mu^x_{eg}\mu^x_{ge}\mu^x_{eg}}{(\Omega_{eg}-\hbar\omega)(\Omega_{eg}-\hbar\omega)(\Omega_{eg}-\hbar\omega)} & \text{N}\\ +\dfrac{\mu^x_{ge}\mu^x_{eg}\mu^x_{ge}\mu^x_{eg}}{(\Omega_{eg}-\hbar\omega)(\Omega_{eg}*-\hbar\omega)(\Omega_{eg}-\hbar\omega)} & \text{N}\end{array}\right. \qquad (2.41)$$

The first two terms in Eq. (2.41) are called **D-terms or Dipolar terms**, which correspond to D-2PA to excited state *e* (shown in Fig.2.1) because these have a two-photon resonance term in the denominator, $\Omega_{eg}-2\hbar\omega$.

We define $\Delta\mu_{ge}=\bar{\mu}_{ee}=\mu_{ee}-\mu_{gg}$, which indicates the change of the permanent dipole moments between the molecule in states *g* and *e*. We consider the near resonance for the two-photon absorption where $\hbar\omega\approx\hbar\omega_{eg}/2$; therefore we have, $\Omega_{eg}-2\hbar\omega=\hbar\omega_{eg}-i\Gamma_{eg}-2\hbar\omega\approx-i\Gamma_{eg}$ and $\Omega_{eg}-\hbar\omega=\hbar\omega_{eg}-i\Gamma_{eg}-\hbar\omega\approx\hbar\omega_{eg}/2-i\Gamma_{eg}$. Then the summation of imaginary parts of the two D-terms gives:

$$\mathrm{Im}[\chi^{(3)}_{xxxx}(D-2PA)_{D-term}] = \mathrm{Im}\left[\frac{2N}{3!\varepsilon_0}\left\{\frac{\mu_{ge}^2\Delta\mu_{ge}^2}{(-i\Gamma_{eg})(\hbar\omega_{eg}/2-i\Gamma_{eg})} \times\left(\frac{1}{\hbar\omega_{eg}/2-i\Gamma_{eg}}+\frac{1}{\hbar\omega_{eg}/2+i\Gamma_{eg}}\right)\right\}\right] \tag{2.42}$$

$$=\frac{N\mu_{ge}^2\Delta\mu_{ge}^2}{3!\varepsilon_0\Gamma_{eg}}\frac{(\hbar\omega_{eg})^2}{\left[(\hbar\omega_{eg}/2)^2+\Gamma_{eg}^2\right]^2}$$

The third and fourth terms in Eq. (2.41) are called **T-terms or two-photon terms**, which correspond to degenerate two-photon absorption (D-2PA) to excited state e' because they have a two-photon resonance term in the denominator, $\Omega_{e'g}-2\hbar\omega$. We also consider the resonance for the two-photon absorption where $\hbar\omega\approx\hbar\omega_{e'g}/2$ shown in Fig. 2.1. So summation of these two terms gives us:

$$\mathrm{Im}[\chi^{(3)}_{xxxx}(D-2PA)_{T-term}] = \mathrm{Im}\left[\frac{2N}{3!\varepsilon_0}\left\{\frac{\mu_{ge}^2\mu_{ee'}^2}{(-i\Gamma_{e'g})(\hbar\omega_{eg}-\hbar\omega_{e'g}/2-i\Gamma_{eg})} \times\left(\frac{1}{\hbar\omega_{eg}-\hbar\omega_{e'g}/2-i\Gamma_{eg}}+\frac{1}{\hbar\omega_{eg}-\hbar\omega_{e'g}/2+i\Gamma_{eg}}\right)\right\}\right] \tag{2.43}$$

$$=\frac{4N\mu_{ge}^2\mu_{ee'}^2}{3!\varepsilon_0\Gamma_{e'g}}\frac{(\hbar\omega_{eg}-\hbar\omega_{e'g}/2)^2}{\left[(\hbar\omega_{eg}-\hbar\omega_{e'g}/2)^2+\Gamma_{eg}^2\right]^2}$$

If we assume that $\Gamma_{eg} << \dfrac{\hbar\omega_{eg}-\hbar\omega_{e'g}/2}{2}$, we have,

$$\mathrm{Im}[\chi^{(3)}_{xxxx}(D-2PA)_{T-term}] = \frac{4N\mu_{ge}^2\mu_{ee'}^2}{3!\varepsilon_0\Gamma_{e'g}}\frac{1}{(\hbar\omega_{eg}-\hbar\omega_{e'g}/2)^2} \tag{2.44}$$

Now we define $\Delta E=\hbar\omega_{eg}-\hbar\omega_{e'g}/2=\hbar\omega_{eg}-\hbar\omega$ as the detuning energy, shown in Fig.2.1.

The last two terms in Eq.(2.41) are called **N-terms or negative term**s, which do not have two-photon resonance denominators, only 1PA resonance terms. This is often called the AC

Stark term, or virtual saturation term. The imaginary part for these two N-terms is zero at resonance $\hbar\omega_{eg} = \hbar\omega$, so there is no contribution to two-photon absorption at resonance.

If we consider an average over the orientation of molecules in an isotropic medium (averaging factor is 1/5) [33], then Eq. (2.42) and Eq. (2.44) become:

$$\mathrm{Im}[\chi^{(3)}_{xxxx}(D-2PA)_{D-term}] = \frac{1}{3!}\frac{N\mu_{ge}^2\Delta\mu_{ge}^2}{5\varepsilon_0\Gamma_{eg}}\frac{(\hbar\omega_{eg})^2}{\left[(\hbar\omega_{eg}/2)^2+\Gamma_{eg}^2\right]^2} \tag{2.45}$$

$$\mathrm{Im}[\chi^{(3)}_{xxxx}(D-2PA)_{T-term}] = \frac{1}{3!}\frac{4N\mu_{ge}^2\mu_{ee'}^2}{5\varepsilon_0\Gamma_{e'g}}\frac{1}{(\hbar\omega_{eg}-\hbar\omega_{e'g}/2)^2} = \frac{1}{3!}\frac{4N\mu_{ge}^2\mu_{ee'}^2}{5\varepsilon_0\Gamma_{e'g}}\frac{1}{(E_{eg}-\hbar\omega)^2} \tag{2.46}$$

If we substitute Eq (2.46) into Eq. (2.31), we have an expression for the 2PA cross section δ in **SI** units:

$$\begin{aligned}\delta &= \frac{3\hbar\omega^2}{2\varepsilon_0 c^2 n^2 N}\times\frac{1}{3!}\frac{4N\mu_{ge}^2\mu_{ee'}^2}{5\varepsilon_0\Gamma_{e'g}}\frac{1}{(\hbar\omega_{eg}-\hbar\omega_{e'g}/2)^2}\\ &= \frac{1}{3!}\frac{6\hbar\omega^2}{5\varepsilon_0{}^2 c^2 n^2}\frac{\mu_{ge}^2\mu_{ee'}^2}{\Gamma_{e'g}}\frac{1}{(\hbar\omega_{eg}-\hbar\omega_{e'g}/2)^2}\end{aligned} \tag{2.47}$$

If we change Eq.(2.47) into **CGS** units, we have:

$$\delta = \frac{1}{3!}(4\pi)^2\frac{6\hbar\omega^2}{5c^2n^2}\frac{\mu_{ge}^2\mu_{ee'}^2}{\Gamma_{e'g}}\frac{1}{(\hbar\omega_{eg}-\hbar\omega_{e'g}/2)^2} = \frac{16\pi^2\hbar\omega^2}{5c^2n^2}\frac{\mu_{ge}^2\mu_{ee'}^2}{\Gamma_{e'g}}\frac{1}{(E_{eg}-\hbar\omega)^2} \tag{2.48}$$

Here we define $\Delta E = \hbar\omega_{eg} - \hbar\omega_{e'g}/2 = \hbar\omega_{eg} - \hbar\omega$ as the detuning energy shown in Fig. 2.1. Eq. (2.48) agrees with Eq.9 in Ref [13].

The dominant parameters which appear in the expression in Eq. (2.47) and Eq. (2.48) are: 1) the transition dipole moment between state *g* and *e*, μ_{ge} ; 2) the transition dipole moment

between state e and e', $\mu_{ee'}$; 3) the change of permanent dipole moments between the molecule in state g and e, $\Delta\mu_{ge}$; and 4) the detuning energy $\Delta E = \hbar\omega_{eg} - \hbar\omega_{e'g}/2 = \hbar\omega_{eg} - \hbar\omega$.

In order to optimize 2PA of molecules we can look at Eq. 2.48 to note what makes the 2PA large. Molecules will show large 2PA if they have a large ground state transition dipole moment μ_{ge} and large excited state transition dipole moment $\mu_{ee'}$ (or $\Delta\mu_{ge}$), and also have a small detuning energy ΔE. Damping factors Γ_{eg} in Eq (2.48) give the natural linewidths of transitions between state g and e. It should be noted that the minimum detuning energy ΔE achievable is limited by this natural linewidth of the transition Γ_{eg}. Beyond that, ESA will occur.

There is another assumption in the above simplified three-state model for 2PA that the orientations of all transition dipole moments are parallel to each other: $\boldsymbol{\mu_{ge}}//\boldsymbol{\mu_{ee'}}$ and $\boldsymbol{\mu_{ge}}//\Delta\boldsymbol{\mu}$. If there is an angle θ between the transition dipole moment $\boldsymbol{\mu_{ge}}$ and $\boldsymbol{\mu_{ee'}}$, Cronstrand suggested an effective excited state transition dipole moment $\mu_{ee'}^{eff}$, which is related to $\mu_{ee'}$ [32]:

$$\mu_{ee'}^{eff} = \mu_{ee'}\sqrt{\frac{2\cos^2(\theta)+1}{3}} \tag{2.49}$$

If $\theta \neq 0^\circ$, we will see $\mu_{ee'}^{eff}$ will be smaller than $\mu_{ee'}$. Then the 2PA probability will be smaller according to Eq.(2.48). In order to optimize 2PA of molecules, we prefer small angle between these transition dipole moments.

There is an alternative method to calculate the 2PA cross section for molecules based on the pertubation theory, called the 2PA tensor method. This method is developed originally by McClain [33], and widely used by Birge [34] and Cronstrand [32], and other researchers [35]. It

is commonly accepted that the degenerate 2PA cross section of molecules at a pump laser frequency ν_p is given in **CGS** Units as [36]:

$$\delta(\nu_p) = \frac{(2\pi)^4 \nu_p^{\,2}}{(ch)^2} g(2\nu_p) \left| \boldsymbol{S}_{f0} \right|^2 \tag{2.50}$$

where *c* is the speed of light and *h* is Planck's constant. Here $g(2\nu_p)$ denotes the normalized line shape function of the 2PA transition defined such that integral over all frequency space is normalized to unity, which is usually taken as a Lorenzian given by,

$$g(2\nu_p) = \frac{1}{\pi} \frac{\Gamma_{f0}}{(\nu_{fo} - 2\nu_p)^2 + \Gamma_{f0}^{\,2}} \tag{2.51}$$

$\left| \boldsymbol{S}_{fo} \right|^2$ is the so-called two-photon tensor and for the degenerate 2PA of randomly oriented molecules is given by perturbation theory:

$$\left| \boldsymbol{S}_{fo} \right|^2 = \frac{1}{30} \sum_{i \neq 0,f}^{M} \sum_{j \neq 0,f}^{M} \left[\begin{array}{l} \dfrac{a(\boldsymbol{\mu}_{io} \cdot \boldsymbol{\mu}_{fi})(\boldsymbol{\mu}_{jo} \cdot \boldsymbol{\mu}_{fj})}{(\nu_{io} - \nu_p)(\nu_{jo} - \nu_p) + \Gamma^2} \\ + \dfrac{b(\boldsymbol{\mu}_{io} \cdot \boldsymbol{\mu}_{jo})(\boldsymbol{\mu}_{fi} \cdot \boldsymbol{\mu}_{fj})}{(\nu_{io} - \nu_p)(\nu_{jo} - \nu_p) + \Gamma^2} \\ + \dfrac{b(\boldsymbol{\mu}_{io} \cdot \boldsymbol{\mu}_{fj})(\boldsymbol{\mu}_{jo} \cdot \boldsymbol{\mu}_{fi})}{(\nu_{io} - \nu_p)(\nu_{jo} - \nu_p) + \Gamma^2} \end{array} \right] \tag{2.52}$$

where $\boldsymbol{\mu}_{mn}$ and ν_{mn} are a transition dipole moment vector and transition energy of the $m \rightarrow n$ transition (*m,n=0, i, j, f*); *0* and *f* denote ground and final states; *i* and *j* denote the intermediate states, the number of which is *M;* Γ is a damping constant related to the intermediate states; *a* and *b* vary depending on the polarization of the two photons and **a=b=8** for the case where both photons are linearly polarized and parallel to each other.

We assume 1) there is only one dominant intermediate state (*i=j, M=1*); 2) transition dipole moments $\boldsymbol{\mu}_{jo}$ and $\boldsymbol{\mu}_{fj}$ are parallel to each other, 3) one final state, (*denoted as f*), and we have:

$$\left|\boldsymbol{S}_{fo}\right|^2 = \frac{1}{30}\left[3\frac{8\left|\boldsymbol{\mu}_{jo}\right|^2\left|\boldsymbol{\mu}_{fj}\right|^2}{(\nu_{jo}-\nu_p)^2+\Gamma_{j0}{}^2}\right] = \frac{4}{5}\frac{\left|\boldsymbol{\mu}_{jo}\right|^2\left|\boldsymbol{\mu}_{fj}\right|^2}{(\nu_{jo}-\nu_p)^2+\Gamma_{jo}{}^2} \tag{2.53}$$

Subsitituting Eq. (2.53) and (2.51) into Eq. (2.50), we get

$$\begin{aligned}\delta(\nu_p) &= \frac{(2\pi)^4\nu_p{}^2}{(ch)^2}\left[\frac{1}{\pi}\frac{\Gamma_{f0}}{(\nu_{fo}-2\nu_p)^2+\Gamma_{f0}{}^2}\right]\left[\frac{4}{5}\frac{\left|\boldsymbol{\mu}_{jo}\right|^2\left|\boldsymbol{\mu}_{fj}\right|^2}{(\nu_{jo}-\nu_p)^2+\Gamma_{jo}{}^2}\right] \\ &= \frac{64\pi^3}{5c^2h}\frac{E_p{}^2}{(E_{jo}-E_p)^2+\Gamma_{jo}{}^2}\frac{\left|\boldsymbol{\mu}_{jo}\right|^2\left|\boldsymbol{\mu}_{fj}\right|^2\Gamma_{f0}}{(E_{fo}-2E_p)^2+\Gamma_{f0}{}^2}\end{aligned} \tag{2.54}$$

where $E_p=h\nu_p$, $E_{j0}=h\nu_{jo}$, $E_{f0}=h\nu_{f0}$.

If there are two 2PA final states (*=f1, =f2*), then Eq.(2.54) changes to

$$\delta(E_p) = \frac{64\pi^3}{5c^2h}\frac{E_p{}^2}{(E_{jo}-E_p)^2+\Gamma_{jo}{}^2}\left[\frac{\left|\boldsymbol{\mu}_{jo}\right|^2\left|\boldsymbol{\mu}_{f1j}\right|^2\Gamma_{f10}}{(E_{f1o}-2E_p)^2+\Gamma_{f10}{}^2}+\frac{\left|\boldsymbol{\mu}_{jo}\right|^2\left|\boldsymbol{\mu}_{f2j}\right|^2\Gamma_{f20}}{(E_{f2o}-2E_p)^2+\Gamma_{f20}{}^2}\right] \tag{2.55}$$

Notably, for Eq. (2.54), if we ASSUME: $E_{jo}-E_p >> \Gamma_{jo}$ and $E_{fo}-2E_p \approx 0$ (only consider the peak value for 2PA), we obtain:

$$\delta(E_p) = \frac{64\pi^3}{5c^2h}\frac{E_p{}^2\left|\boldsymbol{\mu}_{jo}\right|^2\left|\boldsymbol{\mu}_{fj}\right|^2}{\Gamma_{fo}(E_{jo}-E_p)^2} = \frac{32\pi^2}{5c^2\hbar}\frac{E_p{}^2\left|\boldsymbol{\mu}_{jo}\right|^2\left|\boldsymbol{\mu}_{fj}\right|^2}{\Gamma_{fo}(E_{jo}-E_p)^2} \tag{2.56}$$

In **CGS** units, we calculate the constant in Eq. (2.55) and changed it into the Eq. (2.57) used for fitting the measured 2PA spectra of molecules in Chapter 4 and Chapter 5, where the 2PA cross section is in unit of GM (10^{-50} cm^4 • s/(molecule • photon)). Here all energies are input

with units of eV and all dipole moments are input with units of debye (D). The derivation for this equation is shown in APPENDIX A.

$$\delta(E_p) = 4.15\times10^{-3} \times \frac{\left(E_p[eV]\right)^2}{(E_{jo}[eV]-E_p[eV])^2+\left(\Gamma_{jo}[eV]\right)^2} \times \left[\frac{\Gamma_{f10}[eV]\left|\boldsymbol{\mu}_{jo}[debye]\right|^2\left|\boldsymbol{\mu}_{f1j}[debye]\right|^2}{(E_{f1o}[eV]-2E_p[eV])^2+\left(\Gamma_{f10}[eV]\right)^2} + \frac{\Gamma_{f20}[eV]\left|\boldsymbol{\mu}_{jo}[debye]\right|^2\left|\boldsymbol{\mu}_{f2j}[debye]\right|^2}{(E_{f2o}[eV]-2E_p[eV])^2+\left(\Gamma_{f20}[eV]\right)^2}\right][GM] \tag{2.57}$$

With assumption that $E_{f0} \approx 2E_p$ and $E_{j0} - E_p >> \Gamma_{j0}$, the Eq. (2.54) becomes:

$$\delta = \frac{64\pi^3}{5c^2h}\frac{{E_p}^2}{(E_{jo}-E_p)^2}\frac{\left|\boldsymbol{\mu}_{jo}\right|^2\left|\boldsymbol{\mu}_{fj}\right|^2}{\Gamma_{f0}} = \frac{32\pi^2\hbar\omega^2}{5c^2}\frac{\left|\boldsymbol{\mu}_{jo}\right|^2\left|\boldsymbol{\mu}_{fj}\right|^2}{\Gamma_{f0}}\frac{1}{(E_{jo}-\hbar\omega)^2} \tag{2.58}$$

If we compare Eq. (2.58) with Eq. (2.48), we can see that they are in the same form. In Eq. (2.58) $E_p = \hbar\omega$, and n=1 for Eq. (2.48) because the theory assumes the molecule in the vacuum without considering the effect of the solvent. However the constant in Eq. (2.58) is off by 2 compared to Eq. (2.48).

CHAPTER 3 LINEAR AND NONLINEAR SPECTROSCOPY METHODS

3.1 Linear spectroscopic techniques

The linear optical properties of molecules that we measured are one-photon absorption (1PA) spectra, one-photon fluorescence (1PF) spectra, one-photon excitation (steady-state) fluorescence anisotropy spectra and the fluorescence quantum yield.

Linear absorption spectra are measured with a Cary-500 UV-Vis-NIR (170nm to 3300nm) spectrophotometer. These spectra specify linear absorption peak positions and molar absorptivities, or extinction coefficients ε in units of $cm^{-1}M^{-1}$. The relationship between extinction coefficient ε and absorption optical density (OD) is given by:

$$OD = \varepsilon CL \tag{3.1}$$

where C is the solution concentration in units of Molarity (M) or moles per liter (mole/liter); L is the thickness of the solution in units of cm.

Furthermore, with the extinction coefficient ε we can determine ground state transition dipole moments from the ground state to first excited state transition dipole moment, μ_{ge}, which is one of the key factors influencing the strength of 2PA. The transition dipole moment μ_{ge} can be calculated from the integrated strength of the g→e band in the linear absorption spectrum by [36-38]:

$$\mu_{ge} = \sqrt{\frac{1500(\hbar c)^2 \ln 10}{\pi N_A E_{ge}} \int \varepsilon_{ge}(\nu) d\nu} \tag{3.2}$$

where N_A is Avogadro's number (6.022×10^{23}), $\varepsilon_{ge}(\nu)$ is the extinction coefficient in $cm^{-1}M^{-1}$ at the photon energy in wavenumbers υ, in cm^{-1}, and the integral is performed over the main absorption band. All parameters in Eq. (3.2) are in **CGS** unit.

One-photon fluorescence spectra are measured with a PTI quantamaster spectrofluorimeter under 90 degree excitation in a T-format method [39], i.e. irradiate from one direction and look at the fluorescence in a direction perpendicular to this excitation. Material solutions are put into a 1cm cuvette, and we used dilute solutions with peak optical density OD ≤ 0.1 for 1PF measurements.

One-photon excitation fluorescence anisotropy spectra are also measured with the PTI quantamaster spectrofluorimeter in the T-format configuration [39]. Upon excitation with linearly polarized light, the fluorescence emission from the molecule solution is also polarized. The extent of polarization of the fluorescence is expressed in terms of the anisotropy *r*.

There are many phenomena contributing to the depolarization of the fluorescence, and rotational diffusion of molecules is one common cause of depolarization. In order to avoid rotation of molecules during the emission process, we prepared the solution with high viscosity solvents such as glycerol (Viscosity = 934 mPa • S) and silicon oil (Viscosity ≥ 200 mPa • S). We also prepared the solution in 1cm cuvettes with peak optical density OD ≤ 0.1 to avoid reabsorption of the fluorescence and subsequent depolarization of the fluorescence.

One-photon fluorescence anisotropy spectra give information about locations of excited states and the orientation of the transition dipole moment from the ground to excited state

relative to the emission dipole moment. More experimental and theoretical details will be discussed in Section 5.6.

Fluorescence quantum yields of the molecular samples are measured against a standard molecule. In our case we use Rhodamine6G in ethanol (η = 0.95) [39][40], where η is the fluorescence quantum yield fraction.

3.2 Nonlinear spectroscopy

3.2.1 Femtosecond 1KHz laser system

As mentioned in Chapter 2, we are more interested in electronic nonlinear optical properties, especially two-photon absorption of molecules. Two-photon absorption depends on the irradiance of light. We use a femtosecond pulsed laser source to provide light with high intensity.

The femtosecond laser we used is a CPA2010 from Clark-MXR inc. This includes a Ti: Sapphire regenerative chirped pulse amplifier with output at 775nm, 1mJ/pulse, 140fs (FWHM) pulsewidth and a 1KHz repetition rate. The seed beam injected into the Ti: Sapphire regenerative amplifier cavity at 775nm, has a pulsewidth of 180-200ps at a repetition rate of 38-40MHz, and comes from a diode laser (980nm) pumped, mode-locked, frequency-doubled fiber laser. The pump beam for the regenerative amplifier at 532nm, having a 1ns pulsewidth at a 1KHz repetition rate, comes from a flashlamp pumped, Q-switched, frequency-doubled Nd:YAG laser.

In order to perform the nonlinear spectroscopy study, we need to have a source with a tunable output wavelength. In order to obtain this, the output from the CLK-MXR CPA2001 is split into two beams to pump two identical optical parametric amplifiers (OPA), TOPAS from

Light Conversion Inc, which outputs 1100nm to 2200nm. With additional SHG (second harmonic generation) and DFG (Difference Frequency Generation) crystals attachments, the output of the TOPAS could be expanded to the range from 280nm to 10μm. One beam pumping the TOPAS is also able to be redirected to pump a "TOPAS WHITE", which has an output with a 10-30fs pulsewidth, and a wavelength tuning range from 490nm to 1600nm. A schematic of the laser system with the pumping scheme is shown in Fig. 3.1.

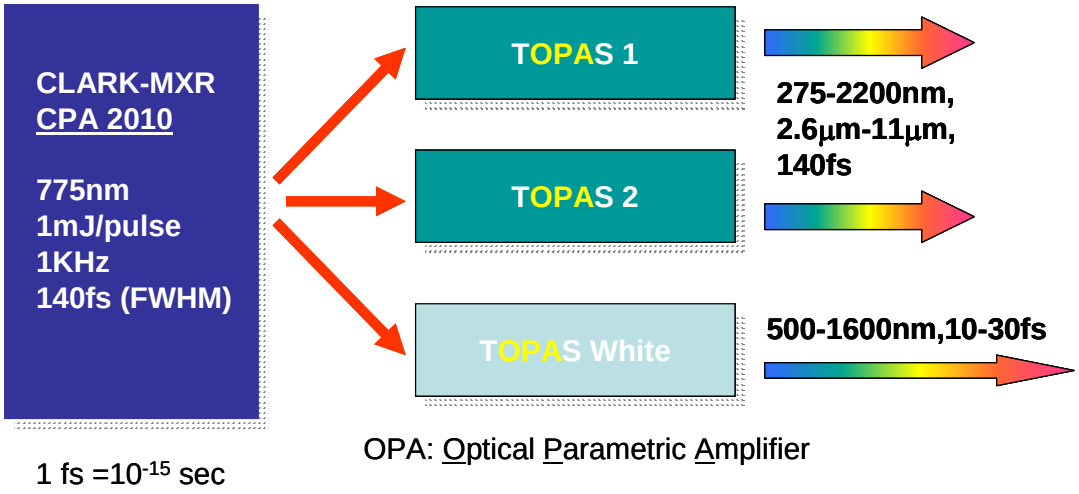

Figure 3.1 Femto-second 1KHz laser system with tunable wavelength output

3.2.2 Z-scan

The Z-scan [41] is a sensitive single-beam technique to separately determine the nonlinear absorption and nonlinear refraction of materials. Z-scan can be used to measure both fluorescent samples and nonfluorescent samples, and due to its experimental simplicity, is probably the most widely used technique to measure these nonlinear properties.

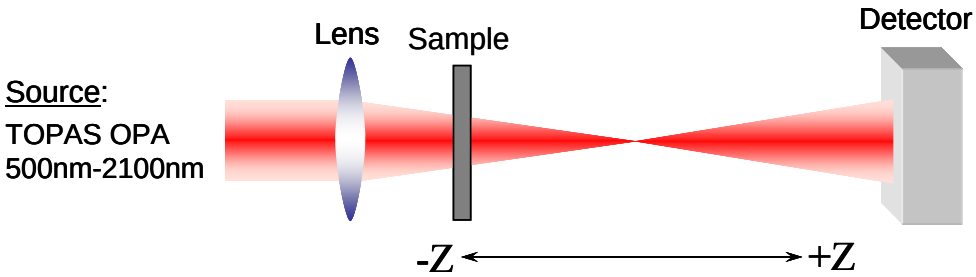

(a)

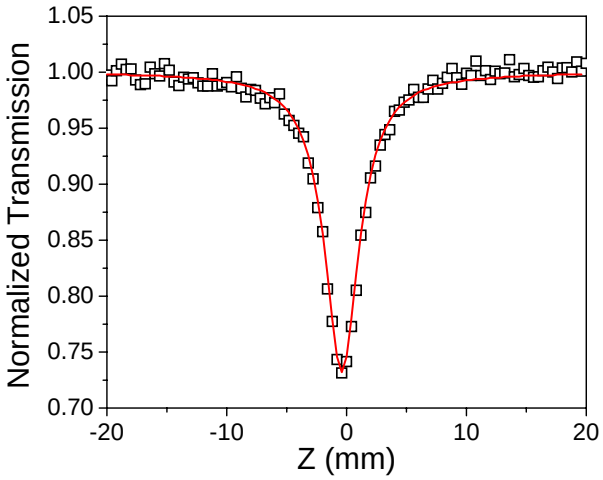

(b)

Figure 3.2 (a) Z-scan experimental setup (b) typical open-aperture Z-scan experimental data (square) with theoretical fitting (red line)

The Z-scan setup is shown in Fig.3.2 (a). The transmission of a focused Gaussian laser beam is measured as a function of the position of the sample with respect to the laser beam waist. Typical Z-scan experimental data with theoretical fitting is shown in Fig. 3.2 (b). Here a plot of the normalized transmission as a function of position Z is displayed. By this theoretical fitting, the 2PA coefficient is determined. 2PA measured by the Z-scan technique is degenerate 2PA because the two photons absorbed come from one beam with the same photon energy. By tuning the wavelength of the beam from the TOPAS, the whole 2PA spectrum can be obtained.

There are assumptions for the Z-scan method and its theoretical fitting: 1) Thickness of sample should be much smaller than Rayleigh range of focused laser beam, or "thin sample" assumption, so changes in the beam diameter within the sample due to diffraction can be neglected. 2) The nonlinear phase shift should be small enough that no change of the beam profile occurs within the sample.

If the pump beam experiences linear absorption loss (this is the case when the pump wavelength is moved to be close to the linear absorption edge), ESA could also happen in a Z-scan experiment. Because both 2PA and ESA are two-photon processes, a single Z-scan using a single pulsewidth cannot determine which physical process is occuring. However, we can separate them with time-resolved experiments, such as using a pump-probe setup in Section 3.2.4. The details will be discussed in Section 3.2.5

The absolute errors associated with the Z-scan technique using the optical source described here are estimated to be ±15 ~ 20%.

3.2.3 Two-Photon Fluorescence (2PF) Spectroscopy

Another single beam technique for measuring degenerate 2PA cross section of molecules is two-photon fluorescence (2PF) spectroscopy, first developed by C. Xu and W. W. Webb in 1996 [42].

In the 2PF technique, we do not measure the transmission of the beam like in the Z-scan. Instead, we measure fluorescence due to 2PA. Figure.3.3 shows the fluorescent process due to 1PA (a) and 2PA (b). Fluorescent molecules can absorb one photon to reach an excited state S_2, then, through nonradiative processes, decay to the first excited state S_1. The fluorescent molecules can come back to the ground state S_0 by releasing a fluorescence photon, and this

process is referred to as radiative decay. The molecule can also absorb two photons simultaneously to reach an excited state, and then through the same decay processes can come back to the ground state by emitting a fluorescence photon. Because the photon energy of the emitted photon is higher than that of a single photon absorbed via 2PA, 2PF spectroscopy is also called up-conversion fluorescence spectroscopy. By measuring the photon flux of the fluorescence with respect to a known standard, we can retrieve the 2PA coefficient or cross section of 2PA of the molecules [42].

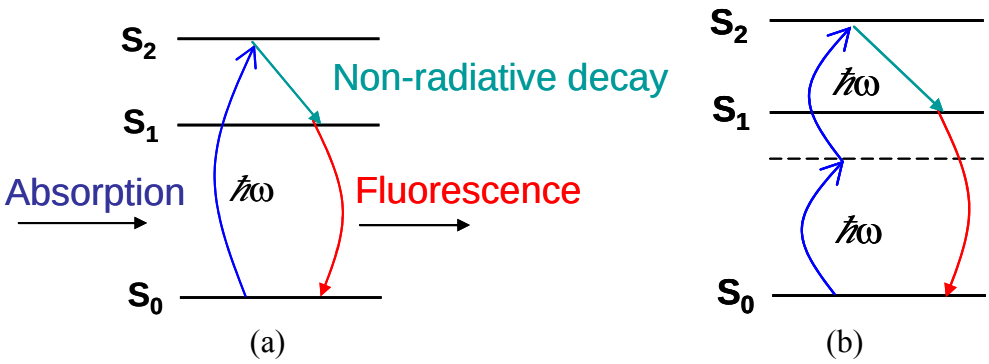

Figure 3.3 Fluorescence following one-photon absorption (a) and two-photon absorption (b)

The experimental setup is shown in Fig.3.4, where a λ/2 WP is a half wave plate, P is a GLAN-Laser calcite Polarizer. We use them to control the energy and polarization of the input beam. We use the telescope made of lenses L1 and L2 to expand the beam by 4×, use the iris A2 to truncate the beam and only allow the central part of the beam to reach the focusing lens L3. By doing this, the spatial profile of the beam on the focusing lens L3 is independent of the pump wavelength from the TOPAS (usually the spatial profile of the beam from the TOPAS changes when tuning the wavelength). Thus, the spatial profile of the beam on L3 will be nearly a flat top beam, so that the intensity distribution at the focal spot after L3 will be a diffraction-limited Airy

pattern, which will be considered in the calculation of the fluorescence due to 2PA shown below [42]. Fluorescent samples experience 2PA at the focal spot to emit fluorescence. Fluorescence is collected by lens L4 and detected by a photomultiplier tube (PMT). The PMT is very sensitive detector, allowing 2PF spectroscopy to be a very sensitive method to measure the molecules' 2PA cross section with values even smaller than 1GM. Also, the concentration of the solution can be less than 10^{-4} M.

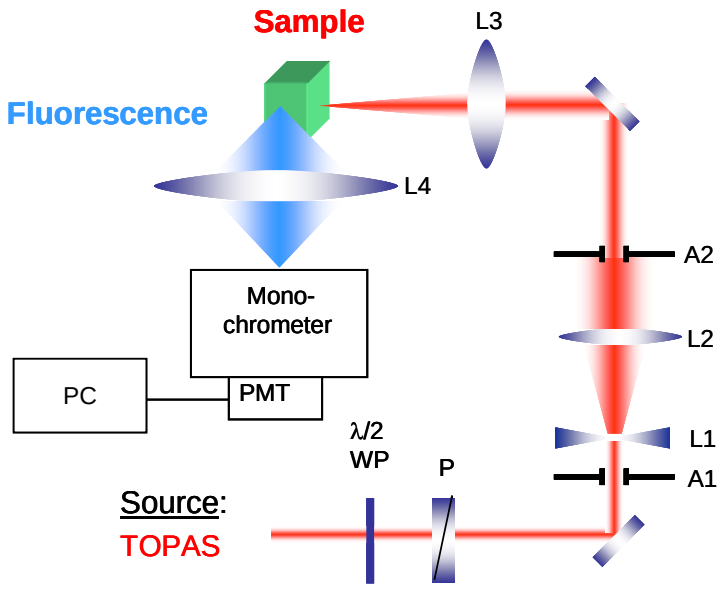

Figure 3.4 Experimental setup for two-photon fluorescence spectroscopy using femtosecond laser pulses from the TOPAS

There are two separate PMT detectors available covering the different spectral ranges (R928, 250-800nm; P1524, 250-700nm). The detectors are operated in the analog mode (DC voltage output) for 2PF measurements. The dynamic range of the PMTs is limited to between 0.03-3 Volts in order to operate in the linear regime of the detector. The fluorescence spectrum is corrected for the spectral responsivity of the fluorimeter (monochrometer and PMT), and then

integrated over the entire emission range to obtain the total integrated fluorescence for a certain excitation wavelength.

In order to determine the 2PA cross section of molecules, we have to determine the photon flux of fluorescence based on the spatial and temporal distribution of the pump beam at the focal point. Here I gave a brief description of this calculation. More details can be found in Ref. [42].

It is known that the number of photons absorbed per molecule per unit time by 2PA is proportional to the 2PA cross section δ and to the square of the incident intensity, I [43]. So the time-averaged fluorescence photon flux $\langle F(t)\rangle$ is measured as:

$$\langle F(t)\rangle = \frac{1}{2} g\phi\eta C\delta \langle I_0(t)\rangle^2 \int_V dV S^2(\mathbf{r}) \tag{3.3}$$

where $S(\mathbf{r})$ and $I_0(t)$ describe the spatial and temporal distribution of the incident light at the focal spot respectively. η is the fluorescence quantum yield of the molecule, and ϕ is the fluorescence collection efficiency of the fluorimeter. C is the concentration of the solution. $g = \langle I_0^2(t)\rangle / \langle I_0(t)\rangle^2$ is a measure of the second-order temporal coherence of the excitation source. δ is the 2PA cross section of the molecule.

If we assume the spatial profile of the pump beam is a flat-top beam at the focus of lens L3, we have the time averaged fluorescence photon flux $\langle F(t)\rangle$ as:

$$\langle F(t)\rangle \approx \frac{1}{2}\phi\eta C\delta \frac{g_p}{f\tau} \frac{8n\langle P(t)\rangle^2}{\pi\lambda} \tag{3.4}$$

where f is the pulse repetition rate, τ is the pulsewidth (FWHM), $g_p = g \times (f\tau)$ ($g_p = \tau \int_{-1/2f}^{1/2f} I_0{}^2(t)dt \Big/ \left[\int_{-1/2f}^{1/2f} I_0{}^2(t)\right]^2$) is equal to 0.664 for a Gaussian temporal profile pulse and 0.558 for a hyperbolic-secant squared pulse. Equation (3.4) is valid for thick samples where the sample thickness is much greater than the focal depth. The time averaged fluorescence photon flux $\langle F(t) \rangle$ is the signal detected by the PMT in the analog mode.

We can see in Eq. (3.4) that the 2PF signal $\langle F(t) \rangle \propto \langle P(t) \rangle^2$. We can check this quadratic power dependence of the fluorescence signal to determine that the fluorescence signal detected is only due to 2PA, not to 1PA or other higher order absorption processes.

From Eq. (3.4), we can see that $\langle F(t) \rangle$ is proportional to the 2PA cross section δ and inversely proportional to the pulsewidth τ and wavelength λ, or $\langle F(t) \rangle \propto \delta \frac{1}{\tau\lambda}$. If other experimental conditions are the same for all excitation wavelengths used (such as collection coefficient ϕ, power $\langle P(t) \rangle$), knowing the 2PA cross section δ_1 and fluorescence signal $(F(t))_1$ for one excitation wavelength λ_1, we can approximately estimate the 2PA cross section δ_2 for any other excitation wavelength λ_2 by the relation:

$$\delta_2 = \delta_1 \frac{\langle F(t) \rangle_2 \tau_2 \lambda_2}{\langle F(t) \rangle_1 \tau_1 \lambda_1} \tag{3.5}$$

We use this method when there is no standard molecule available for the excitation wavelength range.

Based on the Eq. (3.4), we use a relative method to determine the 2PA cross section δ_S of the sample by using standard reference molecules with known 2PA cross sections, δ_R. We

measure the 2PF signal for both the reference molecules and the unknown sample under the same excitation wavelength. Using Eq. (3.4), we can eliminate the 2PA cross section dependency on the spatial and temporal profile of the excitation light and the 2PA cross section of an unknown sample δ_S can be obtained as:

$$\delta_S = \frac{\langle F(t)\rangle_S \phi_R \eta_R C_R \langle P(t)\rangle_R^2}{\langle F(t)\rangle_R \phi_S \eta_S C_S \langle P(t)\rangle_S^2} \delta_R \tag{3.6}$$

where the subscripts S and R refer to the sample and reference respectively. The reference standard molecules we used are: Fluorescein in water (PH=11, quantum yield = 0.9) [42], and Rhodamine B in methanol (quantum yield=0.7) [42]

For the reference molecules and the unknown sample, the difference of the collection efficiencies is mainly due to different slit widths W used for the emission monochrometer, indicated by the micrometer installed on it. The collection efficiency is proportional to the square of this slit width, $\phi \propto W^2$ [39].

Another factor affecting the collection efficiency is the refractive index of solutions. Usually the collection efficiency can be expressed as $\phi = \phi_{disp} \times \phi_n$ [13]. ϕ_{disp} is the collection efficiency related to the fluorescence spectrum range and corresponding PMT's response to this range. And $\phi_n \propto n^{-2}$ (n is refractive index of the solution) takes into account the difference in the solid angles under which the illuminated portion of the solution is seen from the PMT, when the solvents for the reference and the sample are different. This effect is usually considered when the fluorescence quantum yield is measured. However in our 2PF experimental setup, the excitation beam is directed close to one side of the cuvette window and the fluorescence emitted passes through a negligible amount of solvent. Therefore this factor is normally neglected.

We can determine the fluorescence quantum yield of the sample by linear spectroscopy. In 2PF spectroscopy, we assume the fluorescence quantum yield due to 1PA and 2PA are the same. We also assume that the fluorescence spectrum due to 1PA and 2PA are identical.

There is another issue we need to deal with, called the inner filter effect, indicating significant reabsorption of the emission beam because we use relatively high concentrated solutions (~ 10^{-4} M). We measure the one-photon fluorescence spectrum with very low concentration solutions (peak OD < 0.1 in a 1cm cuvette) by linear spectroscopy, and then correct the fluorescence spectrum due to 2PA with this one-photon fluorescence spectrum. Details are described in Ref [28]

The absolute errors associated with this characterization technique are estimated to be ±20%.

3.2.4 White-Light Continuum Pump-Probe Spectroscopy

The two-beam technique we used to measure 2PA is White-Light Continuum (WLC) pump-probe spectroscopy [44][45]. With this pump-probe technique, we are not only able to measure nondegenerate 2PA of materials, but we can also study the dynamics of the nonlinearity in the time regime. For the weak probe beam we can detect additional absorption of the probe due to nondegenerate 2PA (one photon from the pump, the other photon from the probe) with the presence of the strong pump beam to determine the 2PA spectra of samples. The pump beam and probe beam overlap in space and in time (by adjusting the temporal delay) at sample. We can also use the strong pump pulse to induce the nonlinearity within the sample and the weak probe pulse monitors the dynamics of that nonlinearity – again by adjusting the temporal delay. Since

we use ultrashort pump and probe pulses (~140fs), we can distinguish the "short-lived" processes (such as 2PA) from the "long-lived" processes (such as excited state absorption).

Pump-probe experimental setup is shown in Fig.3.5

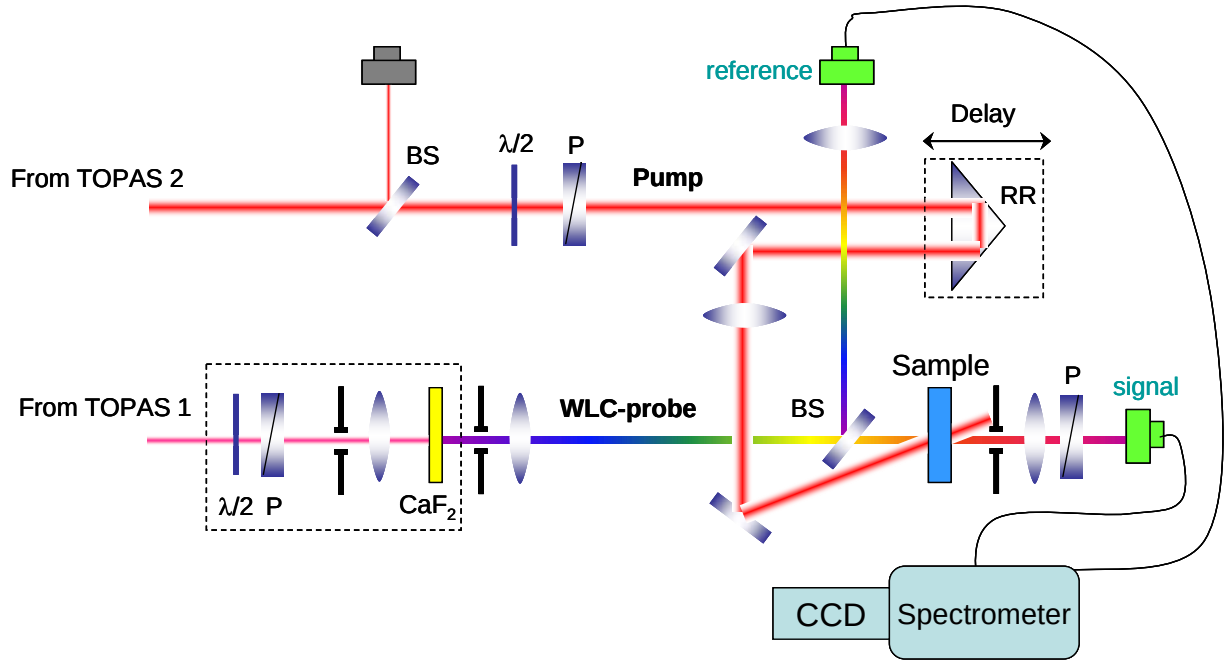

Figure 3.5 Experimental setup for white-light continuum pump-probe nonlinear spectroscopy. BS-Beam Splitter, λ/2-half waveplate, P-polarizer, RR-retroreflector

In this White-Light Continuum (WLC) pump probe spectroscopy, in order to generate the WLC probe beam, we focus a 140fs (FWHM), 2-3 μJ, 1300nm beam from the TOPAS into a 2.5mm thick CaF_2 window with a 5cm focal length lens. According to research by Brodeur and Chin [46], the spectral broadening of the WLC or supercontinuum scales as the bandgap energy of the generation medium, and CaF_2 is one of the transparent media with the largest bandgap (E_{gap}=10.2eV). The spectral range of the WLC generated by this method is from 400nm to 1600nm.

With 140fs pulse excitation, the duration of the WLC probe pulse is much longer than 140fs due to group velocity dispersion (GVD) of the broad WLC spectrum in CaF_2. In order to characterize the temporal properties of the WLC probe, we perform an Optical Kerr Effect (OKE) pump-probe experiment [44]. The OKE method is a cross-correlation technique used to fully characterize the chirp of the WLC (relation between the wavelength and time) and furthermore can measure the GVD of an unknown sample. More details can be found in Ref [44]. The duration of the WLC is around 2ps with 1600nm at the front in time and 400nm toward the back (i.e. normal dispersion).

Nondegenerate 2PA requires that the pump and probe pulses reach the sample at the same time. The single wavelength pump pulse from another TOPAS has a duration of ~140fs, much shorter than the WLC probe. Thus it is necessary to scan the temporal delay of the pump pulse to reach zero delay with different wavelength components of the WLC probe, i.e. only a narrow spectral portion of the WLC undergoes 2PA for a fixed temporal delay.

In addition, photons from the pump and WLC probe have different wavelengths so that they travel at different speeds inside the sample. This causes temporal walk off making the effective interaction length in the sample between the pump and probe pulses to be significantly reduced. Thus, the magnitude of the nonlinear signal will be reduced as well. Therefore, experimentally determined raw data is corrected for this temporal walk off due to group-velocity mismatch (GVM). GVM can be completely corrected for provided the linear dispersion of the sample is known. We can characterize the dispersion of the sample by the OKE method mentioned above.

We derived a single dynamical equation to describe the transmission of the WLC probe due to nondegenerate 2PA including the walk-off correction as [44]:

$$Q(\sigma,\tau_d,W,\rho,\Gamma)=\frac{e^{-2\sigma}}{W\sqrt{\pi}}\int_{-\infty}^{+\infty}\exp\left\{-\left(\frac{\tau+\tau_d-\rho}{W}\right)^2-\frac{\Gamma\sqrt{\pi}}{\rho}\left[erf(\tau)-erf(\tau-\rho)\right]\right\}d\tau \quad (3.7)$$

where Q is the transmission of the WLC probe, σ is the linear absorption coefficient, τ_d is the delay time between the pump and probe pulses, and W is the ratio of the band-limited probe pulsewidth to pump pulsewidth. ρ is the parameter related to the GVM between pump and probe pulses. Γ is the parameter related to the nondegenerate 2PA coefficient; $\Gamma = LI_e\beta_{ND}$, here L is the sample length and I_e is the pump beam intensity.

3.2.5 Pump-probe experiments to study ESA and 2PA processes

In order to investigate 2PA bands located at high energy (or shorter wavelength) region where the large 2PA cross sections usually could be observed, we have to use the pump wavelengths as short as possible, i.e. move the pump wavelength close to longer wavelength edge of linear absorption band. Therefore, pump light might experience some linear absorption. In the Z-scan experiment. as discussed in Section 3.2.4, If the pump beam experiences linear absorption, excited state absorption (ESA) could also happen. Because both 2PA and ESA are two-photon processes, a single wavelength Z-scan using a single pulsewidth cannot determine which physical process is occurring. However, we can separate them with time-resolved experiments, such as using a white-light continuum pump-probe setup in Section 3.2.4. Because ESA and 2PA have different time responses, ESA shows a longer time response (usually hundreds of ps to ns) than 2PA (which is essentially "instantaneous")

1) Let's see the case of the molecule TOR-I-103. The molecular structure and 2PA data for this molecule are presented in Section 5.4. The peak 2PA cross sections are observed to be ≈ 34000 GM at 515nm correponding pump wavelength 1030nm with Z-scan technique. The time-

resolved pump-probe experiments with femtosecond pulses are performed for this molecule with pump wavelength 1020nm and probe wavelengths 1064nm. The linear absorption spectrum for TOR-I-103 in THF are shown in Fig.3.6 (a), and the results of pump-probe experiments are shown in Fig.3.6 (b) including three different pump energies:

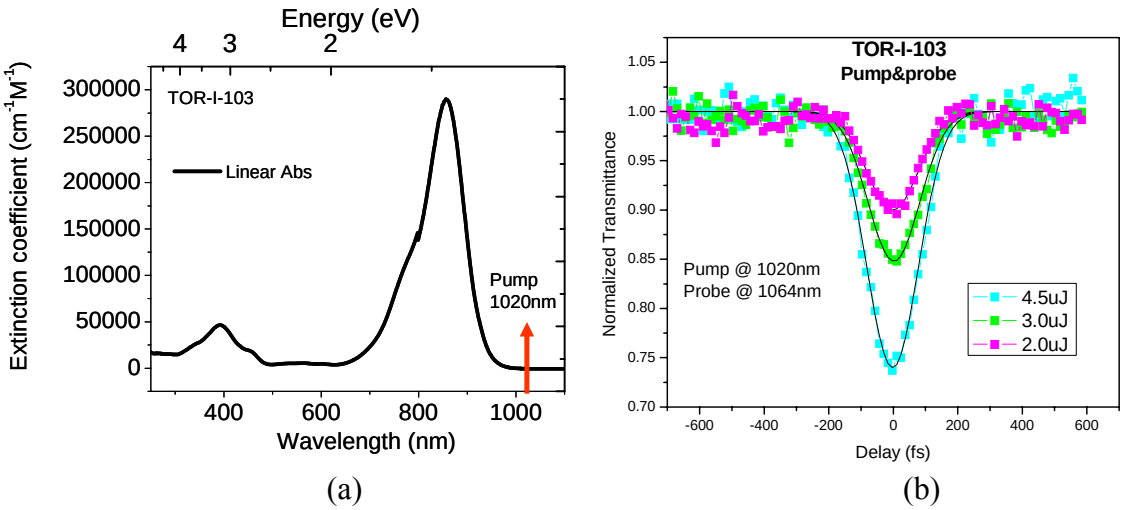

Figure 3.6 (a) Linear absorption spectrum for TOR-I-103 in THF (b) The normalzied transmission of probe as a function of the time delay between pump and probe pulses for TOR-I-103 with pump 1020nm (2uJ, 3uJ and 4.5uJ) and probe 1064nm. Solid lines are for eye-guide.

It is seen that pump 1020nm is located at the long wavelength edge of the linear absorption band in Fig. 3.6 (a). In Fig. 3.6 (b), the transmission of weak probe beam is plotted as a function of time delay between pump and probe pulses for three pump energies. The positive delay indicates that strong pump pulse hits the TOR-I-103 solution before the arrival of the weak probe pulse, negative delay indicates the pump pulse is behind of probe pulse temporally. So at the negative delay, the transmission can be considered as the linear transmission of the probe beam without presence of strong pump beam. The linear transmission of the probe is normalized to unity in Fig. 3.16 (b). We observed that the transmission of probe decreases around zero delay region (-150fs < Delay < 150fs) and then goes back to the same linear transmission as that in the

negative delay. We can conclude that the probe transmission "instantaneous" change around zero delay region is due to nondegenerate 2PA (one photon from pump, the other photon from probe). There is no ESA occurring for this case. We can trust the signal we see in the single wavelength Z-scan experiment with pump 1030nm is from the pure 2PA process.

2) Let's look at the case for molecule Sjz-3-16 in THF. The spectroscopic data for this molecule can be found at Appendix C.3. The linear absorption spectrum of Sjz-3-16 in THF is shown in Fig. 3.7 (a), and the pump probe data in Fig. 3.7 (b) and (c)

Pump 600nm is located at edge of linear absorption band of Sjz-3-16 in THF shown in Fig. 3.7 (a). In Fig 3.7 (b), at after delay ≈ 150 fs, the transmission of weak probe beam is smaller than normalized linear transmission at negative delay, and staying almost same for the delay up to 1.4 ps. We can conclude that this decrease of transmission of the probe (Δ) after zero-delay region (-150fs – 150fs) is because of ESA, which is evidenced by its long time response behavior (usually hundreds ps to ns). In addition, the dip of the probe transmission at zero delay have contributions both from the non-degenerate 2PA and ESA.

Because the strong pump 600nm femtosecond pulse may experience both 2PA and 1PA. In order to tell which absorption process dominates here, we plot the logarithm of ESA signal (Δ) as a function of logarithm of pump energy and fit the experimental data with linear function in Fig. 3.7 (c). The relationship of 1PA and 2PA induced electron population of first excited state N_1 that is responsible to ESA without considering lifetime of the excited state can be expressed as:

$$\frac{dN_1}{dt} = \frac{\alpha I(t)}{\hbar\omega} + \frac{\beta I^2(t)}{2\hbar\omega} \qquad (3.8)$$

Where α is 1PA coefficient, β is 2PA coefficient, I(t) is irradiance of pump beam and $\hbar\omega$ is pump photon energy. In Fig 3.7 (c), the slope of 1.1 is observed to indicates that 1PA dominates here, and ESA signal is mainly due to 1PA of pump beam. So if we use 600nm as the pump beam in single wavelength open-aperture Z-scan experiment, the signal we see is due to 2PA plus 1PA followed with ESA, even although the Z-scan signal can be well fitted with 2PA theory.

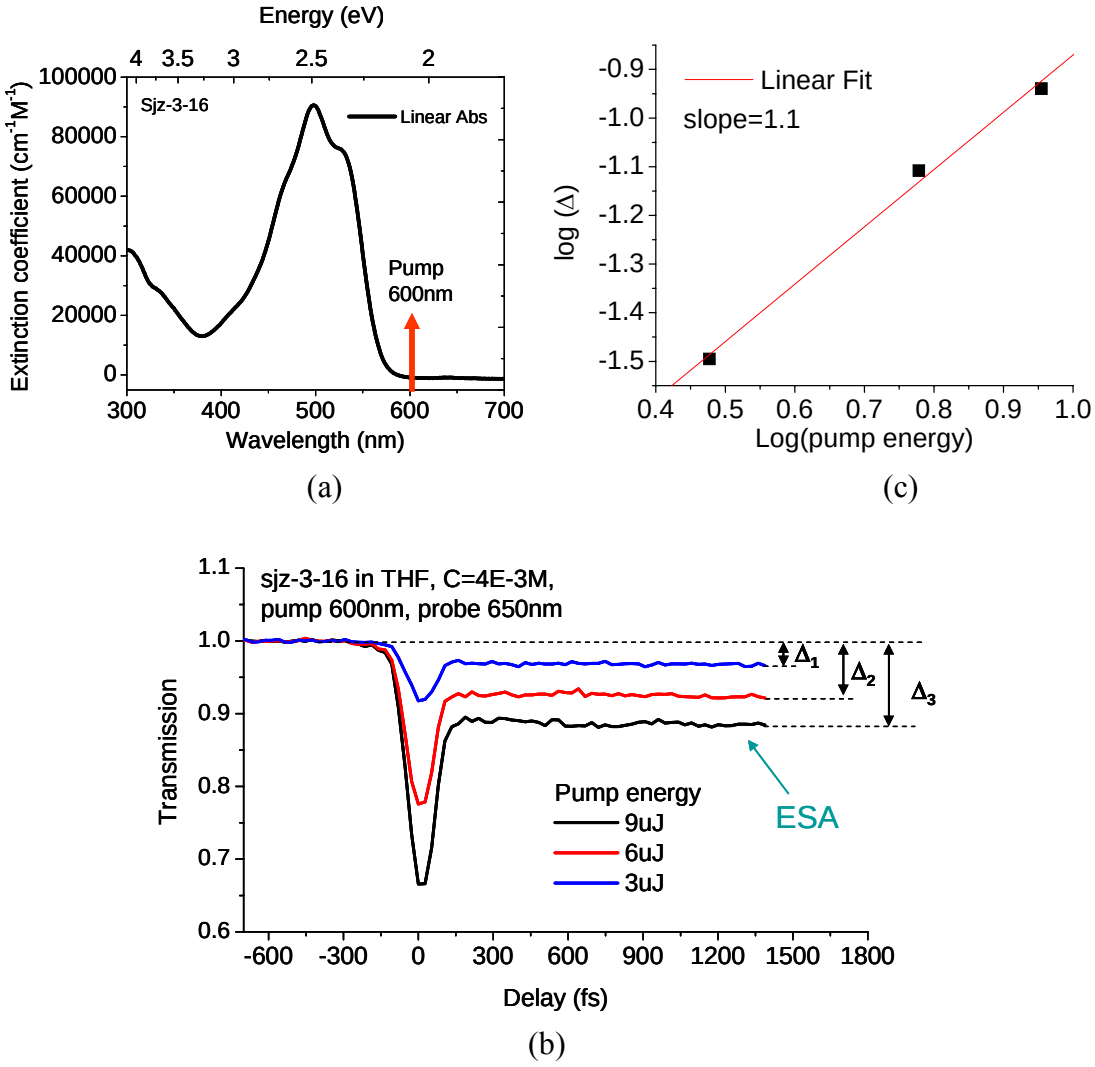

Figure 3.7 (a) Linear absorption spectrum of Sjz-3-16 in THF; (b) The normalized transmission of probe 650nm as a function of the time delay between pump and probe pulses for Sjz-3-16 with pump 600nm (3uJ, 6uJ and 9uJ) and probe 650nm. ESA signals are indicated by Δ_1, Δ_2 and Δ_3 for three pump energies respectively; (c) Plot of logarithm of ESA signal (Δ) as a function of logarithm of pump energy

3) In addition, let's look at the case for LB-II-80 in THF. The spectroscopic data are shown in Appendix C.3. The linear absorption spectrum of LB-II-80 in THF is shown in Fig. 3.8 (a), and the pump probe data in Fig. 3.8 (b) and (c)

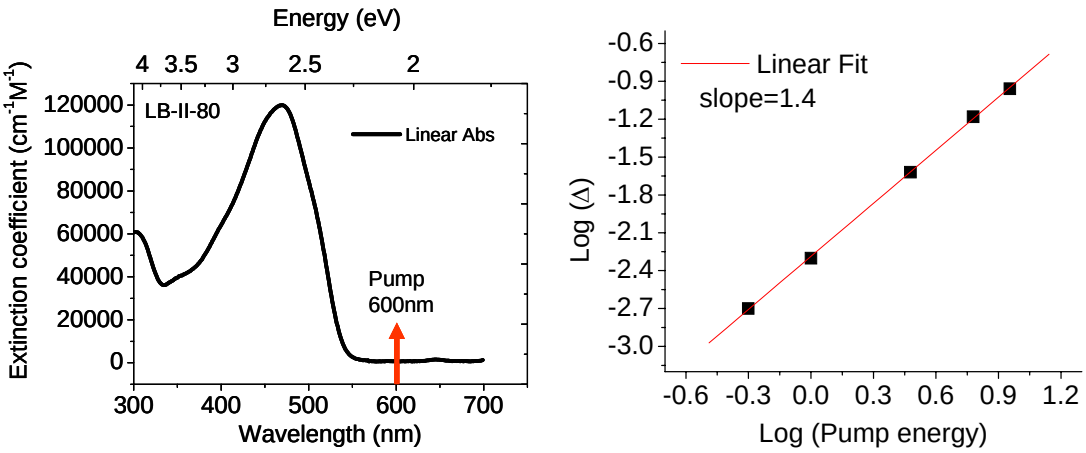

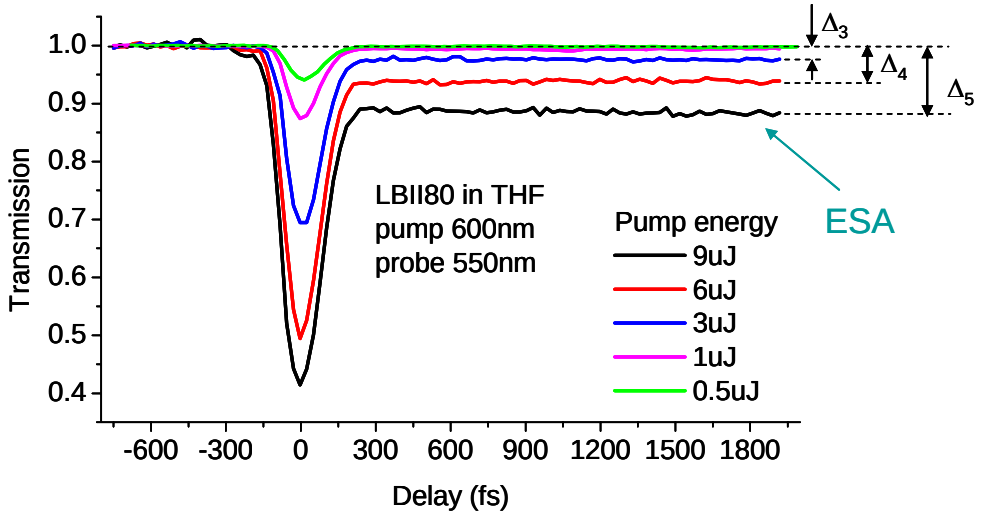

Figure 3.8 (a) Linear absorption spectrum of LB-II-80 in THF; (b) The normalized transmission of probe 550nm as a function of the time delay between pump and probe pulses for LB-II-80 with pump 600nm. ESA signals are indicated by Δ_3, Δ_4 and Δ_5 for pump energies 3uJ, 6uJ and 9uJ respectively. ESA signals for pump enegies 0.5uJ and 1uJ are equal to $\Delta_1 = 0.002$, $\Delta_2 = 0.005$ respectively (not shown in the graph); (c) Plot of logarithm of ESA signal (Δ) as a function of logarithm of pump energy.

The pump 600nm is located quite close to linear absorption band for LB-II-80 in THF shown in Fig. 3.8 (a). ESA with probe 550nm is observed for all the pump energies shown in Fig. 3.8 (b). In Fig 3.8 (c), Slope is equal to 1.4 indicates that ESA have contributions from both 2PA and 1PA of pump 600nm according to Eq. (3.8), i.e. pump 600nm beam experiences both 1PA and 2PA here.

4) We performed the pump-probe experiment for LB-II-80 in THF with another pump wavelength 690nm that is far from linear absorption edge shown in Fig. 3.9 (a), therefore experiences negligible 1PA. The pump probe data in Fig. 3.9 (b) and (c), non-smooth curves in Fig. 3.9 (b) are due to the crosstalk between motor cable and detector cables.

Shown in Fig. 3.9 (b), ESA is observed for all the pump energies, and the slope in Fig. 3.9 (c) is observed to be equal to 2.15, which indicates that here 2PA dominates absorption process for strong pump 690nm. Here ESA is mainly due to 2PA, i.e. a three-photon process. If we use pump 690nm in the single wavelength Z-scan experiment, we prefer to use smaller pump energy to minimize higher order ESA+2PA effect. If pump energy is high, Z-scan signal will not be able to be fitted with pure 2PA theory.

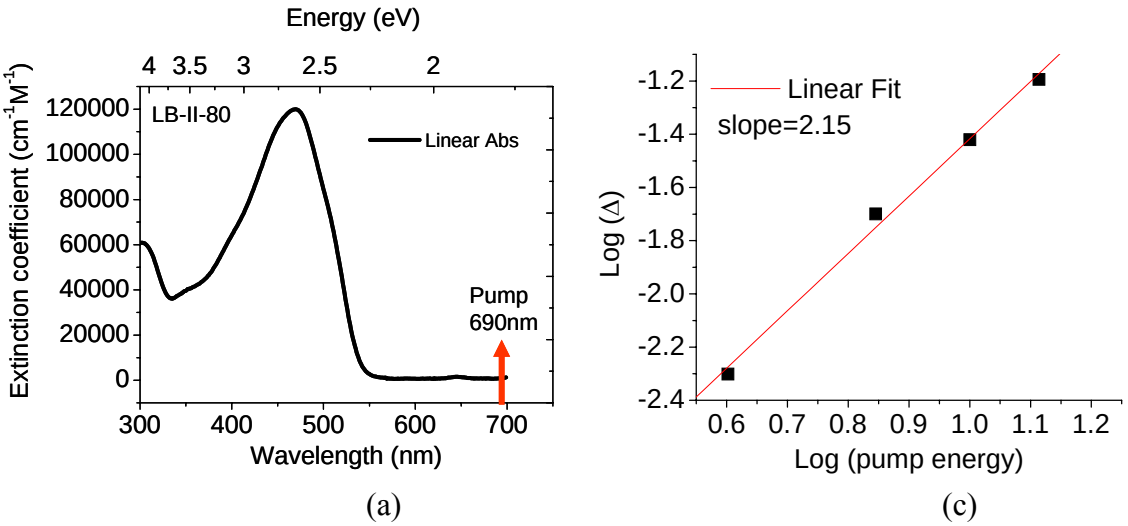

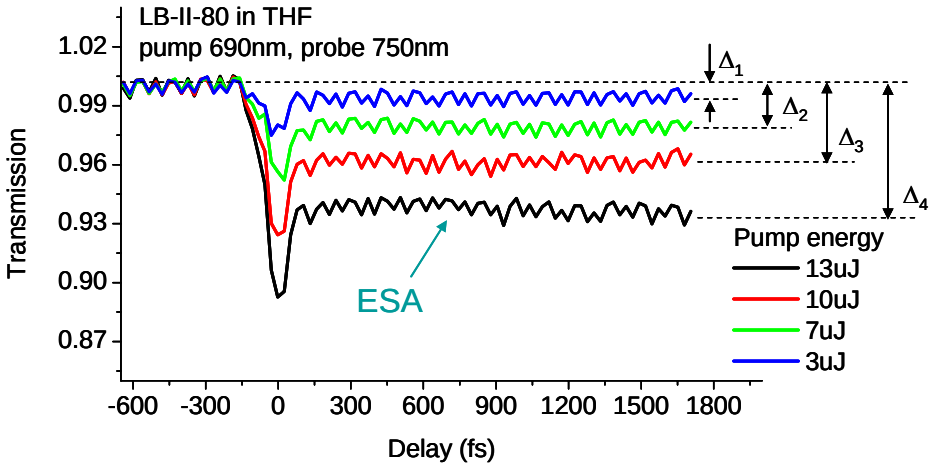

(b)

Figure 3.9 (a) Linear absorption spectrum of LB-II-80 in THF; (b) The normalized transmission of probe 750nm as a function of the time delay between pump and probe pulses for LB-II-80 with pump 690nm. ESA signals are indicated by Δ_1, Δ_2, Δ_3 and Δ_4 for pump energies 3uJ, 7uJ, 10uJ and 13uJ respectively. (c) Plot of logarithm of ESA signal (Δ) as a function of logarithm of pump energy

CHAPTER 4 STRUCTURE-PROPERTY RELATIONSHIP OF POLYMETHINE DYES

4.1 Cyanines

The generic cyanine dyes consist of two nitrogen centers, one of which is positively charged and is linked by a conjugated chain of a number of carbon atoms to the other nitrogen. For example, the structures of PDs are shown in Fig. 4.1.Both polymethine dyes and squaraine dyes belong to the family of cyanine dyes. Polymethine dyes are also called cationic streptopolymethine-cyanines, and squaraine dyes are referred as Zwitterionic squaraine-based cyanine dyes. In this chapter, we will discuss relationships of molecular structure to linear and nonlinear optical properties for polymethine dyes. The squaraine dyes will be discussed in Chapter 5.

In the middle of the 19^{th} century, cyanine dyes were first used as the spectral sensitizers for silver halide photography, and dominate the field of photography since then [47]. Although polymethine and squaraine dyes are substances with a variety of colors in solution, they are not widely used for dyeing purposes because they are decolorized by light and acid, i.e. bleached. However, they have been widely used in optical disks as recording media [48], saturable absorbers for Q-switching and modelocking [49], and gain media in dye lasers [50]. Cyanines are also used for initiation of photopolymerization, as molecular probes in polymer science and biology [51], as nonlinear media for exploring excited-state absorption [52] [53]**.** Polymethine molecules are also useful objects for developing new theoretical concepts and effective quantum-chemical models.

4.2 Polymethine dyes

The name polymethine refers to the π conjugated chromophore chain, which is composed of the methine groups and serves as a light absorbing chromophore of the molecule. The general structure of a polymethine dye (PD) is shown in Fig. 4.1(a), where R_1 and R_2 represent terminal groups. PDs are a special type of the charged (ionic) linear π-electron conjugated system.

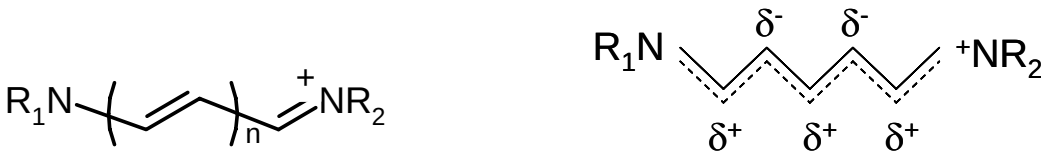

(a) (b)

Figure 4.1 (a) General molecular structure of PD, R_1 and R_2 are terminal groups; (b) π-electron distribution in polymethine chromophore.

The key feature of the polymethine chromophore is an alternating partial charge (δ^+ and δ^- are positive and negative charge, respectively) at the carbon atoms within the polymethine chain along with an equalization of the bond lengths as shown in Fig.4.1(b). This property allows a large delocalization of the π-electron system, which gives rise to a large polarizability and promises a strong nonlinear interaction upon excitation.

Altering the chromophore via the addition of terminal groups to the two end positions gives us the ability to generate different chemical archetypes by affecting the electron accepting and donating properties of the system. By placing the terminal groups with high (accepting) or low (donating) electron affinities we can create the following motifs: 1) Donor-π conjugated chromophore-Donor (D-π-D), 2) Donor-π conjugated chromophore-Acceptor (D-π-A). We can also control the strength of these electron accepting/withdrawing terminal groups, which gives us

further freedom to address the effect these structural changes having on the molecule's NLO properties.

Polymethine dyes (PDs) have highly intense and comparatively narrow absorption and fluorescence bands which can be shifted from the visible to infrared (>1600nm) region by lengthening the polymethine chain (up to n=13) [54] or by introducing specific terminal groups.

The PDs we studied in this thesis are shown in Fig. 4.2:

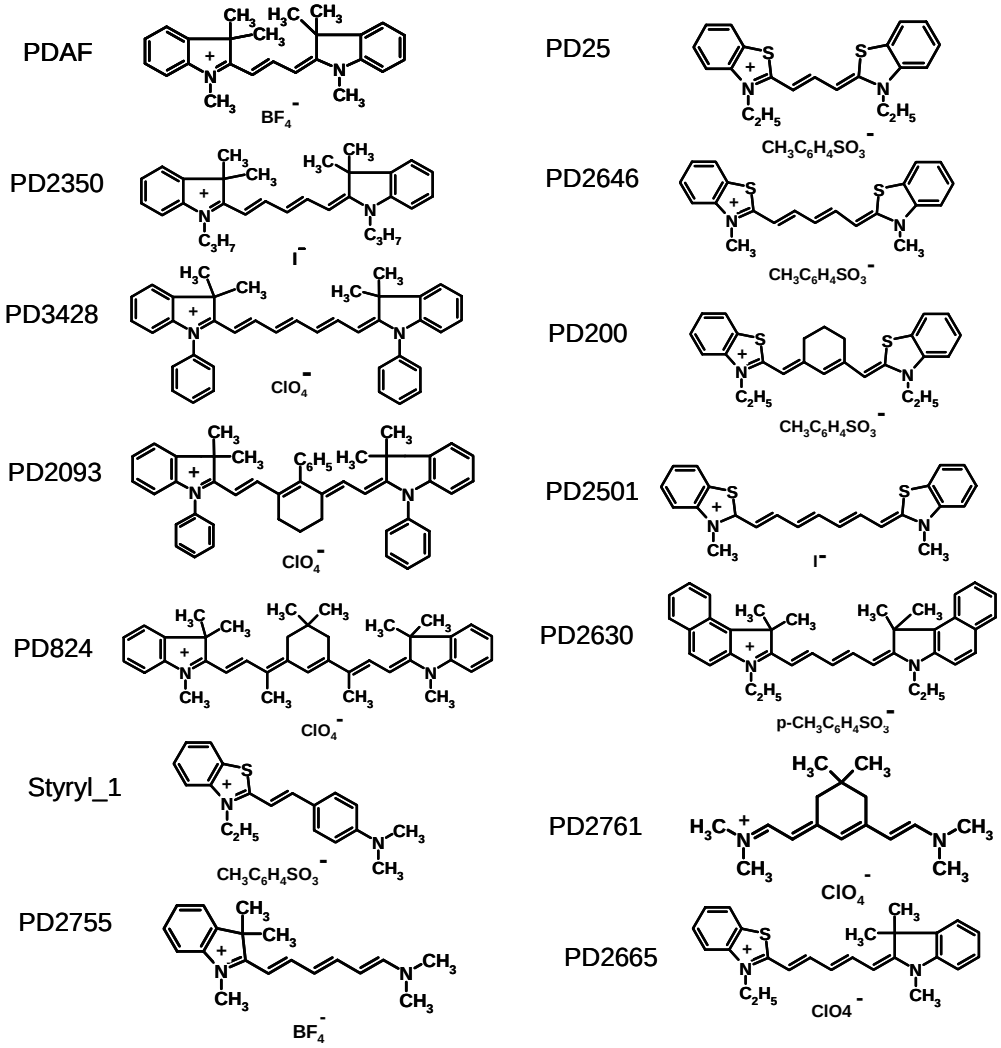

Figure 4.2 Molecular structures of Polymethine Dyes (PDs)

The photochemical stability of PDs degrades as the chain length is increased from the lowest cyanine limit (n=0) to the carbocyanine (n=1) and on to the di- (n=2), tri-, etc. carbocyanine structures. It should be noted that much work has been spent on making this series of dyes photochemically stable [52], with the exception of the pentacarbocyanine dyes which were only recently synthesized.

PDs are attractive for 2PA due to three advantages: 1) they show large ground-state transition dipole moments; 2) they have close to parallel orientation of their ground- and excited-state transition dipole moments [55]; 3) the sharp low-energy side of their linear absorption spectra allows significant intermediate state resonance enhancement of the 2PA [56]

Linear properties such as peak linear absorption wavelength, λ_{abs}max and fluorescence spectra peak wavelength λ_{flu}max, quantum yield η and peak extinction coefficient ε_{max} of the polymethine dyes studied in ethanol are summarized at Table 4.1 below:

Table 4.1 Linear optical properties of polymethine dyes in ethanol

PD	λ_{abs} (nm)	λ_{flu} (nm)	η	ε_{max} (cm^{-1} M^{-1})
AF	547	566	0.035	149000
2350	649	665	0.38	235000
3428	756	-	-	292000
2093	771	-	-	294000
824	863	-	-	224000
25	560	572	0.063	151000
200	648	670	0.0656	160000
2646	654	675	0.3	240000
2501	762	788	-	228000
2630	682	704	-	211900
Styryl 1	527	598	0.013	61500
2665	644	667	0.243	197000
2755	570	605	0.066	168500
2761	536	553	0.11	250200

4.3 Symmetry

It is well known that materials with symmetry through their center of inversion have ground and excited states with a definite parity. These materials are referred to as centro-symmetric systems. Their states are usually separated as symmetric or unsymmetric states. Quantum mechanics dictates that in centro-symmetric systems, linear excitation and two-photon excitation processes access states of differing parity. One-photon absorption will gain access to a state which is opposite in symmetry to that of the ground state, whereas 2PA will access a state of like symmetry [57][58] [59].

We consider the effect of molecular symmetry on 2PA by comparing results for the symmetrical PD 2350 (indolium terminal groups, n = 2) with the weakly asymmetrical PD 2665 (indolium – thiazolium terminal groups, n = 2), and also with the strong asymmetrical molecule PD2755 (indolium-terminal groups, n=2).

Degenerate 2PA spectra of these molecules in ethanol were taken by using 2PF spectroscopy and the Z-scan technique. Experimental results and theoretical fittings based on Eq. (2.55) in chapter 2 are shown in Fig. 4.3. Here the two-photon absorption cross section δ is plotted versus half the wavelengths of the input photons. The 2PA cross-section is a unit expressed in 10^{-50} cm^4*sec/photon that is defined as Goppert-Mayer (GM).

It is commonly known that asymmetrical dyes are characterized by blue-shifted and broader linear absorption bands $S_0 \rightarrow S_1$ as compared to those for symmetrical dyes. We can see this in Fig. 4.3 where the solid lines indicate linear absorption spectra. Absorption shapes for asymmetrical molecules strongly depend on solvent polarity which is connected to the charge localization [55].

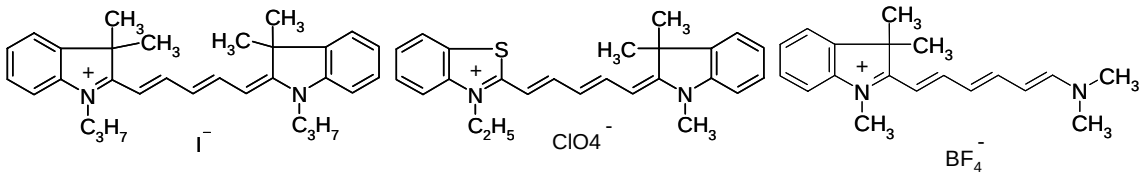

(a)

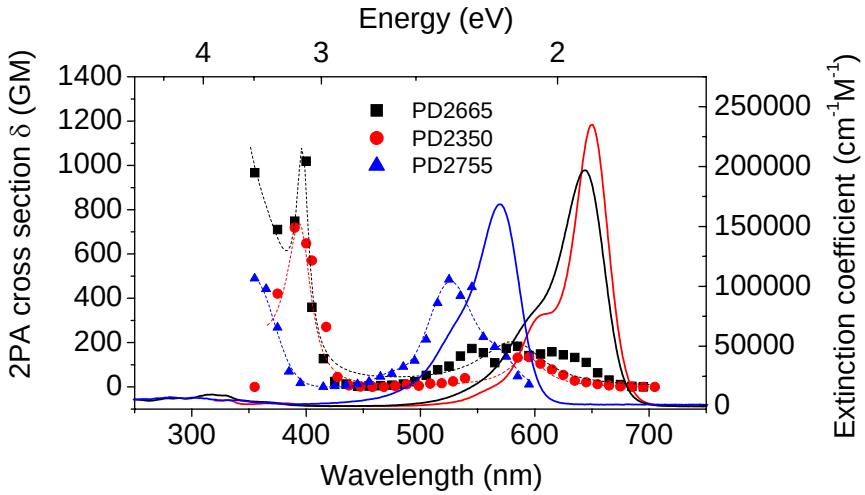

(b)

Figure 4.3 (a) Molecular structures (b) Degenerate 2PA spectra for PD2350 (red), PD2665 (black) and PD2755 (blue). Dashed line is the theoretical fitting based on Eq. (2.55), and the linear absorption spectra (solid line) are shown for reference.

2PA spectra also show some differences. As was expected, for the strongly asymmetrical PD2755, the first 2PA band is much broader than that for the symmetrical PD 2350; however, δ_{2PA} for the second band is smaller. The same, but less pronounced effect was observed for the weakly asymmetrical PD 2665 when compared to the symmetrical PD 2350. We note that for PD 2665 the beginning of the third 2PA band is observed while this is not the case for the symmetrical PD 2350. PD2350, a symmetric dye, shows negligible 2PA into the peak of the first singlet excited state, but displays a first 2PA band corresponding to its vibration shoulder due to

the effect of vibronic coupling partly breaking the molecular symmetry. We will discuss the nature of symmetry breaking in Chapter 5 and 6.

We also compare results for the symmetrical molecule PD 25 (thiazolium terminal groups, n = 1) with the strongly asymmetrical molecule Styryl 1 (thiazolium – styryl terminal groups, n = 1). Molecular structures and experimental results are presented in Fig.4.4.

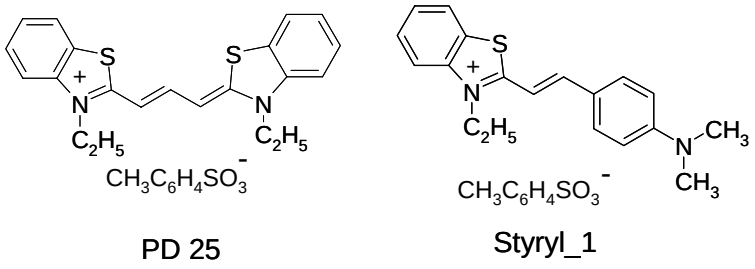

(a)

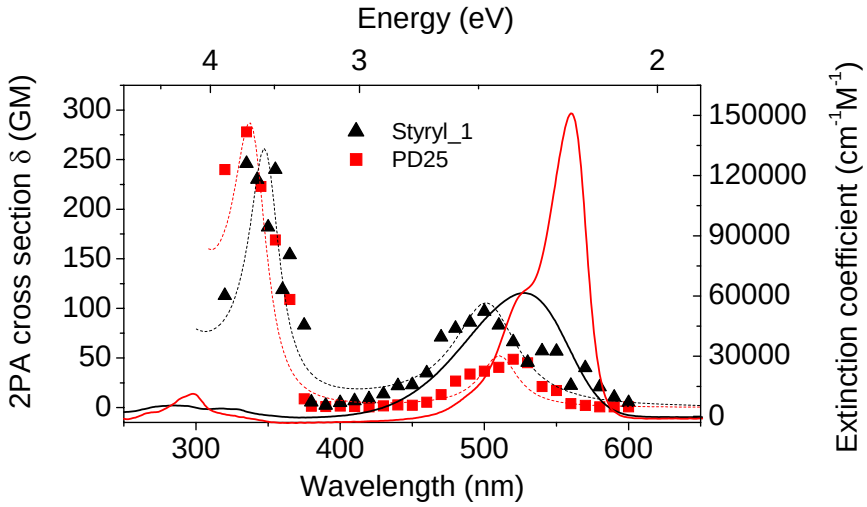

(b)

Figure 4.4 (a) Molecular structures (b) Degenerate 2PA spectra for PD25 (red), Styryl_1 (black). The dashed line is for theoretical fitting based on Eq. (2.55), and linear absorption spectra (solid line) are shown for reference.

Styryl_1, a strongly asymmetrical molecule, shows a relatively strong and broad 2PA band within the linear absorption band when the two-photon absorption cross section δ is plotted

versus half the wavelength of the input photons. PD 25 shows a less intense vibrationally induced 2PA band close to the position of its vibration shoulder.

4.4 Terminal groups

Altering the chromophore of PDs via the addition to the two end groups gives us the ability to generate different chemical archetypes by affecting the electron accepting and donating properties of the system. By placing terminal groups (TGs) at these positions with low (donating) electron affinities we can create the following motifs such as Donor-π conjugated core-Donor (D-π-D). We can also control the strength of these electron donating end groups which gives us further freedom to address the effect these structural changes having on the molecule's NLO properties.

We consider the effect of the three terminal groups: thiazolium, indolium and benzoindolium, on the one- and two-photon absorption properties. Fig. 4.5 represents experimental results for PDs with the same length of the chromophore n = 2 and different terminal groups placed in order of a decrease of their donor strength: PD 2630 (benzoindolium), PD 2350 (indolium) and PD 2646 (thiazolium), respectively. Degenerate 2PA spectra of these molecules in ethanol were taken by using 2PF spectroscopy and Z-scan. Molecular structures are shown in Fig. 4.5 (a). The 2PA spectra are shown in Fig. 4.5 (b). Here the two-photon absorption cross section δ is plotted versus half of the wavelengths of the input photons. A summary of ground state transition dipole moments μ_{01}, calculated excited state transition dipole moments μ_{12} (obtained by fitting the 2PA spectra with Eq. (2.55)), as well as maximum 2PA cross sections δ_{max}, are shown in Table 4.2.

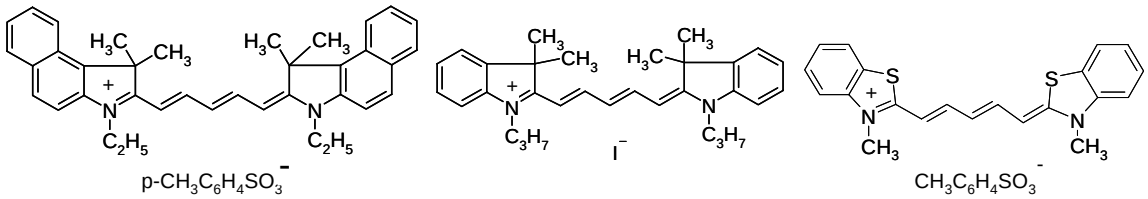

(a)

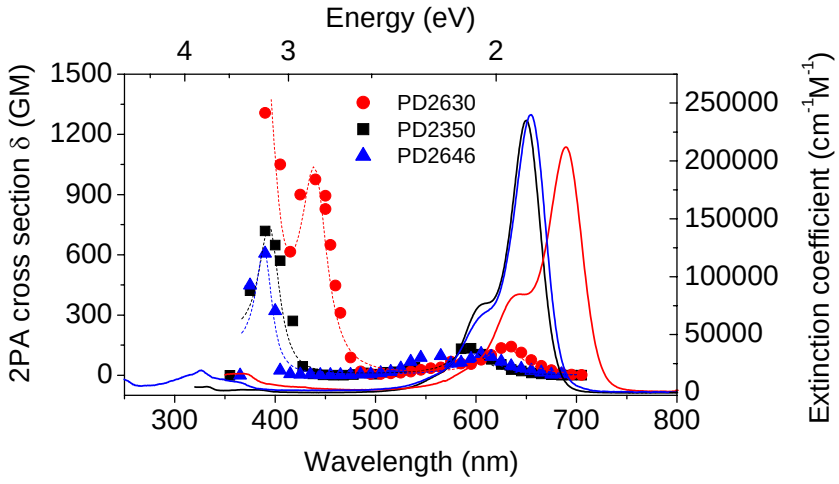

(b)

Figure 4.5 (a) Molecular structures; (b) Degenerate 2PA spectra for PD 2630, PD 2350 and PD 2646. The dashed line is for theoretical fitting based on Eq. (2.55), and linear absorption spectra (solid line) are shown for reference.

Table 4.2 Parameters for PDs having the same conjugate length with benzoindolium (PD2630); indolium (PD2350); thiazolium (PD2646) terminal groups

Molecules	μ_{01}(debye)	μ_{12}(debye)	δmax (GM)	ΔE (eV)
PD2630	14	3.1	980	0.35
PD2350	15	2.0	720	0.31
PD2646	14	1.5	600	0.29

All linear and nonlinear parameters for PD 2646 and PD 2350 are very close in accordance with the similar donor strength and similar contribution of π-conjugation from their terminal groups to the polymethine chain. However, we note that δ_{2PA} in both 2PA bands of PD 2350 is 20-40 % larger than those of PD 2646.

For PD 2630, with the larger π-conjugation (larger contribution to the chain) and increased donor strength in the benzoindolium terminal groups, the positions of the one- and two-photon absorption peaks are red-shifted, and δ_{2PA} for the second band is ≈ 1.5× larger than for PD 2646. The 2PA spectrum for PD 2630 is more complicated than for PD 2350. In contrast to PD 2350, the beginning of the next, third 2PA band, is seen for PD 2630, with δ_{2PA} reaching 1320 GM. Further tuning of the excitation wavelength into the short wavelength region was restricted by the presence of linear absorption. Quantum chemical calculations related to the effect of terminal groups will be addressed in Chapter 5.

All three terminal groups we studied here contain their own π-conjugated system, which will change the effective conjugation length of the molecules. When we discuss the effect of terminal groups on 2PA properties, besides the strength of donors, we also have to consider the change of the effective molecular conjugate length due to the terminal groups. From Section 4.5, we observed the trend that increasing the conjugation length of the molecules leads to an increase of the ground-state transition dipole moments in Section 4.5. However, we do not see this trend with different terminal groups (see the Table 4.2). It should be an interesting topic to study the change of the effective conjugation length due to terminal groups on the 2PA properties of molecules.

Comparing the 2PA properties of PD 200 and PD 2761 gives us some insights about this. They have the same length of the chromophore n = 2 and different terminal groups, i.e. TGs for PD 200 and PD 2761 have similar donor strength but very different conjugation length, which will make the effective conjugation length of PD 2761 smaller. Both of them have benzene bridges in the middle of the chromophore chain. Degenerate 2PA spectra of these molecules in ethanol were also taken by using 2PF spectroscopy and Z-scan. Molecular structures are shown

in Fig. 4.6 (a). The 2PA spectra are shown in Fig. 4.6 (b). Here the two-photon absorption cross-section δ is plotted versus the half of input photon wavelengths. A summary of ground state transition dipole moment μ_{01}, as well as maximum 2PA cross section δ_{max} are shown in Table 4.3.

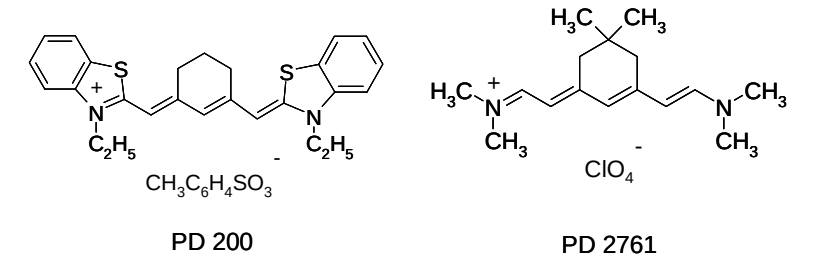

(a)

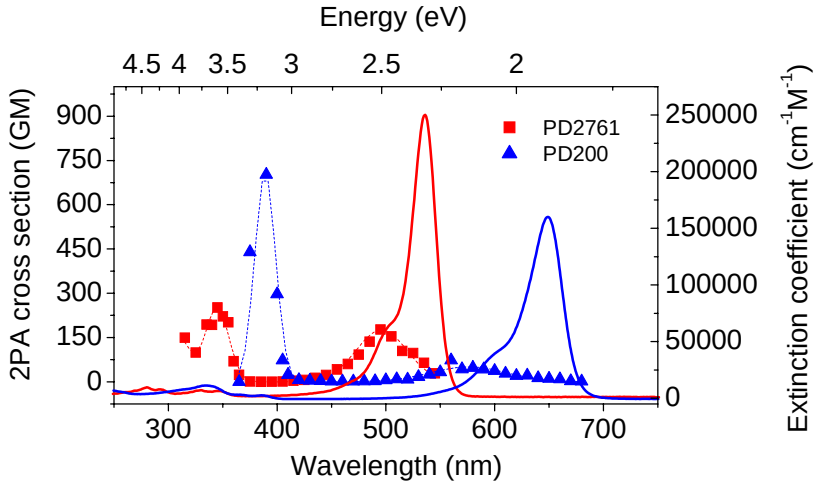

(b)

Figure 4.6 (a) Molecular Structure (b) Degenerate 2PA spectra for PD 200 and PD 2761. The dashed line is for theoretical fitting based on Eq. (2.55), and linear absorption spectra (solid line) are shown for reference

Table 4.3 Parameters for PD 200 and PD 2761 having the same chromophore conjugation length with different terminal groups

Molecules	μ_{01}(debye)	μ_{12}(debye)	δmax (GM)	ΔE (eV)
PD 200	11	2.2	703	0.32
PD 2761	12.8	1.5	248	0.52

The main difference between PD 2761 and PD 200 is that PD 2761 has a very simplified terminal group (TG) without conjugation, which will make the effective conjugation length of

PD 2761 smaller, and is the reason why the linear absorption band of PD 2761 is so shifted to the "blue" region. Here we observe that the one-photon absorption band of PD 2761 is blue-shifted by ~ 110nm compared to PD 200. This shift is approximately equal to the shift upon lengthening of the chain by one unit. Thus, this is a manifestation of the conjugation in TG on the linear properties. The two-photon absorption band is also shifted by a smaller amount ~ 50nm, which is also observed for the dyes upon lengthening of the chain by one unit.

It is interesting to observe that PD 2761 shows a smaller peak 2PA cross section. From the Table 4.3, PD 2761 possesses a larger ground state transition dipole moment than PD 200, a shorter effective conjugation length, but a much smaller observed 2PA cross section. This could be considered as evidence that π-conjugation in TG of PD 200 improves the 2PA probability by increasing the excited state absorption dipole moments and decreasing the detuning energy shown in Table 4.3. It is noticable that extending π-conjugation in chromophore chain of polymethine will increase 2PA cross setions by increasing ground state transition dipole moments shown in Section 4.5

4.5 Conjugation length

For symmetric molecules the first accessible two-photon state is $2A_1$ (numbering is the following: A_g only for the neutral molecules like polyenes and squaraine dyes, and A_1 for polymethine dyes) corresponds to the second singlet excited state. Based on perturbation theory for a three-state model having one-intermediate state for 2PA shown in Chapter 2, the dominant terms which affect the two-photon properties of this transition are the ground to first excited state (intermediate state) with the transition dipole moment μ_{01} as well as the first to second excited

state with the transition dipole moment μ_{12}. A very straightforward way to maximize μ_{01} is by extending the chromophore length of the conjugated molecule. By increasing the ground state transition dipole moment by lengthening the molecule, we can increase the distance over which charge can be transferred to the excited state. Certainly there are limits to the extent to which the value of μ_{01} can be increased by this method.

Here we study two series of symmetric PDs: one series of PDs with indolium terminal groups (from n = 1 to n = 4) is shown in Fig. 4.7 (a), the other series of PDs with thiazolium terminal groups (from n =1 to n = 3) is shown in Fig. 4.8 (a). Degenerate 2PA spectra of these molecules in ethanol were taken by using 2PF spectroscopy and Z-scan. 2PA spectra as well as linear absorption spectra are shown in Fig. 4.7 (b) and Fig. 4.8 (b). Here the 2PA cross section δ is plotted versus the half of input photon wavelengths. A summary of ground state transition dipole moments μ_{01}, calculated excited state transition dipole moments μ_{12} (obtained by fitting the 2PA spectra with Eq. (2.55)), maximum 2PA cross sections δ_{max}, as well as detuning energies ΔE are shown in Table 4.4 and Table 4.5.

Calculations show that an increase in the chain length leads to an increase of the ground state transition dipole moment from 12.2 debye (n = 1) to 17 debye (n = 4) for indocarbocyanines (see Table 4.4), and 10.5 debye (n = 1) to 15.5 debye (n = 3) for thiacarbocyanines (see Table 4.5).

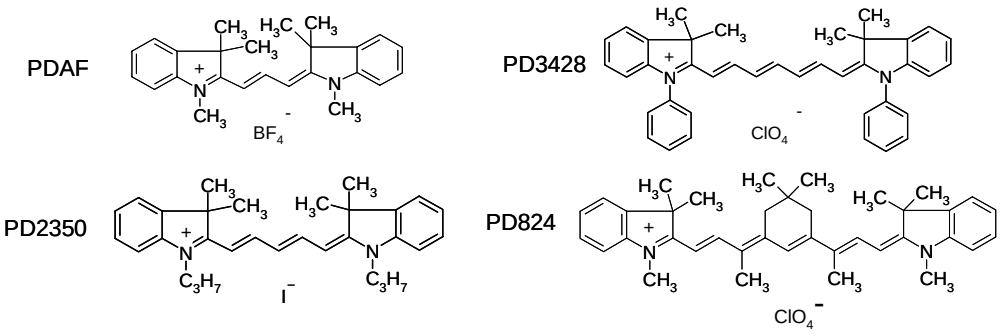

(a)

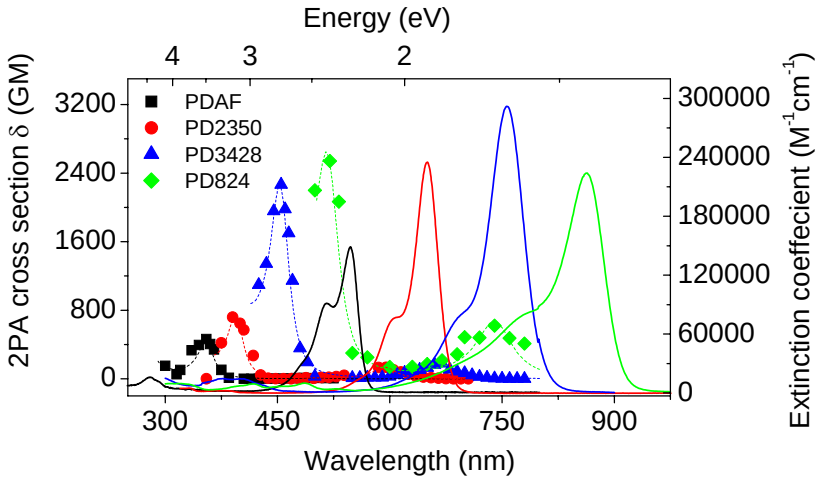

(b)

Figure 4.7 (a) molecular structures; (b) degenerate 2PA spectra for PDAF, PD2350, PD3428 and PD824. The dashed line is for theoretical fitting based on Eq. (2.55), and linear absorption spectra (solid line) are shown for reference.

Table 4.4 Parameters for PDs having indolium terminal groups with conjugation length from n=1 to n=4. Detuning energy ΔE is calculated for the 2PA peak at δ_{exp}max2; Q. C. is from the quantum chemical calculation

PD	n	μ_{01}(debye) Exp	μ_{01}(debye) Q.C.	μ_{12}(debye) Fit	μ_{12}(debye) Q. C.	δ_{exp}max1 (GM)	δ_{exp}max2 (GM)	ΔE^* (eV)
AF	1	12.2	10.2	2.8	3.4	10	465	0.51
2350	2	14.7	12.4	2.0	3.9	140	720	0.31
3428	3	16.8	13.8	2.8	2.3	180	2260	0.26
824	4	17	12.4	2.9	2.3	600	2550	0.25

* Detuning energy ΔE calculated for peak of 2PA spectra δ_{exp}max2

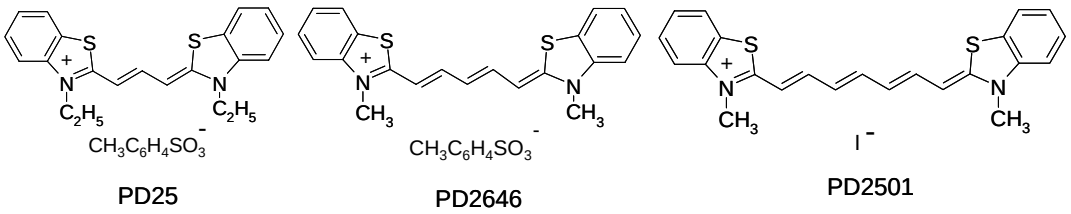

(a)

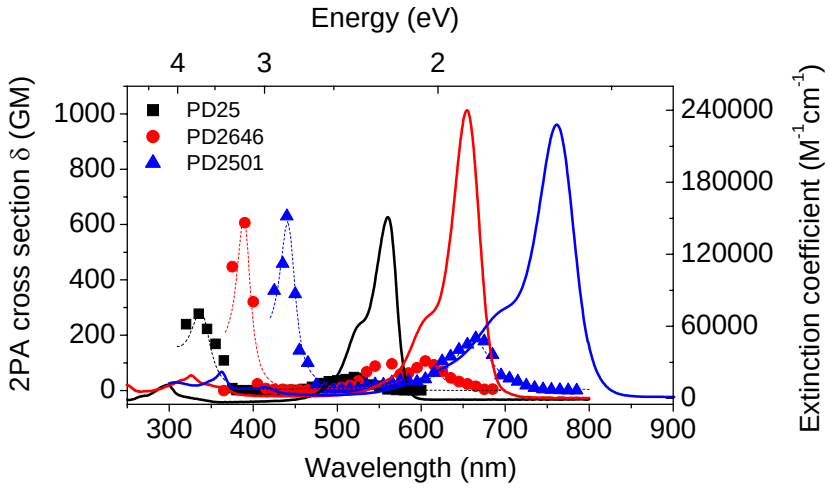

(b)

Figure 4.8 (a) molecular structures; (b) degenerate 2PA spectra for PD25, PD2646 and PD2501. The dashed line is for theoretical fitting based on Eq. (2.55), and linear absorption spectra (solid line) are shown for reference.

Table 4.5 Parameters for PDs having tiazolium terminal groups with conjugation length from n=1 to n=3. Detuning energy ΔE is calculated for a 2PA peak at δ_{exp}max2; Q. C. is from the quantum chemical calculation

PD	n	μ_{01}(debye) Exp	μ_{01}(debye) Q.C.	μ_{12}(debye) Fit	μ_{12}(debye) Q.C.	δ_{exp}max1 (GM)	δ_{exp}max2 (GM)	ΔE^* (eV)
25	1	10.5	10.7	2.1	1.5	50	280	0.36
2646	2	14.0	12.4	1.5	1.4	100	600	0.29
2501	3	15.5	13.4	1.1	1.6	200	630	0.22

* Detuning energy ΔE calculated for peak of 2PA spectra δ_{exp}max2

In addition, it is commonly known that an increase in the chromophore length of the polymethine by one chain unit (n) with the same terminal groups leads to a red shift in the peak of the linear absorption of about 100 nm, which provides another advantage of longer molecules

for 2PA performance: possible have smaller detuning energy ΔE, so the larger 2PA cross section. Based on perturbation theory with a three-state model, the 2PA cross section δ is proportional to $1/\Delta E$, As ΔE becomes small, the increase in δ is referred to intermediate state resonance enhancement [56]. We also calculated the detuning energy ΔE for peaks of 2PA δ_{exp}max2 for these molecules shown in Table 4.4 and Table 4.5.

Broadening of the linear absorption band for PD 824 (n = 4) in polar solution such as ethanol is connected with a partial ground state symmetry breaking and the appearance of a form of the molecule with an asymmetrical distribution of the charge density. Detailed information on our experimental and theoretical investigations of this symmetry breaking effect in different solvents can be found in [55] and are discussed in Section 4.6.

Two-photon absorption spectra for all PDs show the existence of two 2PA bands. Experimental results demonstrate that lengthening of the polymethine chromophore generally results in an increase in the 2PA cross section δ. First, a weakly allowed 2PA band is always positioned within the shoulder of the first absorption band $S_0 \rightarrow S_1$. In the indolium series δ increases from ≈ 10 GM for PD AF (n = 1) to 600 GM for PD 824 (n = 4) and in the thiazolium series from 50 GM for PD 25 (n = 1) to 200 GM for PD 2501 (n = 3).

Secondly, a more intense 2PA band is positioned at a shorter wavelength region, (see Fig. 4.7 and 4.8 and data in Table 4.4, 4.5). The peak 2PA cross section δ_{exp}max2 in the indolium series increases from 470 GM for PD AF (n = 1) to 2550 GM for PD 824 (n = 4) and in the thiazolium series increases from 280 GM for PD 25 (n = 1) to 630 GM for PD 2501 (n = 3). We explain this increase of δ_{2PA} upon lengthening of the polymethine chromophore by the

corresponding increase of the ground state dipole moments and decrease of the detuning energies ΔE (between excitation wavelength and intermediate S1 state), see Eq. (2.48) and (2.56).

4.6 Polarity of solvents

Now we consider the nature of the weakly allowed 2PA bands. Two-photon excitation to the S_1 state involves at least two dipole moments: $\boldsymbol{\mu}_{01}$ and $\Delta\boldsymbol{\mu}$ (vector difference between permanent S_0 and S_1 dipole moments). According to the traditional quantum-chemical theories [59], 2PA to the S_1 state is symmetry forbidden for 2PA in centro-symmetric molecules such as squaraines with C_{2i} symmetry ($\Delta\boldsymbol{\mu} = 0$), and is only slightly allowed for symmetrical polymethines with C_{2v} symmetry ($\Delta\boldsymbol{\mu}$ is oriented perpendicular to $\boldsymbol{\mu}_{01}$). However, these bands have been observed for cyanines and cyanine-like molecules (squaraines [60], Rhodamine B and fluorescein [42]) and explained by the effect of symmetry breaking due to vibronic coupling which can lead to a change of the dipole selection rules, resulting in the appearance of a 2PA band within the $S_0 \rightarrow S_1$ absorption band [61][62]. Indications of some forms of symmetry breaking were also observed by two-photon anisotropy measurements, which show relatively high and nearly constant values over the entire spectral range studied [63]. These results can be explained by taking into account the deviation of $\Delta\boldsymbol{\mu}$ from being perpendicular to $\boldsymbol{\mu}_{01}$. Details will be discussed in Chapter 6.

Our current and ongoing studies of 2PA spectra in this series of PDs with different conjugation lengths discussed in Section 4.5, made it possible to assume that processes other than vibronic coupling can break the symmetry of the molecules. The frequency of the chain skeleton vibration observed in the linear absorption of PDs is ≈ 1450 – 1500 cm^{-1} and is almost

chain-length independent. However, for the weak 2PA band, we observed a different trend. For the shorter molecules, the peak of the weak 2PA band corresponds approximately to the 1PA vibrational shoulder (again plotting as in, for example, Figs. 4.7 and 4.8), but for the longer PDs, this 2PA peak is more blue-shifted and depends upon the solvent polarity.

Based on the discussions above, we studied the behavior of this weak 2PA band in different solvents (methanol, ethanol, 1,2-Dichlorobenzene) for symmetric molecules PD 2646 and asymmetric molecule PD 2755. The molecular structures are shown in Fig. 4.9

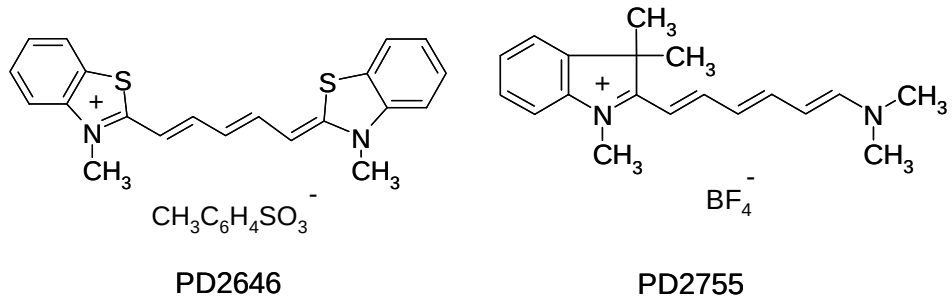

Figure 4.9 Molecular structures for the study of the solvent effect on the weak 2PA band

The polarity of solvents can be evaluated by their orientational polarizability which is expressed as [39]:

$$\Delta f = \frac{\varepsilon - 1}{2\varepsilon + 1} - \frac{n^2 - 1}{2n^2 + 1} \tag{4.1}$$

where ε is the dielectric constant of the solvent, and n is the refractive index of the solvent. From Eq. (4.1), we can see that if the solvent has no permanent dipole moment, or a completely nonpolar solvent, $\varepsilon \cong n^2$ and $\Delta f \cong 0$.

These parameters for three solvents used in this study are listed with decreasing polarity in Table 4.6:

Table 4.6 Dielectric constant ε, refractive index n and polarity Δf of the three solvents (methanol, ethanol and 1,2-Dichlorobenzene)

Solvent	ε	n	Δf
methanol	33.1	1.326	0.31
ethanol	24.3	1.35	0.30
1,2 dichlorobenzene	2.8	1.551	0.166

Table 4.7 Linear optical properties of PD 2646 and PD 2755 in different solvents.

PD	Solvent	$\lambda_{abs}max$	$\lambda_{flu}max$	η	ε_{max}($cm^{-1}M^{-1}$)
2646	methanol	652 nm	672 nm	0.26	219500
	ethanol	654 nm	674 nm	0.3	240000
	1,2 Dichlorobenzene	671 nm	693 nm	0.52	222700
2755	ethanol	570 nm	604 nm	0.07	168500
	1,2 Dichlorobenzene	592 nm	625 nm	0.2	

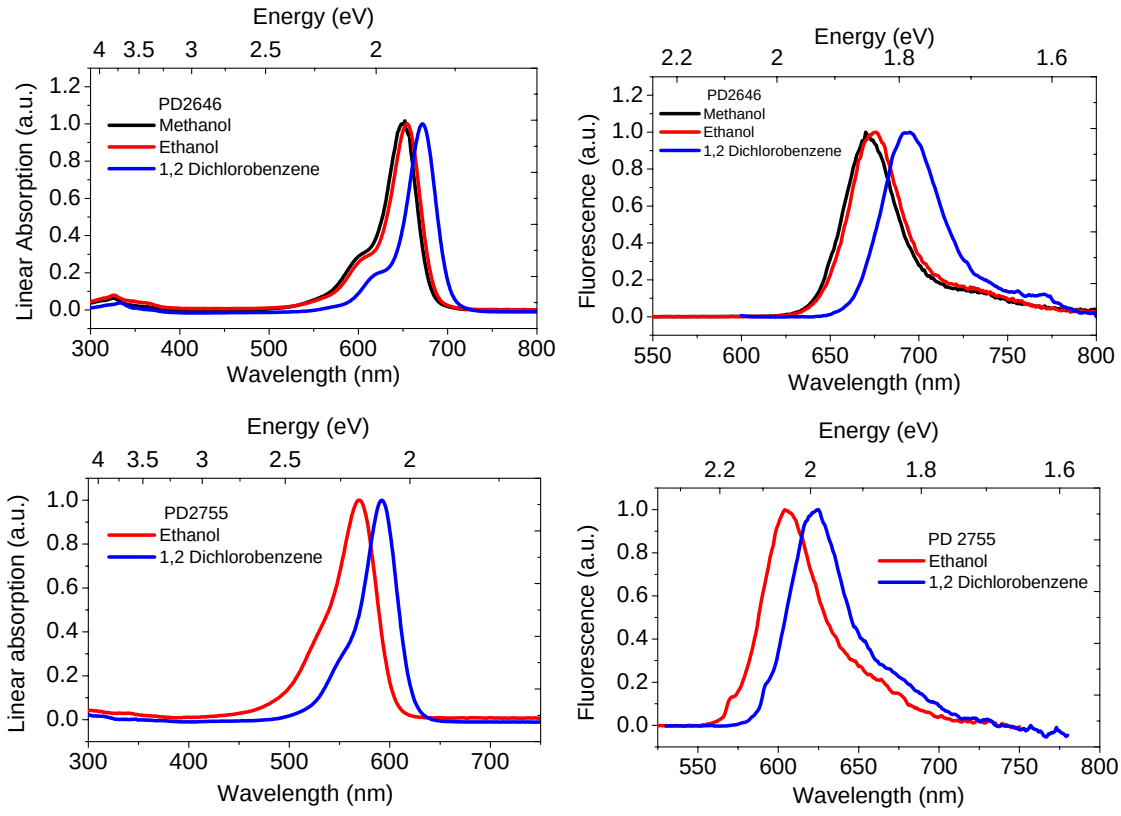

Figure 4.10 Linear absorption and fluorescence spectra for PD 2646 and PD 2755 in different solvents

Linear properties, such as peak linear absorption $\lambda_{abs}max$ and fluorescence wavelength $\lambda_{flu}max$, quantum yield η and peak extinction coefficient ε_{max} of PD 2646 and PD 2755 in

different solvents are listed in Table 4.7. Linear absorption and fluorescence spectra are shown in Fig. 4.10

We can see that linear properties of these two polymethine dyes strongly depend on the polarity of the solvents. Because methanol and ethanol have very similar polarity, PD 2646 shows very similar linear properties in these two solvents. For both asymmetric PD 2755 and symmetric PD 2646 molecules in the less polar solvent 1,2-dichlorobenzene, linear absorption and fluorescence spectra exhibit a 20 ~ 30nm red shift. Fluorescence quantum yields are also higher for dyes in 1,2-dichlorobenzene than in methanol and ethanol.

Our current understanding is that besides vibrational symmetry breaking, a molecular form having an asymmetrical charge distribution may also be present. It was shown in [55], that symmetrical PDs can exist in the ground state as an equilibrium of two forms with symmetrical and asymmetrical charge distributions. Observed both theoretically and experimentally, the total charge (positive and negative) in the charged π-electron system is not delocalized uniformly along the polymethine chain, but instead is distributed at the π-centers as a wave of alternating positive and negative partial charges, i.e. as a soliton of the electron or hole type respectively. For PDs beyond a certain length, i.e. when the width of the charge or solitonic wave is comparable with the length of the chromophore of the molecule, the peak of the charge wave in the ground state can be shifted to on of the TGs. This is called symmtry breaking due to degeneracy of the potential energy. Any fluctuation in the bond length can lead to a shift of this wave. Polar solvents can stabilize the asymmetric form.

However, for the shorter molecules, the fraction of molecules with an asymmetrical charge distribution is small, therefore the shapes of their linear absorption bands do not show a

pronounced solvent dependence as shown in Fig. 4.10. This small amount of the asymmetrical form could be seen by 2PA measurements due to the strong effects of symmetry breaking.

2PA spectra for PD 2646 in methanol, ethanol and 1,2-Dichlorobenzene are taken with the 2PF method and are shown in Fig. 4.11. The polarity of solvents clearly show their profound effect on the 2PA bands in the spectra region 500-700nm. We observed two 2PA bands in the range from 500nm to 700nm (indicated by arrows in Fig. 4.11). In all solvents, the positions of 2PA bands (2) are located exactly at the position of the vibronic shoulder of the linear absorption spectra, so this 2PA band results from vibronic coupling breaking the system symmetry of molecule PD 2646. Therefore, the other 2PA band (1) could result from the existence of an asymmetric charge distribution for the symmetric molecule. The "fraction" of the asymmetric charge distribution decreases in less polar solvents, which can explain in Fig. 4.11 how the 2PA cross section for band (1) is smaller in the less polar solvent 1,2-dichlorobenzene than in methanol and ethnaol. We also notice that the 2PA cross section for band (2) is bigger in 1,2-Dichlorobenzene than that in methanol and ethanol.

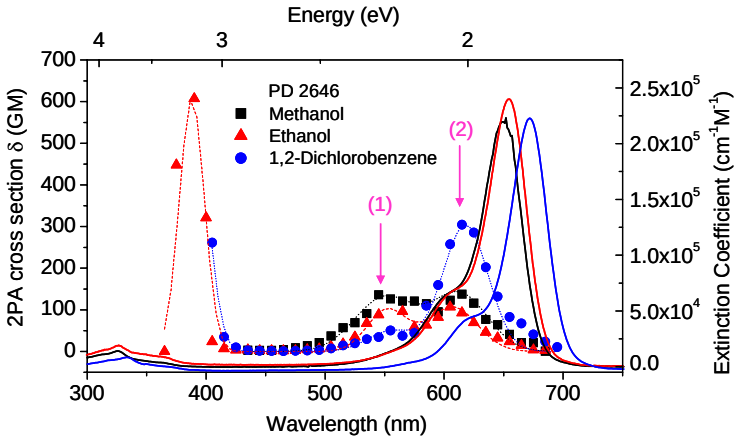

Figure 4.11 2PA spectra for PD 2646 in different solvents: methanol (black), ethanol (red) and 1,2-Dichlorobenzene (blue). Dashed line is a guide for the eye. Solid lines are linear absorption spectra in different solvents for comparison.

2PA spectra for asymmetric PD 2755 in methanol, ethanol and 1,2-Dichlorobenzene are taken with the 2PF method and are shown in Fig. 4.12. Two arrows indicate that there are two 2PA bands for PD 2755 in ethanol. We also can see the similar two 2PA bands for PD 2755 in Dichlorobenzene. Band (1) is located at the position of the vibronic shoulder of the linear absorption spectrum due to vibrational coupling. Band (2) corresponds to the linear absorption peak. Because PD 2755 is an asymmetric molecule, 2PA into the first excited state S_1 is allowed. We can also consider band (2) is due to the asymmetric charge distribution of PD 2755, so the 2PA cross section of band (2) is smaller in the less polar solvent 1,2-dichlorobenzene than it is in ethanol, as experimentally observed.

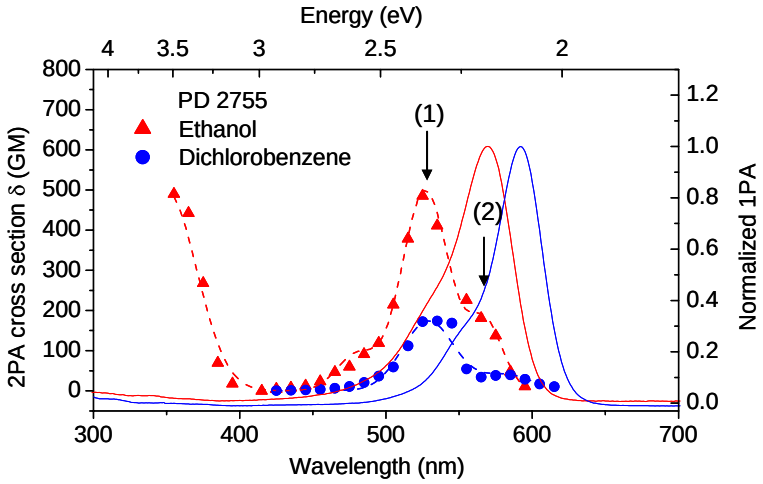

Figure 4.12 2PA spectra for PD 2755 in different solvents: ethanol (blue) and 1,2-dichlorobenzene (red). Dashed line is for a guide for the eye. Solid lines are linear absorption spectra in different solvents for comparison.

These experimental studies are just preliminary results for investigating the nature of the weak 2PA band and symmetry breaking for symmetric molecules. More experiments and detailed quantum chemical calculations are needed to fully understand this nature.

4.7 Effect of bridge

We studied the effect of placing bridge molecules in the middle of conjugated chains on the 2PA properties by comparing PD 2646 with PD 200, as well as PD 3428 with PD 2093. Molecular structures are shown in Fig. 4.13 (a) and Fig. 4.14 (a). Degenerate 2PA spectra of these molecules in the solvent ethanol were taken by using 2PF spectroscopy and Z-scan. 2PA spectra as well as linear absorption spectra with extinction coefficients are shown in Fig. 4.13 (b) and Fig. 4.14 (b). Here the 2PA cross-section δ is plotted versus the half of input photon wavelengths.

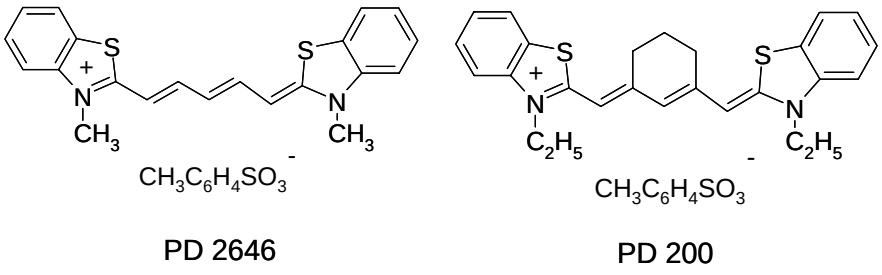

(a)

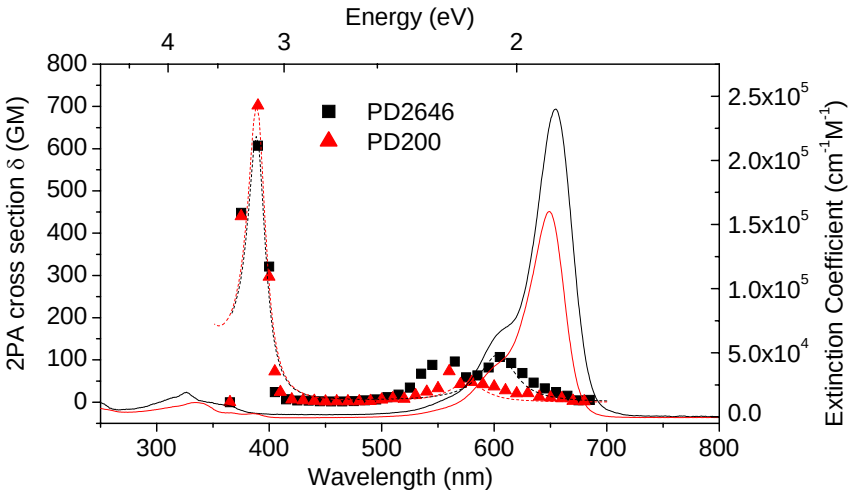

(b)

Figure 4.13 (a) molecular structures; (b) degenerate 2PA spectra for PD200, PD2646, dashed line is for theoretical fitting based on Eq. (2.55), and linear absorption spectra (solid line) are shown for reference.

Introduction of the bridges (or partial cyclization of the chain) with the goal of increasing the photochemical stability, depending on the position of cyclization, leads to blue shifts (compare PD 2646 with PD 200) or red shifts (compare PD 3428 with PD 2093) of the linear absorption peaks relative to the unbridged chromophores.

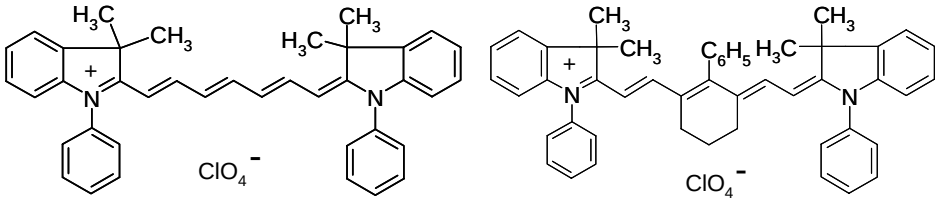

(a)

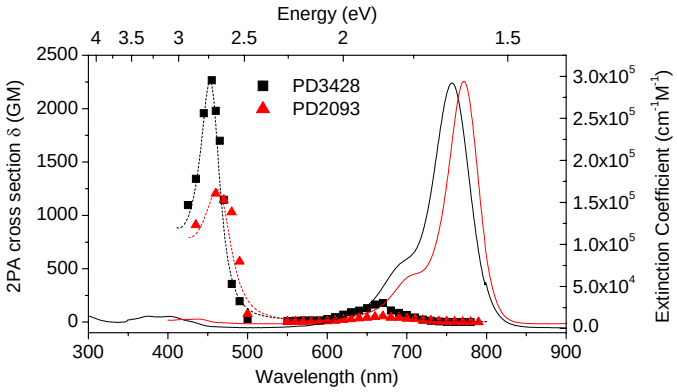

(b)

Figure 4.14 (a) molecular structures; (b) degenerate 2PA spectra for PD3428, PD2093, dashed line is for theoretical fitting based on Eq. (2.55), and linear absorption spectra (solid line) are shown for reference.

We note that the bridged structures (PD 200, PD 2093) are characterized by smaller values of 2PA cross section δ in the first 2PA band. From Section 4.6, this weak 2PA band is due to symmetry breaking of symmetric molecules. So it is reasonable to consider that the

introduction of the bridges can protect the symmetric molecular structure from this symmetry breaking, thus the smaller 2PA cross section δ.

CHAPTER 5 STRUCTURE-PROPERTY OF SQUARAINE, CROCONIUM AND TETRAON

5.1 Squaraine dyes

Squaraine dyes (SDs) also belong to the family of cyanines. SDs insert an electron acceptor C_4O_2 fragment at the center of the chromophore chain, which can be chemically considered as a simultaneous cyclization of the polymethine chain by the C=O bridge shown in Fig.5.1 (a). Introduction of the anionic substitute O^- to the central position of the polymethine molecule makes the squaraine molecule formally neutral, or more correctly, it can be considered as a bi-ionic molecule with separated positive and negative charges. By placing terminal groups R_1 and R_2, we studied SDs with different structures shown in Fig.5.1 (b), which are synthesized at the Institute of Organic Chemistry, National Academy of Science, Kiev, Ukraine by standard methods as described in Ref. [64]. There are other SDs shown in Fig.5.11 in Section 5.4, which are synthesized by Dr. Seth Marder's group at the School of Chemistry and Biochemistry and Center for Organic Photonics and Electronics, Georgia Institute of Technology, Atlanta.

Similar to polymethine dyes (PDs), Squaraine dyes are also attractive for 2PA due to three advantages: 1) they show large ground-state transition dipole moments; 2) they have close to parallel orientation of their ground- and excited-state transition dipole moments; 3) their even sharper (than for PDs) low-energy side of the linear absorption spectra allows significant intermediate state resonance enhancement of the 2PA. The comparison of 2PA property between SDs and PDs will be discussed in Section 5.2

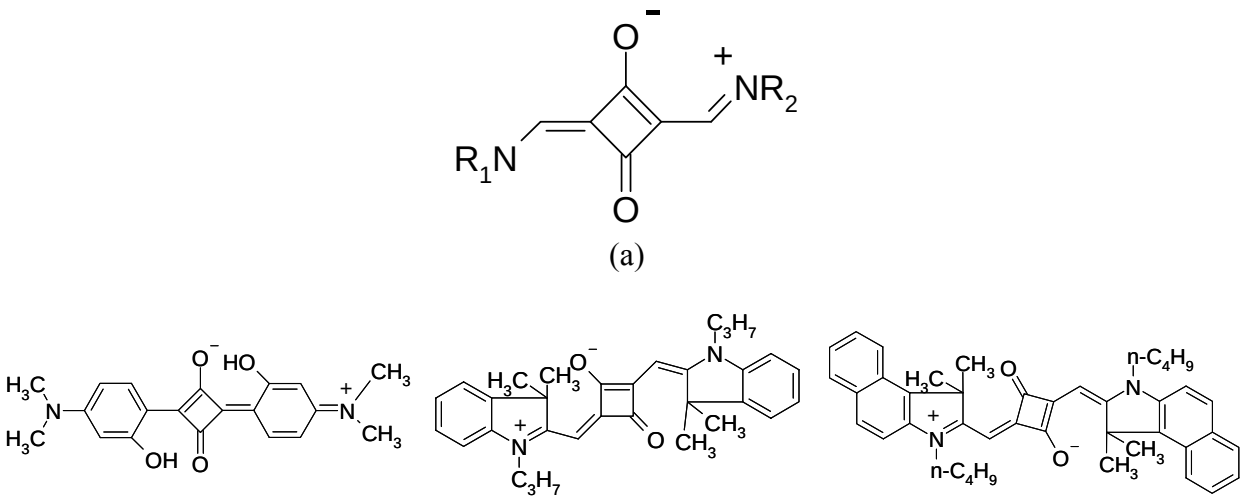

Figure 5.1 Squaraine dyes (SDs): (a) electron acceptor C_4O_2 fragment at the center of the chain, R_1 and R_2 are terminal groups; (b) SDs synthesized in Institute of Organic Chemistry, National Academy of Sciences, Ukraine

5.2 Comparison between polymethines and squaraines

We performed experimental and theoretical studies for two polymethine dyes (PDs) and two squaraine dyes (SDs) with analogous structures to study the effects of the squaraine on the 2PA properties and provide a deeper insight into the nature of 2PA processes.

The molecular structures are shown in Fig. 5.2 (a) and Fig. 5.3 (a). SD 2577 and PD 2350 have the same indolium terminal groups and similar conjugation lengths. SD 2243 and PD 2630 also have the same benzoindolium terminal groups and similar conjugation lengths. Linear absorption and fluorescence spectra are shown in Fig. 5.2 (b) and 5.3 (b). Experimental data show that SDs have narrower linear absorption bands than PDs allowing a smaller detuning energy, ΔE, to be accessed for 2PA, leading to a larger intermediate state resonance enhancement, and thus a larger 2PA cross section. SDs typically are characterized by narrower absorption

bands because of the smaller change in bond lengths when excited by a photon. The Central acceptor group leads to a less pronounced bond alternation as compared to PDs. Therefore their Frank-Condon potential curves (ground and excited) are less shifted with respect to each other.

Degenerate 2PA spectra of these molecules were also taken by using 2PF spectroscopy and Z-scan. 2PA spectra as well as linear absorption spectra with extinction coefficients are shown in Fig. 5.2 (c) and 5.3 (c). The 2PA cross section δ is plotted versus the half of input photon wavelengths. A summary of ground state transition dipole moments μ_{01}, calculated excited state transition dipole moments μ_{12}, maximum 2PA cross section δ_{max}, as well as detuning energy ΔE are shown in Table 5.1 and Table 5.2. PD 2350, SD 2577 and PD 2630 are measured in ethanol, but SD 2243 is measured in CH_2CL_2 due to poor solubility in ethanol.

Table 5.1 Parameters for polymethine and squaraine with analogous structures: PD2350 and SD2577 in ethanol

Molecules	μ_{01}(debye)	μ_{12}(debye)	$\delta_{max}1$	$\delta_{max}2$	$\delta_{max}3$	ΔE^*
PD2350	14.7	2.8	130 GM	710 GM	N/A	0.31eV
SD2577	12.2	4.2	36 GM	740 GM	5000 GM	0.21eV

* Detuning energy ΔE for PD 2350 is calculated for 2PA peak $\delta_{max}2$, and ΔE for SD2577 is calculated for 2PA peak $\delta_{max}3$

Table 5.2 Parameters for polymethine and squaraine with analogous structures: PD2630 and SD2243

Molecules	μ_{01}(Debye)	μ_{12}(Debye)	$\delta_{max}1$	$\delta_{max}2$	$\delta_{max}3$	ΔE
PD2630	14	3.1	140 GM	980 GM	> 1200 GM	0.21 eV
SD2243	13.8	3.5	80 GM	1000 GM	>7000 GM	0.2 eV

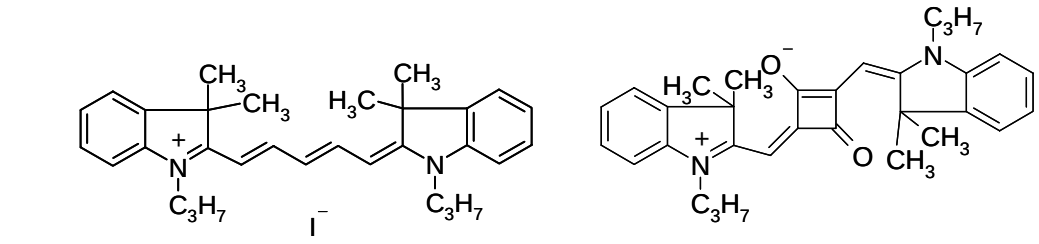

(a)

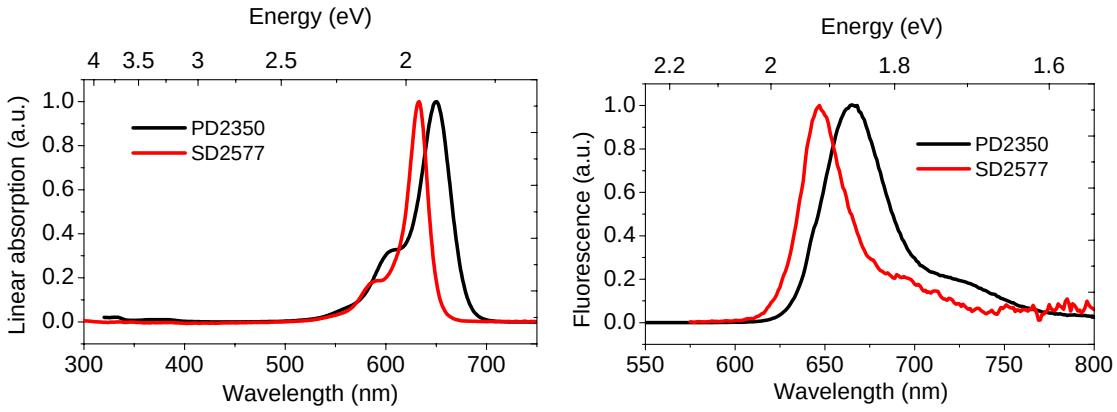

(b)

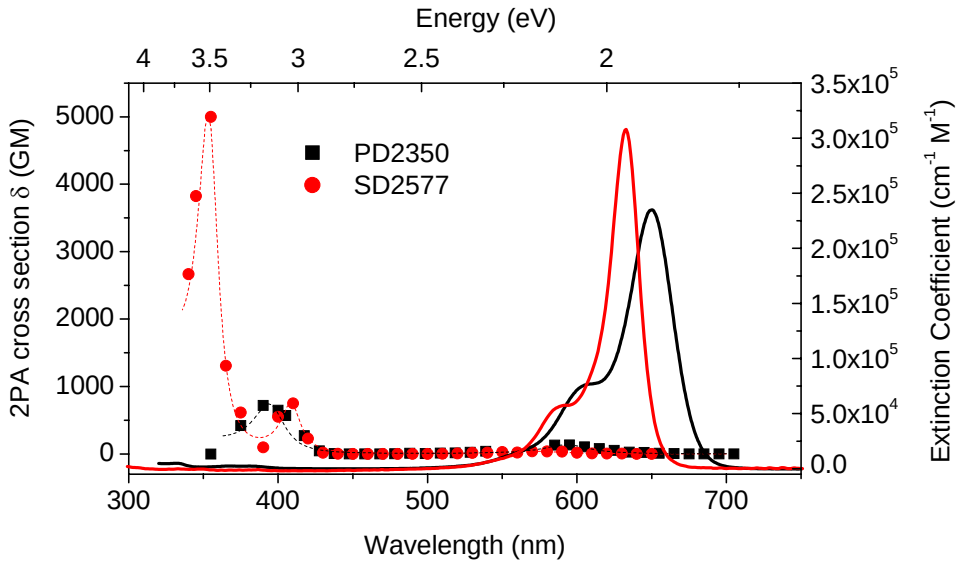

(c)

Figure 5.2 (a) Molecular structure of PD2350 and SD2577; (b) Linear absorption and fluorescence spectra in ethanol; (c) 2PA spectra in ethanol (dotted, dashed line for theoretical fitting) and linear absorption spectra (solid lines) shown as extinction coefficient

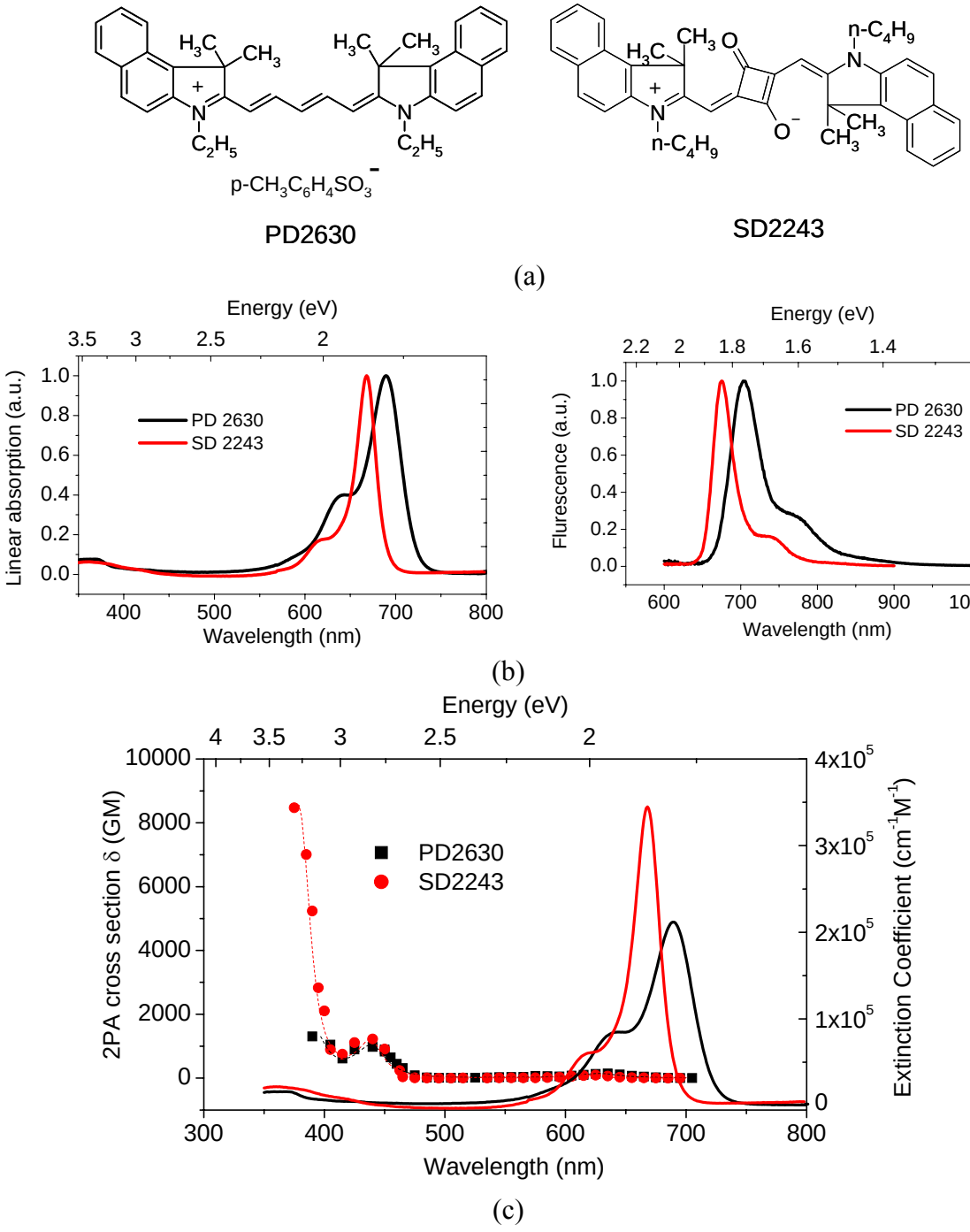

Figure 5.3 (a) Molecular structure of PD2630 and SD2243; (b) Linear absorption and fluorescence spectra; (c) 2PA spectra (doted, dashed line for theoretical fitting) and linear absorption spectra shown as extinction coefficient. PD 2630 in ethanol and SD 2243 in CH_2CL_2

1) Weakly allowed 2PA band:

Our measurements show the existence of a weakly allowed 2PA band within the vibronic shoulder of the first absorption band, $S_0 \rightarrow S_1$, for which the transition is forbidden by dipole selection rules for these symmetrical molecules. It is commonly accepted that two-photon excitation to S_1 involves two dipole moments: $\boldsymbol{\mu_{01}}$ and $\boldsymbol{\Delta\mu}$ (vector difference between permanent S_0 and S_1 dipoles). According to the traditional quantum-chemical theories [59], for symmetrical polymethine dyes (symmetry C_{2v}) $\boldsymbol{\Delta\mu}$ is oriented perpendicular to $\boldsymbol{\mu_{01}}$ and for the symmetrical squarylium dyes (symmetry C_{2i}) $\boldsymbol{\Delta\mu} = 0$ which would both prohibit 2PA to the S_1 state.

Cross sections for these weak 2PA bands are: 140 GM for PD 2350 (peak position at ≈ 590 nm); 40 GM for SD 2577 (peak position at ≈ 570 nm); 160 GM for PD 2630 (peak position at ≈ 625 nm), and 85 GM for SD 2243 (peak position at ≈ 625 nm). We note that cross sections for squaraine dyes are smaller than for polymethines, which may be connected with the different molecular symmetry. As was already mentioned, symmetrical polymethine dyes have C_{2v} symmetry and a non-zero $\boldsymbol{\Delta\mu}$ value. As a result, this band is slightly allowed by dipole selection rules in contrast to being a forbidden band in the centrosymmetrical SDs with $\boldsymbol{\Delta\mu} = 0$.

2) Main 2PA bands:

Considering the more intense 2PA bands, for PD 2350 shown in Fig. 5.2 (c), our measurements reveal the position of the second 2PA band at ~ 390 nm (~780nm excitation) with $\delta_{2PA} \approx 720$ GM. Further tuning of the excitation wavelength into the shorter wavelength region is impossible due to the presence of one-photon absorption from the $S_0 \rightarrow S_1$ band.

Fig. 5.2 (c) shows the analogous information for SD 2577. In contrast to PD 2350, the 2PA spectrum for SD 2577 includes three bands: a weakly allowed band at the vibronic shoulder

of the $S_0 \rightarrow S_1$ transition, a more intense band at ~ 408 nm with $\delta_{2PA} \approx 760$ GM, and a much more intense band at ~ 350 nm with $\delta_{2PA} \approx 5200$ GM.

Between the peak of the first absorption band and the position with twice that energy, i.e. the "double resonance" position, there are *two* 2PA bands for PD2350 and *three* 2PA bands for SD2577 that are experimentally observable

The 2PA spectrum for PD 2630, presented in Fig. 5.3 (c), is more complicated than for PD 2350. In contrast to PD 2350, there is no strong decrease in δ_{2PA} after the second 2PA band ($\delta_{2PA} \approx 920$ GM at 440 nm). We observe an increase in δ_{2PA} to ≈ 1320 GM at an excitation wavelength of 780 nm, the shortest wavelength at which 2PA measurements may be performed in this molecule due to the linear absorption tail. This increase in δ_{2PA} may be the beginning of a third 2PA band. This new band is connected with the larger π conjugation length in the benzoindolium terminal groups, and will be discussed more in Section 5.3.

Figure 5.3 (c) also shows the 2PA spectrum for SD 2243 with the same terminal groups as for PD 2630. The 2PA trends for both dyes are similar. For the second 2PA peak at 440 nm, SD 2243 shows a similar value of $\delta_{2PA} \approx 1200$ GM, however, for the next 2PA band, the experimentally observable δ_{2PA} is considerably larger, reaching ≈ 8660 GM for the shortest possible excitation wavelength of 730 nm. The peak position and strength of this band cannot be resolved for the same reason as for PD 2630, i.e. linear absorption loss.

In summary, PDs and SDs show comparable 2PA cross sections and positions for the second 2PA band ($\delta_{max}2 \approx 720$ GM for PD2350 and 760 GM SD2577 at around 400nm, see Table 5.1; $\delta_{max}2 \approx 980$ GM for PD2630 and 1000 GM SD2243 at around 421nm, see Table 5.2). For the case of PD2350 and SD2577, as determined by quantum-chemical calculations as shown

in Section 5.3, introduction of the donor indolium terminal groups to the unsubstituted polymethine chain increases the density of the occupied molecular orbitals, and thus the number of electronic transitions between the first band $S_0 \rightarrow S_1$, and the position of twice the energy of the first band. Relatively high $\delta_{2PA} \approx 700$ GM can be observed due to a strong coupling of initial and final molecular orbitals via the intermediate level.

Quantum-chemical calculations (see Section 5.3) show another way to increase the number of active two-photon transitions by increasing the density of unoccupied molecular orbitals. This was achieved by introducing acceptor fragments to the squaraine molecules. The distinguishing feature of SD2577 is the possibility to access the third and most intense 2PA band. This higher lying third 2PA band ($\delta_{max}3 \approx 5200$ GM for SD2577) displays a much larger δ due to a decrease in the detuning energy ΔE leading to a large enhancement of cross section values, i.e. significant resonance enhancement of the 2PA cross section for both the intermediate and final states.. This peak is observable just below the linear absorption edge.

5.3 Quantum-chemical calculations and analysis

5.3.1 Methodology of quantum-chemical calculations

Quantum-chemical calculations are performed by Dr. Olga V. Przhonska and her colleagues at Institute of Organic Chemistry, National Academy of Sciences, Ukraine. Quantum-chemical calculations were performed with the goal of understanding the spectral position of 2PA bands and revealing the origin of the high 2PA cross section δ_{2PA} in squaraine molecules. Quantum-chemical calculations were carried out at the Institute of Organic Chemisty, National Academy of Sciences, Ukraine. For the calculations of the positions of the electronic levels and

the shapes of the molecular orbitals, a well-known MOLCAO (Molecular Orbital as a Linear Combination of Atomic Orbitals) method was used [59]. The wavefunction of the *i*-th molecular orbital (MO) φ_i was written as an expansion of the atomic orbitals χ_μ:

$$\varphi_i = \sum_\mu C_{i\mu}\chi_\mu \tag{5.1}$$

where $C_{i\mu}$ are the corresponding coefficients, and the summation runs over all the atomic orbitals. We note that $C_{i\mu}^2$ is the probability of the location of an electron in the *i*-th MO in the neighborhood of the μ-th atom [59]. Calculations were performed in the framework of the standard semi-empirical approximations (HyperChem package). The equilibrium molecular geometries were calculated employing the Austin Model 1 (AM1) method with the energy change step, i.e. gradient, 0.01 kcal/mol. It was established previously that the lengths of the carbon-carbon bonds calculated in this method are in good agreement with the corresponding values obtained by an ab initio approximation [65].

The π-system of all molecules was found to be planar. Characteristics of the electron transitions were obtained in the ZINDO/S approximation with spectral parameterization. The wavefunction of the *p*-th excited state Ψ_p was built as an expansion of the electronic configurations $\Phi_{i\to j}$ corresponding to electron transfer from the occupied *i*-th to vacant *j*-th orbital:

$$\psi_p = \sum_{i,j} T_{p,i\to j}\Phi_{i\to j} \tag{5.2}$$

where $T_{p,i\to j}$ are the normalized coefficients, and indices *i* and *j* run over all MOs. $\sum_{i,j} T_{p,i\to j}^2 = 1$ is a normalization condition. In our calculations we used all $\pi \to \pi^*$ single excited

configurations, with the overlap weight factor (OWF) equal to 0.5. All calculations were performed on isolated molecules neglecting solvent effects.

Here quantum-chemical calculations have been performed with the goal of understanding the 2PA spectra for cationic polymethines and neutral squaraines having analogous structures and uncover the origin of the high 2PA cross section δ_{2PA} for squaraine molecules. For these purposes we considered the evolution of the molecular orbitals and electronic transitions from the unsubstituted polymethine chain: $H_2C^+ – (CH = CH)_2 – CH = CH_2$ to the cationic PD 2350, PD 2646, PD 2630 and neutral SD 2577. Schemes of some higher occupied and lower unoccupied molecular orbitals, as well as the corresponding transitions between them are presented in Figs. 5.4 and Table 5.3. In our considerations we limited the number of molecular orbitals to the number of electronic transitions participating in one- and two-photon absorption between $S_0 \rightarrow S_1$ and its "double resonance" position.

Table 5.3 Calculated parameters for the unsubstituted polymethine chain, PD 2350 and SD 2577

Dye	Transition	Symmetry of final states	λ nm	Oscillator strength	Main configuration
Unsubstituted chain	$S_0 \rightarrow S_1$	$1B_1$	551	1.65	0.96| H→L>
	$S_0 \rightarrow S_2$	$2A_1$	315	0.002	0.97| H-1→L>
	$S_0 \rightarrow S_3$	$3A_1$	291	0.08	0.97| H→L+1>
PD 2350	$S_0 \rightarrow S_1$	$1B_1$	655	1.6	0.96| H→L>
	$S_0 \rightarrow S_2$	$2A_1$	460	0.01	0.94| H-1→L>
	$S_0 \rightarrow S_3$	$2B_1$	410	0.07	0.92| H-2→L>
	$S_0 \rightarrow S_4$	$3A_1$ (local)	395	0.02	0.95| H-3→L>
	$S_0 \rightarrow S_5$	$3B_1$	386	0.06	0.93| H-4→L>
	$S_0 \rightarrow S_6$	$4A_1$	352	0.05	0.95| H→L+1>
SD 2577	$S_0 \rightarrow S_1$	$1B_u$	630	1.7	0.97| H→L>
	$S_0 \rightarrow S_2$	$2A_g$	480	0	0.87| H-1→L>
	$S_0 \rightarrow S_3$	$2B_u$	465	0.005	0.85| H-2→L>
	$S_0 \rightarrow S_4$	$3A_g$ (O-O)	456	0.34	0.45| H→L+2> + 0.85| H→L+3>
	$S_0 \rightarrow S_5$	$4A_g$	410	0	0.87| H→L+1>
	$S_0 \rightarrow S_6$	$3B_u$	386	0.03	0.54| H-4→L> + 0.66| H→L+3>
	$S_0 \rightarrow S_7$	$5A_g$ (local)	384	0	0.96| H-3→L>
	$S_0 \rightarrow S_8$	$4B_u$	378	0.2	0.63| H-4→L> + 0.52| H→L+3>

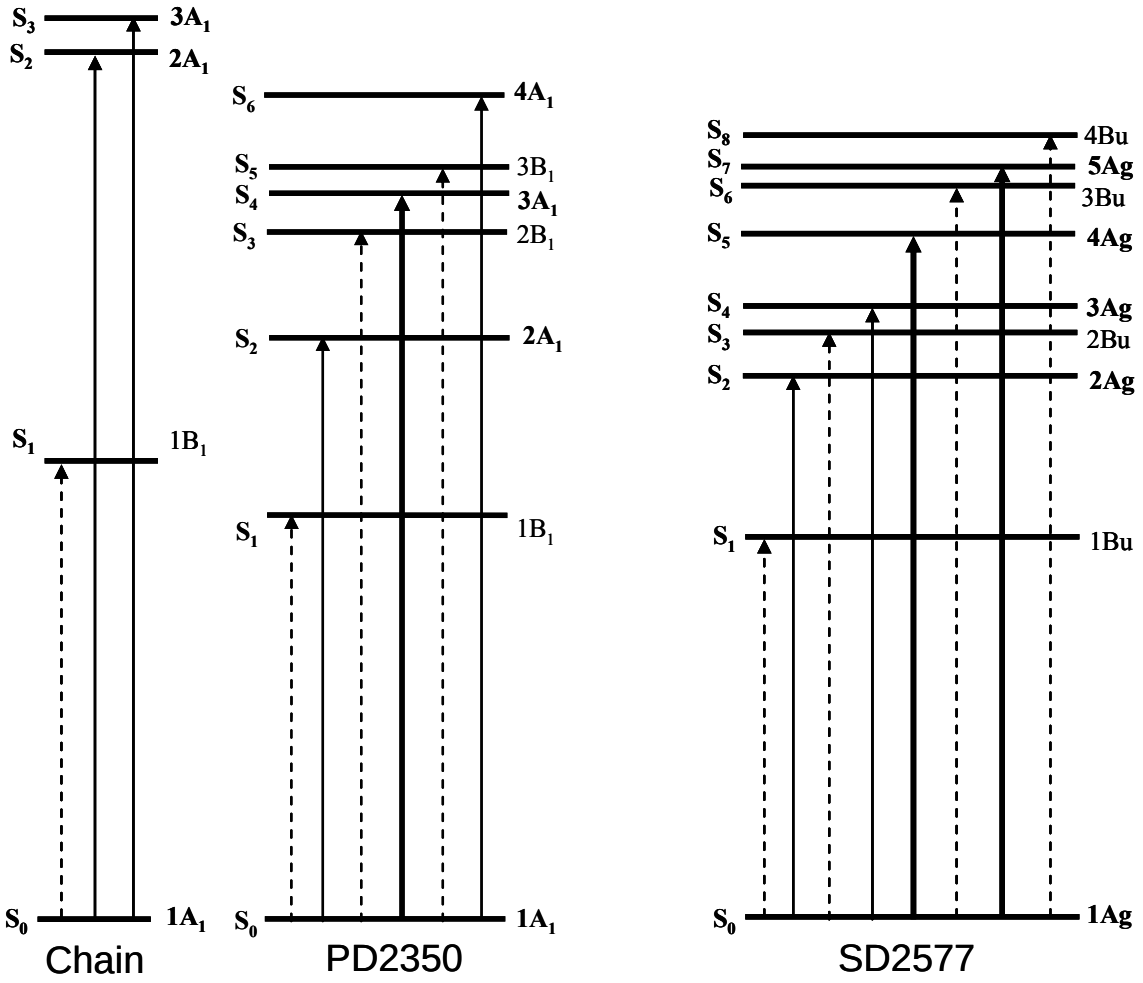

Figure 5.4 Scheme of the electronic transitions for the unsubstituted chain, PD 2350 and SD 2577. Dashed lines indicate one-photon allowed transitions; solid lines indicate allowed two-photon transitions; bold solid lines indicate experimentally observed two-photon transitions.

5.3.2 Unsubstituted polymethine chain

Quantum-chemical calculations of the unsubstituted polymethine chain show in Fig.5.4 – Fig. 5.6 that the ground to first excited state transition $S_0 \rightarrow S_1$ is allowed by symmetry rules ($1A_1 \rightarrow 1B_1$) and is connected with the electron transfer between the highest occupied molecular orbital (HOMO) and the lowest unoccupied molecular orbital (LUMO). The two next electronic

transitions, $S_0 \rightarrow S_2$ ($1A_1 \rightarrow 2A_1$) and $S_0 \rightarrow S_3$ ($1A_1 \rightarrow 3A_1$), are forbidden and correspond to HOMO-1 → LUMO and HOMO → LUMO+1 respectively (see Table 5.3).

These transition energies are close but not exactly equal to each other. The calculated spectral shift between the corresponding $S_0 \rightarrow S_2$ and $S_0 \rightarrow S_3$ absorption bands is ≈ 20 nm, i.e. no degeneracy. This is the origin of the main difference between the spectra of the cationic polymethine chain and its neutral polyene analogue. The polyene chain is characterized by the formation of double (for $A_u \rightarrow A_u$) and triple (for $B_g \rightarrow B_g$) degenerate configurations leading to energy level splitting and to a redistribution of oscillator strengths [22]. This makes the least energetic transition disallowed for 1PA but allowed for 2PA.

For the polymethine chain, one of the $A_1 \rightarrow A_1$ transitions approximately corresponds to a "double resonance" position of the main absorption band, which makes it impossible to reach this 2PA peak experimentally, again due to linear absorption. We emphasize that all molecular orbitals in the unsubstituted conjugated polymethine chain are totally and uniformly delocalized, and all electronic transitions are described mainly by single configurations with coefficients $T_{p,i\rightarrow j} > 0.9$ (see Table 5.3).

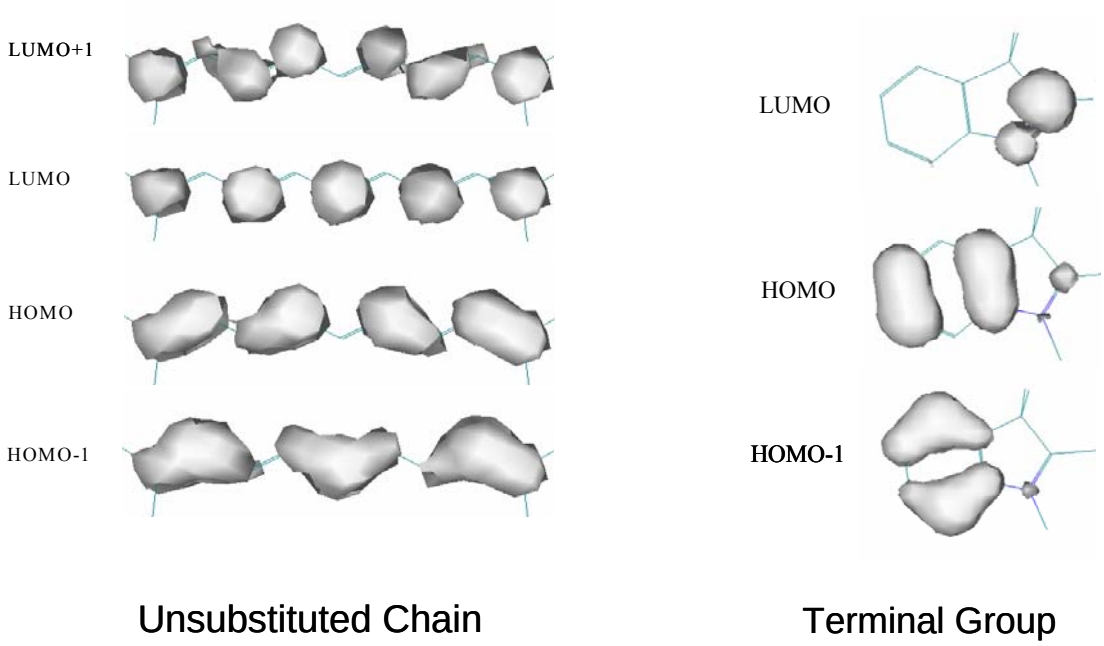

Figure 5.5 Electron density distribution in the molecular orbitals for the unsubstituted polymethine chain and indolium terminal groups.

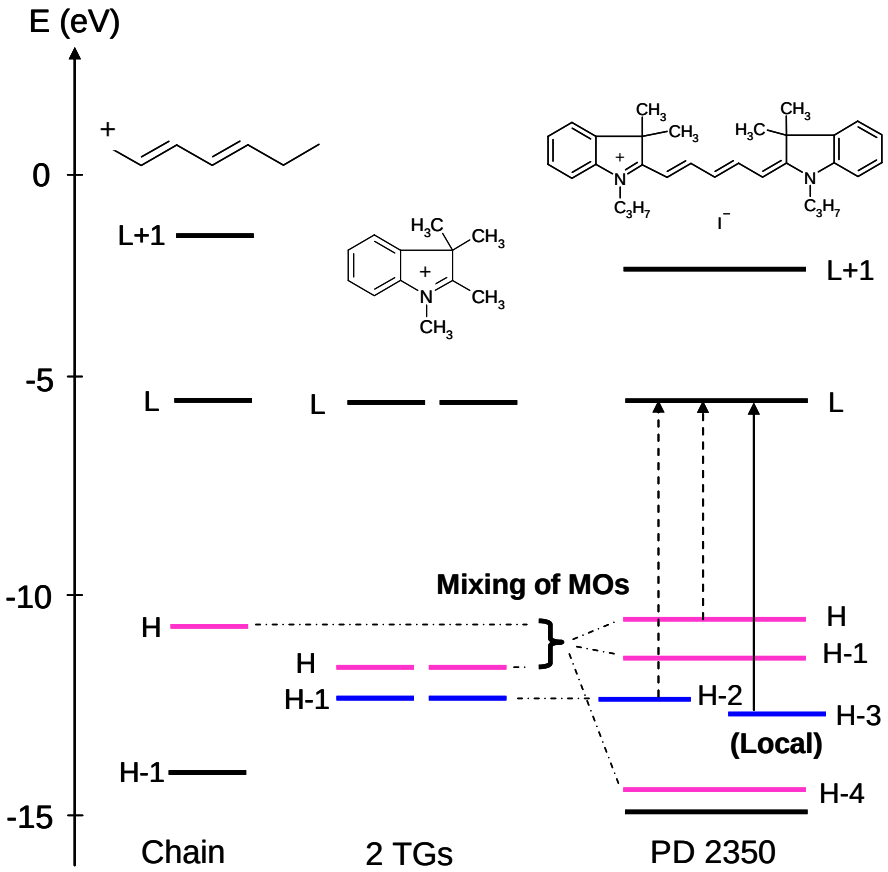

Figure 5.6 Scheme of the energy levels for molecular orbitals of the unsubstituted polymethine chain, indolium terminal groups and PD 2350. H identifies Highest Occupied Molecular Orbital (HOMO) and L identifies Lowest Unoccupied Molecular Orbital (LUMO). Dashed arrow lines indicate experimentally observed one-photon transitions and solid arrow line indicates the experimentally observed two-photon transition.

5.3.3 Polymethines

Introduction of the donor indolium terminal groups (TGs) to the polymethine chain will increase the density of the occupied molecular orbitals and thus the number of electronic transitions. Figure 5.5 presents three MOs (HOMO-1, HOMO and LUMO) belonging to each TG.

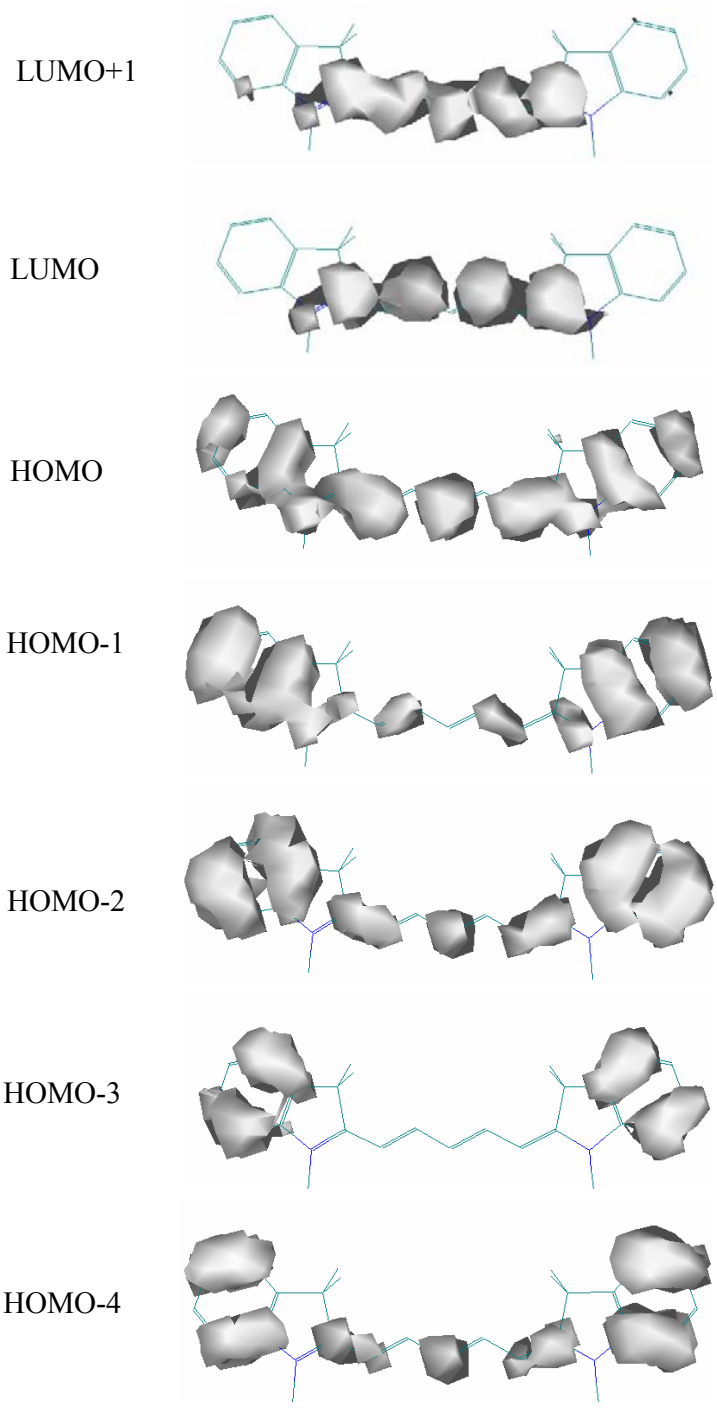

Figure 5.7 Electron density distribution in the molecular orbitals for PD 2350

As shown in Fig. 5.6 and Fig. 5.7, two HOMO orbitals of both TGs are completely mixed with the HOMO of the unsubstituted polymethine chain producing three delocalized molecular orbitals HOMO, HOMO-1 and HOMO-4. In symmetrical PDs such as PD 2350, there are two identical HOMO-1s of TGs (with charge localization only at TGs see in Fig. 5.5). This is an origin of the energy splitting. The splitting energy depends on the TG's donor properties. After splitting, one of these MOs typically mixes with the orbital of the chain producing a delocalized molecule orbital, HOMO-2, shown in Fig. 5.6 and Fig. 5.7, and the other MO remains localized at the TGs (see HOMO-3 shown in Fig. 5.6 and Fig. 5.7). Thus, the interaction of the MOs of all the molecular fragments (mixing among HOMOs from chain and two TGs) in PD 2350 leads to delocalization of the three highest occupied MOs of PD 2350 (HOMO, HOMO-1, HOMO-2 shown in Fig. 5.6). This occurs not only along the polymethine chain, but also extends through the TGs. Therefore, introduction of the indolium TGs with their own conjugated systems causes a considerable effective lengthening of the chromophore.

Note that LUMO and LUMO+1 extend the chain conjugation to the nitrogen atoms of both TGs, while the π-electron conjugations at HOMO, HOMO-1 and HOMO-2 spread out over the entire molecule. In total, 7 molecular orbitals (from HOMO-4 to LUMO+1), shown in Fig. 5.7, are necessary for the quantum-chemical analysis.

It is commonly accepted that the electron transfer between the HOMO and LUMO ($S_0 \rightarrow S_1$, $1A_1 \rightarrow 1B_1$ transition) corresponds to the intense long wavelength band in the one-photon absorption spectrum. The next transition involving practically pure HOMO-1 and LUMO (see coefficients $T_{p,i\rightarrow j}$ in the Table 5.3) and being of the $1A_1 \rightarrow 2A_1$ symmetry, should correspond to the lowest two-photon transition. However, based on the results of the quantum-chemical calculations, we suggest that only the next $1A_1 \rightarrow 3A_1$ ($S_0 \rightarrow S_4$) transition in Fig. 5.4 for PD2350,

corresponding to the electron transfer between the localized HOMO-3 and delocalized LUMO is the most active in 2PA for PD 2350. This is in agreement with the experimental spectral position of the second 2PA band seen in Fig. 5.2 at ~ 390 nm.

The existence of this local molecular orbital is of great importance for the 2PA. The transition from HOMO-3 to LUMO ($1A_1 \rightarrow 1A_3$, $S_0 \rightarrow S_4$ in Table 5.3) gives zero overlap (see in Fig.5.7), thus it requires an intermediate (HOMO) state and forms a two-photon absorbing transition. Our understanding is that the localized – delocalized electron transition, such as HOMO-3 $\rightarrow$ LUMO, which appears in the energy interval between the $S_0 \rightarrow S_1$ and its "double resonance", is responsible for the strong 2PA band with peak at 390nm.

The main characteristic feature of the 2PA spectrum for the PDs is the relatively high 2PA cross section δ_{2PA} of $\approx$ 600 – 1000 GM (for dicarbocyanines with different TGs, see the Section 4.4) due to the strong coupling of these orbitals with the intermediate HOMO, see Fig. 5.7.

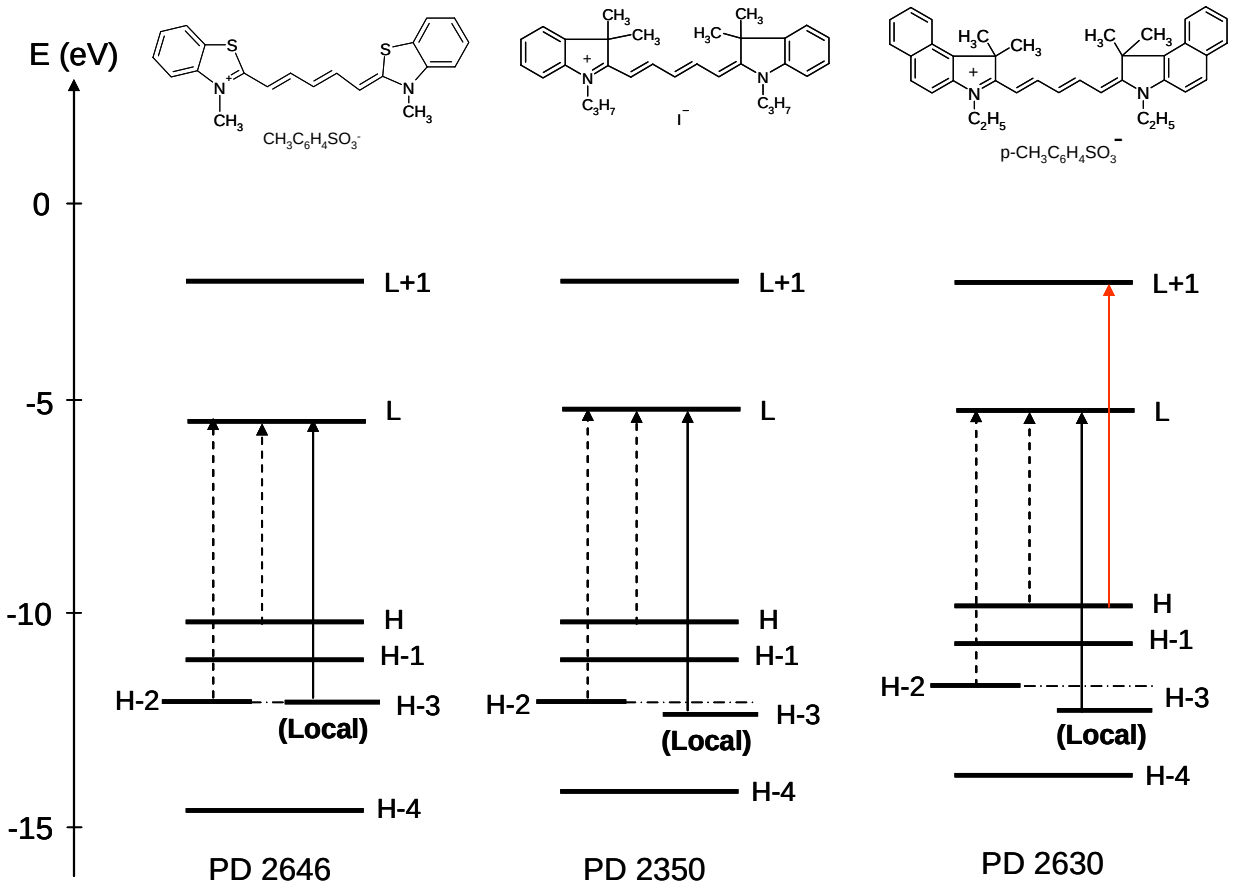

Figure 5.8 Scheme of the energy levels for molecular orbitals of PD 2646, PD 2350 and PD 2630. H identifies the Highest Occupied Molecular Orbital (HOMO) and L identifies the Lowest Unoccupied Molecular Orbital (LUMO). Dashed arrow lines indicate experimentally observed one-photon transitions and solid arrow lines indicate experimentally observed two-photon transitions.

In order to further increase the density of occupied molecular orbitals and thus the number of electronic transitions, we choose TGs with more extended π-systems. This idea was realized in PD 2630 containing more complicated benzoindolium terminal groups (see Section 4.4 and Fig. 5.8). As compared to PD 2350, this dye is characterized by red-shifted absorption bands. Note that experimentally the main one-photon absorption peak is shifted by ≈ 0.1 eV, and the 2PA band

is shifted more to the red by ≈ 0.18 eV. Due to this shift, the beginning of the next, third 2PA band (corresponding to transition HOMO → L+1 in Fig. 5.8, 1A1 → 4A1 and S_0 → S_6 in Fig. 5.4), has been experimentally measured (see Fig. 4.5(b)). Analyzing the evolution of the 2PA bands from the unsubstituted chain to PD 2350, and then to PD 2630, we assume that the spectral shift of the 2PA peak is primarily due to the terminal groups. More extended TGs may provide an additional shift increasing the number of experimentally reachable 2PA bands.

5.3.4 Squaraines

An alternative way to increase the number of active two-photon transitions, $1A_1 \rightarrow mA_1$, can be provided by an increase of the density of unoccupied molecular orbitals. This has been achieved in the dyes of another type – squaraines. Inserting the high acceptor C_4O_2 fragment in the center of the polymethine chain, while keeping the same TG, can be chemically considered as a simultaneous cyclization of the chain by the C=O bridge and introduction of the anionic substituents O^- to the central position of the PD 2350 (or PD 2630). The latter makes the SD-molecule formally neutral, or more correctly, it can be considered as a bi-ionic molecule with separated positive and negative charges.

In the case of SD 2577, five HOMO's and five LUMO's have to be considered to elucidate the nature of the allowed and forbidden transitions in the spectral area of interest, see Fig. 5.9. Shown in Fig. 5.10 the molecular orbitals of the neutral dye SD 2577 are shifted up in energy, and the distance between LUMO and LUMO+1 decreases as compared to the corresponding PD 2350. Therefore, the energies of the electronic transitions involving LUMO+1 can be smaller than twice the energy of the transition $S_0 \rightarrow S_1$, i.e. the "double resonance" energy, thus allowing experimental observation.

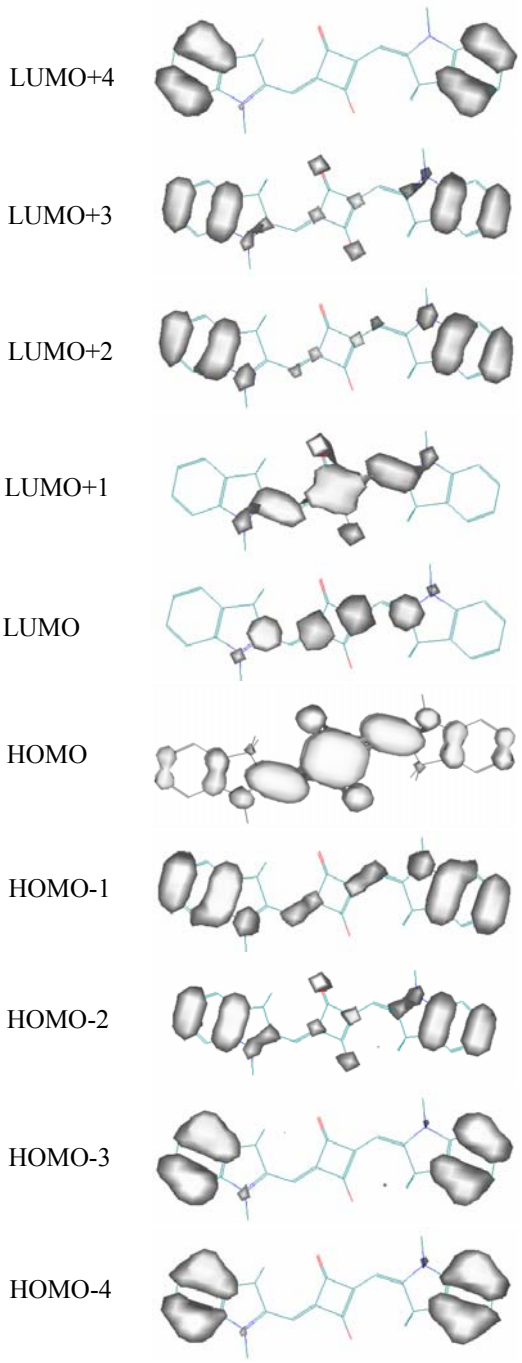

Figure 5.9 Electron density distribution in the molecular orbitals for SD 2577

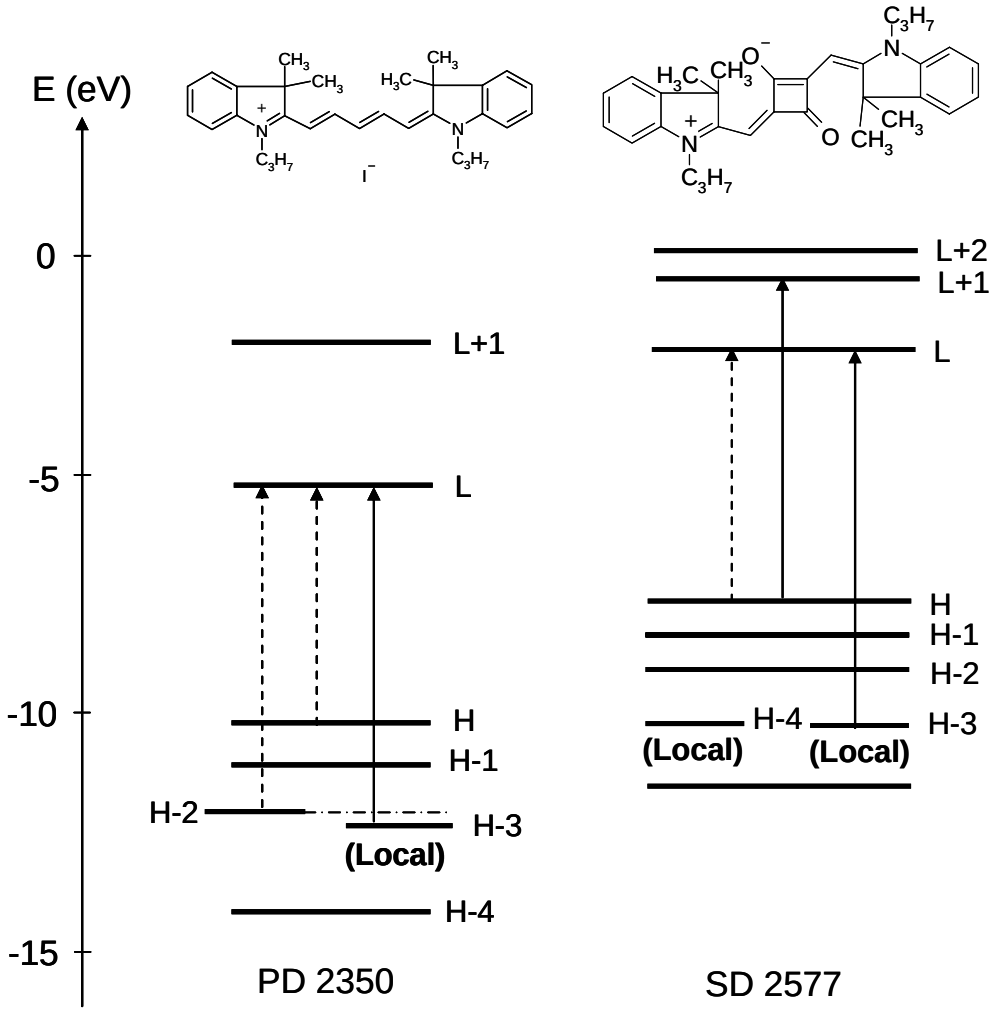

Figure 5.10 Scheme of the energy levels for molecular orbitals of PD 2350 and SD 2577. H identifies the Highest Occupied Molecular Orbital (HOMO) and L identifies the Lowest Unoccupied Molecular Orbital (LUMO). Dashed arrow lines indicate experimentally observed one-photon transitions and solid arrow lines indicate experimentally observed two-photon transitions.

The nature of the allowed $S_0 \rightarrow S_1$ transition for SD 2577 remains the same as for the PD 2350, and is connected with the electron transfer between HOMO and LUMO. Similar to PD 2350, two HOMO orbitals of both TGs for SD 2577 are also completely mixed with the orbitals of the chain producing HOMO, HOMO-1 and HOMO-2. The HOMO-1 orbitals of TGs produce

two localized molecular orbitals HOMO-3 and HOMO-4 in SD 2577 that remain mostly localized in the TGs with only a small participation of the chain, see in Fig. 5.9.

For the neutral SD 2577, the influence of the LUMOs associated with the TGs is very significant. Although the nature of LUMO and LUMO+1 is similar for PD 2350 and SD 2577 which preliminarily are associated with LUMOs from the chain, other unoccupied molecular orbitals (LUMO+2, LUMO+3) are connected to LUMOs from the TGs that mix with the molecular orbital located at the central C_4O_2.

Analysis of the quantum-chemical data shows that the following two electronic transitions are the most active for 2PA in agreement with the spectral positions of the measured bands: HOMO → LUMO+1 in Fig. 5.10 (presumably the $1A_g \rightarrow 4A_g$, $S_0 \rightarrow S_5$ transition in Fig.5.4 for SD 2577), which was unreachable in PD 2350 due to linear absorption, but becomes shifted to a lower energy region in the neutral SD2577 and thus becomes experimentally reachable. Also, the transition between the localized HOMO-3 and delocalized LUMO in Fig. 5.10 (presumably the $1A_g \rightarrow 5A_g$, $S_0 \rightarrow S_7$ transition in Fig. 5.4 for SD2577), which is analogous to the $1A_1 \rightarrow 3A_1$ transition in PD2350, is similarly shifted and can now be observed just below the linear absorption edge. These higher lying $4A_g$ and $5A_g$ states are strongly coupled to the intermediates state as is displayed in Fig. 5.9

The lower lying $3A_g$ state, connected with the charge distribution in the direction perpendicular to the long molecular axis, cannot be coupled to the intermediate state and therefore, the $1A_g \rightarrow 3A_g$ transition is not active in 2PA. As predicted, we did not observe this 2PA band experimentally. We did not observe the $1A_1 \rightarrow 2A_1$ transition for PDs and $1A_g \rightarrow 2A_g$ transition for SDs. This may be partially due to the large detuning from the intermediate level S_1, leading to smaller 2PA.

5.4 Squaraine molecules showing large 2PA cross sections

Seth Marder's group at the School of Chemistry and Biochemistry and Center for Organic Photonics and Electronics at the Georgia Institute of Technology synthesized a series of squaraine molecules in which the terminal donor groups are separated from the central acceptor squarylium core by longer conjugated bridges. The molecular structures are shown in Fig. 5.11. The 2PA spectra were acquired using open-aperture Z-scan (D-2PA) and the white-light continuum pump-probe (ND-2PA) method [44]. The experimental results are shown in Fig. 5.12

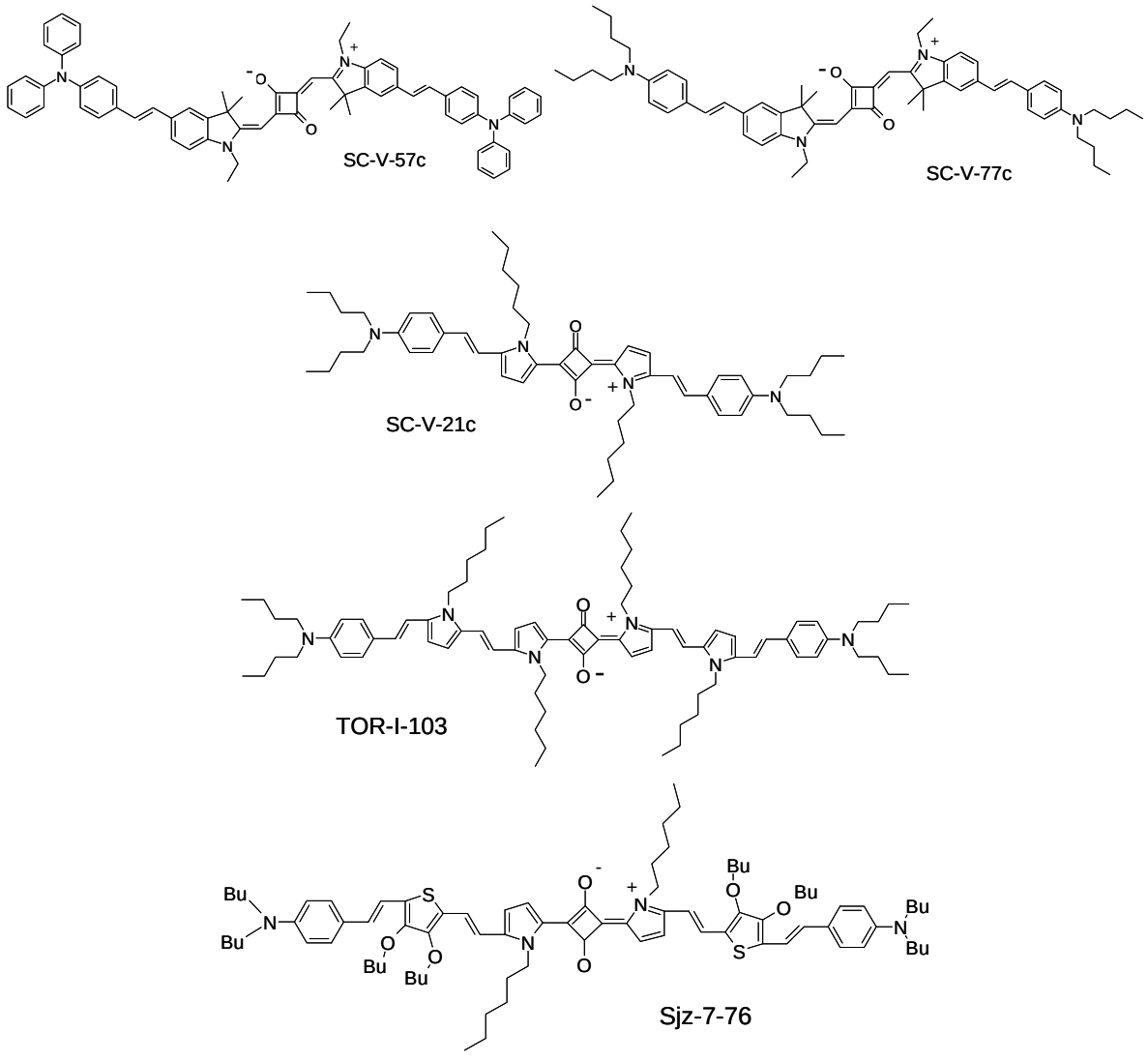

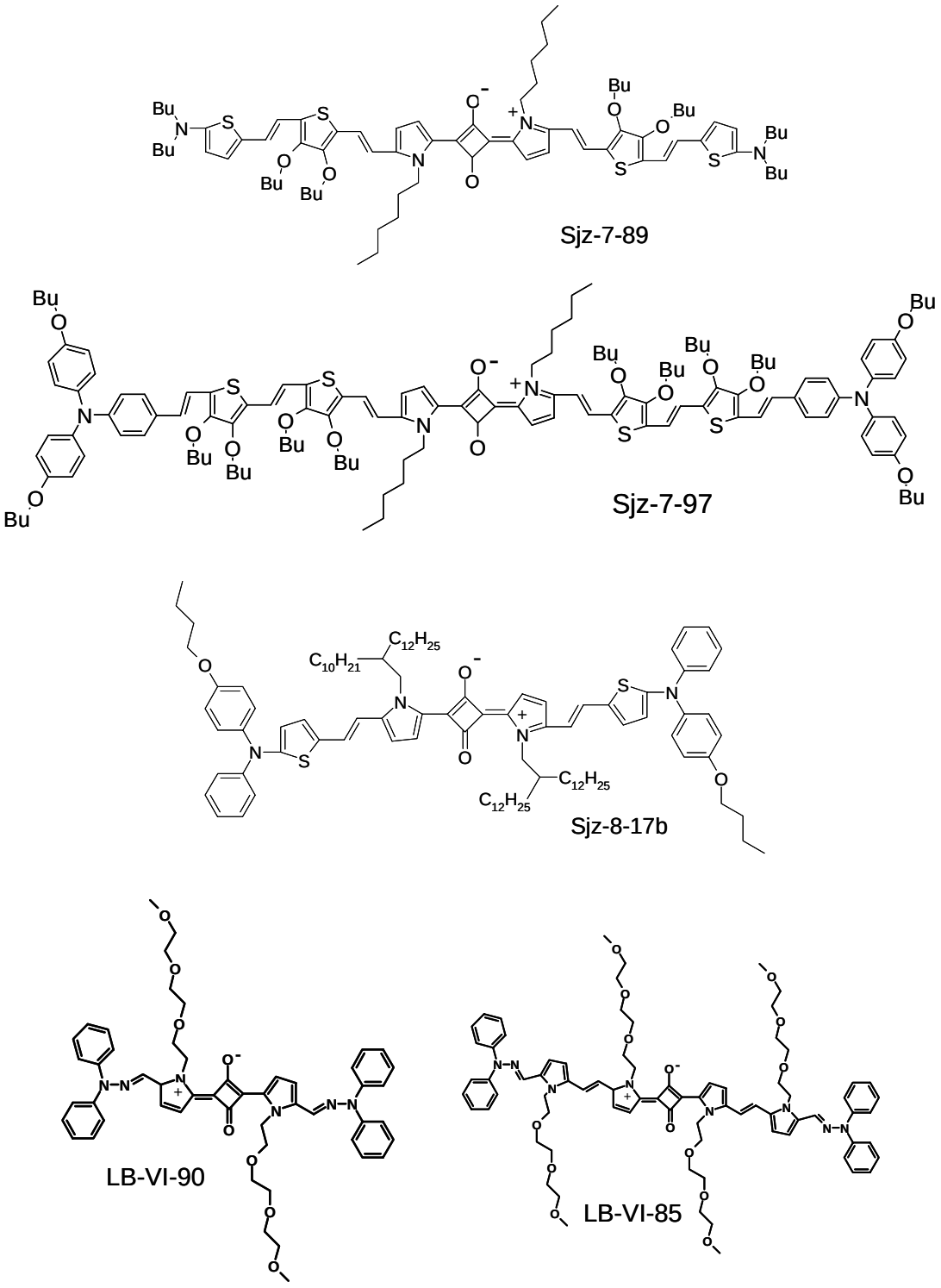

Figure 5.11 Molecular structures of squaraine dyes synthesized by Seth Marder's group at the Georgia Institute of Technology

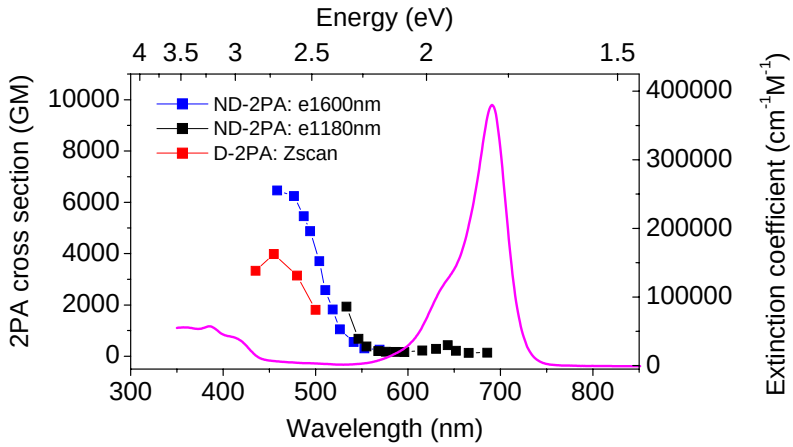

(a) **SC-V-57c** in CH_2CL_2

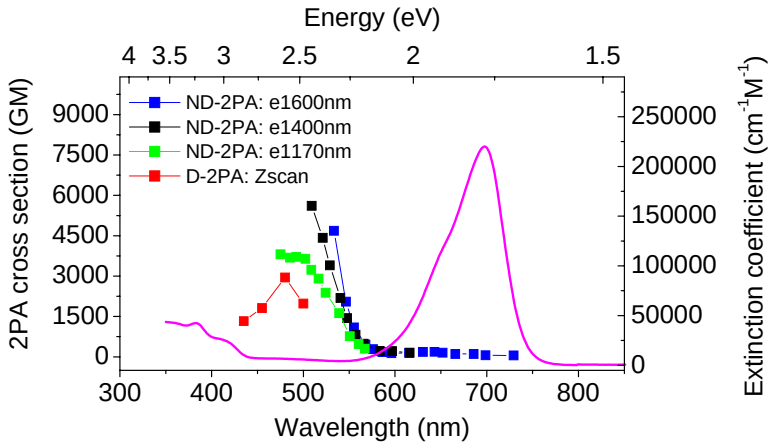

(b) **SC-V-77c** in CH_2CL_2

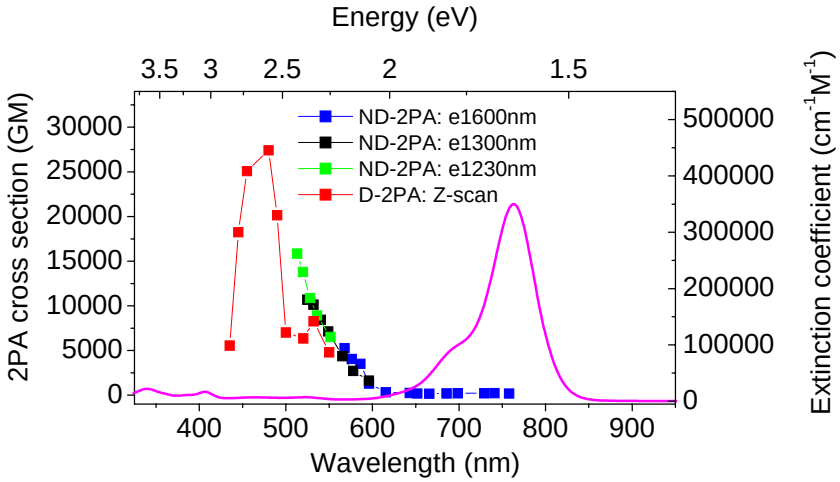

(c) **SC-V-21c** in CH_2CL_2

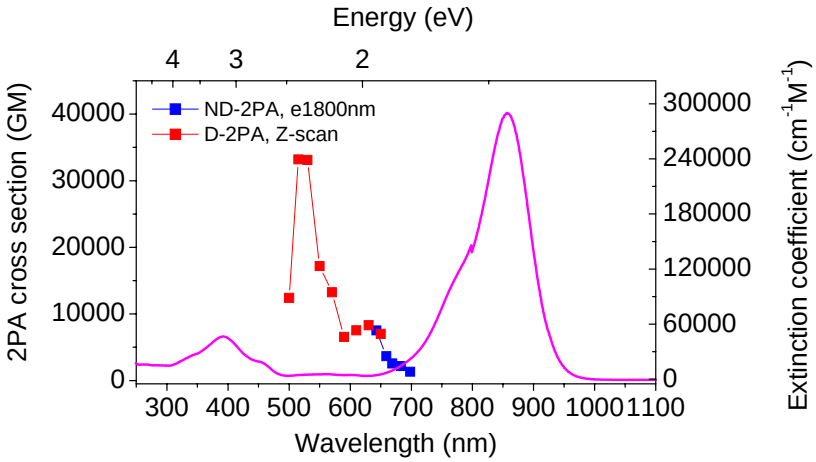

(d) **TOR-I-103** in THF

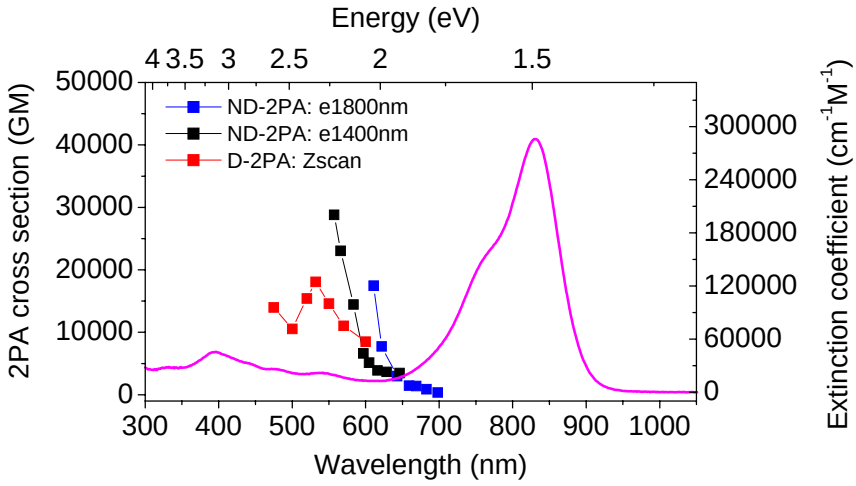

(e) **Sjz-7-76** in THF

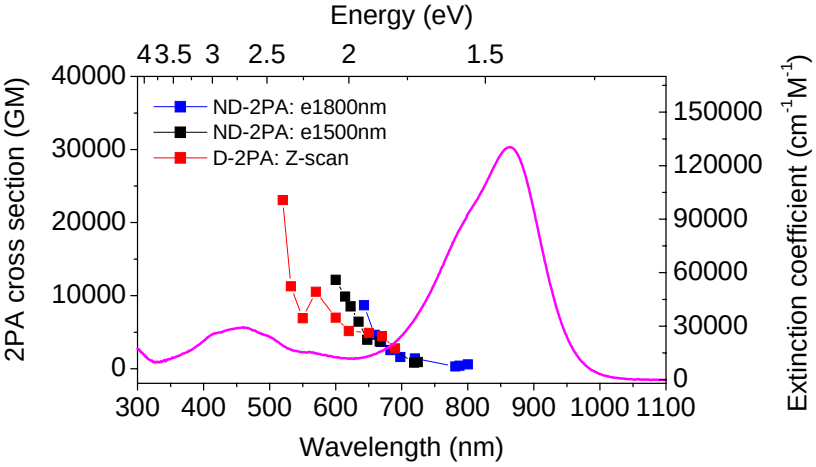

(f) **Sjz-7-89** in THF

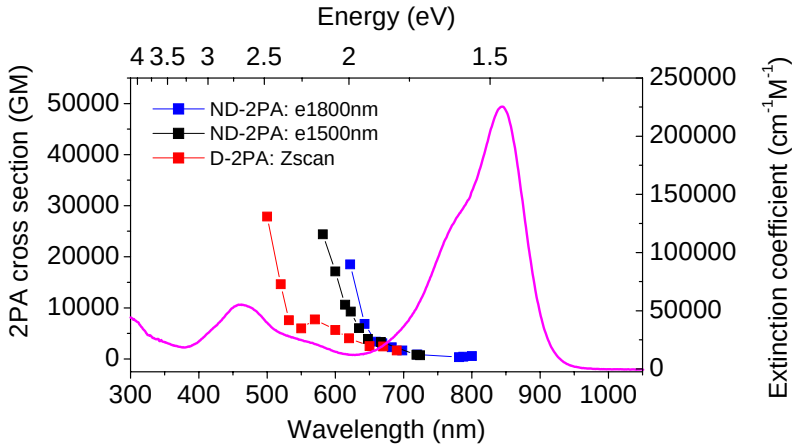

(h) **Sjz-7-97** in THF

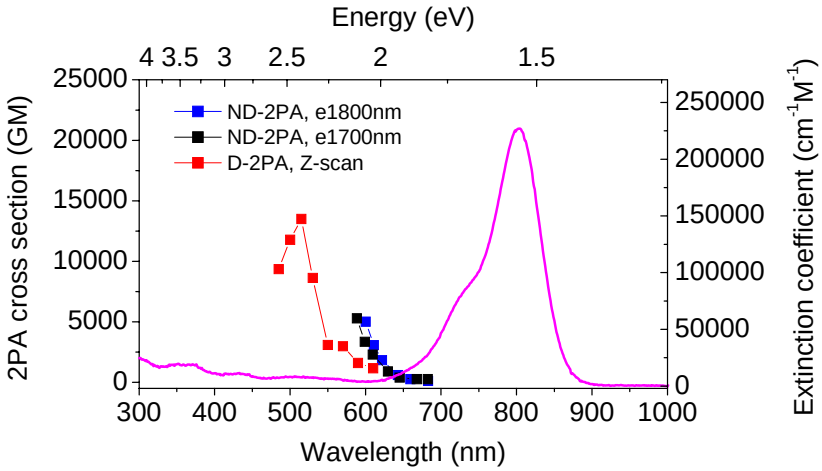

(i) **Sjz-8-17b** in THF

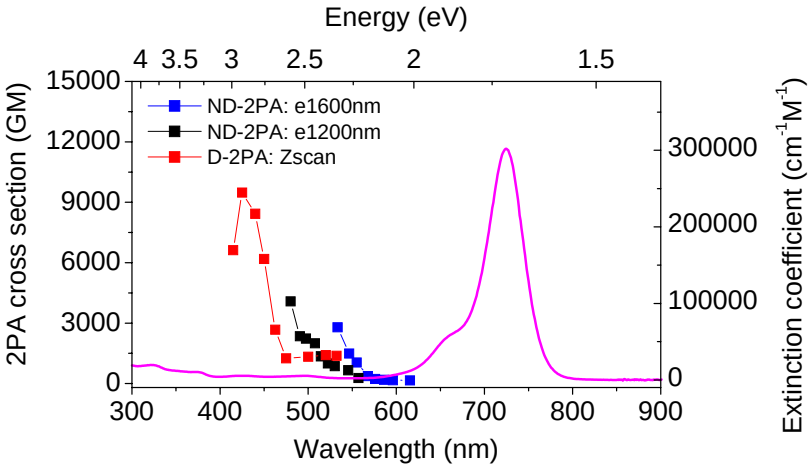

(j) **LB-IV-90** in THF

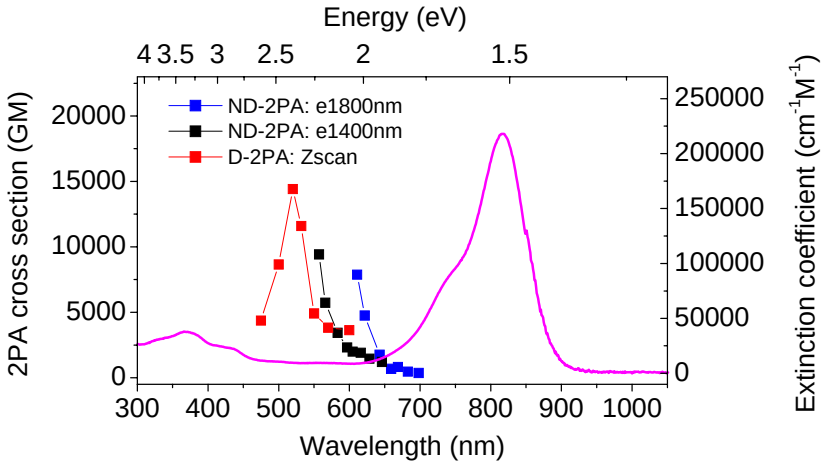

(k) **LB-IV-85** in THF

Figure 5.12 2PA spectra for squaraine dyes synthesized by Seth Marder's group at Georgia Institute of Technology. 2PA cross-section δ is plotted versus the wavelength for the 2PA state (equivalent to the sum of the two excitation photons' energies, for D-2PA, two photons have the same energies, for ND-2PA, pump and probe photons have the different energies). The pump wavelength of WLC pump-probe measurements for ND-2PA is shown in the graph.

Due to the extensive π systems of chromophores or long conjugated chains of these molecules, the peaks of the linear absorption bands are around 800nm. SC-V-21c and TOR-I-103 show extremely large peak 2PA cross sections of ≈ 30000 GM [66].

Quantum-chemical calculations [66] were carried out by Jean-Luc Bredas's group at the Georgia Institute of Technology for these two molecules, SC-V-21c and TOR-I-103 (alkyl groups replaced with CH_3). They used model structures in which hexyl and butyl groups were replaced with methyl groups. In the case of TOR-I-103, both centrosymmetric conformers with both cisoid and transoid arrangement of the two vinylene groups about the outermost pyrrole were considered, as shown in Fig.5.13:

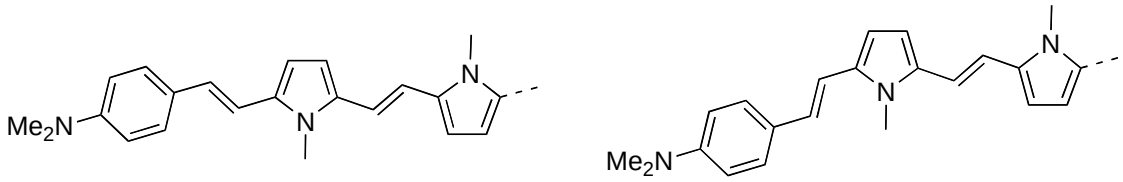

Figure 5.13 Two centrosymmetric conformers of TOR-I-103 considered in quantum chemical calculations

The molecular geometry was optimized with the semi-empirical AM1 method [67] without symmetry constraints. The excited-state energies and transition dipole moments were computed applying the intermediate neglect of differential overlap (INDO/S) method [68] (using the Mataga-Nishimoto potential to describe Coulomb repulsion terms [69]) combined with two different schemes to include correlation effects: the Coupled Cluster method with singles and doubles (CCSD-EOMs)[70][71], and the multi-reference double-configuration-interaction (MRD-CI) technique[72][73]. For the latter method, they have fully modified the codes so that the maximum number of CI configurations can exceed the 6000 limit and that an identical MO-active space is required for single and multiple excitations. With the upper computational limit of ~10^6 configurations they can consider MO active spaces comprising up to 26 molecular orbitals. The high numerical efficiency is achieved by implementing Davidson's diagonalization algorithm. Both approaches incorporate multiply excited determinants in the description of the excited states, which are necessary for providing more quantitative predictions. In particular, doubly excited determinants constitute a significant portion of the excited states that are active in two-photon absorption [73][74][75][76][77].

The two-photon absorption cross-section was computed from the excited states and transition dipole moments among them using the sum-over-states approach [31] and by the S-

tensor [32]. The damping constant Γ was set to 0.1 eV, which for the S-tensor calculations corresponds to a convolution with a Lorentzian lineshape function with a FWHM of 0.4 eV for spectra plotted as a function of transition energy.

For the MRD-CI calculations, the determinants dominant in the description of the ground state and the lowest excited states were selected as references: These are the SCF determinant, singly excited determinants (HOMO→LUMO, HOMO→LUMO+1, HOMO-1→LUMO), and one doubly excited determinant (HOMO, HOMO→LUMO, LUMO). The same set of reference determinants was found necessary to reliably describe the excited states of other quadrupolar molecules [22] [78]. In order to ensure that the obtained picture is independent on the (somewhat ambiguous) choice of the MO-active space, it was varied between 5/5 (including the five highest occupied and five lowest unoccupied) π-orbitals to 11/11 (MRD-CI) for SC-V-21c, and 8/9 to 11/11 (MRDCI) for TOR-I-103. For CCSD, the MO-active space included both σ– and π– orbitals; the largest probed were 15/15 for SC-V-21c and 15/16 for TOR-I-103.

In the geometry optimizations, the total energy of TOR-I-103 is essentially independent of the chosen conformer; the transoid conformation being 0.005 eV more stable than the cisoid. All excited state and detuning energies of the conformers agree quantitatively within 1%, while transition dipole moments [2PA cross-sections] differ by up to 7% [13%] between the conformers. Below, the results for the "cisoidal" conformer of TOR-I-103 are presented.

The validity of the few-state model for describing 2PA from the $1A_g$ ground state (g) into $3A_g$ (e') is ensured by the very small detuning factor of the channel associated with the intermediate state e ($1B_u$) and e', which leads to this channel dominating over all possible alternative pathways. Table 5.4 compares the 2PA cross sections and few-state model parameters

obtained with MRD-CI and CCSD. The chosen MO-active spaces for MRD-CI and CCSD were scaled between SC-V-21c and TOR-I-103 to account for the increased number of π-electrons in TOR-I-103. Additionally, the results for the largest MO-active space used for each molecule and method are given.

Independent of the method (MRD-CI or CCSD) and the CI-active space used, the same qualitative (and expected) picture arises: With extending the molecular length from SC-V-21c to TOR-I-103 by an additional pyrrol-vinylene unit, the energies of $1B_u$ and $3A_g$ decrease, while the calculated transition dipole moments μ_{ge}.and $\mu_{ee'}$ increase (Table 5.4).

Table 5.4 Theoretical one and two-photon parameters for SC-V-21c and TOR-I-103 [a]

	MRD-CI			**CCSD**		
SC-V-21c	7/7 (11/11)			7/7 (15/15)		
	E (eV)	Configuration	Coefficient	E (eV)	Configuration	Coefficient
E ($1B_u$)	1.92 (1.96)	H→ L	0.91 (0.90)	1.90 (1.69)	H → L	0.93 (0.88)
E' ($3/4A_g$)	3.19 (3.29)	H-1 → L	0.81 (0.80)	3.17 (2.82)	H-1 → L	0.81 (0.58)
		H → L+1	0.31 (0.30)		H → L+1	0.32 (<0.1)
		HH → LL	0.16 (0.10)		HH → LL	0.17 (0.20)
Detuning (eV)	0.32 (0.31)			0.31 (0.28)		
μ_{ge} (debye)	18.4 (17.3)			17.2 (13.7)		
$\mu_{ee'}$ (debye)	15.4 (14.9)			13.9 (12.2)		
$\delta_{S\text{-tensor}}$ (10^3 GM)	42 (40)			32 (16)		
TOR-I-103	11/9 (11/11)			12/12 (15/16)		
	E (eV)	Configuration	Coefficient	E (eV)	Configuration	Coefficient
E ($1B_u$)	1.83 (1.83)	H→ L	0.90 (0.90)	1.72 (1.71)	H→ L	0.91 (0.90)
E' ($3/4A_g$)	2.88 (2.90)	H-1 → L	0.77 (0.77)	2.59 (2.57)	H-1 → L	0.53 (0.57)
		H → L+1	0.38 (0.37)		H → L+1	0.25 (0.20)
		HH → LL	0.17 (0.17)		HH → LL	0.30 (0.27)
Detuning (eV)	0.39 (0.38)			0.42 (0.43)		
μ_{ge} (debye)	20.4 (20.1)			20.4 (19.4)		
$\mu_{ee'}$ (debye)	15.4 (18.7)			14.2 (14.7)		
$\delta_{S\text{-tensor}}$ (10^3 GM)	41 (42)			20 (19)		

[a]the CI active space chosen has been scaled consistently with the varying number of π-electrons in the system; equivalent π-orbitals were used in the MRD-CI and CCSD calculations for each molecule. The values corresponding to the largest MO-active space are given in parentheses.

The one-photon active state $1B_u$ (*e*) corresponds to a HOMO→LUMO transition whereas the main two-photon active state, $3A_g$ (*e′*) [$4A_g$ for some MO-active spaces], is mainly composed of the configurations representing the HOMO→LUMO+1, HOMO-1→LUMO, and HOMO, HOMO→LUMO, LUMO transitions (*cf.* Table 5.4). However, the participation of the above mentioned configurations into $3A_g$ varies with the method (MRD-CI vs. CCSD) as well as with the size of the MO-active space. CCSD calculations for SC-V-21c show particularly pronounced variations. This unsteadiness in the description of $3A_g$ can be partially held responsible for the observed deviations of up to 25% in all 3-state model parameters contributing to δ (see Table 5.4); deviations that, in combination, lead to a CCSD calculated δ being a factor of up to two smaller than the MRD-CI calculated δ.

To eliminate the uncertainty related to the MRD-CI vs. CCSD computed 3-state model parameters, they studied the impact of the computed transition dipole moments on 2PA cross section δ by inserting them with the experimentally observed detuning and transition energies, E_{ge} and $E_{ge'}$, into the few-state model expression. They note that owing to its smaller detuning energy, SC-V_21c possesses a comparable if not even larger cross-section than the more elongated compound TOR-I-103. The extraordinarily strong dependence of the actual cross-section on the detuning energy upon approaching double resonance (and thus on only minor errors affecting the calculations of the excited-state energies) together with larger experimental errors upon approaching linear absorption, can be held to some extent responsible for quantitative deviations between theoretical and experimental peak values.

In summary, quantum chemical calculations suggest that an excited singlet state, $3A_g$, is strongly 2PA allowed, with δ_{max} values of the same order of magnitude as observed

experimentally, and lies at a similar energetic position relative to the 1PA-allowed S_1 state as the experimentally observed 2PA peaks. The calculations also suggest that 2PA into $3A_g$ can be well described by considering a single 3-level model with S_1 as the intermediate state (see Eq. (2.48) and (2.56) in Chapter 2). Consistent with the experimental result, the calculations give comparable μ_{ge} for SC-V-21c (18.4 debye) and TOR-I-103 (20.4 debye), and small detuning energies (0.32eV for SC-V-21c, 0.39 eV for TOR-I-103). Furthermore, the calculated $\mu_{ee'}$ is somewhat larger for TOR-I-103 (18.5 debye) than for SC-V-21c (15.4 debye). Although 2PA into $3A_g$ results from the combination of two large (albeit not exceptional) transition dipole moments that scale with molecular size, the resulting 2PA cross section δ_{max} for SC-V-21c and TOR-I-103 (42 and 41 $\times 10^3$ GM, respectively) are found to be comparable.

5.5 Croconium and Tetraon

From section 5.2-5.4, we can see that inserting the squarylium center core into the conjugated chain of polymethine dyes can generate neutral squaraine dyes that show much larger 2PA cross sections than the counterpart PDs. Following this strategy, we are trying to insert different types of acceptor cores into the conjugated polymethine chain to study their effects on 2PA properties.

5.5.1 Squaraine Vs Croconium

First, we compared the squaraine molecule TOR-I-110 with the croconium molecule TOR-I-95. Molecular structures are shown in Fig. 5.14. Both of these two molecules are synthesized by Seth Marder's group at the Georgia Institute of Technology, Atlanta. They have the same terminal donor groups and conjugation length.

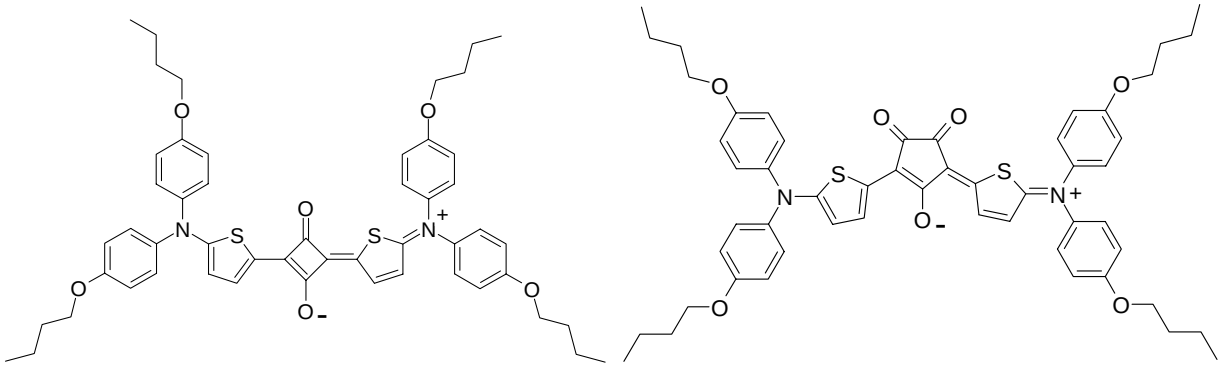

(a) TOR-I-110 (b) TOR-I-95

Figure 5.14 Molecular structure for (a) Squaraine TOR-I-110 (b) Croconium TOR-I-95

Linear optical properties of these two molecules are listed in Table 5.5. We can see that the peak wavelength of linear absorption of croconium, TOR-I-95, is ≈150nm red-shifted compared to that of its counterpart squaraine TOR-I-110. But they show similar extinction coefficients and ground state transition dipole moments (TOR-I_95 is a little bit larger).

Table 5.5 Linear properties of squaraine TOR-I-110 and croconium TOR-I-95 in THF: linear absorption peak λ_{abs}max, extinction coefficient ε_{max}, ground state transition dipole moment. μ_{ge}

Molecule	λ_{abs}max (nm)	ε_{max} ($cm^{-1}M^{-1}$)	μ_{ge} (debye)
TOR-I-110	703	200000	13.6
TOR-I-95	854	180000	14.3

Degenerate 2PA spectra as well as linear absorption spectra are shown in Fig. 5.15. The 2PA cross section δ is plotted versus the half of input photon wavelengths. Degenerate 2PA cross sections were measured with Z-scan and two-photon fluorescence (2PF) techniques.

Measuring the 2PA properties, we cannot resolve the peak of the main 2PA band for both molecules due to linear absorption. The highest 2PA cross section of the squaraine dye TOR-I-

110 observed by experiment is much larger than that of croconium TOR-I-95. The reason for this difference is still under study. In general, croconium dyes are a type of PD, and their 2PA properties should be very similar to PDs. Here we observed that the relationships of both linear and 2PA properties between SD and croconium dyes with analogous structures are similar to the relationships between SDs and PDs discussed in Section 5.2.

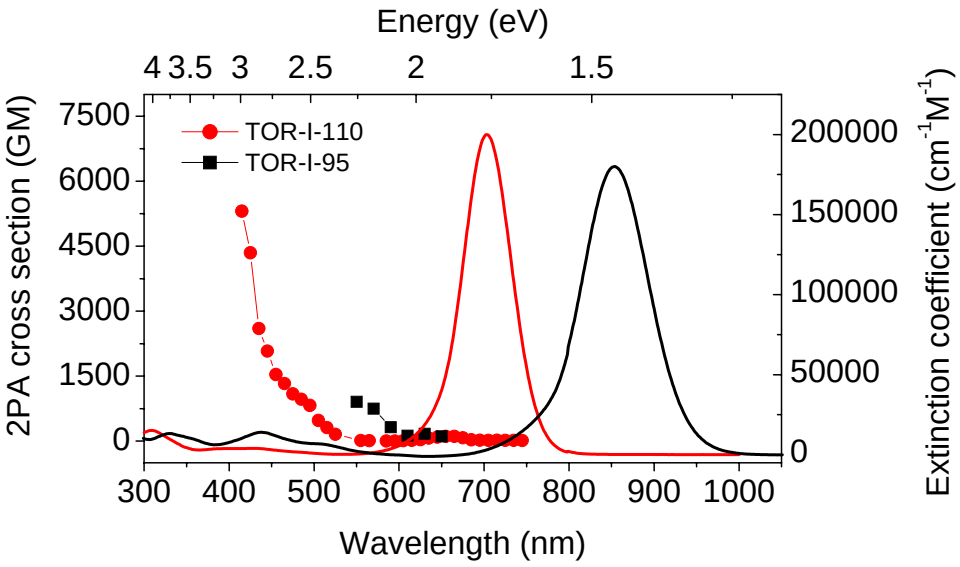

Figure 5.15 2PA spectra for squaraine TOR-I-110 and croconium TOR-I-95. Linear spectra also are plotted for comparison.

5.5.2 Squaraine Vs Tetraon

We also compared the squaraine dye SD 2243 and tetraon dye TOD 2765. They are synthesized at the Institute of Organic Chemistry, National Academy of Sciences, Ukraine. Molecular structures are shown in Fig. 5.16. They have the same terminal groups. SD 2243 has a squarylium acceptor core at the center of the conjugated chain, but TOD 2765 has a $C_6H_{12}O_4$ acceptor core at the center that separates the conjugated chain of the left part of the molecule from the right part. The effective conjugation length of TOD 2765 is shorter than that of SD

2243 because the central structure in the Tetraon breaks the conjugation chain connected from the left to the right.

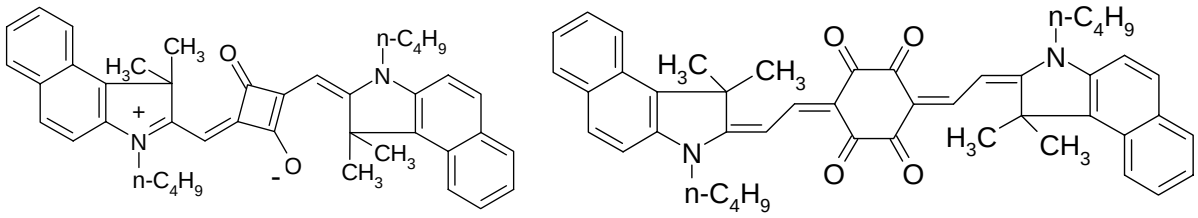

(a) SD 2243 (b) TOD 2765

Figure 5.16 Molecular structure for (a) Squaraine dye SD 2243 and (b) Tetraon dye TOD 2765.

The linear optical properties of SD 2243 and TOD 2765 are summarized in Table 5.6. Due to the shorter effective length of TOD 2765, we can see that the linear absorption band of TOD 2765 is blue-shifted ≈ 60nm compared to SD 2243, and the ground state transition dipole moment μ_{01} for TOD 2765 is smaller than that of SD2243. TOD 2765 also exhibits a stronger linear absorption vibrational shoulder shown in Fig. 5.17.

Table 5.6 Linear properties of squaraine SD 2243 in CH_2CL_2 and tetraon TOD 2765 in ethanol: linear absorption peak λ_{abs}max, extinction coefficient ε_{max} and ground state transition dipole moment μ_{01}

Molecule	λ_{abs}max (nm)	ε_{max} ($cm^{-1}M^{-1}$)	μ_{01} (debye)
SD 2243	668	345000	13.8
TOD 2765	624	230900	13.0

The 2PA spectra of SD 2243 in CH_2CL2 and TOD 2765 in ethanol are shown in Fig. 5.17. The 2PA cross-section δ is plotted versus the half of input photon wavelengths. 2PA spectra are measured by Z-scan and two-photon fluorescence (2PF).

We experimentally observed three 2PA bands for SD 2243 ($\delta_{max}1 \approx 80$ GM at ≈ 615nm, $\delta_{max}2 \approx 1000$ GM at ≈ 440nm and $\delta_{max}3 > 8000$ GM at wavelengths shorter than 375nm), however, we observed four 2PA bands for TOD 2765 ($\delta_{max}1 \approx 130$ GM at ≈ 550 nm, $\delta_{max}2 \approx 877$ GM at ≈ 483 nm, $\delta_{max}3 \approx 2700$ GM at ≈ 410nm and $\delta_{max}4 > 8000$ GM at wavelengths shorter than 340nm). Similar to linear absorption, 2PA bands of TOD 2765 are also blue-shifted compared to those of SD 2243. We cannot resolve the peak of the 2PA band at shorter wavelengths due to linear absorption. We conclude, based experimental data, that the introduction of $C_6H_{12}O_4$ at the center of the conjugated chain in TOD 2765 further increases the density of electronic transitions between the linear absorption band and its "double resonance" position. The molecular orbitals associated with this could be revealed by undergoing quantum chemical calculations.

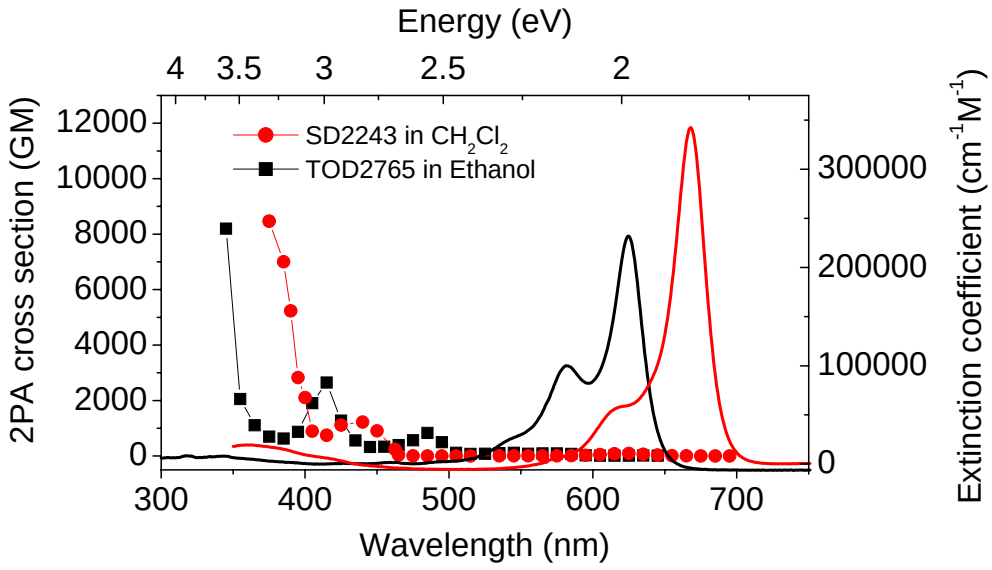

Figure 5.17 2PA spectra for squaraine SD 2243 in CH_2CL_2 and tetraon TOD 2765 in Ethnaol. Linear spectra also are plotted for comparison.

5.6 Relations of one-photon anisotropy to 2PA spectra

5.6.1 One-photon excitation fluorescence anisotropy

Steady-state one-photon excitation fluorescence anisotropy spectra of organic molecules were measured in high viscosity solvents to avoid reorientation of molecules, and in low concentration solutions (peak OD < 0.1) to avoid reabsorption of fluorescence, with a PTI Quantamaster Spectrofluorimeter. The experimental setup is shown as below:

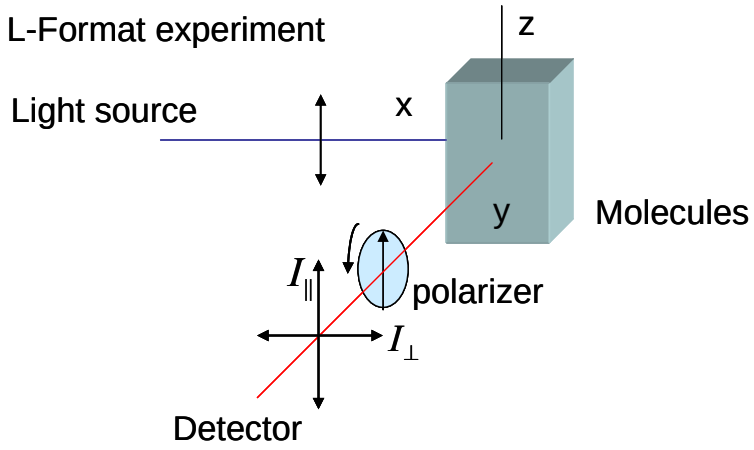

Figure 5.18 Experiment setup for one-photon and two-photon excitation fluorescence anisotropy measurement

The solutions of molecules are excited with vertically polarized light. One then measures the intensity of the fluorescence emission through a polarizer at 90 degree (L-format configuration) with the detector. When the emission polarizer is oriented parallel (||) to the direction of the polarized excitation, the observed intensity is referred as $I_{||}$. Likewise, when the polarizer is perpendicular (⊥) to the excitation polarization, the intensity is called $I_{\perp}$.

It is well-known that the excitation anisotropy spectrum, *r(λ)*, can be calculated as a function of the excitation wavelength λ at a fixed emission wavelength, usually near a fluorescence maximum:

$$r(\lambda) = \frac{I_{//}(\lambda) - I_{\perp}(\lambda)}{I_{//}(\lambda) + 2I_{\perp}(\lambda)} \tag{5.3}$$

where $I_{//}$ and $I_{\perp}$ are the fluorescence intensities polarized parallel and perpendicular to the excitation light [39].

One-photon anisotropy measurements can give information about the spectral position and orientation of the transition dipole moments from the ground (S_0) to the first (S_1) and higher (S_n) excited-states relative to the orientation of the emission dipole moment. The angle between the absorption and emission dipole moments (β) can be determined from one-photon anisotropy,

$$r_{1PA} = \frac{3\cos^2\beta - 1}{2} \tag{5.4}$$

In the range: $90^0 \le \beta \le 0^0$, one-photon anisotropy ranges between, $-0.2 \le r_{1PA} \le 0.4$

5.6.2 Polymethine dyes

Here we show experimental results for three typical polymethine dyes with different terminal groups: PD 2350, PD 2646 and PD 2630. The molecular structures are shown in Fig. 5.19. The 2PA cross section is plotted versus the wavelengths equal to half of input photon wavelengths. One-photon excitation fluorescence anisotropy (all three molecules in Glycerol) and degenerate 2PA spectra (all three molecules in ethanol), as well as linear absorption spectra are shown in Fig; 5.20. All three PDs show strong correlation between one-photon anisotropy spectra and 2PA spectra.

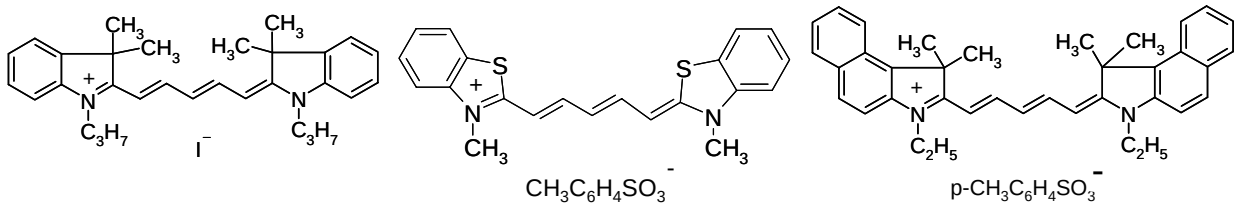

Figure 5.19 Molecular structures for polymethine dyes: PD 2350, PD 2646 and PD 2630

Analysis of one-photon excitation fluorescence anisotropy, $r(\lambda)$, for PD 2350 revealed the alternation of the allowed and forbidden (by symmetry) one-photon transitions. One-photon forbidden transitions, as transitions between states of the same symmetry, can indicate a possible position of 2PA bands. Shown in Fig. 5.20 (a), the first dip in $r(\lambda)$ was observed at 412 nm (r_{1PA} = 0.22) corresponding to the angle $\beta \approx 33^0$ between μ_{01} and μ_{10}. However, the peak of 2PA for PD 2350 is shifted to the blue region by ≈ 22 nm relative to this anisotropy dip. A second dip in $r(\lambda)$ at 330 nm ($r_{1PA} \approx 0$) corresponds to the angle $\beta \approx 55^0$. Since this wavelength is almost exactly half that of the absorption peak in the $S_0 \rightarrow S_1$ transition, degenerate 2PA into this band would be enhanced by an intermediate state resonance [56]. However, as we observed from Fig. 5.20, this "double resonance" cannot be experimentally reached by 2PA due to the influence of the tail in the linear absorption band.

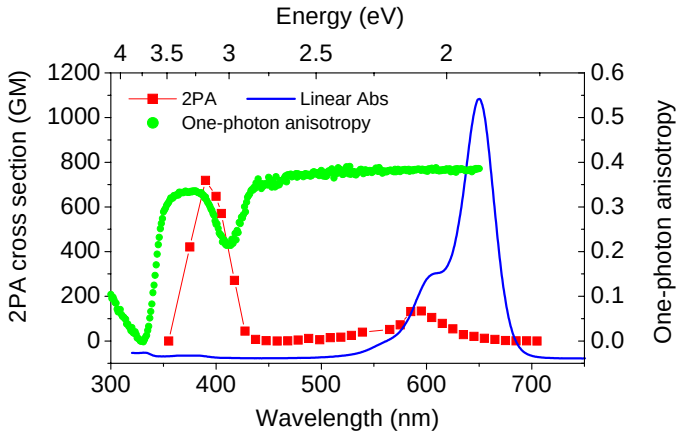

(a) PD 2350

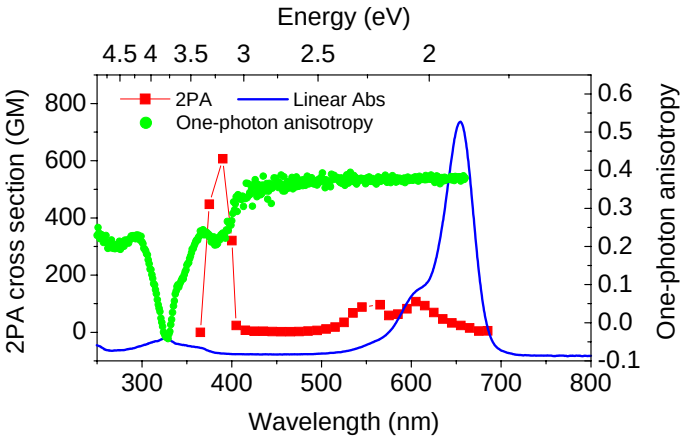

(b) PD 2646

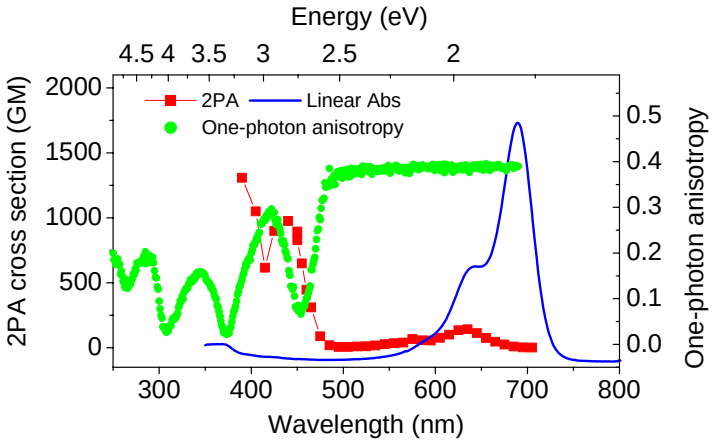

(c) PD 2630

Figure 5.20 One-photon excitation fluorescence anisotropy and 2PA spectra for three PDs with different terminal groups. Linear spectra also are plotted for comparison.

Let's go back to see the quantum chemical calculations in Section 5.3 (Fig. 5.6) to reveal the origin of this correlation. As shown in Fig. 5.6 for PD 2350, there are two identical HOMO-1s of the isolated TGs (with charge localization only at TGs, see in Fig. 5.5). Introduction of the symmetrical terminal groups leads to the formation of doubly degenerate configurations resulting in their energies splitting. After splitting, one of these MOs typically mixes with the orbital of the chain producing a delocalized molecule orbital, HOMO-2, shown in Fig. 5.6 and Fig. 5.7. The transition from HOMO-2 to LUMO ($1A_1 \rightarrow 2B_1$, $S_0 \rightarrow S_3$ shown in Table 5.3) can be seen in one-photon absorption (non zero transition dipole moment). The peak of this one-photon transition band (410nm in Table 5.3) corresponds to a dip in the one-photon anisotropy spectrum (412nm in Fig. 5.20 (a)).

The other MO remains localized at the benzene rings of the TGs (see HOMO-3 shown in Fig. 5.6 and Fig. 5.7). The existence of this local molecular orbital is of great importance for 2PA. The transition from HOMO-3 to LUMO ($1A_1 \rightarrow 1A_3$, $S_0 \rightarrow S_4$ in Table 5.3) gives zero overlap (see in Fig.5.7), thus it requires an intermediate (HOMO) state and forms a two-photon absorbing transition. Our understanding is that the localized – delocalized electronic transition, such as HOMO - 3 $\rightarrow$ LUMO, which appears in the energy interval between the $S_0 \rightarrow S_1$ and its "double resonance", is responsible for the strong 2PA band with peak at 390nm.

Similar to PD 2350, for PD 2630 in Fig. 5.20 (c) there is a shift of $\approx$ 13 nm between the second 2PA peak (440nm) and the first one photon excitation fluorescence anisotropy dip (453nm). The splitting energy for polymethine dyes with indolium and benzoindolium TGs is larger. Therefore, for these molecules, the 2PA peaks are blue-shifted relative to the anisotropy dips (see Appendix B).

The energy splitting depends on the energy position of the orbitals from the isolated terminal groups relative to the chain orbitals and thus on the terminal groups' structure (length of conjugation, donor strength). A small splitting energy leads to approximate overlap between one-photon anisotropy dips and the positions of the 2PA peaks. Figure5.20 (b) shows a strong correlation between the 2PA peak and the one-photon anisotropy dip for PD 2646 with the thiazolium terminal groups. The same trend was observed for all other polymethine molecules (see Appendix B).

5.6.3 Squaraine dyes

We also compared one-photon anisotropy spectra with 2PA spectra for two squaraine dyes. Experimental data for other squaraines can be found at Appendix B. Molecular structures are shown in Fig. 5.21. SD 2577 was synthesized at the Institute of Organic Chemistry, National Academy of Sciences, Ukraine. SC-V-21c was synthesized by Seth Marder's group at the Georgia Institute of Technology, Atlanta. The one-photon excitation anisotropy spectra (SD 2577 in Glycerol, SC-V-21c in Silicon Oil) as well as degenerate 2PA spectra (SD 2577 in ethanol, and SC-V-21c in CH_2CL_2) are shown in Fig. 5.22. The 2PA cross section is plotted versus the wavelengths equal to half of input photon wavelengths.

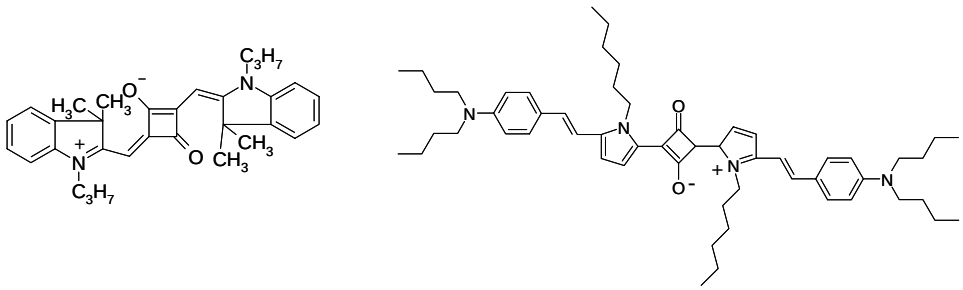

(a) SD 2577 (b) SC-V-21c

Figure 5.21 Molecular structures for squaraine dyes (a) SD 2577 (b) SC-V-21c

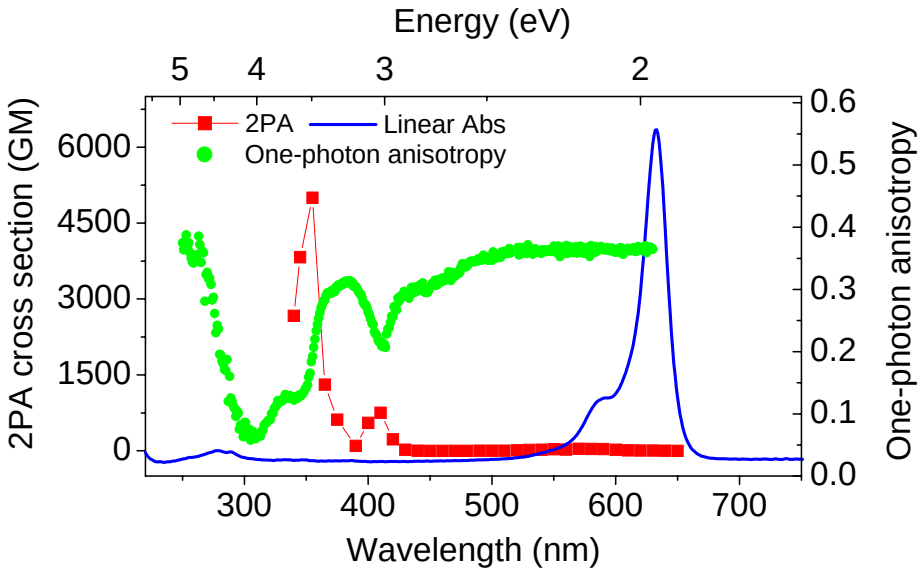

(a) SD 2577

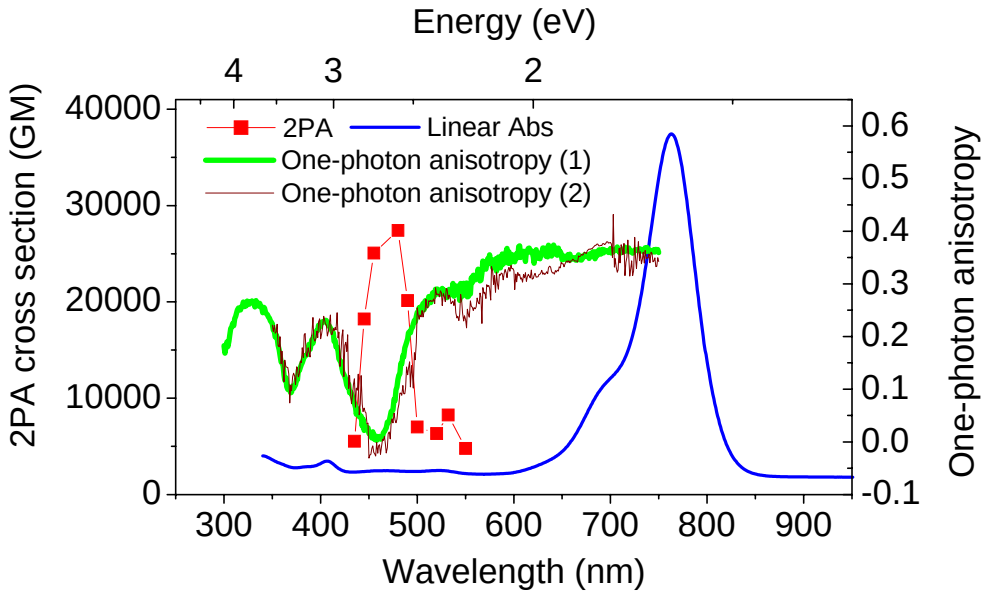

(b) SC-V-21c

Figure 5.22 One-photon excitation fluorescence anisotropy and 2PA spectra for two SDs: (a) SD 2577 (b) SC-V-21c. There are two curves for one-photon anisotropy spectra: (1) measured by the visible detector, PMT R928b (2) measured by the near IR PMT. Linear spectra are also plotted for comparison.

The 2PA spectrum for SD2577 can be directly mapped onto the one-photon anisotropy function $r(\lambda)$. The observed dips of one-photon anisotropy at 410 nm (r_{1PA} = 0.22, $\beta \approx 33^0$) and at 345 nm (r_{1PA} = 0.13, $\beta \approx 42^0$) correspond to the peak positions of the 2PA bands. Analogous to PD 2350, the last dip at 309 nm (r_{1PA} = 0.06, $\beta \approx 49^0$), corresponding to a position of twice the energy of the main allowed $S_0 \rightarrow S_1$ absorption band (or "double resonance" position) is obscured by one-photon absorption.

We also observed this strong correlation for SC-V-21c. The observed dips of one-photon anisotropy at 460nm and at 546nm correspond to the peak positions of the experimentally observed 2PA bands as well.

Explanation for this correlation for SDs is not so straightforward as for PDs. More research needs to be carried out to understand this.

CHAPTER 6 TWO-PHOTON EXCITATION FLUORESCENCE ANISOTROPY

6.1 Introduction

A much less investigated approach for understanding the 2PA properties of organic molecules is the study of one-photon and two-photon excitation fluorescence anisotropy. Such studies can give additional information about the nature of intermediate states and the molecular symmetry. It is commonly known that one-photon excitation fluorescence anisotropy measurements, especially linked to quantum-chemical calculations, can reveal the spectral positions and orientations of the transition dipole moments from the ground to the first, μ_{01}, and higher excited-states, μ_{0n}, relative to the orientation of the emission dipole moment, μ_{10}, which cannot be obtained from one-photon absorption spectra, but is important for understanding 2PA processes.

It was shown theoretically [79] that the range of two-photon anisotropy, r_{2PA}, values is much broader than for r_{1PA} indicating potential advantages of two-photon excitation. In practice, as will be shown in this dissertation and in a previous paper [80], r_{2PA} spectra for many organic dyes are almost wavelength independent within several electronic transitions. It is necessary to note that r_{2PA} literature studies are very limited. Most of the measurements were performed only within one electronic band, and their analysis is usually directed at a comparison of the values of r_{1PA} and r_{2PA}. An overview of the existing experimental data was presented by Lakowicz and Gryczynski in Ref. [81]. However, to our knowledge, an explanation of the wavelength

independent behavior of r_{2PA} as well as its potential for understanding the properties of 2PA has not been reported.

6.2 Experimental setup

The light source for one-photon excitation fluorescence anisotropy measurements is a Xenon lamp. However the light source for two-photon excitation fluorescence anisotropy measurements is our Clark-MXR, CPA2010, Ti:Sapphire amplified femtosecond laser system followed by an optical parametric generator/amplifier (model TOPAS 4/800, Light Conversion) providing laser pulses of 140 fs (FWHM) duration with 1 kHz repetition rate. Experimental setup for two-photon excitation fluorescence anisotropy is same as that for one-photon anisotropy shown in Fig. 5.18

The anisotropy of up-converted fluorescence of all molecules under two-photon excitation was measured in 1 cm quartz cuvettes with the same PTI Quantamaster Spectrofluorimeter and the same experimental configuration as shown in Fig .6.1. Special care was taken to minimize reabsorption of the emission, especially for the dyes with a small Stokes shift as, for example, for PDs with a typical Stokes shift of ≈ 15-20 nm. We controlled this reabsorption by comparing the shape of up-converted fluorescence (usually red-shifted due to the high concentration typically used for 2PA studies) with one-photon fluorescence obtained from the diluted solution. We found experimentally that for all the molecules studied the up-converted fluorescence at concentrations ≤ 10^{-5} M completely overlaps the one-photon fluorescence band, confirming that reabsorption is negligible. Therefore, we used 10^{-5} M or smaller concentrations

for all two-photon anisotropy studies. The measurements and calculations of r_{2PA} were performed as described above in Eq. 6.2.

6.3 Two-photon anisotropy: four-state and three-state model

Derivation of the formula for two-photon excitation fluorescence anisotropy is based on two theoretical approaches. The first was made by P. R. Callis [82], who used McClain's original treatment for the two-photon absorption (2PA) tensor and added the fluorescence transition dipole moment to develop the equation for the two-photon anisotropy function. The second theoretical approach was made by P. Cronstrand et al [32]. They derived the equation for 2PA cross section in a more general four-state/two-intermediate-level model taking into account the influence of an additional second excitation channel.

We obtain the equation for the two-photon excitation fluorescence anisotropy r_{2PA} in the four-state/two-intermediate-state approximation shown in Fig. 6.2 (a). The assumptions are 1) the two photons for excitation have identical photon energies and the same polarization (degenerate 2PA case); 2) all transition dipole moments are in one plane, or planar molecule assumption. In the final formula, r_{2PA} should be expressed in terms of absorbing dipoles μ_{01}, μ_{0n}, μ_{1f}, μ_{nf} (not their projections), angles α, β, γ, θ between transitions (α is the angle between emission dipole moment $\boldsymbol{f}$ and isometric line of ground state transition dipole moment μ_{01} and excited state transition dipole moment μ_{1f}, β is the angle between transition dipole moments μ_{01} and μ_{0n}, γ is the angle between ground state transition dipole moment μ_{01} and excited state transition dipole moment μ_{1f}, θ is the angle between transition dipole moments μ_{01} and μ_{0n} in

Fig.6.2 (b)) and detuning energies ΔE_1, ΔE_2. After algebraic transformation, we can write the expression (detailed derivation is shown in Appendix D):

$$r_{2PA} = \frac{18(K_1 + K_2)K_3 - 8K_3^2 + K_4}{7(K_3^2 + K_4)} \tag{6.3}$$

where $K_1 = \Delta E_2 \mu_{01}\mu_{1f} \cos(\frac{\gamma}{2} + \alpha)\cos(\frac{\gamma}{2} - \alpha)$;

$K_2 = \Delta E_1 \mu_{0n}\mu_{nf} \cos(\frac{\gamma}{2} - \alpha + \theta)\cos(\frac{\gamma}{2} + \alpha - \beta)$;

$K_3 = \Delta E_2 \mu_{01}\mu_{1f} \cos\gamma + \Delta E_1 \mu_{0n}\mu_{nf} \cos(\gamma + \theta - \beta)$;

$K_4 = \Delta E_1^2 \mu_{0n}^2 \mu_{nf}^2 [1 + \cos^2(\gamma + \theta - \beta)] + \Delta E_2^2 \mu_{01}^2 \mu_{1f}^2 (1 + \cos^2\gamma) +$
$+ 2\Delta E_1 \Delta E_2 \mu_{01}\mu_{0n}\mu_{1f}\mu_{nf} [\cos(\gamma + \theta)\cos(\gamma - \beta) + \cos\theta\cos\beta]$

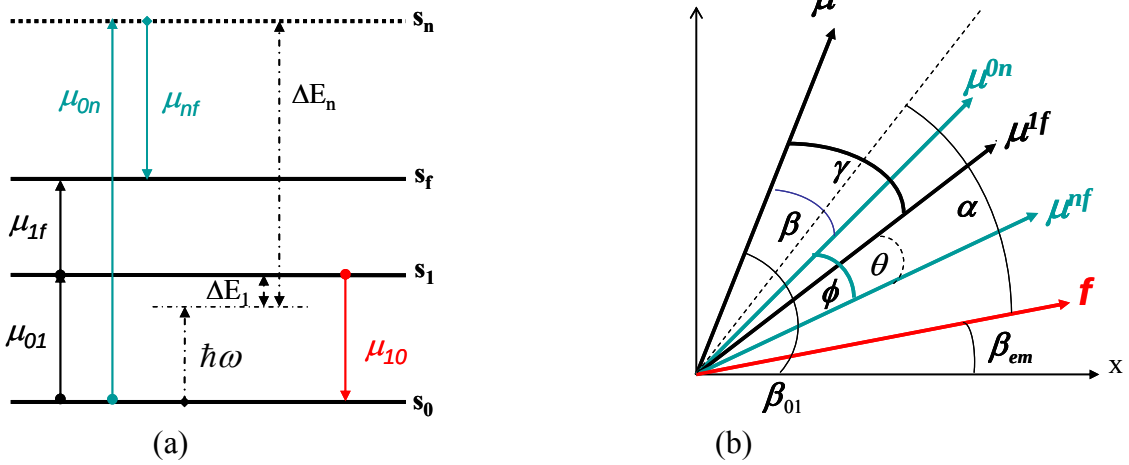

Figure 6.1 Four-state, two-intermediate level (S_1 and S_n), model for two-photon anisotropy, (a) energy states S_0, S_1, S_f and S_n diagram; (b) transition dipole moments schematic diagram

In case of the simplest three-state/one-intermediate-state model shown in Fig. 6.3 (α is the angle between emission dipole moment ***f*** and isometric line of ground state transition dipole moment μ_{01} and excited state transition dipole moment μ_{1f}, γ is the angle between ground state

transition dipole moment μ_{01} and excited state transition dipole moment μ_{1f}, α_{em} is the angle between emission dipole moment ***f*** and ground state transition dipole moment μ_{01} in Fig.6.3 (b)): $S_0 \rightarrow S_1$ and $S_1 \rightarrow S_f$ (S_1 is the only intermediate state and S_f is the final state), Eq. 6.3 can be simplified to Eq. 6.4, which is the same as the formula derived in Ref. [82] using a 3-state model,

$$r_{2PA} = \frac{18\cos(\frac{\gamma}{2}-\alpha)\cos(\frac{\gamma}{2}+\alpha)\cos\gamma - 7\cos^2\gamma + 1}{7(2\cos^2\gamma + 1)} \tag{6.4}$$

The main difference between Eq. (6.3) and (6.4) is that in the three-state model, two-photon anisotropy, r_{2PA}, depends only on the mutual orientation (α and γ) in 2D-space of three transition dipole moment vectors participating in the 2PA process (μ_{01}: $S_0 \rightarrow S_1$, μ_{1f}: $S_1 \rightarrow S_f$ and f_{em}: $S_1 \rightarrow S_0$), and does not depend on the values of the absorbing dipole moments and detuning energy.

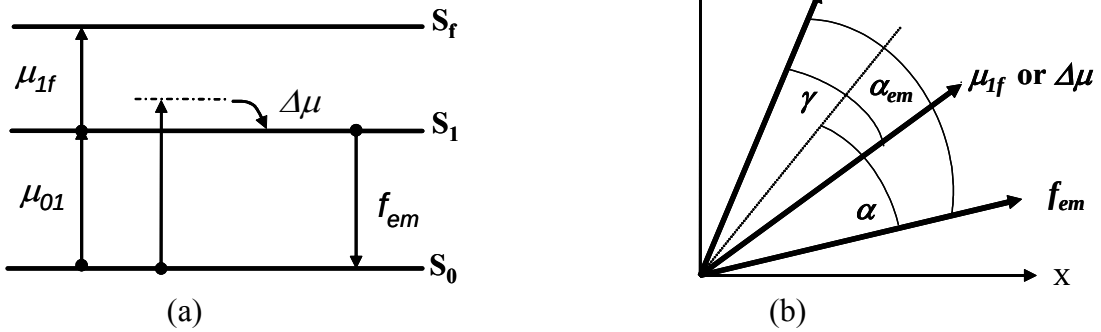

Figure 6.2 Three-state one-intermediate level (S_1) model for two-photon anisotropy: (a) energy states S_0, S_1, S_f diagram; (b) transition dipole moments schematic diagram

The angle $\alpha_{em} = \alpha + \frac{\gamma}{2}$ in Fig. 6.3 (b) is the angle of orientation of μ_{01} relative to the orientation of f_{em}, which could be calculated from the one-photon excitation anisotropy spectra.

If the absorbing dipole $\boldsymbol{\mu_{01}}$ is parallel to $\boldsymbol{\mu_{1f}}$, $\gamma = 0$ ($\alpha_{em}=\alpha$) and the angle α becomes equal to the angle between absorbing and emitting dipoles, then *r* reduces to the well-known formula [39]:

$$r_{2PA} = \frac{6\cos^2 \alpha_{em} - 2}{7} \tag{6.5}$$

In the case of $\alpha_{em} = 0°$, r_{2PA} reaches its maximum value 0.57. If $\alpha_{\text{em}}= 90°$, the value of r_{2PA} is minimal: -0.29.

6.4. Symmetric molecules

We measured two-photon excitation anisotropy spectra for most of the polymethine and squaraine dyes (see Appendix B) synthesized at the Institute of Organic Chemistry, National Academics of Sciences, Ukraine. Here, we choose only four polymethine dyes for our two-photon excitation fluorescence anisotropy measurement and analysis. We also choose two fluorene molecules synthesized by Kevin Belfield's group in the Department of Chemistry, University of Central Florida in Orlando for analysis. Three of them are symmetric molecules (PD2350, PD3428 and Fluorene 2), the other three are asymmetric molecules (PD2665, Styryl 1 and Fluorene 1). The molecular structures of polymethine dyes are shown in Fig. 6.4, and the molecule structures of two fluorene molecules are shown below in Fig. 6.5:

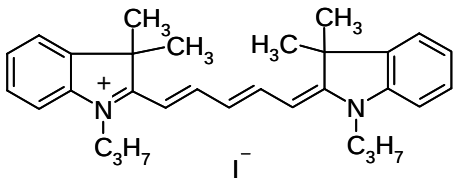

PD 2350

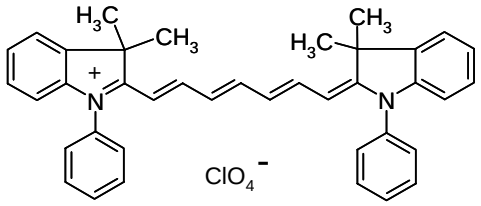

PD 3428

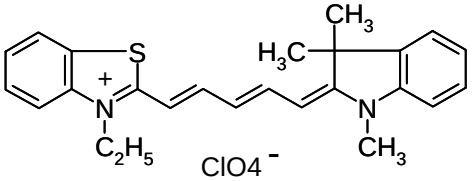

PD 2665

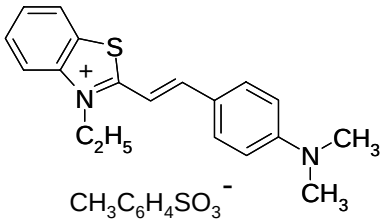

Styryl_1

Figure 6.3 Molecular structures for polymethine dyes PD2350, PD3428, PD2665 and Styryl_1

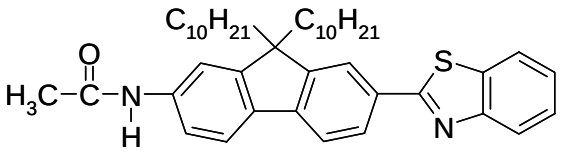

Fluorene 1

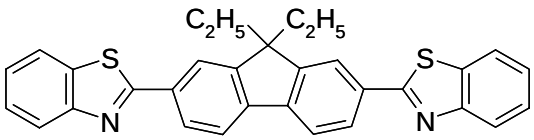

Fluorene 2

Figure 6.4 Molecule structures of two fluorene derivatives for two-photon excitation fluorescence anisotropy measurements.

The experimental results for the three symmetric molecules are shown in Fig. 6.6. For comparison with linear absorption, 2PA and two-photon anisotropy spectra are presented as functions of wavelength equal to half of input photon wavelengths.

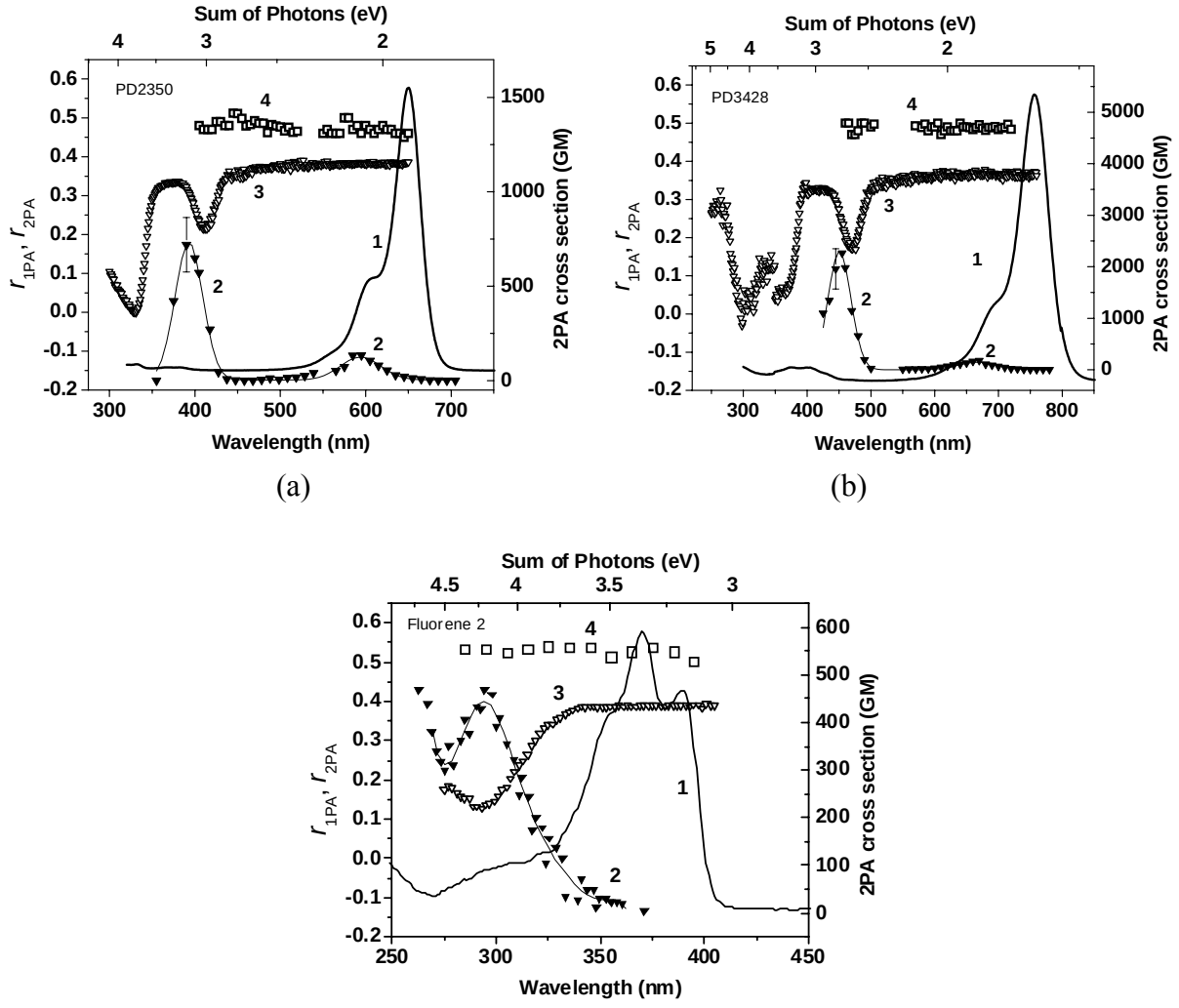

Figure 6.5 (1) linear absorption, (2) 2PA, (3) one-photon fluorescence anisotropy and (4) two-photon fluorescence anisotropy spectra for symmetric molecules; (a) PD2350; (b) PD3428; (c) Fluorene 2.

For both three-state (Eq. 6.4) and four-state models (Eq. 6.3), r_{2PA} depends on angle α, or $\alpha_{em} = \alpha + \frac{\gamma}{2}$ (angle between the absorbing dipole moment $\boldsymbol{\mu_{01}}$ and emission dipole moment $\boldsymbol{f_{em}}$), which can be calculated from the maximum value of the one-photon anisotropy $r_{1PA}^{\max}$. From Fig. 6.6, $r_{1PA}^{\max} \approx 0.38$ for all three symmetric molecules indicating that α_{em} does not exceed ~10°.

6.4.1.Analysis: Three-state model

Based on three-state model of Eq. 6.4, we can plot a set of curves for r_{2PA} as a function of γ ranging from 0° to 180° at several α_{em} as shown in Fig. 6.7. All curves converge to a point $r_{2PA} = 0.14$ at $\gamma = 90°$ independent of the value of α_{em}.

For symmetric molecules, quantum-chemical theory predicts that for 2PA to S_2 state, the transition dipoles $\boldsymbol{\mu_{01}}$ and $\boldsymbol{\mu_{12}}$ are parallel $\gamma = 0°$ (or anti-parallel γ=180°), for 2PA to the S_1 state $\boldsymbol{\mu_{01}}$ and $\boldsymbol{\Delta\mu}$ are perpendicular $\gamma = 90°$. Thus from curve 3 (α_{em}=10° do) in Fig. 6.7, the theoretical value of $r_{2PA} \approx 0.55$ for 2PA to the S_2 state ($\gamma = 0°$) and 0.14 for 2PA to the S_1 state ($\gamma = 90°$). Compared with experimental data, we found that for PD 2350 and PD 3428, $r_{2PA} \approx 0.47 - 0.49$ for both 2PA to S_1 and S_2 states, and contradicted the theoretical predictions. For fluorene 2, we measured $r_{2PA} \approx 0.53$ for both transitions, which is close to the theoretical value for 2PA to the S_2 state, but also disagrees with the theoretical result for 2PA to the S_1 state.

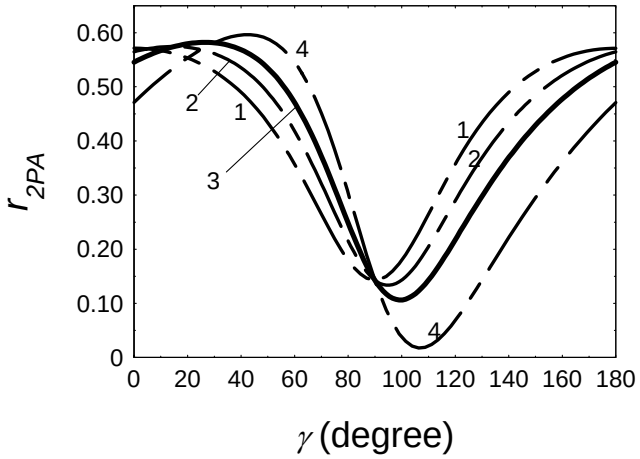

Figure 6.6 Two-photon anisotropy as a function of the angle γ with the three-state model at (1) α_{em}=0° ; (2) 5°; (3) 10°; and (4) 20°.

In order to understand the reason for this disagreement between the three-level model and experiments for symmetric molecules, we propose two ways as described in the next two sections

6.4.2. Analysis: Four-state model

Here we go to a more complete four-state model with Eq. 6.3. As shown in Fig.6.2, r_{2PA} becomes a function of the mutual orientation (angles $\alpha, \gamma, \beta, \theta$) in 2D-space of all 5 transition dipoles participating in the 2PA process, and also a function of the magnitudes of the four transition dipole moments and two detuning energies. We made this four-state model analysis with molecule PD2350 (experimental data shown in Fig. 6.6 (a)).

We assume that 2PA to S_2 includes two simultaneous scenarios or channels: $S_0 \rightarrow S_1$ then $S_1 \rightarrow S_2$ (first), and $S_0 \rightarrow S_4$ then $S_4 \rightarrow S_2$ (second), which is shown in Fig. 6.2 (a) where $S_n = S_4$ and $S_f = S_2$. The choice of S_4 as the second intermediate state for PDs is connected with our observation, taken from one-photon anisotropy spectra, that the angle β (between two scenarios or between $\boldsymbol{\mu}_{01}$ and $\boldsymbol{\mu}_{04}$) is typically one of the largest angles ($\approx 60^0$) among the measurable $S_0 \rightarrow S_n$ transitions. According to traditional quantum-chemical theories for symmetric molecules, the transitions within each scenario can be anti-parallel (($\gamma = \phi = 180^0$) or parallel ($\gamma = \phi = 0^0$) to each other, where γ is an angle inside of the first scenario (between $\boldsymbol{\mu_{01}}$ and $\boldsymbol{\mu_{12}}$), and ϕ is the angle inside of the second scenario (between $\boldsymbol{\mu_{04}}$ and $\boldsymbol{\mu_{42}}$) (see in Fig. 6.2 (b)). The dependence of r_{2PA} upon the angle γ calculated by Eq. 6.3 is shown in Fig. 6.8(a). Typically, for polymethines, the contribution of the second channel is small: $\mu_{04}\mu_{42} << \mu_{01}\mu_{12}$, therefore, the curve in Fig. 6.8 (a) completely overlaps with curve 3 in Fig. 6.7 which is calculated by the three-state model. In

this case, r_{2PA} depends mainly on γ and α_{em}, and does not change significantly with changes of β and ϕ, which is shown in the 3D plot in Fig. 6.8(b).

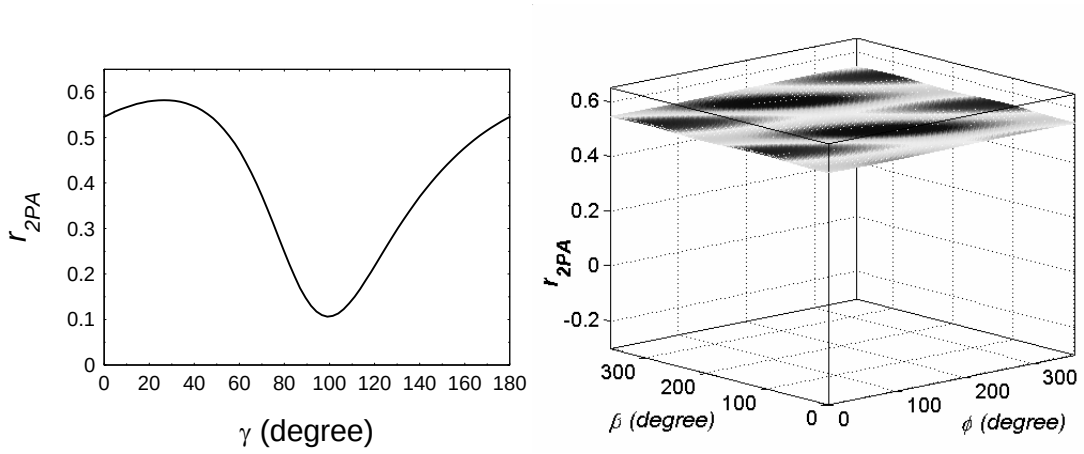

Figure 6.7 (a) Two-photon anisotropy r_{2PA}, calculated in the four-state model, as a function of γ. $\alpha_{em} = 10^0$; μ_{01} =13.5 D; $\mu_{12} = \mu_{04} = \mu_{42} = 1$ D; $\beta = 60^0$; $\phi = 0^0$ (or 180^0); $\Delta E_1 = 0.5$ eV; $\Delta E_2 = 2.5$ eV. This curve coincides with curve 3 from Fig. 6.7 obtained from the three-state model. (b) 3D picture of r_{2PA}, calculated in the four-state model, as a function of β and ϕ for $\alpha_{em} = 10^0$; μ_{01} =13.5 D; $\mu_{12} = \mu_{04} = \mu_{42} = 1$ D; $\gamma = 180^0$.

6.4.3. Analysis: Symmetry breaking of symmetric molecules

Since the more complete four-state model cannot explain the discrepancy between the theory and experiments for symmetric molecules shown in Fig. 6.6 either, we tried to explain this with the symmetry breaking of symmetric molecules.

For PD2350, based on calculations from the three-state model (Eq.6.4, and curve 3 in Fig. 6.7), in order to achieve $r_{2PA} \approx 0.47 - 0.49$ over two electronic transitions, which is what experiments showed, the deviations of orientation of the participating dipoles should be $\approx 35^0$ for $\Delta\boldsymbol{\mu}$ from the perpendicular "classical" orientation, and $\approx 17^0$ for $\boldsymbol{\mu_{12}}$ from the anti-parallel

"classical" orientation. These deviations could be due to ground-state symmetry breaking. This is illustrated in Fig. 6.9.

Even a small contribution of an asymmetrical form can lead to non-equality in the charge transfer from the terminal groups to the chain center, which will affect the orientation of the transition moments. As shown in Fig. 6.9, this effect cannot essentially change the orientation of the large $S_0 \rightarrow S_1$ transition dipole moment since for both forms charge transfer occurs in the direction of the chromophore. However, for other transition dipole moments, which are at least one order of magnitude smaller, the difference in the charge transfer from the terminal groups to the center of the chain can strongly affect their orientations. An especially strong effect can be observed for the "perpendicular" (to $S_0 \rightarrow S_1$) transitions, such as $\Delta\boldsymbol{\mu}$, $\boldsymbol{\mu_{02}}$ ($S_0 \rightarrow S_2$), $\boldsymbol{\mu_{04}}$ ($S_0 \rightarrow S_4$). It is seen that the asymmetrical charge transfer from the terminal groups can change the direction of $\boldsymbol{\mu_{02}}$ relative to $\boldsymbol{\mu_{01}}$. However, we cannot predict how the deviation of $\boldsymbol{\mu_{02}}$ will change the "classical" orientation of $\boldsymbol{\mu_{12}}$ (parallel or anti-parallel to $\boldsymbol{\mu_{01}}$). Further development of quantum-chemical theory is necessary.

The assumption about the ground-state symmetry breaking, affecting the orientations of higher excited-state transition dipole moments relative to $\boldsymbol{\mu_{01}}$, can explain why in one-photon anisotropy measurements the "classical" minimal anisotropy value $r_{1PA} = -0.2$, corresponding to an angle $\alpha_{em} = 90^0$, has not been observed for PDs (also see this in Appendix B). The maximum angles observed experimentally for the "perpendicular" transitions in PDs were $60^0 - 65^0$.

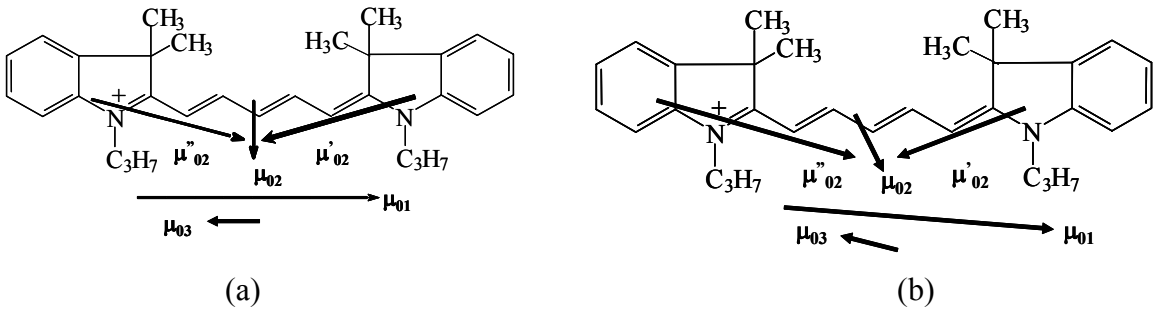

Figure 6.8 Schematic presentation of the orientation of the transition dipole moments for (a) symmetrical and (b) asymmetrical forms of PD 2350. μ''_{02} and μ'_{02} indicate a partial charge transfer from each terminal group to the polymethine chromophore.

6.5. Asymmetric molecules

The experimental results for the three asymmetric molecules (PD2665, Styryl 1 and Fluorene 1) are shown in Fig. 6.10 (a)-(c). For comparison with linear absorption, 2PA and two-photon anisotropy spectra are presented as functions of wavelength equal to half of input photon wavelengths.

We also compare experimental data with the three-state model (Eq. 6.4). Quantum-chemical calculations performed for these molecules, show that μ_{01} and μ_{12} are oriented almost parallel (angles γ are within 10^0) similar to the symmetrical molecules. However, $\Delta\mu$ shows a large deviation from an orientation perpendicular to μ_{01}. These angles γ for Styryl 1, PD 2665 and fluorene 1 equal 26^0, 43^0 and 37^0 respectively. Substituting theseγ's into the three-state model or Eq. 6.4, as well as using the experimental value of $\alpha_{em} = 10^0$, which is the same for all these molecules, we calculated that $r_{2PA} \approx 0.55$ - 0.56 for 2PA to both S_1 and S_2 states. Thus, the three-state model can be used to model the asymmetrical molecules for two-photon excitation fluorescence anisotropy.

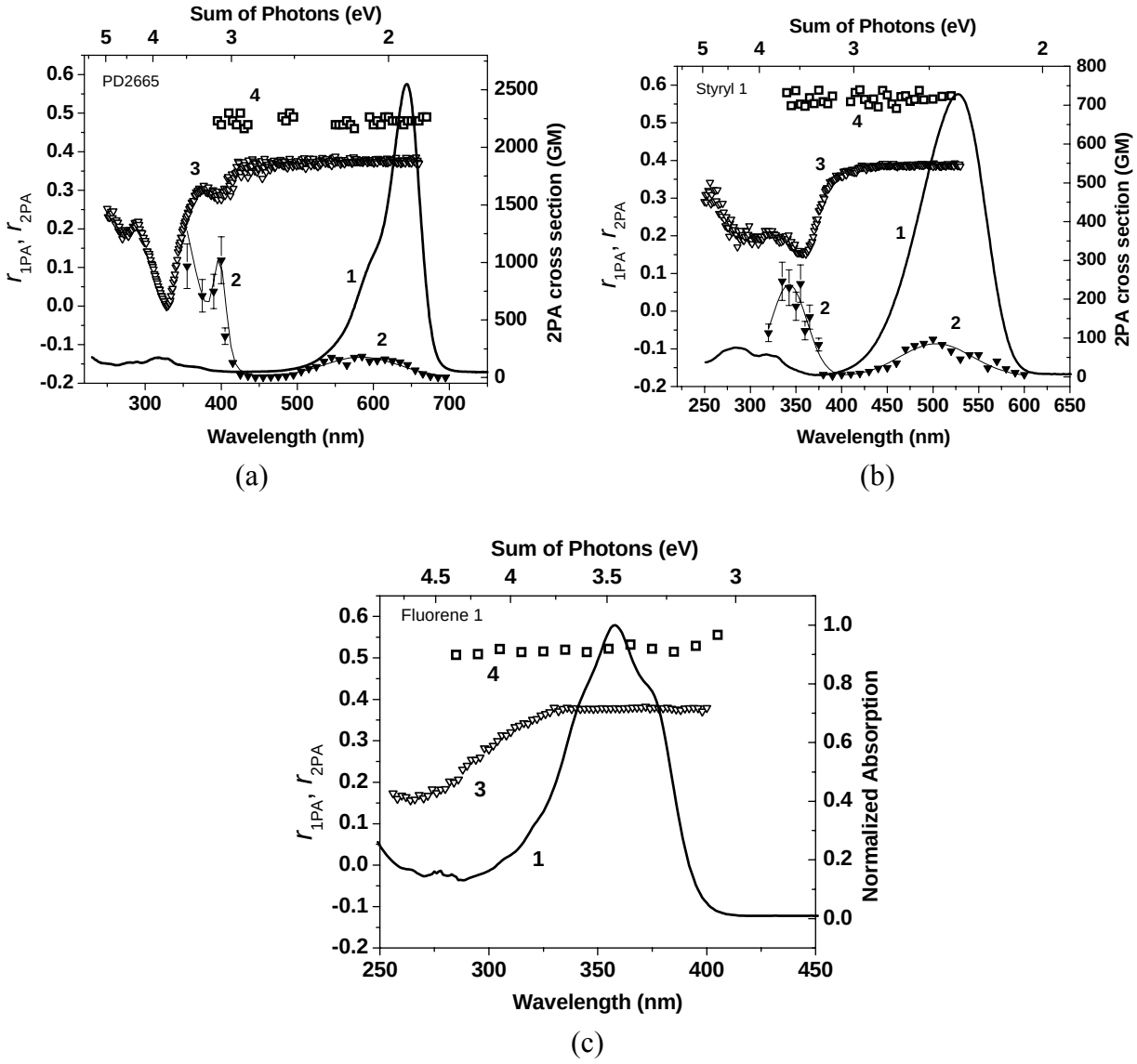

Figure 6.9 Linear absorption (1), 2PA spectra (2), one-photon anisotropy (3) and two-photon anisotropy (4) for asymmetric molecules: (a) PD2665; (b) Styryl 1; (c) Fluorene 1.

6.6 Why do we use the four-state model?

From the above analysis, we see that the three-state model works for asymmetric molecules fairly well, but both three- and four-state models do not work for the symmetric

molecules we studied, and we have to introduce symmetry breaking to explain the lower experimental value of r_{2PA} for symmetrical molecules. So what is the benefit for us to have a more complicated four-state model for two-photon excitation fluorescence anisotropy?

Based on the four-state model, theoretically there is a way to decrease r_{2PA} closer to the experimental values for symmetric molecules without introducing symmetry breaking (means that we can keep the parallel or anti-parallel "classical" orientation of transitions inside each channel for symmetric molecules).

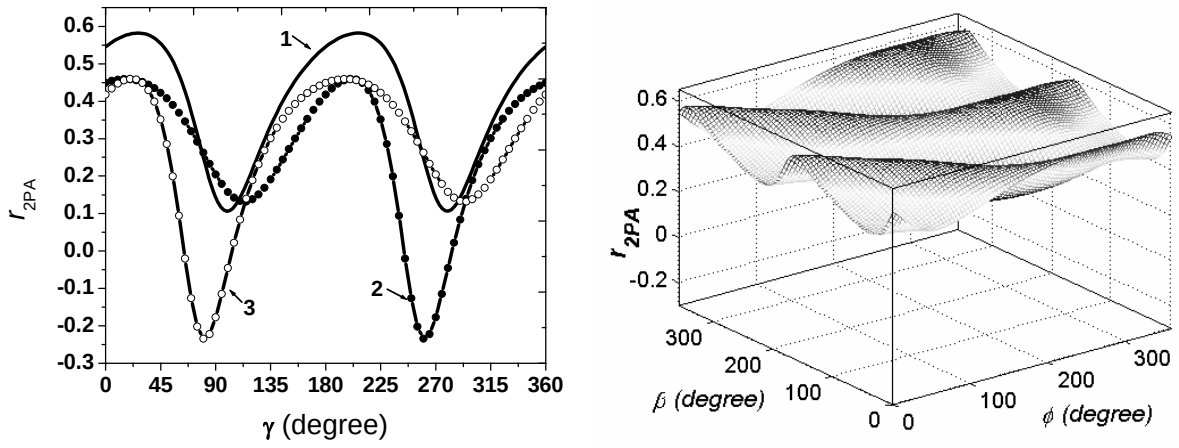

(a) (b)

Figure 6.10 (a) Two-photon anisotropy r_{2PA} for 2PA to S_2 state of PD2350, calculated in the four-state model, as a function of γ. Curve 1: $\alpha_{em} = 10^0$; $\beta = 60^0$; $\phi = 0^0$ (or 180^0); $\Delta E_1 = 0.5$ eV; $\Delta E_2 = 2.5$ eV; $\mu_{01} = 13.5$ D; $\mu_{12} = 1$D; $\boldsymbol{\mu_{04} = \mu_{42} = 1}$ **D**. Curve 2 and 3: $\alpha_{em} = 10^0$; $\beta = 60^0$; $\Delta E_1 = 0.5$ eV; $\Delta E_2 = 2.5$ eV; $\mu_{01} = 13.5$ D; $\mu_{12} = 1$ D; $\boldsymbol{\mu_{04} = \mu_{42} = 6}$ **D**; $\phi = 0^0$ (for curve 2) and $\phi = 180^0$ (for curve 3). (b) 3D plot of r_{2PA}, as functions of β, ϕ, with $\alpha_{em} = 10^0$; $\gamma = 180^0$; $\Delta E_1 = 0.5$ eV; $\Delta E_2 = 2.5$ eV; $\mu_{01} = 13.5$ D; $\mu_{12} = 1$ D; $\boldsymbol{\mu_{04} = \mu_{42} = 6}$ **D**

For this purpose we consider an increase of the contribution of the second channel. Fig. 6.11 (a) (curves 2 and 3) demonstrates these results for the case $\mu_{04}\mu_{42} \geq \mu_{01}\mu_{12}$ ($\mu_{01} = 13.5$ D, $\mu_{12} = 1$ D, $\mu_{04} = \mu_{42} = 6$ D). The 3D plot of r_{2PA}, calculated in the four-state model, as functions

of β, ϕ at an increased contribution of the second channel, is presented in Fig. 6.11 (b), which are compared with Fig.6.8 for $\mu_{04} = \mu_{42} = 1$D.

It is important to note that in contrast to the PDs studied in this dissertation, some molecules from other classes of organic compounds possess strong transitions to the second or higher excited states with dipole moments comparable to μ_{01}. For example, the symmetrical 9,9-didecyl-2,7-bis-(N,N-diphenylamino)fluorene, reported in [76], shows relatively large transition dipole moments (up to 6 debye) to the higher excited-states compared to the ground state transition dipole moment $\mu_{01} = 8$ debye. Its molecular parameters, revealed from quantum-chemical calculations and substituted into the four-state model or Eq. 6.3, give $r_{2PA} \approx 0.27$ without involving symmetry breaking, which is close to its experimental value. This confirms that the four-state model can be used for the explanation of r_{2PA} into the S_1 and S_2 states, if the contribution of the effective second channel to 2PA is comparable with the contribution of the first one.

For the polymethine molecules, this case may be achieved by considering the second channel as a superposition of all possible channels oriented at relatively large angles to the first excitation channel.

In addition, although based on the three-state model, r_{2PA} does not depend on detuning energy ΔE, or pump photon energy. The four-state model provides us a chance to study the wavelength dependence of r_{2PA} by changing the detuning energy. Figure 6.12 shows the two-photon excitation anisotropy r_{2PA} for PD2350 based on the four-state model as a function of wavelength equal to half of input photon wavelength. By including a symmetry breaking effect,

we could get the two-photon excitation fluorescence spectrum, which agrees with the experimentally observed flat r_{2PA} spectra.

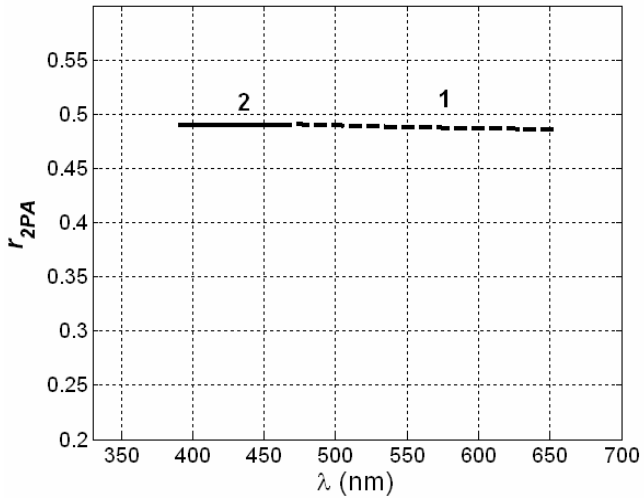

Figure 6.11 Calculated wavelength dependence of r_{2PA} under 2PA to S_1 state (1) and 2PA to S_2 state (2) based on the four-state model. Molecular parameters for (1) are: $\alpha_{em} = 10^0$; μ_{01} =13.5 D; $\Delta\mu = 0.6$; $\mu_{02} = 1.2$ D; $\mu_{21} = 1$ D; $\phi = 90^0$; $\beta = 32^0$; $\gamma = 55^0$. Molecular parameters for (2) are: $\alpha_{em} = 10^0$; μ_{01} =13.5 D; $\mu_{12} = 1$ D; $\mu_{04} = \mu_{42} = 1$ D; $\phi = 180^0$; $\beta = 60^0$; $\gamma = 163^0$.

Although we can understand two-photon anisotropy having the same value within one electronic transition based on the theoretical models, we still do not quite understand the fundamental reason why two-photon anisotropy keeps the same value over several electronic transitions for symmetric molecules, so more analysis has to be made.

CHAPTER 7 CONCLUSIONS

7.1 Conclusions

In this dissertation, the relationships of molecular structures to linear and nonlinear optical properties (especially 2PA properties) for polymethine and squaraine dyes are addressed. Systematically altering the molecular structures provided an effective way to investigate the correlations of structure to their optical properties, and then indicated the pathway to design novel organic molecules exhibiting large nonlinearity and ultimately to make nonlinear optical organic photonic devices for real applications. These studies include effects of molecular symmetry, strength of donor terminal groups, conjugation length of the chromophore chain, polarity of solvents, and bridge molecules within the chromophore chain. We also compared polymethine, squaraine, croconium and tetraon dyes with similar structures to study the effects of the different additions inserted within the chromophore chain on their NLO properties. We used three different nonlinear spectroscopic techniques (Z-scan, two-photon fluorescence and white-light continuum pump-probe) to obtain 2PA spectra, revealing 2PA bands, and to confirm the experimental data by comparing the results from different methods. Two-photon excitation fluorescence anisotropy spectra were measured through several 2PA transitions. This is the first time such measurement have been reported to our knowledge.

To understand the structure-property relationships observed from these experiments, we used a simplified three-level model based on the 2PA tensor method to fit experimental 2PA spectra to reveal the critical parameters for 2PA. Quantum chemical calculations help us

understand the evolution of molecular orbitals with changing to the structures, and transitions between MOs which are responsible for observed linear and 2PA bands.

The conclusions related to the correlations of the molecular structures to their 2PA properties are summarized below:

1) **Symmetry:** Symmetrical PDs and SDs show negligible 2PA into the first excited state, or linear absorption band. But asymmetric molecules clearly show 2PA into any excited state. Both symmetric and asymmetric PDs as well as SDs exhibit a weak 2PA band at the vibrational shoulder of the linear absorption spectra, i.e.2PA from the ground state to the higher lying vibration bands of the first excited state. Symmetry breaking is clearly indicated for symmetric molecules by this 2PA band. The origin of the symmetry breaking was investigated (see sections 4 and 9)).

2) **Terminal Groups:** Three molecules with different terminal groups (Thiazolium, Indolium, Benzoindolium) and the same conjugation length were compared for their 2PA properties. PD 2630 with the strongest donor benzoindolium terminal group exhibits red-shifted linear and 2PA spectra, and the beginning of a third and stronger 2PA band can be observed experimentally. Comparing 2PA properties of PD 200 and PD 2761 provides us some insight about the effect of conjugation strcture in the terminal group on the linear and nonlinear properties.

3) **Conjugation Length:** Increasing the conjugation length of the chromophore chain red-shifts both the linear and 2PA bands, as well as increasing the 2PA cross section due to increases of ground state transition dipole moments and decreases of detuning energies.

4) **Polarity of Solvents:** A way to study the symmetry breaking of symmetric molecules is to study 2PA of molecules in solvents of different polarity. Experimental results indicated

two possible origins for this symmetry breaking. One is vibronic coupling due to the vibrational shoulder in the linear absorption. The other is the existence of an asymmetrical charge distribution in the symmetric molecules.

5) **Bridge:** Inserting a benzene bridge into the chromophore chain can protect the symmetric molecules from symmetry breaking. Thus, we observed that the 2PA cross sections of this weak 2PA band is smaller for bridged symmetric PDs than unbridged symmetric PDs.

6) **Polymethines and Squaraines:** SDs exhibited much larger experimentally observable 2PA cross sections than PDs having the same terminal groups and similar conjugation length. Quantum chemical calculations showed that forming PDs by putting terminal groups on the chromophore chain increases the density of occupied molecular orbitals, thus increases electronic transitions for 2PA. Quantum chemical calculations also showed that forming SDs by inserting a squarylium core into PDs further increases the density of unoccupied molecular orbitals, thus the electronic transitions. Thus, combining with narrower linear absorption bands, SDs move more 2PA bands with larger 2PA cross sections into the experimentally observable region before being obscured by linear absorption. Near IR absorbing squaraine dyes exhibit extremely large 2PA cross sections (≈ 30000GM).

7) **Squaraine, Croconium and Tetraon:** Inserting different additions into the chromophore chain forms squaraine (C_4O_2), Croconium (C_5O_3) and Tetraon (C_6O_4) dyes. Croconium exhibits much smaller 2PA than squaraine, and tetraon dyes show similar large 2PA as squaraine, but exhibits more 2PA bands than squaraines indicating an increase of the number of electronic transitions.

8) **One-photon Fluorescence Anisotropy:** Our experimental results indicate the strong correlation between one-photon excitation fluorescence anisotropy spectra and 2PA spectra for symmetric PDs. Quantum chemical calculations show that this correlation comes from energy splitting of molecular orbitals of two identical terminal groups. After splitting, one molecular orbital corresponds to a one-photon transition, and the other molecular orbital corresponds to a two-photon transition. And this splitting energy depends on the structure of the terminal groups. For symmetric SDs, this correlation is also observed.

9) **Two-photon Fluorescence Anisotropy:** Two-photon excitation fluorescence anisotropy spectra for several 2PA bands are measured experimentally for the first time. A theoretical model based on a four-level, two-intermediate-state model is developed. The observed deviation of the two photon anisotropy from the theoretical prediction for symmetric molecules indicates the existence of symmetry breaking.

7.2 Future work

From the conclusions listed above, a few potential research are are proposed:

1) The conjugation structure of terminal groups will increase the effective conjugation length of molecules. The effect of conjugation length in the terminal groups on 2PA is still an ongoing research project. I will propose to try to quantitatively describe the donor/acceptor strength of different terminal groups, which will help to separate the contributions of donor/acceptor strength in TGs from conjugation structure in TGs on the 2PA properties of the molecules.

2) To investigate the nature of symmetry breaking we need more experiments performed. Linear absorption of long polymethine molecules (such as PD 1659) exhibits a strong dependence on the polarity of solvents. Some short molecules exhibit less of this dependence. It is proposed to measure 2PA of long molecules in solvents of different polarity to study the effects of the asymmetric form in symmetric molecules on 2PA However, two issues make this measurement difficult. One is that molecules with long conjugation lengths will move the linear absorption band as well as the fluorescence spectrum into the NIR region. Only the Z-scan technique can study the weak 2PA band at the vibronic shoulder of the linear absorption band. The other is that the solubility of symmetric molecules strongly depends on the polarity of the solvent, which makes it impossible to prepare high concentration solutions for all solvents for Z-scan measurements. Being able to use the very sensitive 2PF method becomes crucial for this study.

3) Quantum chemical calculations need to be performed to understand the difference in 2PA properties of squaraine, croconium and tetraon for optimizing molecules for 2PA applications in the future.

4) The value of two-photon excitation fluorescence anisotropy is experimentally observed to be constant for several 2PA bands for all the molecules we studied. We can explain this for asymmetric molecules based on a three-level model. However we cannot explain this phenomenon for symmetric molecules with three-level and four-level models. More theoretical study on this is proposed.

APPENDIX A
CGS AND SI UNIT

In chapter two, we derived the formula for the imaginary part of $\chi^{(3)}$ in SI units. But when we used the relation for the 2PA cross section and transition dipole moments to fit experimental 2PA spectra, we use a formula in CGS units because usually transition dipole moments are expressed with units of debye (D) that belongs to CGS unit.

The CGS unit system is an abbreviation for the centimeter-gram-second system, which uses the centimeter, gram and second for length, mass and time. The units most used parameters for 2PA cross section theory are expressed in SI and CGS units listed in Table A.1.

Table A.1 Relationship of CGS to SI unit

	CGS	Definition	SI
Length	centimeter	1 cm	$= 10^{-2}$ m
Mass	Gram	1 g	$= 10^{-3}$ kg
Time	Second	1 s	= 1 s
Energy	Erg	1 erg = 1 g • cm^2/s^2	$= 10^{-7}$ J
Charge	Esu	1 esu = 1 $(g \bullet cm^3/s^2)^{1/2}$	$= 3.3356\times10^{-10}$ C
Dipole moment	debye (D)	1 D = 1 10^{-18} cm • esu	$= 3.3356\times10^{-10}$ C • m

We used Eq. 2.54 in Chapter 2 to fit the 2PA spectra of polymethine and squaraine molecules. We calculated the constant and changed Eq. 2.54 into the Eq. 2.57 for practical use, where the 2PA cross section is in units of GM (10^{-50} cm^4 • s/molecule), all energies are input with units of eV and all dipole moments are input with units of debye (D). The derivation for this equation is shown below to verify the units validity and calculated constant in front.

$$\delta(E_p)[GM]=\frac{64\pi^3}{5c^2h}\frac{{E_p}^2}{(E_{jo}-E_p)^2+{\Gamma_{jo}}^2}\frac{\left|\boldsymbol{\mu}_{jo}\right|^2\left|\boldsymbol{\mu}_{fj}\right|^2\Gamma_{f0}}{(E_{fo}-2E_p)^2+{\Gamma_{f0}}^2}$$

$$=\frac{64\pi^3}{5\times(3\times10^{10})^2\cdot cm^2/s^2\times(6.626\times10^{-27})\cdot erg\cdot s}\times\frac{{E_p}^2[eV^2]}{(E_{jo}[eV]-E_p[eV])^2+{\Gamma_{jo}}^2[eV^2]}\times$$

$$\frac{\Gamma_{f0}[eV]}{(E_{fo}[eV]-2E_p[eV])^2+{\Gamma_{f0}}^2[eV^2]}\times\frac{1}{1.602\times10^{-12}\cdot erg/[eV]}\times\left|\boldsymbol{\mu}_{jo}[debye]\right|^2\left|\boldsymbol{\mu}_{fj}[debye]\right|^2\times(10^{-18}\cdot\frac{esu\cdot cm}{[debye]})^4$$

$$=\frac{64\pi^3\times(10^{-18})^4}{5\times(3\times10^{10})^2\times6.626\times10^{-27}\times1.602\times10^{-12}}\times\frac{{E_p}^2[eV^2]}{(E_{jo}[eV]-E_p[eV])^2+{\Gamma_{jo}}^2[eV^2]}\times$$

$$\frac{\Gamma_{f0}[eV]}{(E_{fo}[eV]-2E_p[eV])^2+{\Gamma_{f0}}^2[eV^2]}\times\left|\boldsymbol{\mu}_{jo}[debye]\right|^2\left|\boldsymbol{\mu}_{fj}[debye]\right|^2\times\frac{esu^4\cdot cm^4}{cm^2/s^2\cdot erg^2\cdot s}$$

$$=\frac{1984.4\times10^{-72}}{477.67\times10^{-19}}\times\frac{{E_p}^2[eV^2]}{(E_{jo}[eV]-E_p[eV])^2+{\Gamma_{jo}}^2[eV^2]}\times$$

$$\frac{\Gamma_{f0}[eV]}{(E_{fo}[eV]-2E_p[eV])^2+{\Gamma_{f0}}^2[eV^2]}\times\left|\boldsymbol{\mu}_{jo}[debye]\right|^2\left|\boldsymbol{\mu}_{fj}[debye]\right|^2\times cm^2\cdot s\cdot\frac{esu^4}{erg^2}$$

$$=4.15\times10^{-3}\times10^{-50}\times\frac{{E_p}^2[eV^2]}{(E_{jo}[eV]-E_p[eV])^2+{\Gamma_{jo}}^2[eV^2]}\times$$

$$\frac{\Gamma_{f0}[eV]}{(E_{fo}[eV]-2E_p[eV])^2+{\Gamma_{f0}}^2[eV^2]}\times\left|\boldsymbol{\mu}_{jo}[debye]\right|^2\left|\boldsymbol{\mu}_{fj}[debye]\right|^2\times cm^2\cdot s\cdot\frac{(\sqrt{g\cdot cm^3/s^2})^4}{(g\cdot cm^2/s^2)^2}$$

$$=4.15\times10^{-3}\times\frac{{E_p}^2[eV^2]}{(E_{jo}[eV]-E_p[eV])^2+{\Gamma_{jo}}^2[eV^2]}\times\frac{\Gamma_{f0}[eV]\left|\boldsymbol{\mu}_{jo}[debye]\right|^2\left|\boldsymbol{\mu}_{fj}[debye]\right|^2}{(E_{fo}[eV]-2E_p[eV])^2+{\Gamma_{f0}}^2[eV^2]}\times10^{-50}\cdot cm^4\cdot s[GM]$$

$$=4.15\times10^{-3}\times\frac{(E_p[eV])^2}{(E_{jo}[eV]-E_p[eV])^2+(\Gamma_{jo}[eV])^2}\times\frac{\Gamma_{f0}[eV]\left|\boldsymbol{\mu}_{jo}[debye]\right|^2\left|\boldsymbol{\mu}_{fj}[debye]\right|^2}{(E_{fo}[eV]-2E_p[eV])^2+(\Gamma_{f0}[eV])^2}[GM]$$

APPENDIX B
EXPERIMENTAL DATA FOR MOLECULES FROM DR. OLGA V. PRZHONSKA

We performed a comprehensive experimental study of PDs, SDs, and tetraon dye that are synthesized at the Institute of Organic Chemistry, National Academy of Sciences, Ukraine. We measured linear absorption spectra, one-photon fluorescence spectra, one-photon excitation fluorescence anisotropy spectra, two-photon absorption spectra and two-photon excited fluorescence anisotropy spectra. Below are listed experimental results for all molecules. Molecular structures can be found in Fig. 4.2 and Fig. 5.1.

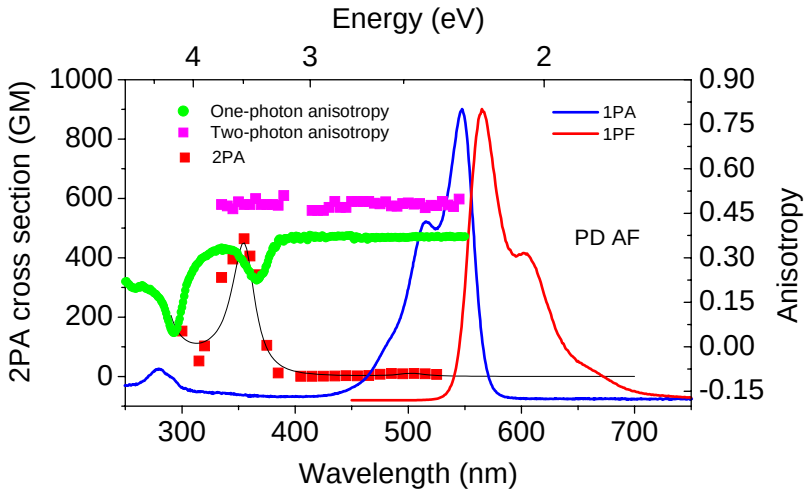

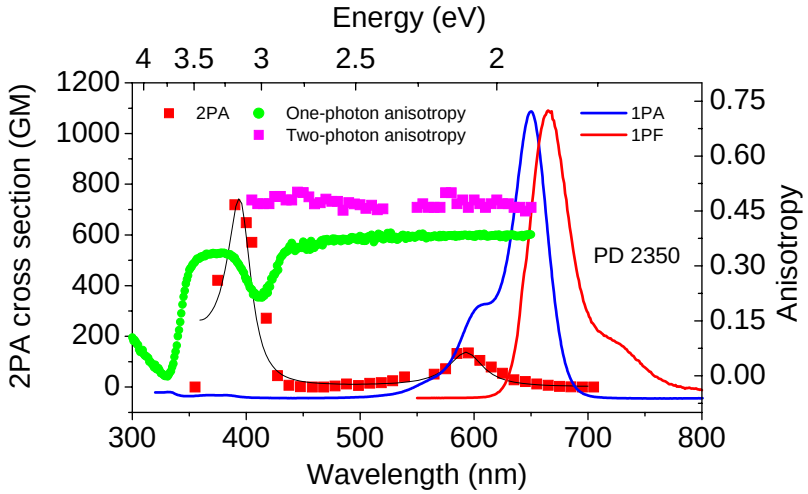

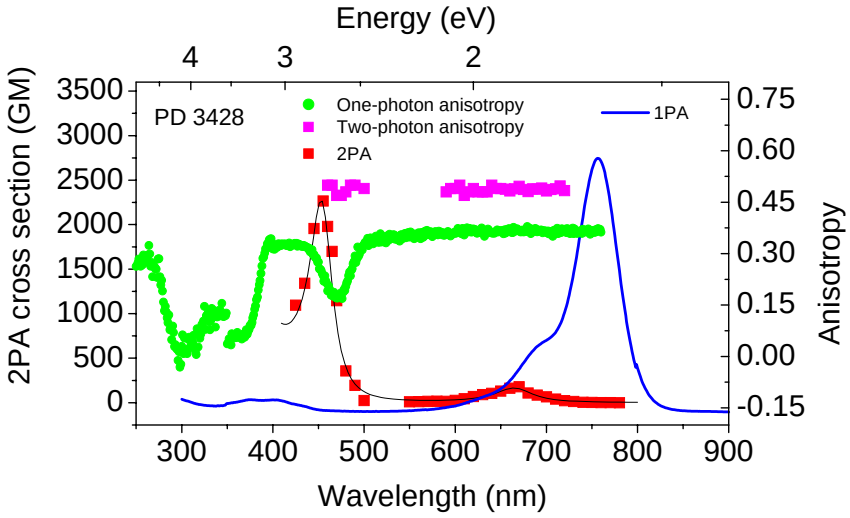
Energy (eV)
4
3
2
PD 3428
One-photon anisotropy
Two-photon anisotropy
2PA
1PA
2PA cross section (GM)
Anisotropy
Wavelength (nm)

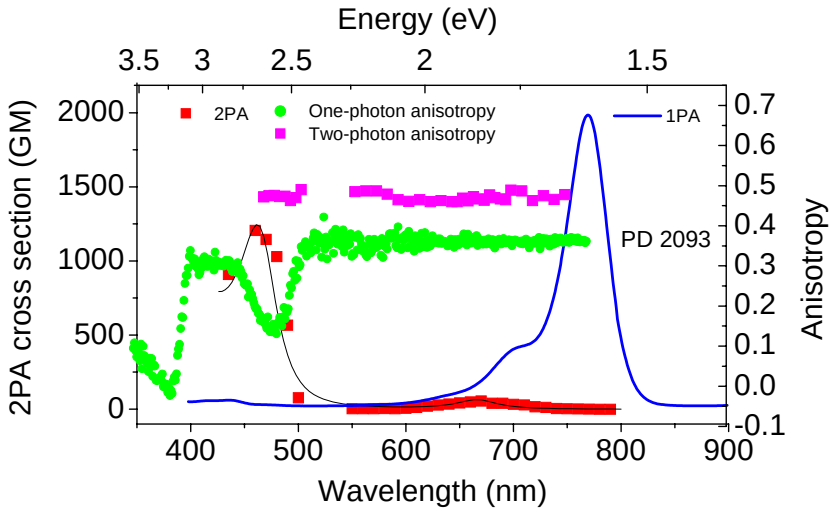
Energy (eV)
3.5
3
2.5
2
1.5
2PA
One-photon anisotropy
Two-photon anisotropy
1PA
PD 2093
2PA cross section (GM)
Anisotropy
Wavelength (nm)

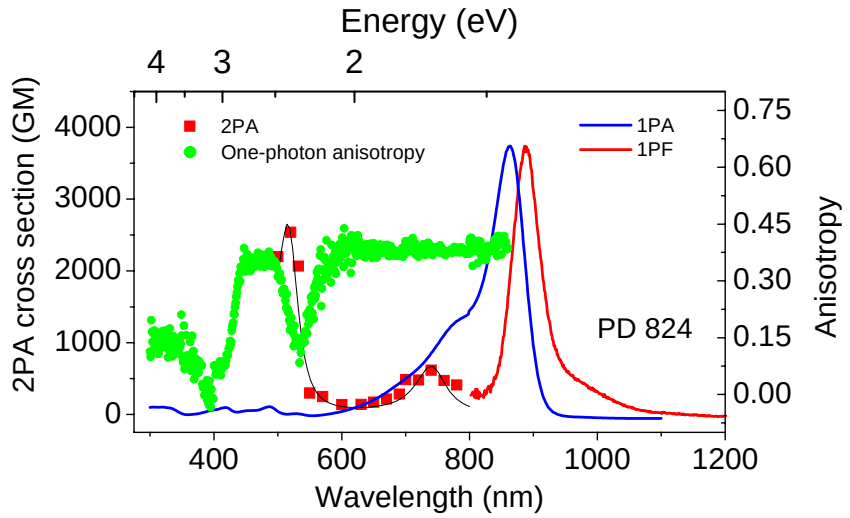
Energy (eV)
4
3
2
2PA
One-photon anisotropy
1PA
1PF
PD 824
2PA cross section (GM)
Anisotropy
Wavelength (nm)

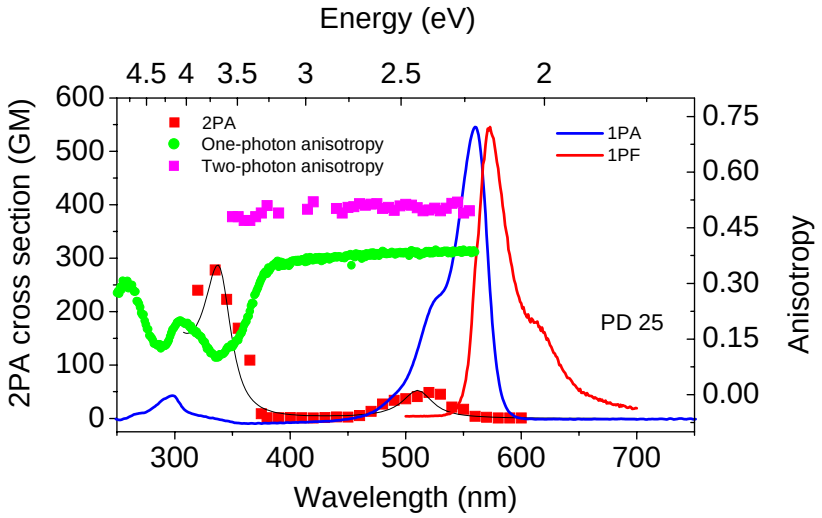
Energy (eV)
4.5 4 3.5 3 2.5 2
2PA cross section (GM)
Anisotropy
Wavelength (nm)
2PA
One-photon anisotropy
Two-photon anisotropy
1PA
1PF
PD 25

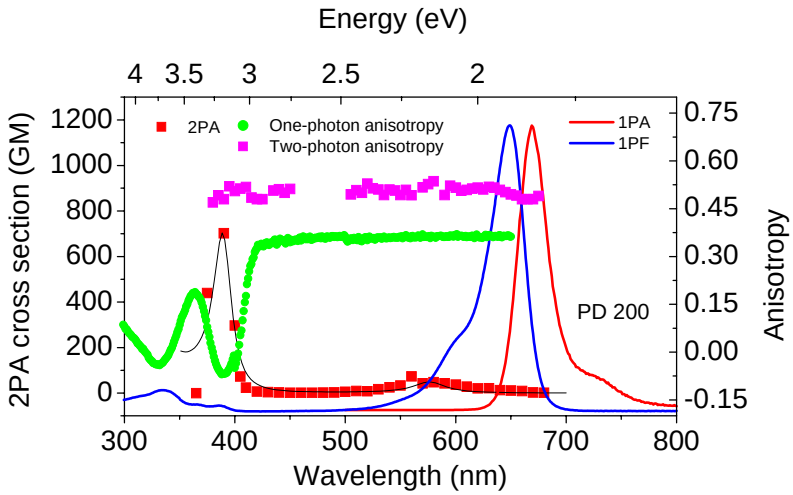
Energy (eV)
4 3.5 3 2.5 2
2PA cross section (GM)
Anisotropy
Wavelength (nm)
2PA
One-photon anisotropy
Two-photon anisotropy
1PA
1PF
PD 200

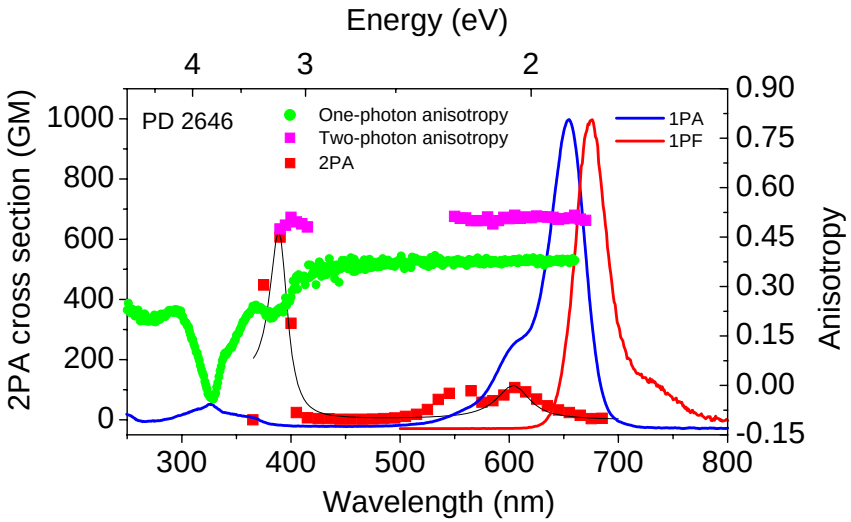
Energy (eV)
4 3 2
2PA cross section (GM)
Anisotropy
Wavelength (nm)
PD 2646
One-photon anisotropy
Two-photon anisotropy
2PA
1PA
1PF

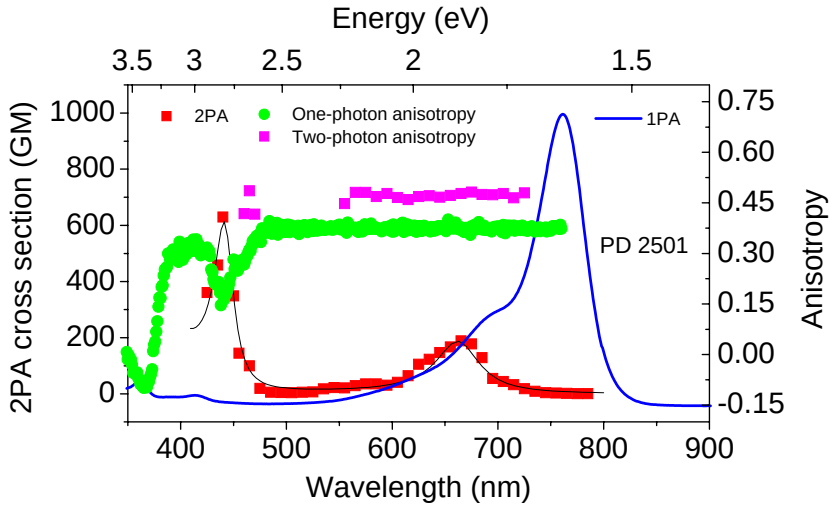
Energy (eV)
3.5
3
2.5
2
1.5
2PA
One-photon anisotropy
Two-photon anisotropy
1PA
PD 2501
2PA cross section (GM)
Anisotropy
Wavelength (nm)

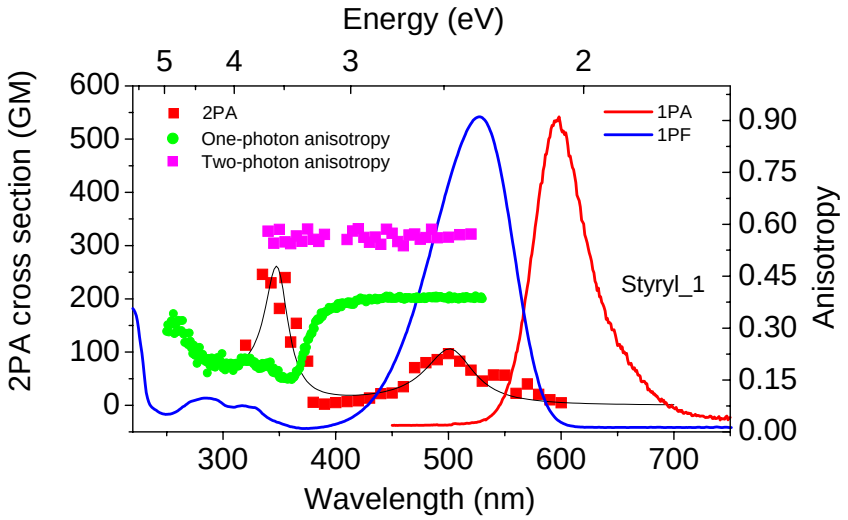
Energy (eV)
5
4
3
2
2PA
One-photon anisotropy
Two-photon anisotropy
1PA
1PF
Styryl_1
2PA cross section (GM)
Anisotropy
Wavelength (nm)

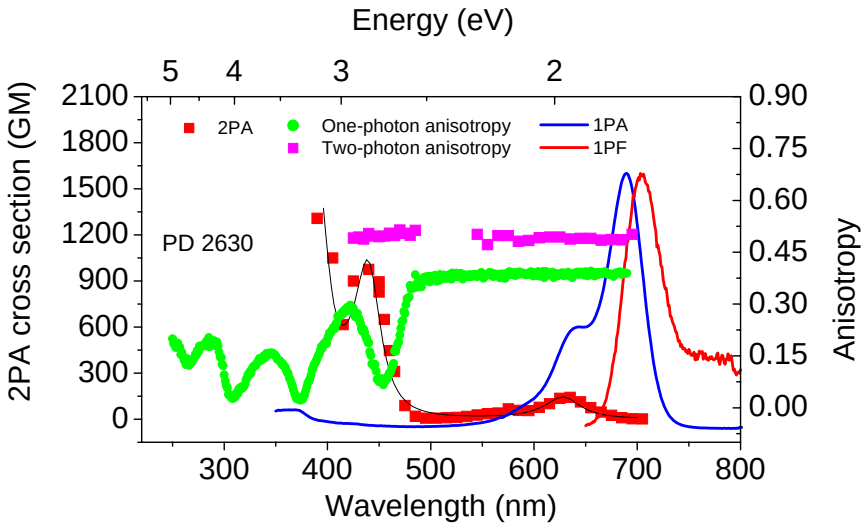
Energy (eV)
5
4
3
2
2PA
One-photon anisotropy
Two-photon anisotropy
1PA
1PF
PD 2630
2PA cross section (GM)
Anisotropy
Wavelength (nm)

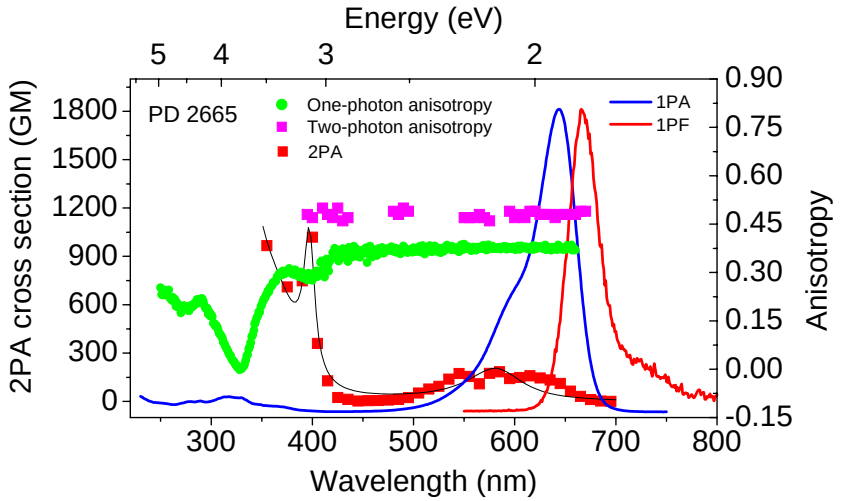
Energy (eV)
5
4
3
2
PD 2665
One-photon anisotropy
Two-photon anisotropy
2PA
1PA
1PF
2PA cross section (GM)
Anisotropy
Wavelength (nm)

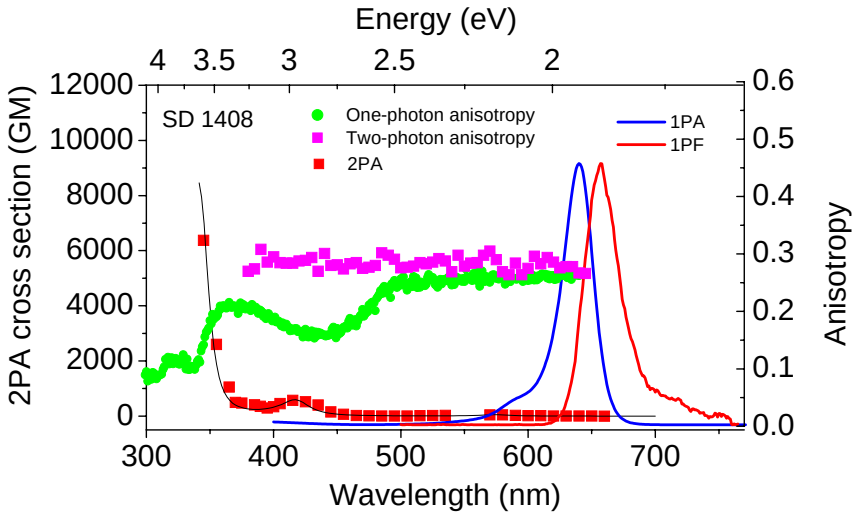
Energy (eV)
4
3.5
3
2.5
2
SD 1408
One-photon anisotropy
Two-photon anisotropy
2PA
1PA
1PF
2PA cross section (GM)
Anisotropy
Wavelength (nm)

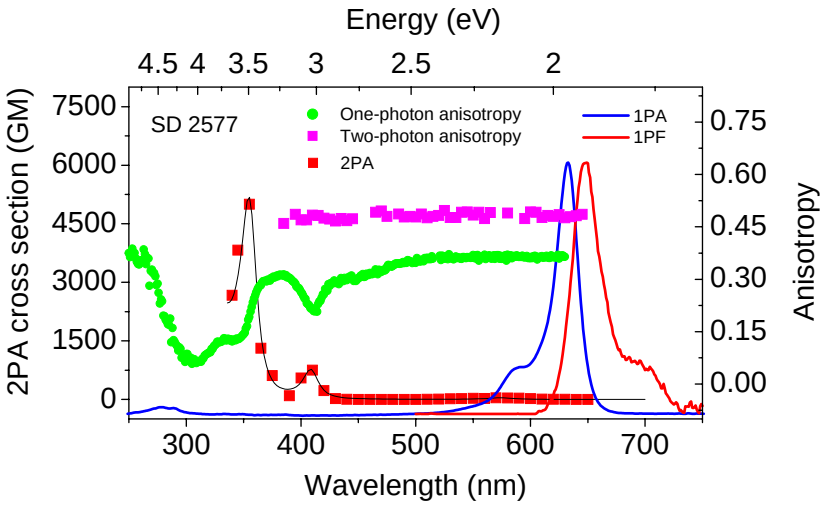
Energy (eV)
4.5
4
3.5
3
2.5
2
SD 2577
One-photon anisotropy
Two-photon anisotropy
2PA
1PA
1PF
2PA cross section (GM)
Anisotropy
Wavelength (nm)

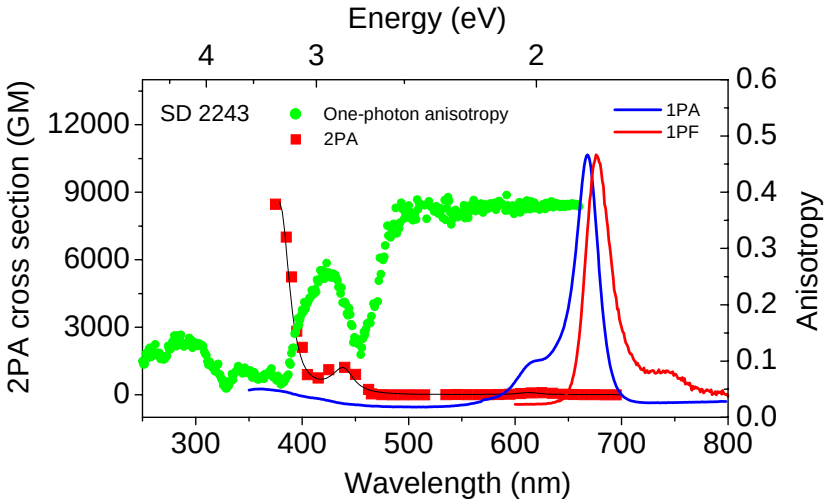
Energy (eV)
4
3
2
SD 2243
One-photon anisotropy
2PA
1PA
1PF
2PA cross section (GM)
Anisotropy
Wavelength (nm)
12000
9000
6000
3000
0
0.6
0.5
0.4
0.3
0.2
0.1
0.0
300
400
500
600
700
800

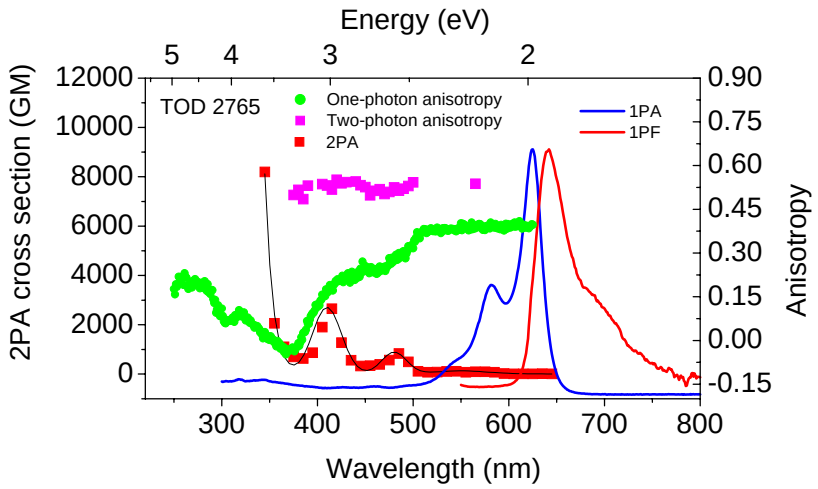
Energy (eV)
5
4
3
2
TOD 2765
One-photon anisotropy
Two-photon anisotropy
2PA
1PA
1PF
2PA cross section (GM)
Anisotropy
Wavelength (nm)
12000
10000
8000
6000
4000
2000
0
0.90
0.75
0.60
0.45
0.30
0.15
0.00
-0.15
300
400
500
600
700
800

APPENDIX C
EXPERIMENTAL DATA FOR MOLECULES FROM DR. SETH R. MARDER'S GROUP

C.1 MOLECULES FOR 2PA AT TELECOMMUNICATIONS WAVELENGTHS [83]

Molecular structures:

LB-II-84a

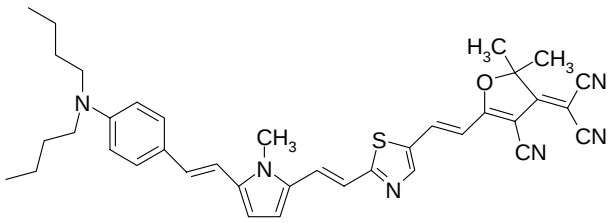

LB-IV-43a

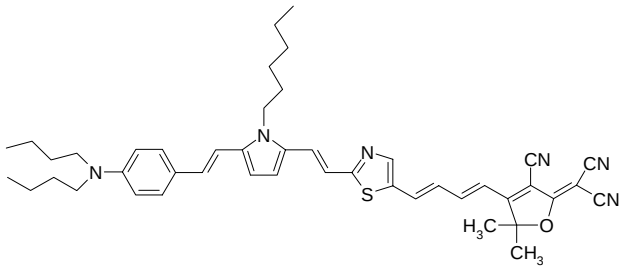

LB-IV-20c

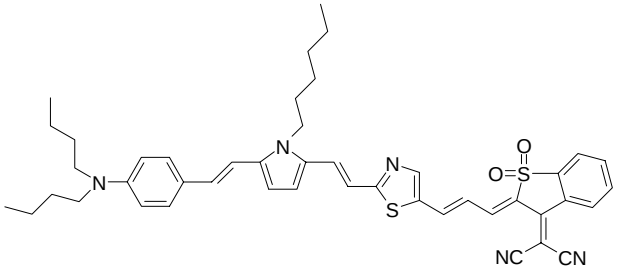

Sjz-6-89

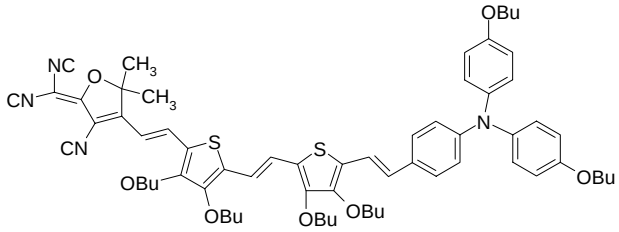

AJC-190

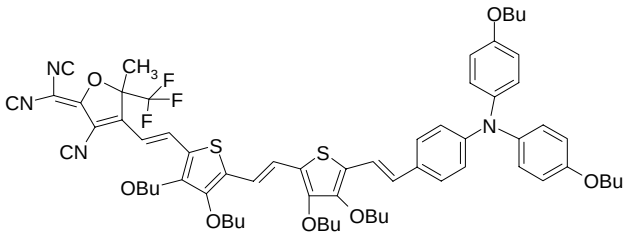

TOR-I-99

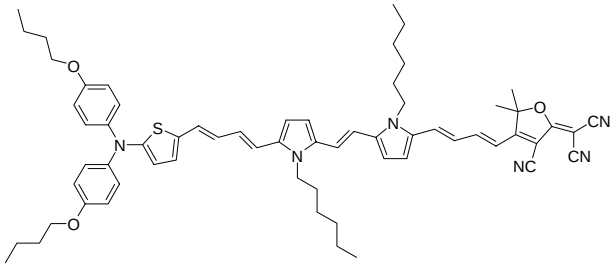

LB-II-84a in THF

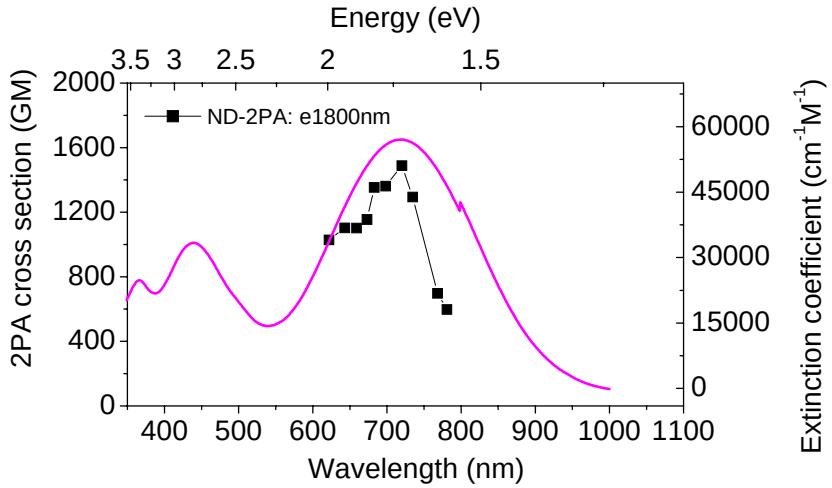

LB-IV-43a in THF

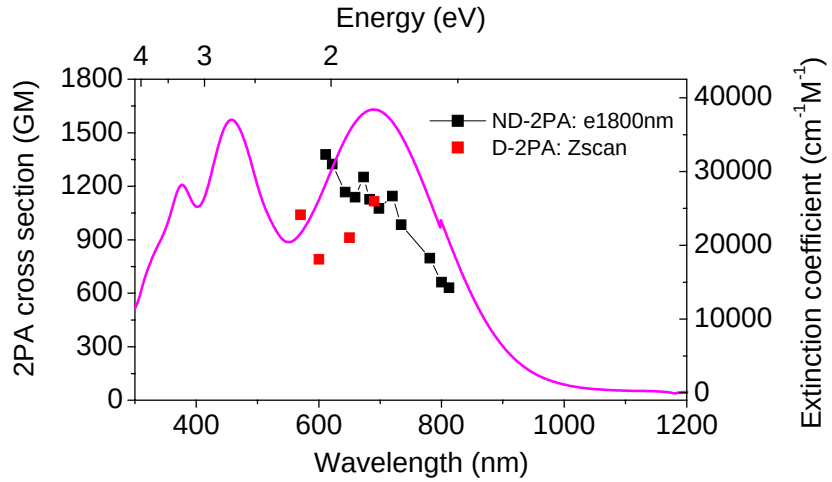

LB-IV-20c in CH_2CL_2

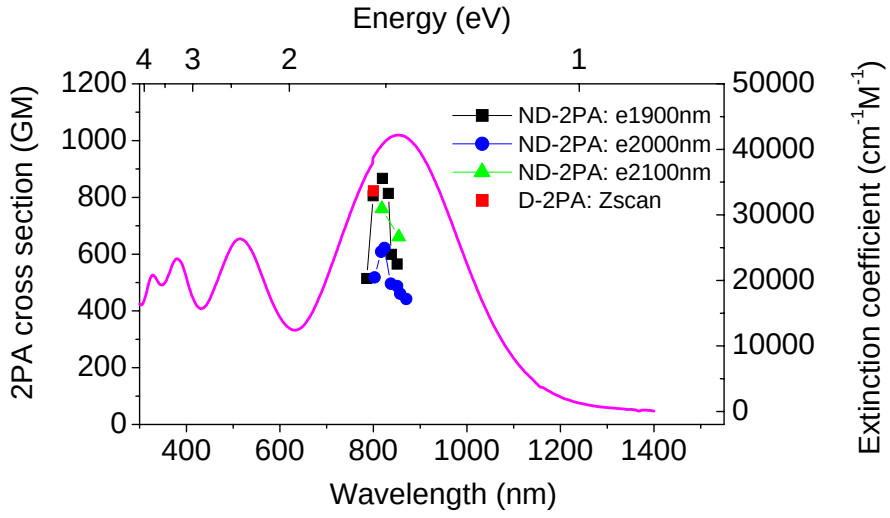

Sjz-6-89 in THF

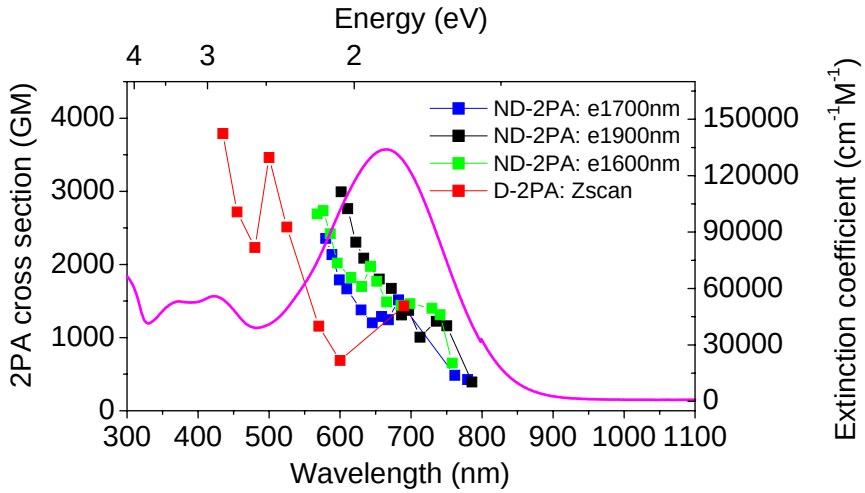

AJC-190 in THF

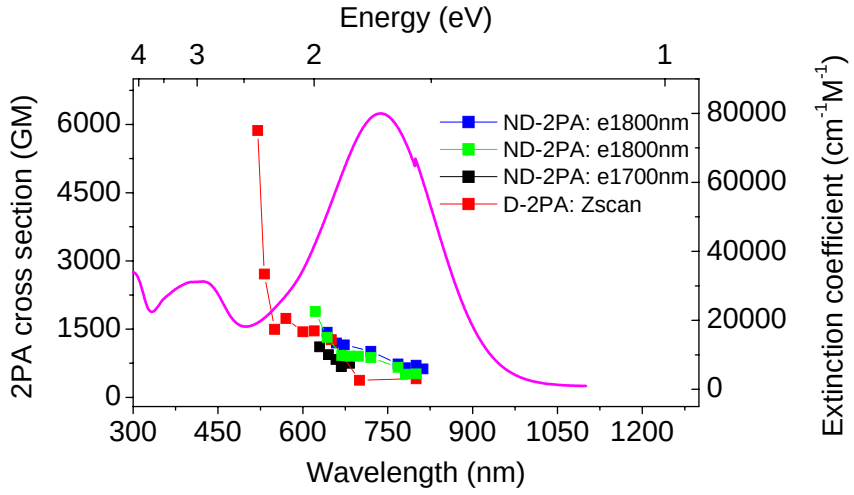

TOR-I-99 in THF

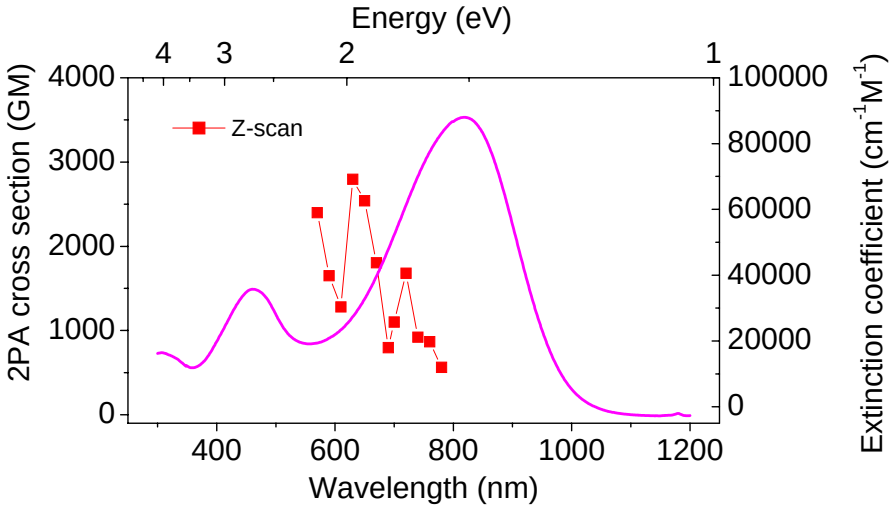

C.2 NI-COMPLEX FOR 2PA AT TELECOMMUNICATIONS WAVELENTHS [84]

Molecular structures:

MB-123

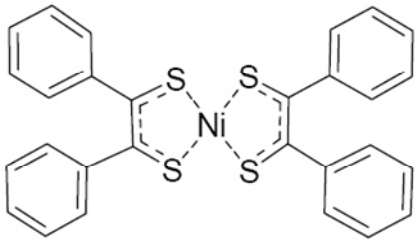

JYC-IV-087c

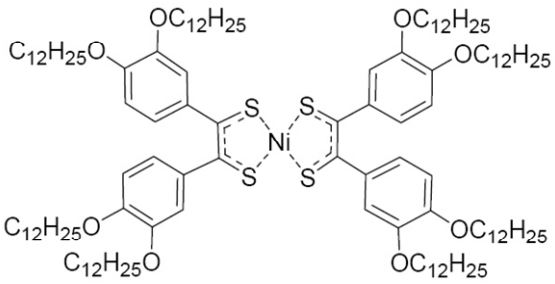

JYC-V-019a

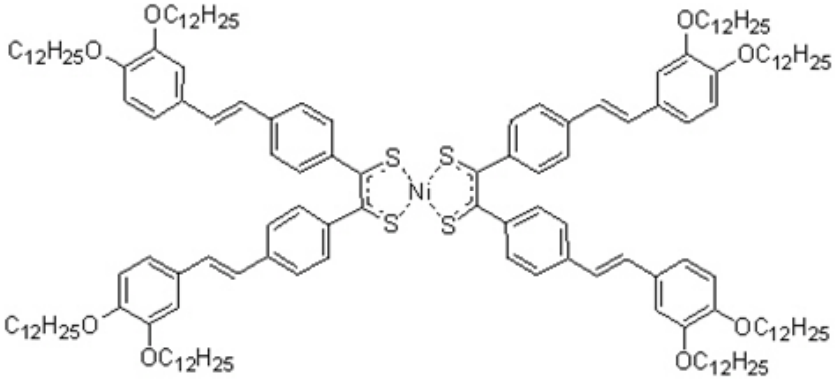

MB-123 in CH_2CL_2

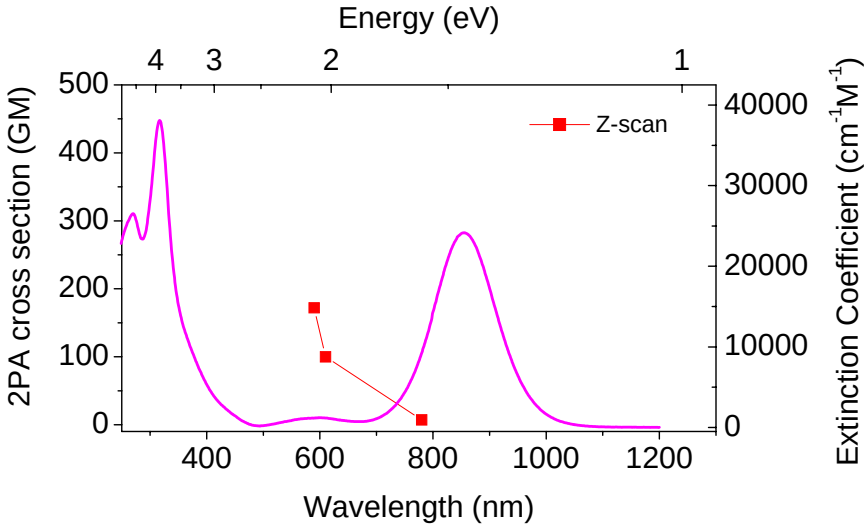

JYC-IV-087c in CHCL3

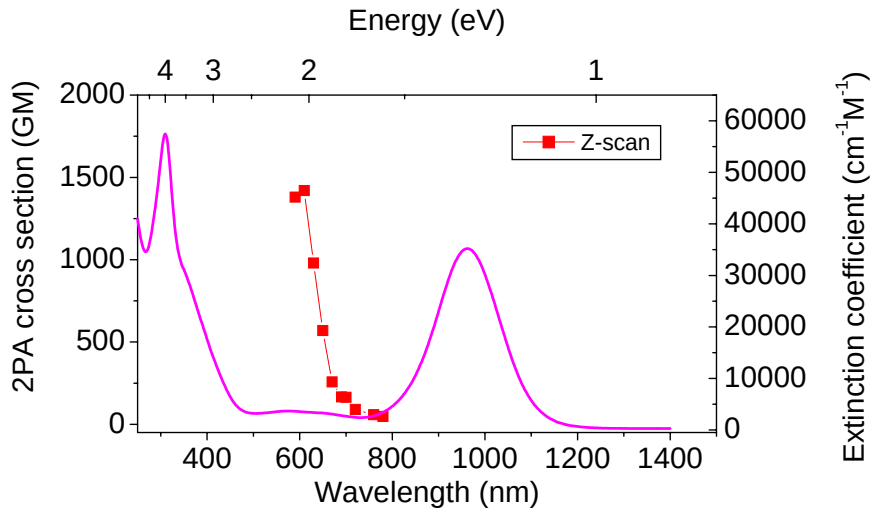

JYC-V-019a in THF

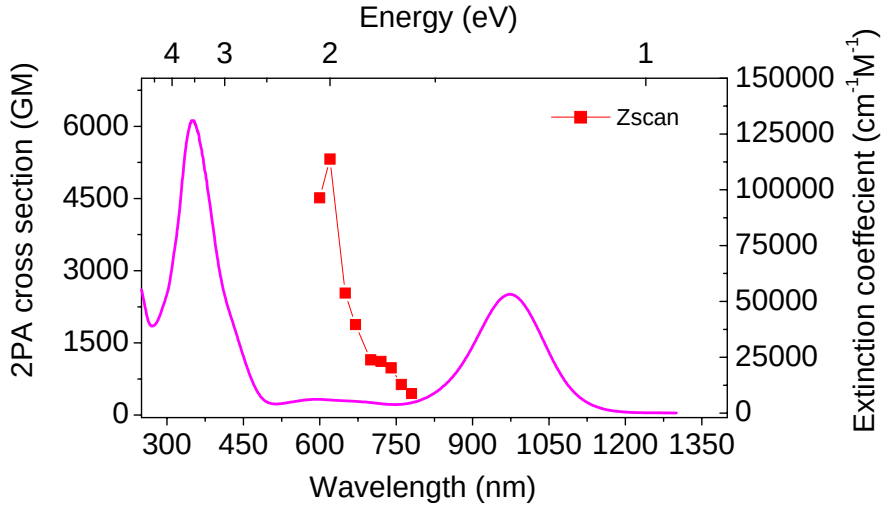

C.3 D-D-D-D MOLECULES [85]

Molecular structures:

LB-II-24

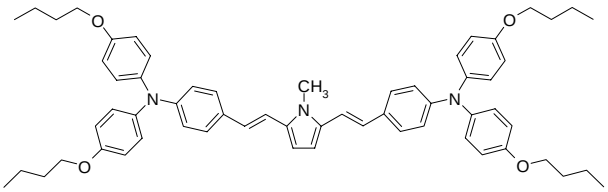

LB-II-80

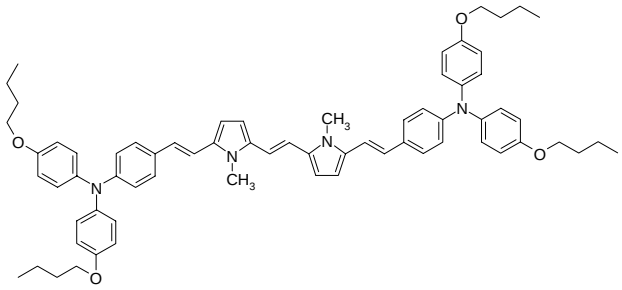

Sjz-3-16

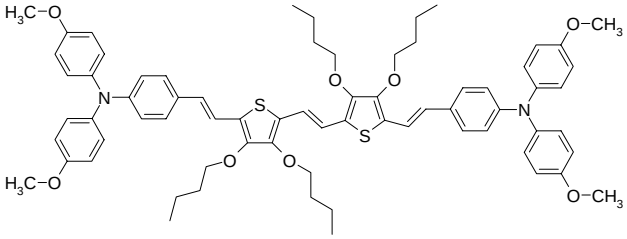

Sjz-3-17

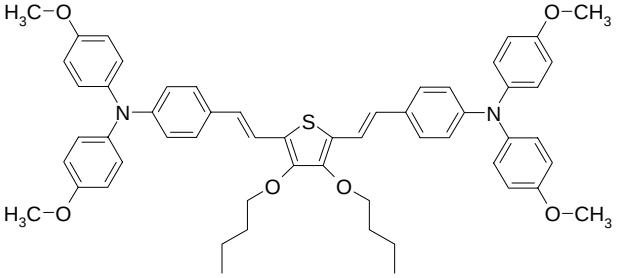

Sjz-4-1

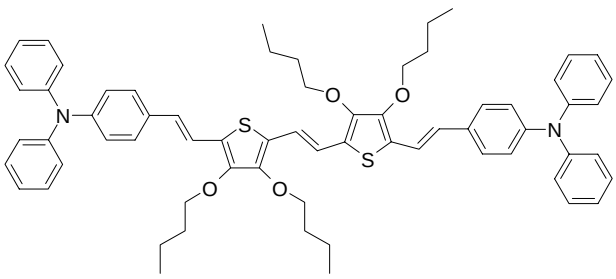

Sjz-4-7

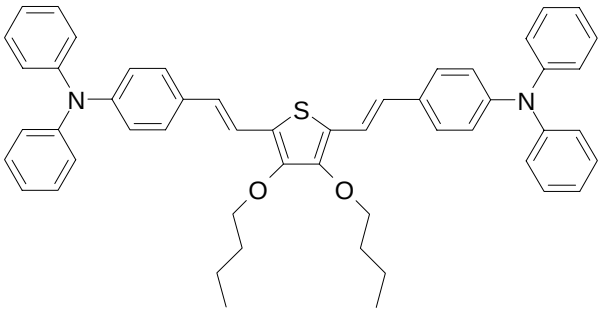

GW-67a

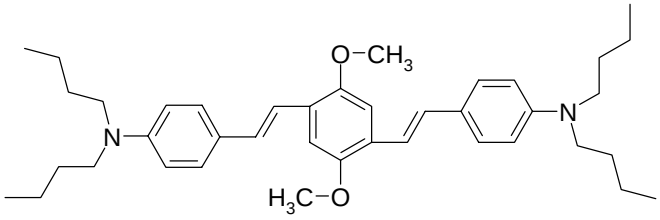

LB-II-24 in THF

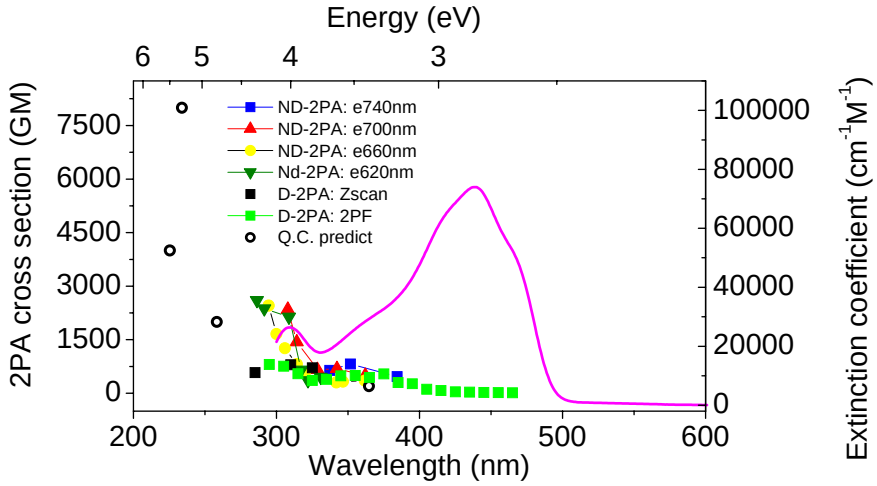

LB-II-80 in THF

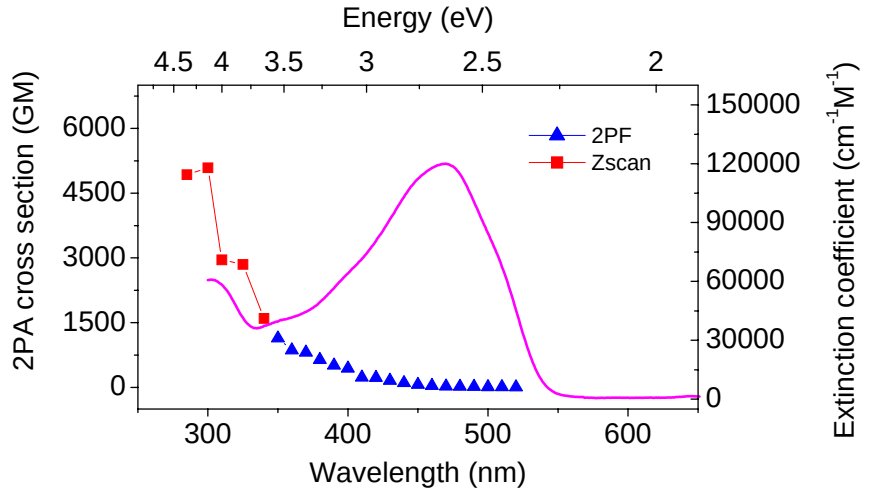

Sjz-3-16 in THF

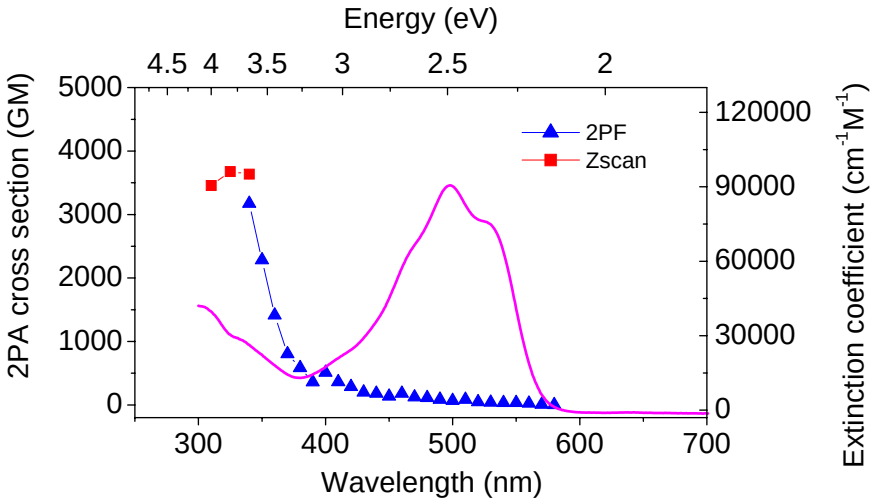

Sjz-3-17 in THF

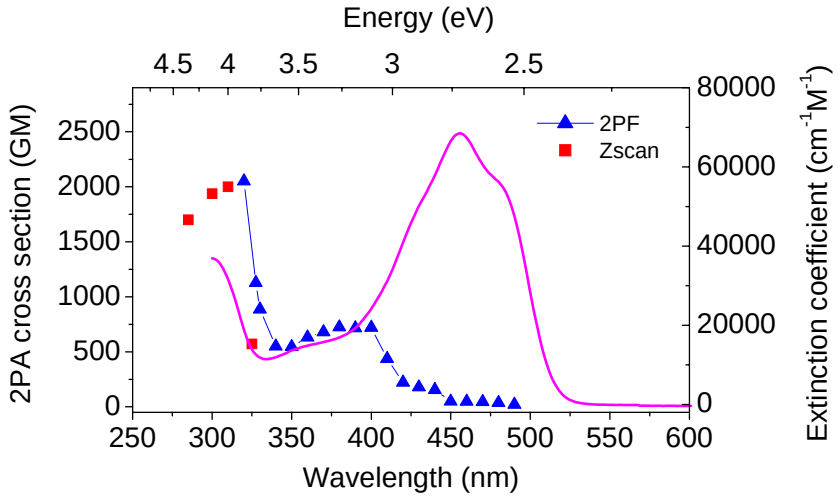

Sjz-4-1 in THF

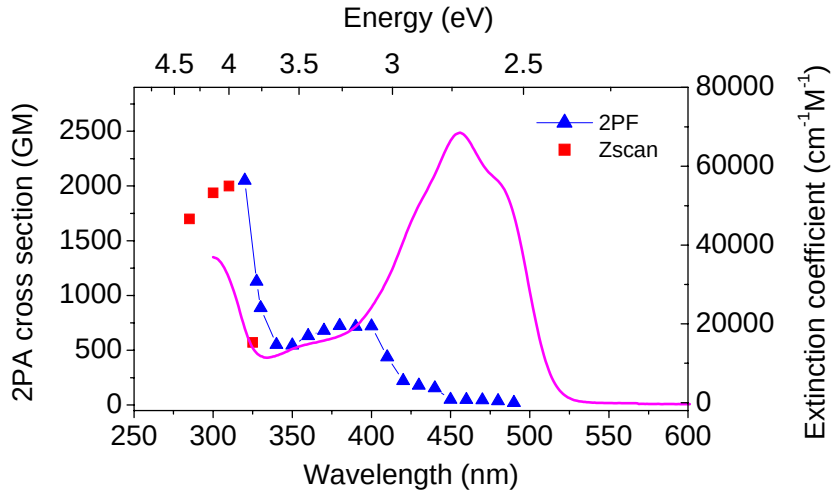

Sjz-4-7 in THF

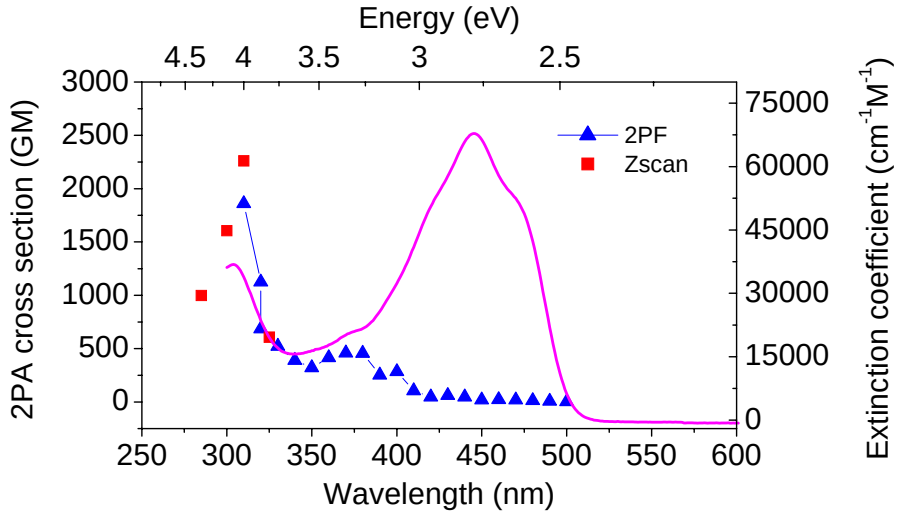

GW-67a in THF

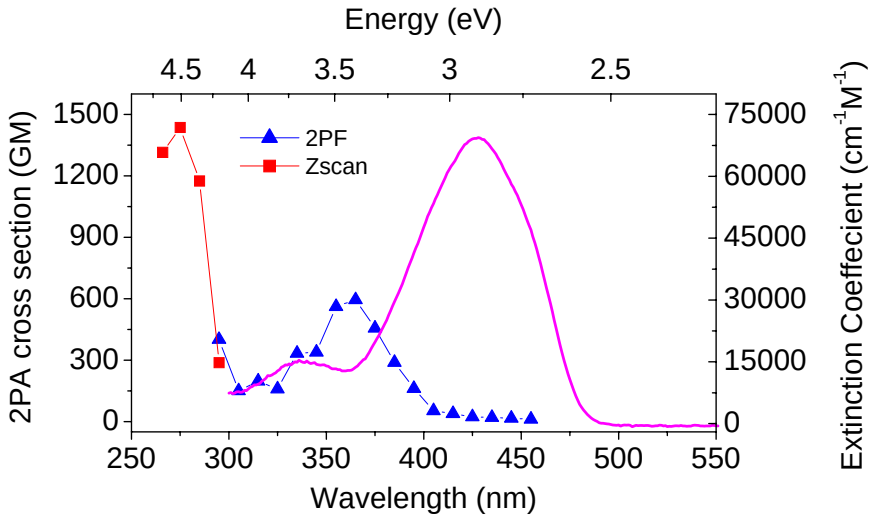
Energy (eV)
4.5
4
3.5
3
2.5
1500
1200
900
600
300
0
2PA cross section (GM)
2PF
Zscan
75000
60000
45000
30000
15000
0
Extinction Coeffecient (cm-1M-1)
250
300
350
400
450
500
550
Wavelength (nm)

C.4 A-D-D-A MOLECULES [86]

Molecular structures:

Sjz-7-26

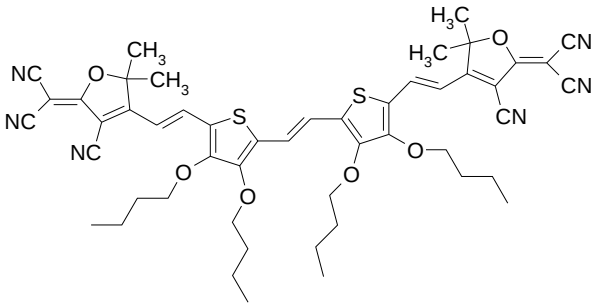

Sjz-7-32b

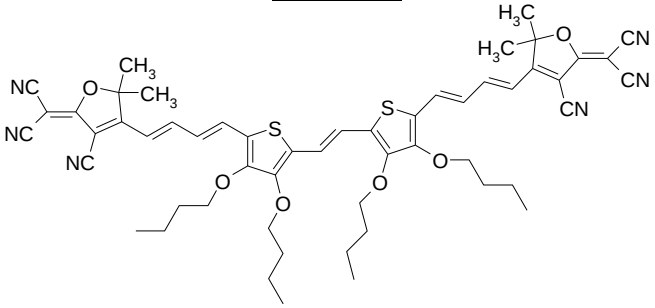

Sjz-7-57

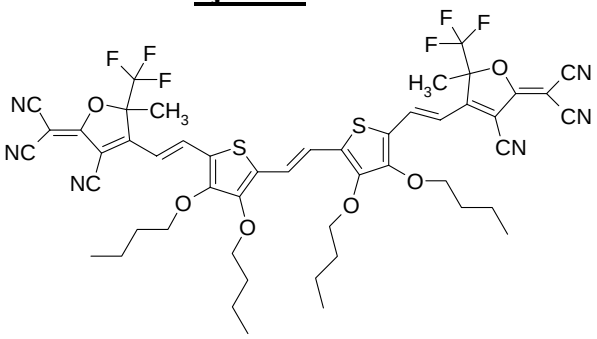

Sjz-7-58

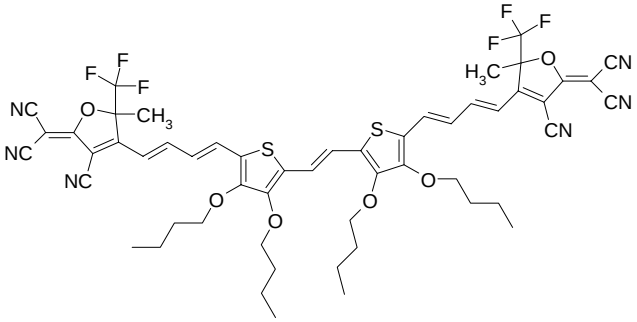

LB-IV-10a

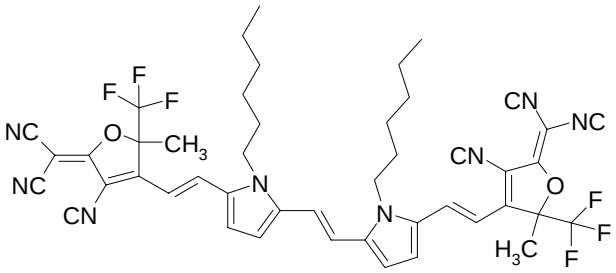

LB-IV-08b

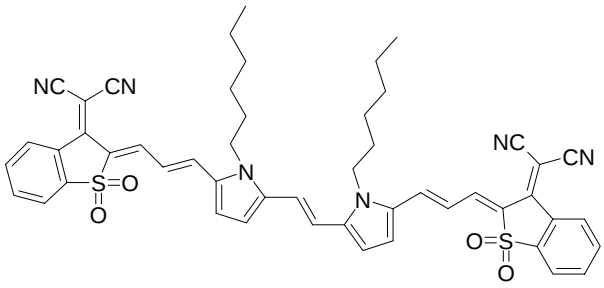

Sjz-8-14d

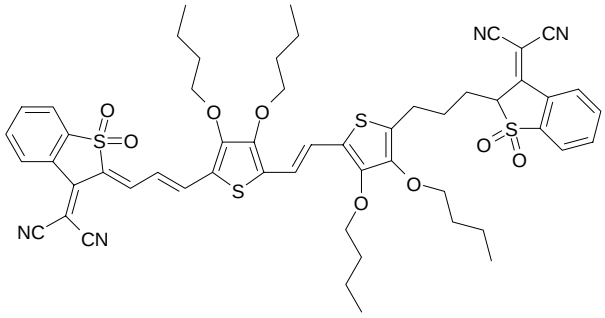

Sjz-7-26 in THF

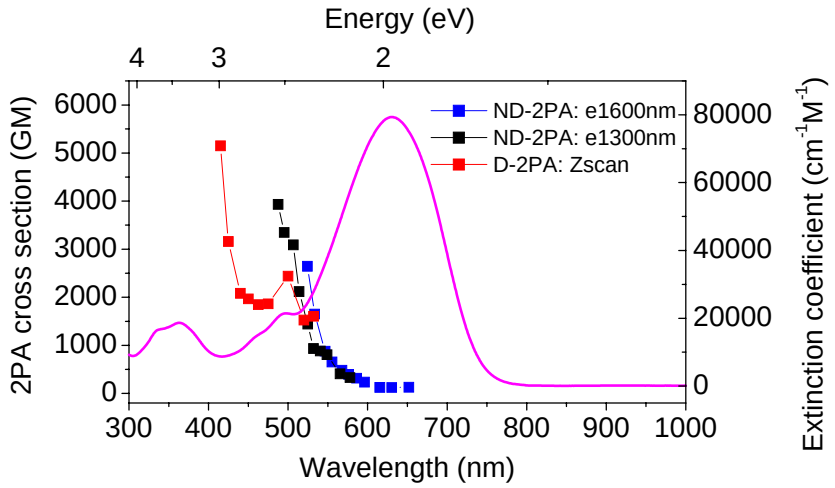

Sjz-7-32b in THF

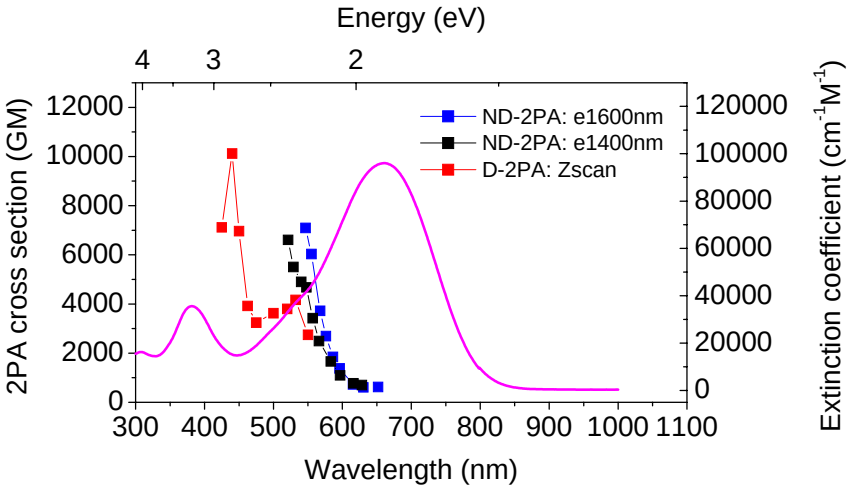

Sjz-7-57 in THF

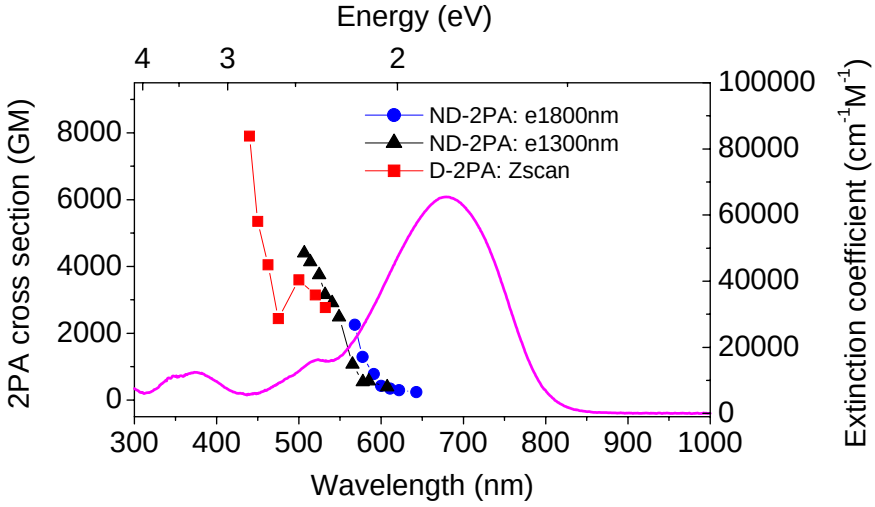

Siz-7-58 in THF

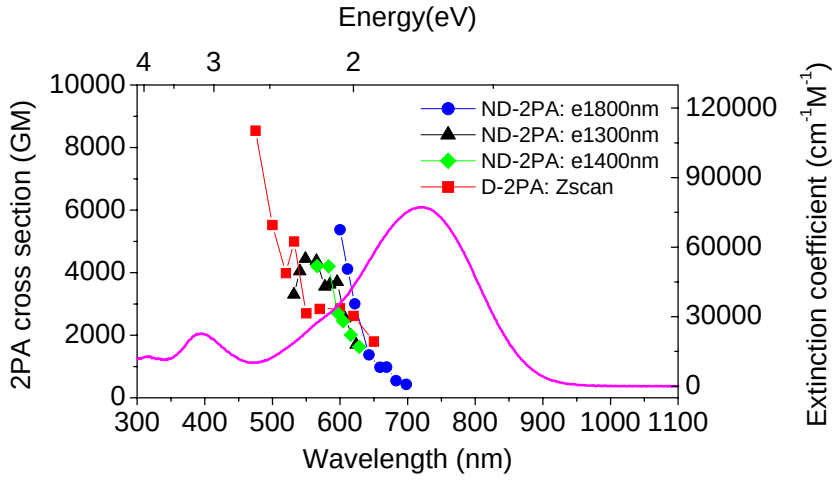

LB-IV-10a in THF

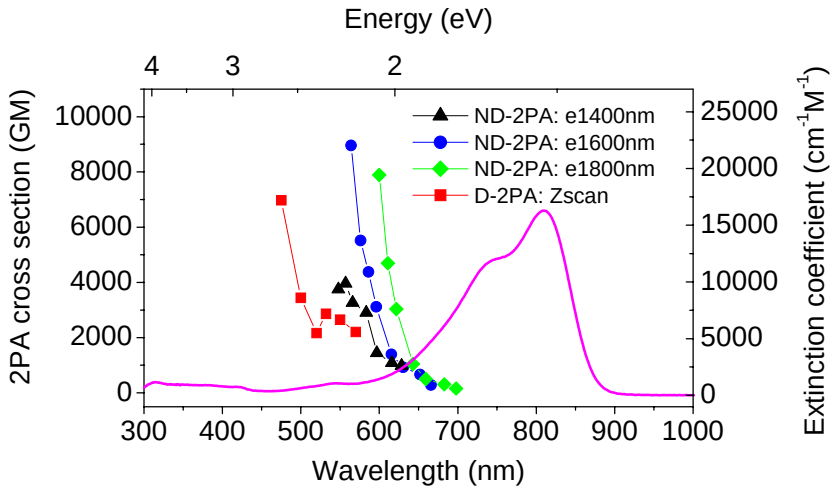

LB-IV-08b in THF

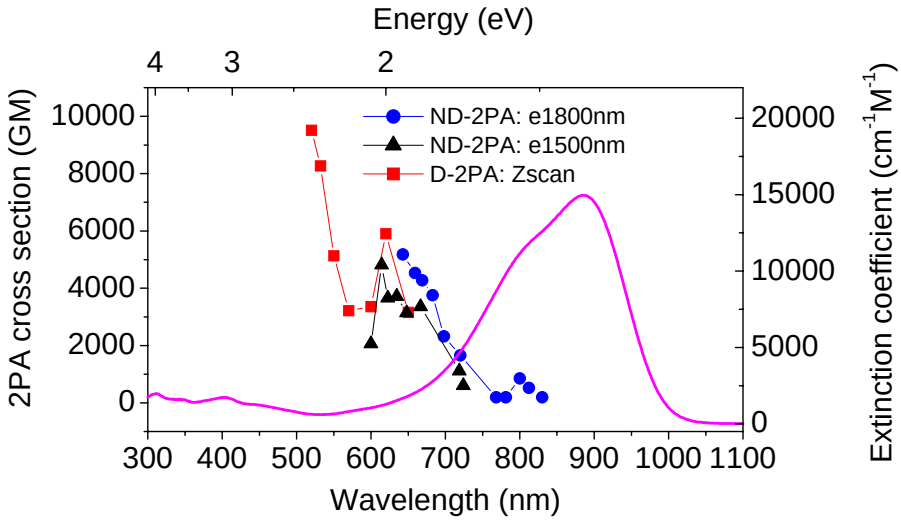

Sjz-8-14d in THF

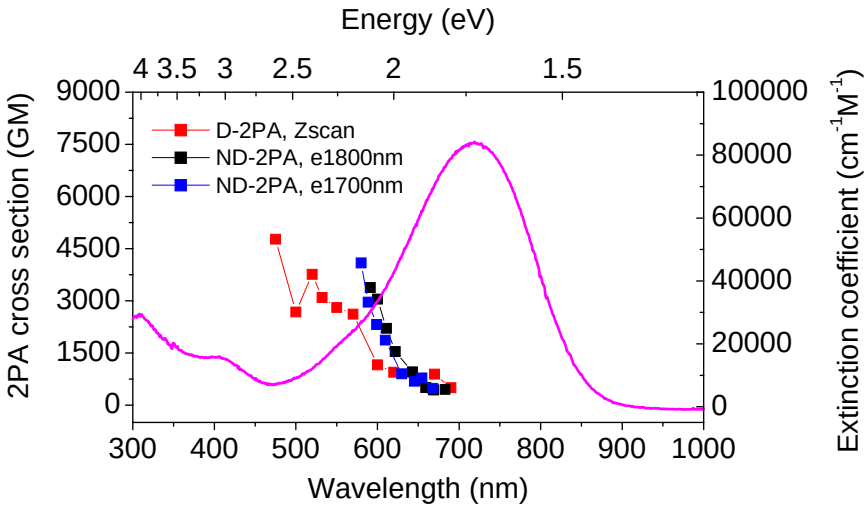

C.5 PERYLENE DYE

Molecular structures:

ZA-III-20

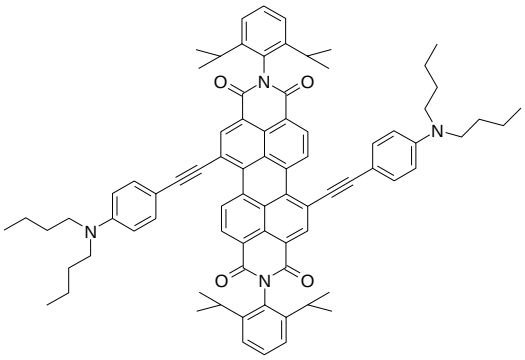

ZA-III-28

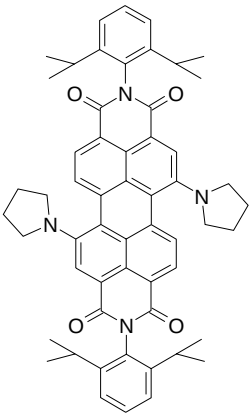

ZA-III-100

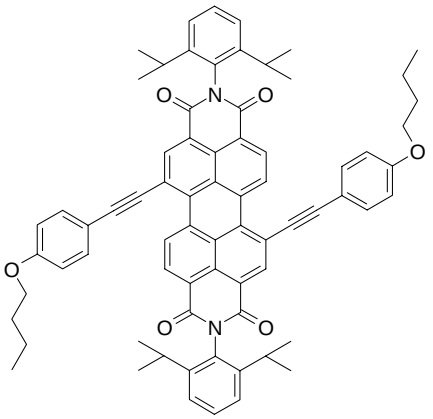

ZA-IV-64

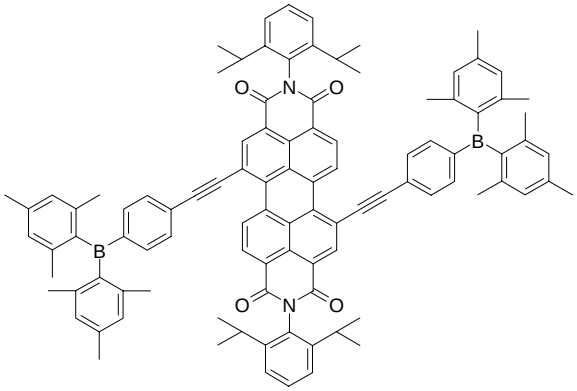

ZA-VII-13b

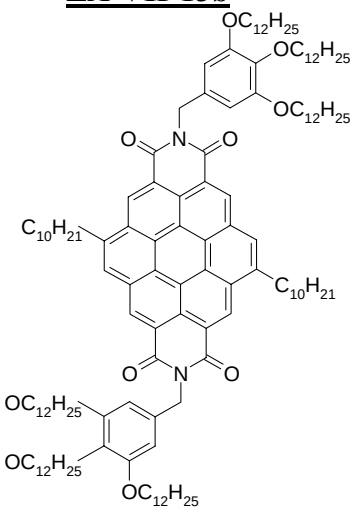

ZA-III-20 in CH_2CL_2

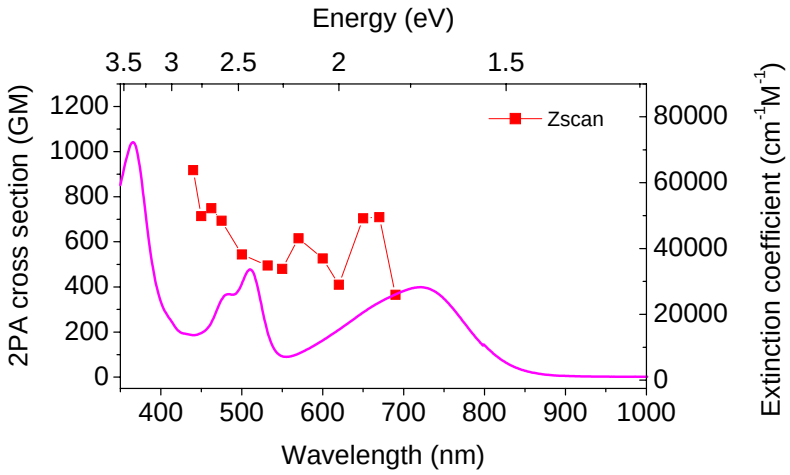

ZA-III-28 in CH_2CL_2

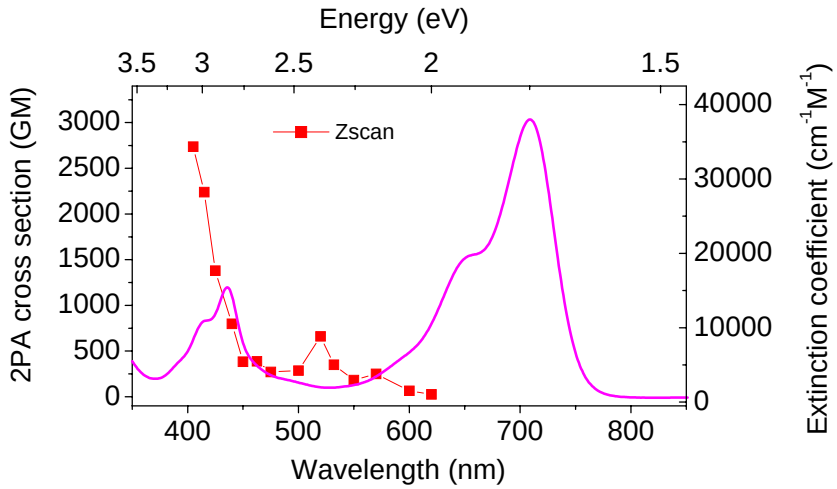

ZA-III-100 in CH_2CL_2

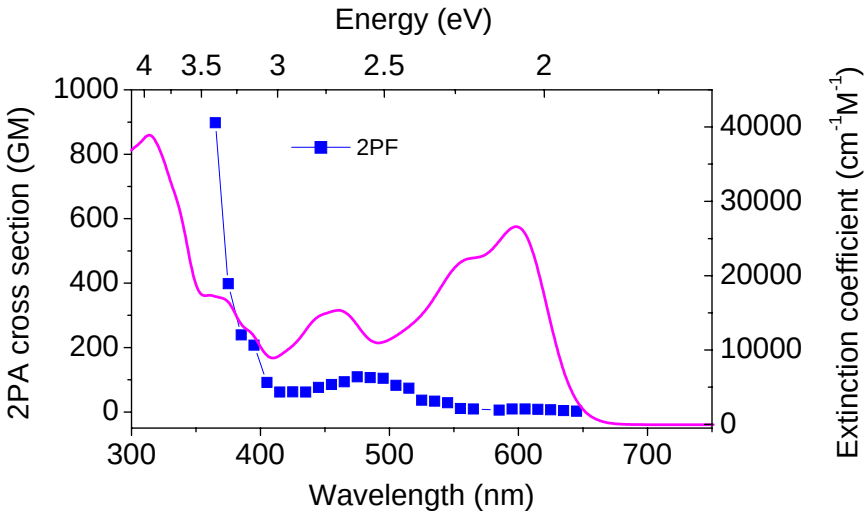

ZA-IV-64 in CH_2CL_2

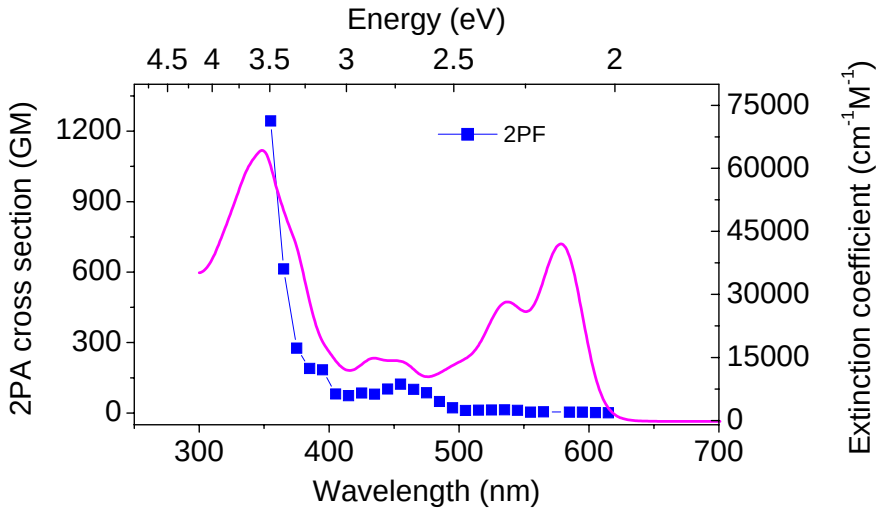

ZA-VII-13b in CH_2CL_2

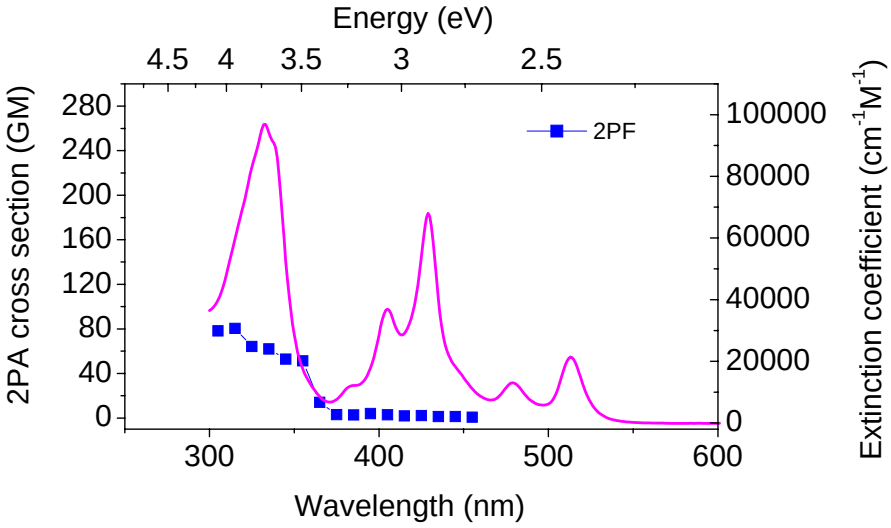

C.6 Naphthalene Derivatives

Molecular Structures:

GJW-DAN

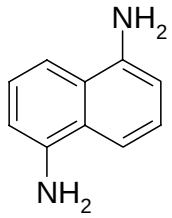

GJW-1-26a

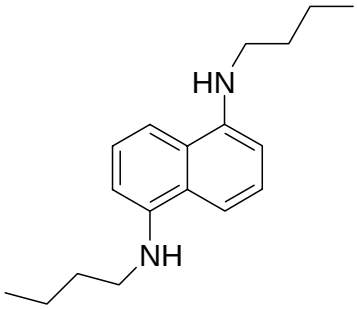

GJW-1-17b

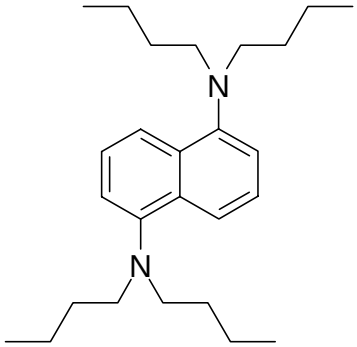

GJW-1-36a

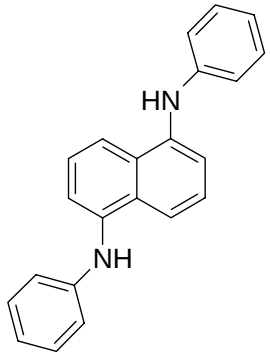

GJW-1-48b

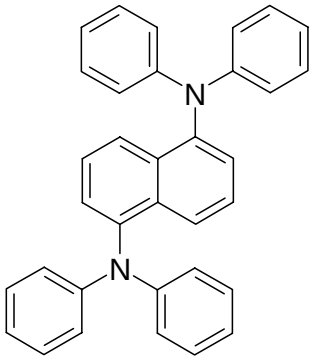

GJW-DAN

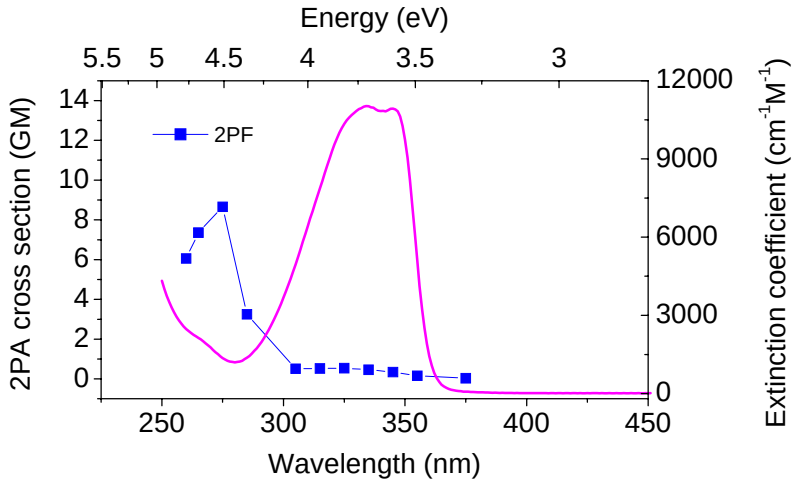

GJW-1-26a

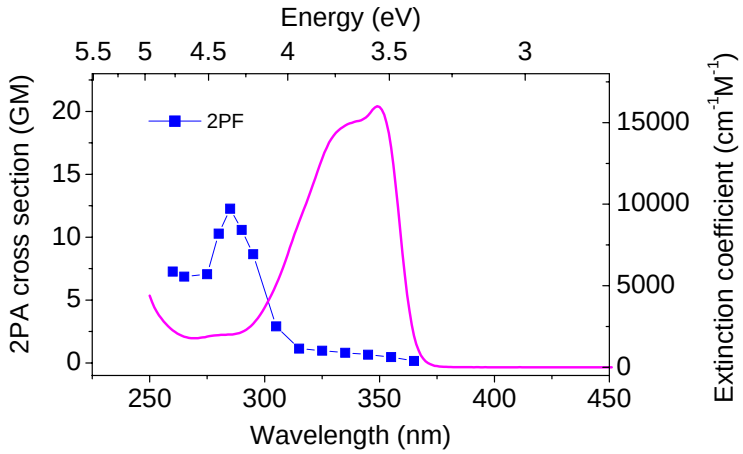

GJW-1-17b

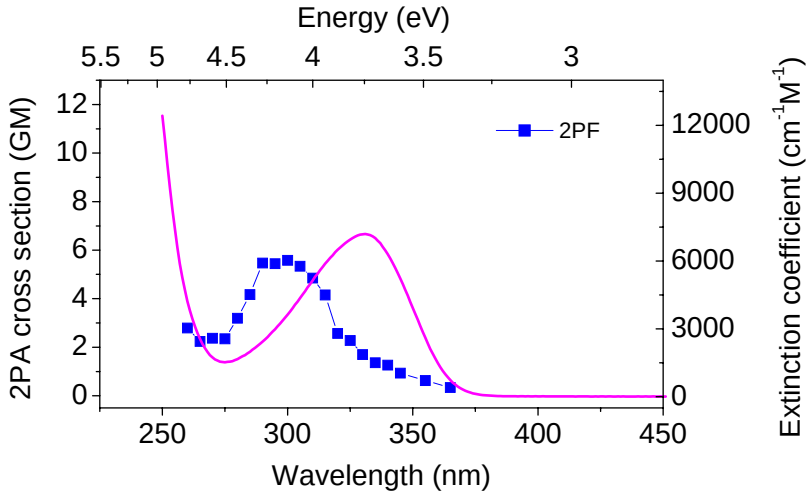

GJW-1-36a

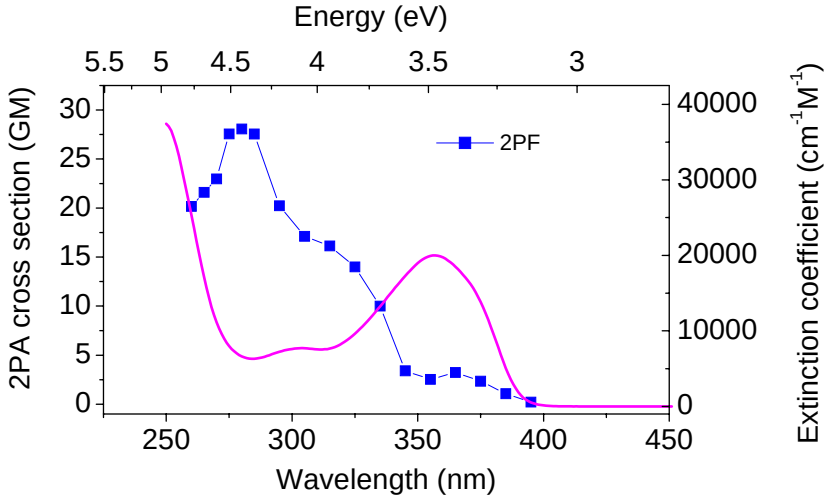

GJW-1-48a

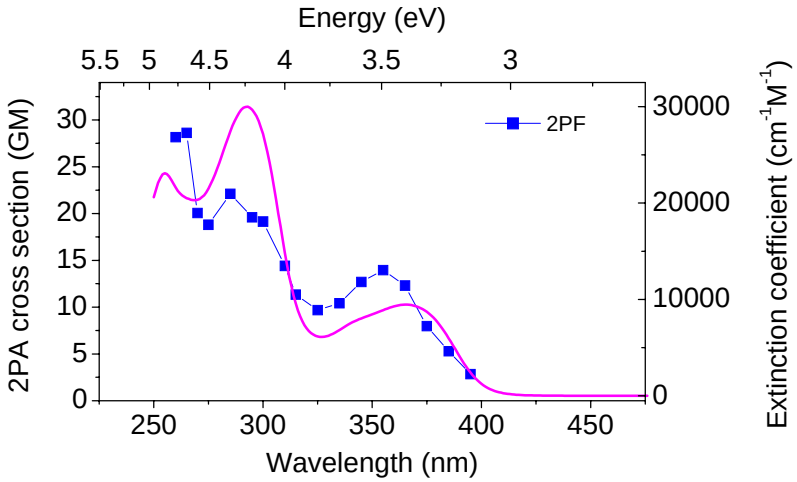
Energy (eV)
5.5
5
4.5
4
3.5
3
2PA cross section (GM)
30
25
20
15
10
5
0
2PF
30000
20000
10000
0
Extinction coefficient (cm-1M-1)
250
300
350
400
450
Wavelength (nm)

C.7 OTHERS

Molecular structures:

Sjz-3-42

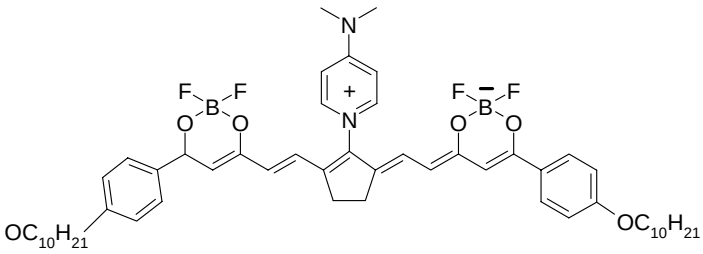

Sjz-6-85

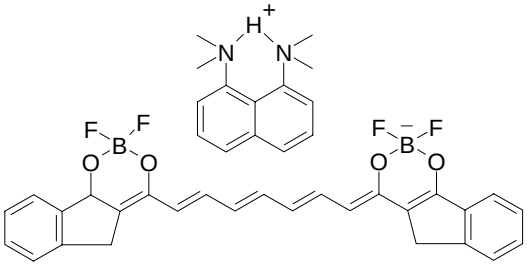

SC-IV-25c

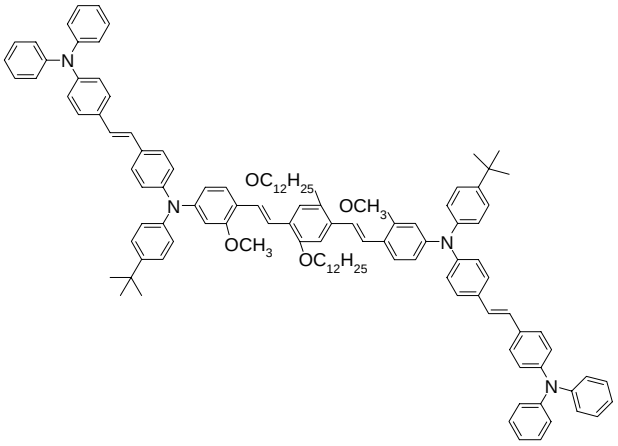

SC-V-10

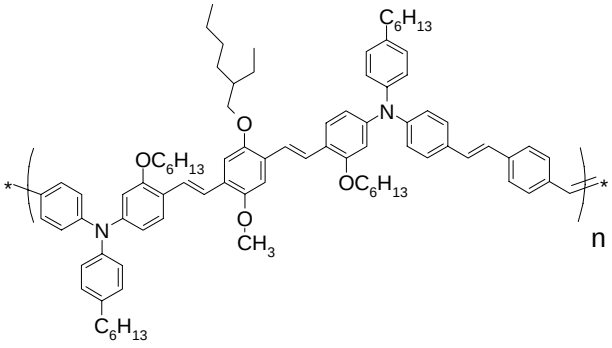

XZ-III-28d

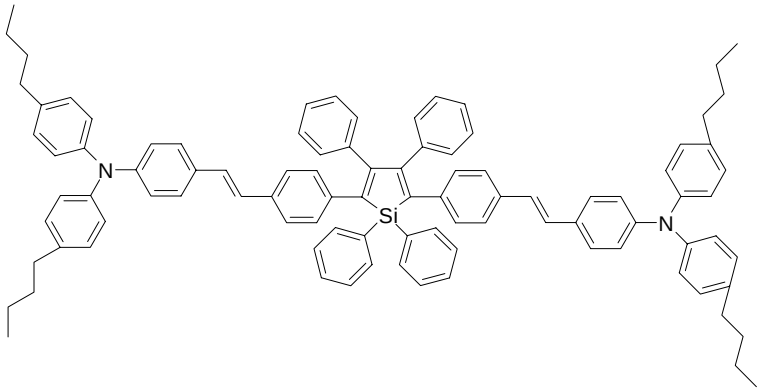

Sjz-3-42 in CH_2CL_2

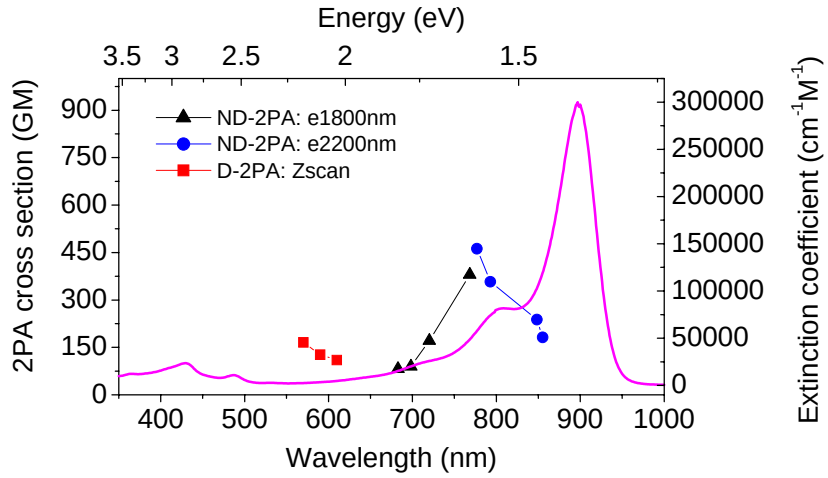

Sjz-6-85 in Acetonitrile

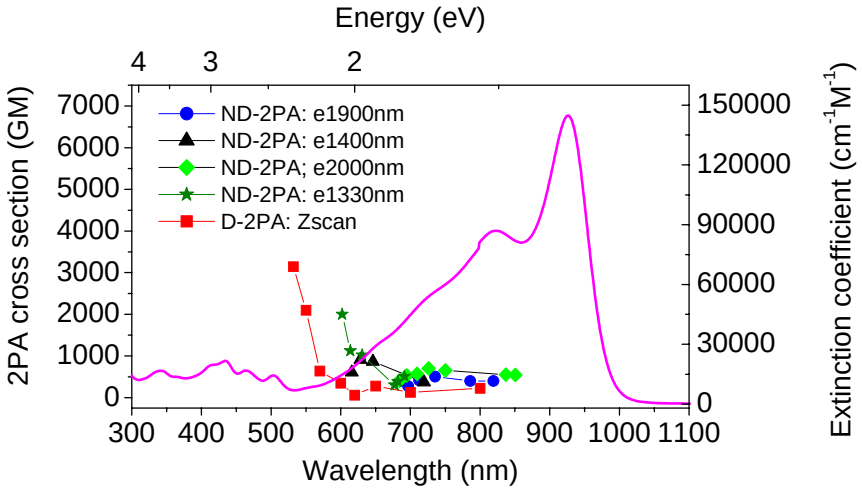

SC-IV-25c in $CHCL_3$

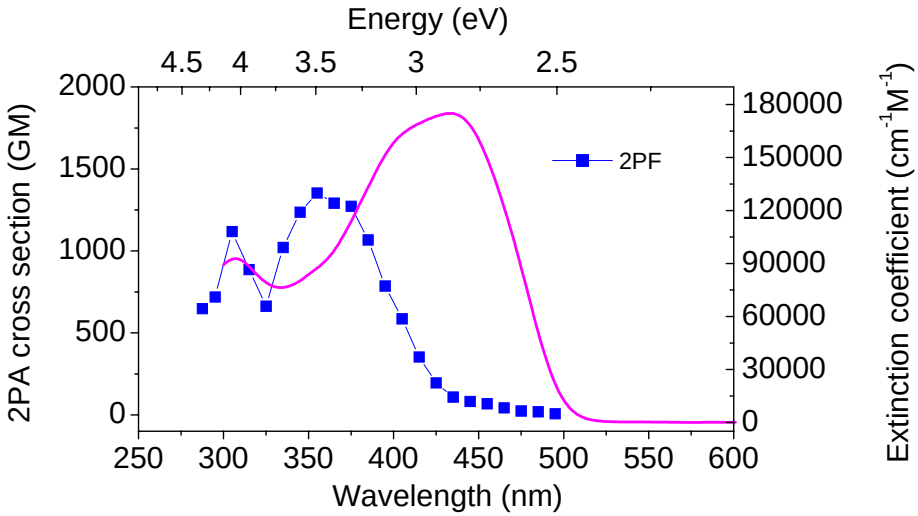

SC-V-10 in Toluene

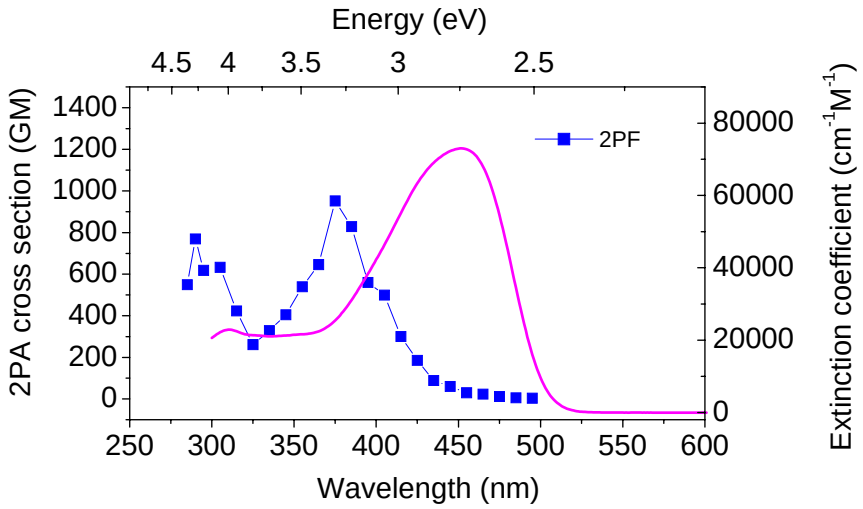

XZ-III-28d in $CHCL_3$

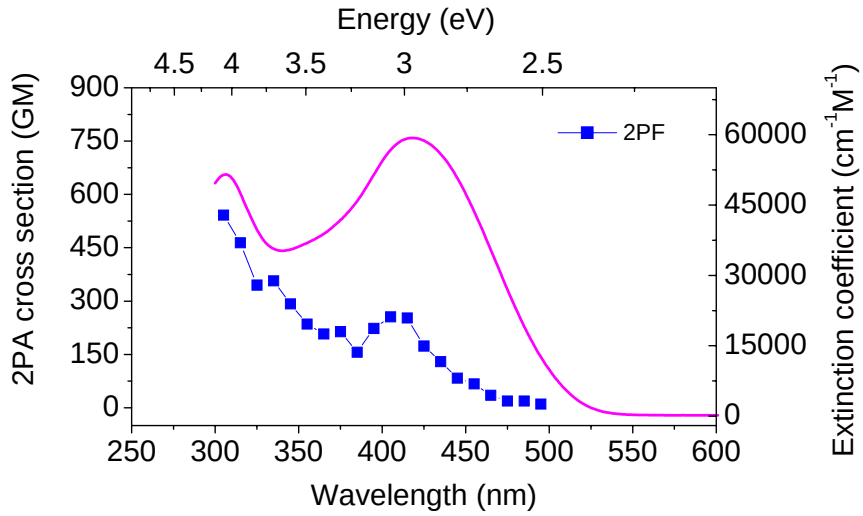

APPENDIX D
DERIVATIONS FOR TWO-PHOTON EXCITATION FLUORESCENCE ANISOTROPY

The two-photon anisotropy formula derivation is based on two theoretical approaches. The first is made by P. Callis [79], who used McClain's original treatment for the two-photon absorption (2PA) tensor and added the fluorescence transition dipole to develop the equation for the two-photon anisotropy function. The second theoretical approach is made by P. Cronstrand, Yi Luo and H. Agren [32]. They derived the equation for the 2PA cross section in a more general four-state, two-intermediate-level model taking into account the influence of an additional (second) excitation channel.

Following Callis' theory, the two-photon anisotropy function, r, is written as

$$r = \frac{18Q_x + Q_y - 7}{7Q_y + 14} \tag{D.1}$$

where Q_x and Q_y are functions depending on the 2PA tensor $\boldsymbol{S}$ and fluorescence transition dipole $\boldsymbol{F}$. Both Callis and Cronstrand considered only a two-dimensional approximation (case of the planar molecule oriented in the x-y plane) and linear polarization of the excitation light. For linear molecules the tensor component S_{zz} is much smaller compared to S_{xx} and S_{yy}, and r depends only on the Q_x and Q_y projections. Also, this formula is limited to steady-state conditions with completely motionless molecules. From [79] it follows that

$$Q_x = f_x^2 s_{xx}^2 + 2 f_x s_{xx} f_y s_{xy} + f_y^2 s_{xy}^2 + f_x^2 s_{xy}^2 + 2 f_x s_{xy} f_y s_{yy} + f_y^2 s_{yy}^2 \tag{D.2}$$

$$Q_y = (s_{xx} + s_{yy})^2 \tag{D.3}$$

where f_x, f_y and s_{xx}, s_{xy}, s_{yy} are normalized matrix elements of $\boldsymbol{S}$ and $\boldsymbol{F}$.

Substituting Eq.D.2 and D. 3 into Eq. D.1 gives the two-photon anisotropy function, r, as

$$r_{2PA} = \frac{2}{7}\left[\frac{9(f_x^2 s_{xx} + 2 f_x f_y s_{xy} + f_y^2 s_{yy})(s_{xx} + s_{yy}) - 4(s_{xx} + s_{yy})^2 + 1}{(s_{xx} + s_{yy})^2 + 2}\right] \tag{D.4}$$

This is the general formula for steady-state two-photon excitation fluorescence anisotropy, which is valid for a model including any number of levels. In order to derive an equation for r_{2PA}, which is possible to apply for analysis of real molecules, we need, first, to choose an adequate molecular model and, second, to connect the normalized matrix elements f_x, f_y and s_{xx}, s_{xy}, s_{yy} with the molecular parameters such as transition dipole moments, angles between these transitions and energy position of the levels.

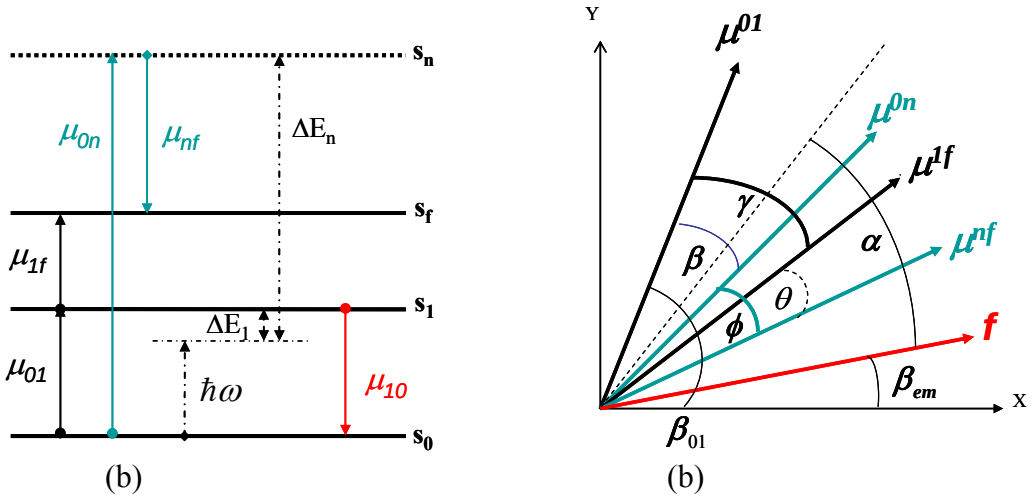

Figure D.1 Four-state, two-intermediate level (S_1 and S_n) model for two-photon anisotropy, (a) energy states S_0, S_1, S_f and S_n diagram; (b) transition dipole moments schematic diagram

First, let's consider a more general four-state-two-intermediate-level model (or two scenario model) described in [32] and presented in Fig. D.1 (a). As shown in [32], for this model the two-photon matrix element S may be presented as $S_{\alpha\beta} = S^{(1)}_{\alpha\beta} + S^{(2)}_{\alpha\beta}$, where upper indexes (1) and (2) indicate the first and the second scenarios of 2PA, and $\alpha, \beta \in \{x, y\}$. If the first scenario involves the transitions $S_0 \rightarrow S_1$ and $S_1 \rightarrow S_f$ (1 is the first intermediate level and f is the final

level) and the second scenario involves transitions $S_0 \rightarrow S_n$ and $S_n \rightarrow S_f$ (n is the second intermediate level), matrix elements $S_{\alpha\beta}^{(1)}$ and $S_{\alpha\beta}^{(2)}$ may be rewritten as

$$S_{\alpha\beta}^{(1)} = \frac{\mu_\alpha^{01}\mu_\beta^{1f}}{\Delta E_1} + \frac{\mu_\beta^{01}\mu_\alpha^{1f}}{\Delta E_1} \tag{D.5}$$

$$S_{\alpha\beta}^{(2)} = \frac{\mu_\alpha^{0n}\mu_\beta^{nf}}{\Delta E_n} + \frac{\mu_\beta^{0n}\mu_\alpha^{nf}}{\Delta E_n} \tag{D.6}$$

where μ_α and μ_β are the dipole moments of the participating transitions; $\Delta E_1 = \hbar\omega_1 - \hbar\omega$, $\Delta E_n = \hbar\omega_n - \hbar\omega$ and ω is the frequency of the excitation. Using Eq. D.5 and D.6, we can write *xx*, *xy* and *yy* components of matrix elements $S_{\alpha\beta}$ as:

$$S_{xx} = \frac{2}{\Delta E_1}\mu_x^{01}\mu_x^{1f} + \frac{2}{\Delta E_2}\mu_x^{0n}\mu_x^{nf};\ S_{yy} = \frac{2}{\Delta E_1}\mu_y^{01}\mu_y^{1f} + \frac{2}{\Delta E_2}\mu_y^{0n}\mu_y^{nf} \tag{D.7}$$

$$S_{xy} = \frac{\mu_x^{01}\mu_y^{1f}}{\Delta E_1} + \frac{\mu_x^{0n}\mu_y^{nf}}{\Delta E_2} + \frac{\mu_y^{01}\mu_x^{1f}}{\Delta E_1} + \frac{\mu_y^{0n}\mu_x^{nf}}{\Delta E_2} \tag{D.8}$$

The next step is to find the normalized matrix elements s_{xx}, s_{yy}, s_{xy} using the normalized condition $s_{\alpha\beta} = \frac{S_{\alpha\beta}}{\sqrt{\sum_{\alpha\beta} S_{\alpha\beta}S_{\alpha\beta}^*}}$ presented in [79].

After normalization

$$s_{xx} = \frac{S_{xx}}{\sqrt{S_{xx}^2 + S_{yy}^2 + 2S_{xy}^2}},\ s_{yy} = \frac{S_{yy}}{\sqrt{S_{xx}^2 + S_{yy}^2 + 2S_{xy}^2}} \text{ and } s_{xy} = \frac{S_{xy}}{\sqrt{S_{xx}^2 + S_{yy}^2 + 2S_{xy}^2}} \tag{D.9}$$

Substituting relation Eq. D.7 and D.8 into Eq. D.9, gives the normalized matrix elements s_{xx}, s_{yy}, s_{xy}, expressed in terms of molecular parameters, for Eq. (D.4). However, two-photon anisotropy (Eq. D.4) includes not only the normalized matrix elements of the 2PA tensor

S but also the normalized components of the emission dipole moment ***F***: $f_x = \frac{F_x}{\sqrt{|\boldsymbol{F}|^2}}$ and $f_y = \frac{F_y}{\sqrt{|\boldsymbol{F}|^2}}$ [79]. To connect these components with the absorbing dipoles, we consider the diagram shown in Fig. D.1 (b). It is possible to show that $f_x = \cos\beta_{em}$ and $f_y = \sin\beta_{em}$, where $\beta_{em} = \beta_{01} - (\frac{\gamma}{2} + \alpha)$. The angle β_{01} can be written as a ratio of the corresponding μ_x and μ_y projections and the normalized absorbing dipole μ_{01}: $\cos\beta_{01} = \frac{\mu_x^{01}}{\mu_{01}}$ and $\sin\beta_{01} = \frac{\mu_y^{01}}{\mu_{01}}$. After transformation:

$$f_x = \frac{\mu_x^{01}}{\mu_{01}} a + \frac{\mu_y^{01}}{\mu_{01}} b \tag{D.10}$$

$$f_y = \frac{\mu_y^{01}}{\mu_{01}} a - \frac{\mu_x^{01}}{\mu_{01}} b \tag{D.11}$$

where $a = \cos(\frac{\gamma}{2} + \alpha)$ and $b = \sin(\frac{\gamma}{2} + \alpha)$

Substituting Eq. D.10, D. 11 as well as Eq. D. 9 into Eq. D. 4, we obtain an equation for r_{2PA} in the four-level-two-intermediate state approximation. In the final formula for the anisotropy, r should be expressed in terms of absorbing dipoles μ_{01}, μ_{0n}, μ_{1f}, μ_{nf} (not their projections), angles α, β, γ, θ between transitions and detuning energies ΔE_1, ΔE_2. After algebraic transformation and taking into account that

$\mu_x^{01}\mu_y^{0n} - \mu_y^{01}\mu_x^{0n} = -\mu_{01}\mu_{0n}\sin\beta$; $\mu_x^{01}\mu_x^{0n} + \mu_y^{01}\mu_y^{0n} = \mu_{01}\mu_{0n}\cos\beta$;

$\mu_x^{01}\mu_y^{1f} - \mu_y^{01}\mu_x^{1f} = -\mu_{01}\mu_{1f}\sin\gamma$; $\mu_x^{01}\mu_x^{1f} + \mu_y^{01}\mu_y^{1f} = \mu_{01}\mu_{1f}\cos\gamma$;

$\mu_x^{1f}\mu_y^{nf} - \mu_y^{1f}\mu_x^{nf} = -\mu_{1f}\mu_{nf}\sin\theta$; $\mu_x^{1f}\mu_x^{nf} + \mu_y^{1f}\mu_y^{nf} = \mu_{1f}\mu_{nf}\cos\theta$;

$\mu_x^{01}\mu_y^{nf} - \mu_y^{01}\mu_x^{nf} = -\mu_{01}\mu_{nf}\sin(\gamma+\theta)$; $\mu_x^{01}\mu_x^{nf} + \mu_y^{01}\mu_y^{nf} = \mu_{01}\mu_{nf}\cos(\gamma+\theta)$;

$\mu_x^{0n}\mu_y^{1f} - \mu_y^{0n}\mu_x^{1f} = -\mu_{0n}\mu_{1f}\sin(\gamma-\beta)$; $\mu_x^{0n}\mu_x^{1f} + \mu_y^{0n}\mu_y^{1f} = \mu_{0n}\mu_{1f}\cos(\gamma-\beta)$;

$\mu_x^{0n}\mu_y^{nf} - \mu_y^{0n}\mu_x^{nf} = -\mu_{0n}\mu_{nf}\sin(\gamma+\theta-\beta)$; $\mu_x^{0n}\mu_x^{nf} + \mu_y^{0n}\mu_y^{nf} = \mu_{0n}\mu_{nf}\cos(\gamma+\theta-\beta)$,

we finally can write the expression for the four-level model for two-photon excitation fluorescence anisotropy:

$$r = \frac{18(K_1+K_2)K_3 - 8K_3^2 + K_4}{7(K_3^2+K_4)} \tag{D.12}$$

where $K_1 = \Delta E_2\mu_{01}\mu_{1f}\cos(\frac{\gamma}{2}+\alpha)\cos(\frac{\gamma}{2}-\alpha)$;

$K_2 = \Delta E_1\mu_{0n}\mu_{nf}\cos(\frac{\gamma}{2}-\alpha+\theta)\cos(\frac{\gamma}{2}+\alpha-\beta)$;

$K_3 = \Delta E_2\mu_{01}\mu_{1f}\cos\gamma + \Delta E_1\mu_{0n}\mu_{nf}\cos(\gamma+\theta-\beta)$;

$K_4 = \Delta E_1^2\mu_{0n}^2\mu_{nf}^2[1+\cos^2(\gamma+\theta-\beta)] + \Delta E_2^2\mu_{01}^2\mu_{1f}^2(1+\cos^2\gamma) +$
$+ 2\Delta E_1\Delta E_2\mu_{01}\mu_{0n}\mu_{1f}\mu_{nf}[\cos(\gamma+\theta)\cos(\gamma-\beta) + \cos\theta\cos\beta]$

LIST OF REFERENCES

[1] M. Goppert-Mayer, "Elementary actions with two quantum leaps", *Ann. Physik*, Vol. 9, 273 (1931)

[2] W. Kaiser, C.G.B. Garrett, "Two-photon excitation in $CaF_2:Eu^{2+}$", *Phys. Rev. Lett.*, Vol. 7, 229 (1961)

[3] R. R. Birge and B. M. Pierce, "Semiclassical time-dependent theory of two-photon spectroscopy. The effect of dephasing in the virtual level on the two-photon excitation spectrum of isotachysterol", *Int. J. Quan. Chem.*, Vol. 29, 639 (1986)

[4] W. Denk, J. H. Strickler, and W. W. Webb, "Two-photon laser scanning fluorescence microscopy", *Science*, Vol. 248, 73 (1990)

[5] W. H. Zhou, S. M. Kuebler, K. L. Braun, T. Y. Yu, J. K. Cammack, C. K. Ober, J. W. Perry, and S. R. Marder, "An efficient two-photon-generated photoacid applied to positive-tone 3D microfabrication ", *Science*, Vol. 296, 1106 (2002)

[6] B. H. Cumpston, S. P. Ananthavel, S. Barlow et al., "Two-photon polymerization initiators for three-dimensional optical data storage and microfabrication ", *Nature*, Vol. 398, 51 (1999)

[7] W. R. Zipfel, R. M. Williams, W. W. Webb, "Nonlinear magic: multiphoton microscopy in the biosciences", *Nature Biotechnology*, Vol. 21, No. 11, 1369 (2003)

[8] A. A. Said, C. Wamsely, D. J. Hagan, E. W. Van Stryland, B. A. Reinhardt, P. Roderer and A. G. Dillard, "Third- and fifth-order optical nonlinearities in organic materials", *Chem. Phys. Lett.*, Vol. 228, 646 (1994)

[9] J. D. Bhawalkar, G. S. He and P. N. Prasad, "Nonlinear multiphoton processes in organic and polymeric materials", *Rep. Prog. Phys.*, Vol. 59, 1041 (1996)

[10] J. E. Ehrlich, X. L. Wu, Ys. L. Lee, Z. Y. Hu, H. Rockel, S. R. Marder and J. W. Perry, "Two-photon absorption and broadband optical limiting with bis-donor stilbenes", *Opt. Lett.*, Vol. 22, 1843 (1997)

[11] T. W. Graham Solomons, *Organic Chemistr*y, New York, Wiley, 1996

[12] M. Albota, D. Beljonne, J. Bredas, J. E. Ehrlich, J. Y. Fu, A. A. Heikal, S. E. Hess, T. Kogej, M. D. Levin, S. R. Marder, D. McCord-Maughon, J. W. Perry, H. Rockel, M. Rumi, G. Subramaniam, W. W. Webb, X. L. Wu, C. Xu, "Design of organic molecules with large two-photon absorption cross section", *Science*, Vol. 281, 1653 (1998)

[13] M. Rumi, J. E. Ehrlich, A. A. Heikal, J. W. Perry, S. Barlow, Z. Hu, D. McCord-Maughon, T. C. Parker, H. Rockel, S. Thayumanavan, S. R. Marder, D. Beljonne, and J. Bredas, " Structure-property relationships for two-photon absorbing chromophores: bis-donor diphenylpolyene and bis(styryl)benzene derivatives", *J. Am. Chem. Soc.,* Vol. 122, 9500 (2000)

[14] K. Ogawa, A. Ohashi, Y. Kobuke, K. Kamada, K. Ohta, "Strong two-photon absorption of self-assembled butadiyne-linked bisporphyrin", *J. Am. Chem. Soc.*, Vol. 125, 13356 (2003)

[15] G. P. Bartholomew, M. Rumi, S. J. K. Pond, J. W. Perry, S. Tretiak and G. C. Bazan, "Two-photon absorption in three-dimensional chromophores based on [2.2]-paracyclophane", *J. Am. Chem. Soc.*, Vol. 126, 11529 (2004)

[16] M. Drobizhev, Y. Stepanenko, Y. Dzenis, A. Karotki, A. Rebane, P. N. Taylor and H. L. Anderson, "Understanding strong two-photon absorption in π-conjugated porphyrin dimers

via double-resonance enhancement in a three-level model", *J. Am. Chem. Soc.*, Vol. 126, 15352 (2004)

[17] S. J. Chung, M. Rumi, V. Alain, S. Barlow, J. W. Perry and S. R. Marder, "Strong, low-energy two-photon absorption in extened amine-terminated cyano-substituted phenylenevinylene oligomers", *J. Am. Chem. Soc.*, Vol. 127, 10844 (2005)

[18] T. K. Ahn, J. H. Kwon, D. Y. Kim, D. W. Cho, D. H. Jeong, S. K. Kim, M. Suzuki, S. Shimizu, A. Osuka and D. H. Kim, "Comparative photophysics of [26]- and [28] hexaphyrins(1.1.1.1.1.1): large two-photon absorption cross section of aromatic [26]hexaphyrins(1.1.1.1.1.1)", *J. Am. Chem. Soc.*, Vol. 127, 12856 (2005)

[19] L. Beverina, J. Fu, A. Leclercq, E. Zojer, P. Pacher, S. Barlow, E. W. Van Stryland, D. J. Hagan, J. L. Bredas, and S. R. Marder, "Two-photon absorption at telecommunications wavelengths in a dipolar chromophore with a pyrrole auxiliary donor and thiazole auxiliary acceptor", *J. Am. Chem. Soc.*, Vol. 127, 7282 (2005)

[20] K. D. Belfield, D. J. Hagan, E. W. Van Stryland, K. J. Schafer, R. A. Negres, "New two-photon absorbing fluorene derivatives: synthesis and nonlinear optical characterization", *Organic Letters*, Vol. 1, No. 10, 1575, (1999)

[21] K. D. Belfield, A. R. Morales, J. M. Hales, D. J. Hagan, E. W. Van Stryland, V. M. Chapela and J. Percino, "Linear and two-photon photophysical properties of a series of symmetrical diphenylaminofluorenes", *Chemistry of Materials*, Vol. 16, No. 11, 2267 (2004)

[22] E. Zojer, D. Beljonne, T. Kogej, H. Vogel, S. R. Marder, J. W. Perry and J-L. Bredas, "Tuning the two-photon absorption response of quadrupolar organic molecules", *J. Chem. Phys.*, Vol. 116, 3646 (2002)

[23] S.R. Marder, "Organic nonlinear optical materials: where we have been and where we are going", *Chem. Commun.* 131-134 (2006).

[24] T. Kogej, D. Beljonne, F. Meyers, J.W. Perry, S.R. Marder, J.L. Bredas, "Mechanisms for enhancement of two-photon absorption in donor-acceptor conjugated chromophores", *Chem. Phys. Lett.* 298, 1-3 (1998).

[25] G.S. He, T.-C. Lin, J. Dai, P.N. Prasad, R. Kannan, A.G. Dombroskie, R.A. Vaia, L.-S. Tan, "Degenerate two-photon-absorption spectral studies of highly two-photon active organic chromophores", *J. Chem. Phys.* 120, 5275-5284 (2004).

[26] C.-K. Wang, P. Macak, Yi Luo, H. Agren, "Effects of π centers and symmetry on two-photon absorption cross sections of organic chromophores", *J. Chem. Phys.* 114, 9813-9820 (2001).

[27] D. B, Hochstrasser R. M. and Trommsdorff H. P., *Nonlinear optical properties of organic molecules and crystals,* Vol.2, ed D. S. Chemla and J. Zyss, New York: Academic press, pp 167-170 (1987)

[28] J. M. Hales, PhD dissertation, "Chemical structure-nonlinear optical property relationships for a series of two-photon absorbing fluorene molecules", 2004

[29] R. W. Boyed, *Nonlinear Optics*, Academic Press, San Diego (1992)

[30] P. Pacher, "Two-photon absorption in organic molecules", Diploma thesis, Graz University of Technology (2003)

[31] B. J. Orr and J. F. Ward, "Perturbation theory of the non-linear optical polarization of an isolated system", *Mol. Phys.*, Vol.20, 513 (1971)

[32] P. Cronstrand, Y. Luo and H. Agren, "Generalized few-state models for two-photon absorption of conjugated molecules", *Chem. Phys. Lett.*, Vol. 352, 262 (2002)

[33] P. R. Monson and W. M. McClain, "Polarization dependence of the two-photon absorption of tumbling molecules with application to liquid 1-chloronaphthalene and benzene", *J. Chem. Phys.*, Vol. 53, No. 1, 29 (1970)

[34] R. R. Birge, J. A. Bennett, B. M. Pierce and T. M. Thomas, "Two-photon spectroscopy of the visual chromophores. Evidence for a lowest excited 1Ag-_Like ππ* state in all-trans-retinol (Vitamin A)", *J. Am. Chem. Soc*., Vol. 100, No. 5, 1533 (1978)

[35] K. Kamada, K. Ohta, Y. Iwase, K. Kondo, "Two-photon absorption properties of symmetric substituted diacetylene: drastic enhancement of the cross section near the one-photon absorption peak", *Chem. Phys. Lett*., Vol. 372, 386 (2003)

[36] R. R. Birge, *Ultrasensitive Laer Spectrosocopy*, Ed. D. S. Kliger, Academic Press: New York, 109 (1983)

[37] G. Herzberg, *Molecular spectra and molecular structure. I. Spectra of diatomic molecules*, Van Nostrand Reinhold Company: New York, 381 (1950)

[38] R. S. Mulliken, "Intensities of electronic transitions in molecular spectra", *J. Chem. Phys.*, Vol.7, 14 (1939)

[39] J. R. Lakowicz, *Principle of fluorescence spectroscopy*, 2nd edition, Kluwer Academic/Plenum Publisher: New York, (1999)

[40] M. Fischer, J. Georges, "Fluorescence quantum yield of rhodamine 6G in ethanol as a function of concentration using thermal lens spectrometry", *Chem. Phys. Lett.*, Vol. 260, 115 (1996)

[41] M. Sheik-Bahae, A. A. Said, T. Wei, D. J. Hagan, E. W. Van Stryland, "Sensitive measurement of optical nonlinearities using a single beam", *IEEE J. Quantum. Electron.*, Vol. 26, 760 (1990)

[42] C. Xu and W. W. Webb, "Measurement of two-photon excitation cross sections of molecular fluorophores with data from 690 to 1050nm", *J. Soc. Opt. Am. B*, Vol. 13, No. 3, 481 (1996)

[43] W. M. McClain and R. A. Harris, *Two-photon molecular spectroscopy in liquids and gases in excited states*, E. C. Lim, ed. Academic, New York, 1 (1977)

[44] R. A. Negres, J. M. Hales, A. Kobyakov, D. J. Hagan, E. W. Van Stryland, "Experiment and analysis of two-photon absorption spectroscopy using a white-light continuum probe", *IEEE J. Quantum Electron*. Vol. 38, No. 9, 1205 (2002)

[45] R. A. Negres, "Ultrafast nonlinear spectrometer for material characterization", PhD thesis, 2001

[46] A. Brodeur, S. L. Chin, "Bandgap dependence of the ultrafast white-light continuum"' *phys. Rev. Lett.*, Vol. 80, 4406 (1998)

[47] C.H.G. Williams, Trans. R. Soc. Edinburg, 211, 377 (1856)

[48] M. T. Spitler, A. Ehret, R. Kietzmann and F. Willig, "Electron transfer threshold for spectral sensitization of silver halides by monomeric cyanine dyes", *J. Phys. Chem. B*, Vol.101, 2552 (1997)

[49] N. Tyutyulkov, et. al., Polymethine dyes structure and properties, Sofia, St. *Kliment Ohridski University Press*, (1991)

[50] Y. Miyazoe and M. Maeda, "Stimulated emission from 19 polymethine dyes-laser action over the continuous range 710-1060 nm," *App. Phys. Lett.* Vol.12, No.5, 206 (1968)

[51] E. Terpetschnig, H. Szmacinski, A. Ozinskas, J. R. Lakowicz, "Synthesis of squaraine-N-hydroxysuccinimide esters and their biological application as long-wavelength fluorescent labels", *Anal. Biochem.*, Vol. 217, 197 (1994)

[52] J. H. Lim, O. V. Przhonska, S. Khodja, S. Yang, T. S. Ross, D. J. Hagan, E. W. Van Stryland, M. V. Bondar, Y. L . Slominsky, "Polymethine and squarylium molecules with large excited-state absorption", *Chem. Phys.*, Vol. 245, 79 (1999)

[53] R. S. Lepkowicz, O. V. Przhonska, J. M. Hales, D. J. Hagan, E. W. Van Stryland, M. V. Bondar, Y. L. Slominsky, A. D. Kachkovski, "Excited-state absorption dynamics in polymethine dyes detected by polarization-resolved pump-probe measurements", *Chem. Phys.*, Vol. 286, 277 (2003)

[54] Y.H. Meyer, M. Pittman, and P. Plaza, "Transient absorption of symmetrical carbocyanines," *J. Photochem. Photobiol. A*, Vol. 114, 1, 1998

[55] R. S. Lepkowicz, Olga V. Przhonska, J. M. Hales, J. Fu, David J. Hagan, E. W. Van Stryland, M. V. Bondar, Y. L. Slominsky, A. D. Kachkovski, "Nature of the electronic transitions in thiacarbocyanines with a long polymethine chain", *Chem. Phys.* Vol. 305, p259 (2004)

[56] J. M. Hales, D. J. Hagan, E. W. Van Stryland, K. J. Schafer, A. R. Morales, K. D. Belfield, P. Pacher, O. Kwon, E. Zojer, J. L. Bredas "Resonant enhancement of two-photon absorption in substituted fluorene molecules", *J. Chem. Phys.*, Vol. 121 (7), 3125, 2004

[57] W. M. McClain, "Excited state symmetry assignment through polarized two-photon absorption studies of fluids", *J. Chem. Phys.*, Vol. 55, 2789-2796 (1971)

[58] D. M. Friedrich and W. M. McClain, "Two-photon molecular electronic spectroscopy", *Annu. Rev. Phys. Chem.*, Vol. 31, 559-577 (1980)

[59] M.J.S. Dewar, *The molecular orbital theory of organic chemistry* (McGrow-Hill, New York, 1969)

[60] D. Scherer, R. Dorfler, A. Feldner, T. Vogtmann, M. Schwoerer, U. Lawrentz, W. Grahn and C. Lambert, "Two-photon states in squaraine monomers and oligomers", *Chem. Phys.*, Vol. 279, 179 (2002)

[61] P. R. Callis, T. W. Scott and A. C. Albrecht, "Perturbation selection rules for multiphoton electronic spectroscopy of neutral alternant hydrocarbons", *J. Chem. Phys.*, Vol. 78, 16 (1983)

[62] T. W. Scott, P. R. Callis and A. C. Albrecht, "Alternant hydrocarbon selection rules in the two-photon spectroscopy of perturbed benzenes", *Chem. Phys. Lett.*, Vol. 93, 111 (1992)

[63] J. Fu, O.V. Przhonska, L.A. Padilha, D.J. Hagan, E.W. Van Stryland, K.D. Belfield, M.V. Bondar, Yu.L. Slominsky, A.D. Kachkovski, "Two-photon anisotropy: Analytical description and molecular modeling for symmetrical and asymmetrical organic dyes", *Chem. Phys.,* Vol. 321, 257 (2006)

[64] M. Hamer, *The Cyanine Dyes and Related Compounds*, Interscience Publisher, New York, 1964

[65] J.S. Craw, J.R. Reimers, G.B. Bacskay, A.T. Wong, N.S. Hush, "Solitons in finite- and infinite-length negative-defect trans-polyacetylene and the corresponding Brooker (polymethinecyanine) cations", *Chem. Phys.* Vol. 167, 77 (1992)

[66] S. J. Chung, S. J. Zheng, T. Odani, L. Beverina, J. Fu, L. A. Padilha, A. Biesso, J. M. Hales, X. W. Zhan, K. Schmidt, A. J. Ye, E. Zojer, S. Barlow, D. J. Hagan, E. W. Van Stryland, Y. P. Yi, Z. G. Shuai, G. A. Pagani, J-L. Bredas, J. W. Perry and S. R. Marder, "Extended squaraine dyes with large two-photon absorption cross sections", submitted to *J. Am. Chem. Soc.*

[67] Dewar, M. J. S.; Zoebisch, E. G.; Healy, E. F.; Stewart, J. J. P., "Development and use of quantum mechanical molecular models. 76. AM1: a new general purpose quantum mechanical molecular model", *J. Am. Chem. Soc*. Vol. 107, 3902 (1985)

[68] Ridley, J.; Zerner, M., "An intermediate neglect of differential overlap technique for spectroscopy: Pyrrole and the azines" *Theo. Chem. Acta* Vol. 32, 111 (1973)

[69] Mataga, N.; Nishimoto, K., Z. " ", *Phys. Chem.* Vol. 13, 140 (1957)

[70] Purvis, G. D.; Bartlett, R. J., "A full coupled-cluster singles and doubles model: The inclusion of disconnected triples**"** *J. Chem. Phys.* Vol. 76, 1910 (1982)

[71] Shuai, Z.; Brédas, J. L., "Coupled-cluster approach for studying the electronic and nonlinear optical properties of conjugated molecules**"** *Phys. Rev. B*. Vol. 62, 15452 (2000)

[72] Buenker, R. J.; Peyerimhoff, S. D., "Individualized configuration selection in CI calculations with subsequent energy extrapolation" *Theo. Chem. Acta* ,Vol. 35, 33 (1974)

[73] Tavan, P.; Schulten, K., "The low-lying electronic excitations in long polyenes: A PPP-MRD-CI study" *J. Chem. Phys*. Vol. 85, 6602 (1986)

[74] Guo, D.; Mazumdar, S.; Dixit, S. N.; Kajzar, F.; Jarka, F.; Kawabe, Y.; Peyghambarian, N., "Role of the conduction band in electroabsorption, two-photon absorption, and third-harmonic generation in polydiacetylenes" *Phys. Rev. B* Vol. 48, 1433 (1993)

[75] Heflin, J. R.; Wong, K. Y.; Zamani-Khamiri, O.; Garito, A. F., "Nonlinear optical properties of linear chains and electron-correlation effects" *Phys. Rev. B* Vol. 38, 1573 (1988)

[76] Tavan, P.; Schulten, K., "Electronic excitations in finite and infinite polyenes" *Phys. Rev. B* 1987, 36, 4337

[77] Shuai, Z.; Beljonne, D.; Brédas, J. L., "Nonlinear optical processes in short polyenes: Configuration interaction description of two-photon absorption and third-harmonic generation" *J. Chem. Phys.* Vol. 97, 1132 (1992)

[78] Zojer, E.; Beljonne, D.; Pacher, P.; Brédas, J. L., *Chem. Eur. J.* Vol.10, 2668 (2004)

[79] P.R. Callis, in: J.R. Lakowicz (Ed.) *Topics in fluorescence spectroscopy*, V. 5, Plenum Press, New York – London, p1. (1997)

[80] K. D. Belfield, M. V. Bondar, J. M. Hales, A. R. Morales, O. V. Przhonska, K. J. Schafer, "One- and two-photon fluorescence anisotropy of selected fluorene derivatives" *J. Fluoresc.* Vol. 15, No. 1, 3 (2005)

[81] J.R. Lakowicz, I. Gryczynski, in J.R. Lakowicz (Ed.), *Topics in fluorescence spectroscopy*, V. 5, Plenum Press, New York – London, p87 (1997)

[82] V. Gaisenok, A. Sarzhevskii, *Absorption and fluorescence anisotropy of complicated molecules*, University Press, Minsk, (1986)

[83] L. Beverina, J. Fu, A. Leclercq, E. Zojer, P. Pacher, S. Barlow, E. W. Van Stryland, D. J. Hagan, J-L. Bredas, S. R. Marder, "Two-photon absorption at telecommunications wavelengths in a dipolar chromophore with a pyrrole auxiliary donor and thiazole auxiliary acceptor", *J. Am. Chem. Soc.*, Vol. 127, 7282 (2005)

[84] J. Y. Cho, S. Barlow, S. R. Marder, J. Fu, L. A. Padilha, E. W. Van Stryland, D. J. Hagan, M. Bishop, "Strong two-photon absorption at telecommunications wavelengths in nickel dithiolene complexes", submitted to *Optics Letters*

[85] S. J. Zheng, L. Beverina, J. Fu, L. A. Padilha, E. Zojer, S. Barlow, C. Fink, O. Kwon, Y. P. Yu, E. W. Van Stryland, D. J. Hagan, J-L. Bredas and S. R. Marder. "High two-photon

cross-sections in bis(diaryaminostyryl) chromophores with electron-rich heterocycle and bis(heterocycle)vinylene bridges", submitted to

[86] S. J. Zheng, A. Leclercq, J. Fu, L. Beverina, L. A. Padilha, E. Zojer, K. Schmidt, S. Barlow, J. D. Luo, S. H. Jiang, A. Jen, Y. P. Yi, Z. G. Shuai, E. W. Van Stryland, D. J. Hagan, J-L Bredas and S. R. Marder, "Two-photon absorption in quadrupolar bis(acceptor)-terminated chromophores with electron-rich bis(heterocycle)viny bridges", submitted to *Chemical Material*